

TROPOSPHERIC COMPOSITION OF
ORGANOHALOGENS AND ALKYL NITRATES:
TROPICAL AND TEMPERATE CASE STUDIES

A thesis submitted to the
School of Environmental Sciences
of the
University of East Anglia
in partial fulfilment of the requirements for the degree of
Doctor of Philosophy

By
Hannah Madeleine Newton

September 2011

© This copy of the thesis has been supplied on condition that anyone who consults it is understood to recognise that its copyright rests with the author and that no quotation from the thesis, nor any information derived therefrom, may be published without the author's prior, written consent.

Abstract

The tropospheric composition of organohalogenes and alkyl nitrates have been investigated from tropical and temperate environments. Ground based measurements and aircraft data are presented from the Oxidant and Particle Photochemical Processes (OP3) project, conducted in Borneo, 2008. Controlled experiments of temperate vegetation were also conducted to assess the emission of methyl halides from crop plants. Methyl halide results from OP3 contradict current assumptions of a strong source from tropical vegetation. High mixing ratios of methyl chloride and chloroform were observed in the boundary layer over oil palm plantations. OP3 aircraft data suggests that the oil palm plantations facilitate the formation of C₂ to C₄ alkyl nitrates. There was evidence that the southeast coast of Sabah is a source region for the bromocarbons measured. The short lived bromocarbons contribute to a bromine budget of 4- 6 ppt; this corroborates recent modelling estimates of their contribution to the stratospheric burden.

In controlled experiments it was confirmed that the gene responsible for the emission of methyl halides is the HOL (HARMLESS TO THE OZONE LAYER) gene. The current WMO estimate for rapeseed contribution to the natural methyl bromide budget was shown to be an overestimate, based on the varieties studied in this thesis. Methyl iodide emissions from rice plants grown in soils were observed to be significantly lower than reported from rice paddies in the literature, suggesting that the growth conditions contribute to the production of methyl iodide.

I almost wish I hadn't gone down that rabbit-hole - and yet - and yet - it's rather curious, you know, this sort of life!

Alice, from Alice in Wonderland

Lewis Carroll, 1865

Acknowledgements

I would like to thank Claire Reeves and Graham Mills for their supervision, assistance and guidance throughout my Ph.D. I feel fortunate to have been a part of the Trace Gas Laboratory and wider Atmospheric Chemistry Group at UEA, within which there has always been a door to turn to with a query. I greatly enjoyed the opportunity to work with Lars Ostergaard's group at the JIC, and I thank them for their patience when explaining crop genetics to me. I am grateful to Faye and Nem who were a reassuring, sharing their own Ph.D experiences.

Thanks are also due to the OP3 group with whom it was a privilege to be conducting field work in Borneo. I learnt a great deal from my OP3 colleagues and I would like to express my thanks to them for their assistance in the field and during the data work up. Big thanks are due to Ayu, Felicity and Dave for providing alternative meal-time conversation to that of vacuum pumps, at Danum Valley Field Centre (DVFC). I wish to acknowledge the support services provided by the Malaysian staff at DVFC and NERC for funding my Ph.D.

On a personal note, I am indebted to my wonderful parents, Margaret and Stephen, for their emotional and financial support throughout my Ph.D. Their upbeat spirits and excellent perspectives on life are an inspiration. Likewise my brother, Robert, and sister-in-law, Sanchia, have been wholly supportive and a great comfort. I am very lucky to have Paul in my life and my great friends Vicki, Nina, Ben, Rob, Matthew and Kirsty, who all deserve huge thanks for having kept me sane(ish) over the last four years!

Finally, I remember my good friend Kate who sadly died in 2009. I have great memories of the two of us staying in the ladies hostel at DVFC during OP3 deciding which of the

48 beds to sleep in, the huge amounts of assorted/unknown tropical fruit we consumed and the alarmingly coloured cakes! Also, there was the incident with the snake...good times. Thank you.

Contents

Abstract	iii
Acknowledgements	vi
1 Introduction	1
1.1 Structure of the atmosphere	2
1.1.1 Atmospheric transport	6
1.2 Ozone and climate	7
1.2.1 Tropospheric ozone	7
1.2.2 Stratospheric ozone depletion	9
1.3 Sources of atmospheric organohalogens	12
1.3.1 Direct and indirect effects of organohalogens	17
1.4 Alkyl nitrates	18
1.5 Aims and objectives	20
2 Experimental methodologies	23
2.1 Analytical system	23
2.1.1 Gas chromatography	23
2.1.2 Mass Spectrometry	26
2.1.3 Sensitivity and detection limits.	30
2.1.4 OP3 analytical setup	32
2.1.5 JIC analytical setup	33
2.2 Sampling techniques	34
2.2.1 OP3 project ground based site, Bukit Atur	34
2.2.2 OP3 aircraft campaign	36
2.2.3 Methyl halide plant emission experiments, John Innes Centre	38
3 OP3: Organohalogens	39
3.1 Introduction	39

3.2	Spatial characterisation of Sabah	43
3.3	Wind directions during the OP3 campaigns.	44
3.4	Back trajectories for OP3	44
3.4.1	OP3-I	45
3.4.2	OP3-III	46
3.5	Methyl halides	53
3.6	Short lived bromocarbons	64
3.6.1	Bromine budget	88
3.7	Chloroform and methyl chloroform	90
3.8	Back trajectories and source attribution analysis of select halocarbons	98
3.9	Conclusions	102
3.10	Further work	103
4	OP3: C₁-C₄ Alkyl nitrates	105
4.1	Introduction	105
4.1.1	Formation of alkyl nitrates	105
4.1.2	NO _x observations during OP3	107
4.2	Spatial observations of alkyl nitrates over Borneo	110
4.2.1	Relationship between alkyl nitrates and their parent hydrocarbons in the OP3-III aircraft data	119
4.3	Temporal trends in alkyl nitrate observations	121
4.3.1	Back trajectory analysis of alkyl nitrates from measurements at Bukit Atur	127
4.4	Summary	132
5	Methyl halide emissions from crop plants	133
5.1	Introduction	133
5.1.1	The methylation process and the HOL gene	136
5.1.2	Plant varieties studied here	137
5.2	Pilot study of methyl halide emissions from <i>Arabidopsis thaliana</i>	140
5.2.1	Hypothesis 1	140
5.2.2	Methodology	140
5.2.3	Results from HOL vs. wild type experiment	140
5.2.4	Hypothesis 2	144
5.2.5	Methodology	144
5.2.6	Results of overexpressor experiment	144
5.2.7	Summary of <i>Arabidopsis thaliana</i> experiments	144

5.3	<i>Brassica napus</i> field experiment	147
5.3.1	Hypothesis 3	147
5.3.2	Methodology	147
5.3.3	Results and Discussion	148
5.3.4	Summary of <i>Brassica napus</i> field experminet	154
5.4	Effect of NaCl salinity on emission of methyl halides from <i>Brassica rapa</i>	156
5.4.1	Hypothesis 4	156
5.4.2	Rationale	156
5.4.3	Methodology for NaCl <i>Brassica rapa</i> experiment	156
5.4.4	Results of NaCl treatment experiment	157
5.4.5	Conclusions of NaCl treatment experiment.	158
5.5	Methyl halide emissions from rice, <i>Oryza sativa</i>	160
5.5.1	Hypothesis 5	160
5.5.2	Methodology	160
5.5.3	Results from rice experiment	160
5.6	Global emission estimates based on the plant varieties measured	162
5.6.1	Emission calculations	164
5.7	Conclusions	171
6	Summary and Conclusions	173
	References	178
	Appendix	193

List of Tables

1.1	Summary of VSLS source gases	13
1.2	Sources of methyl bromide to the atmosphere.	16
2.1	Detection limits for EI and NI	32
3.1	Mean mixing ratios (pptv) of CHBr_3 and CH_2Br_2 from OP3-I and OP3-III campaigns and compared to the literature.	82
3.2	Comparison of bromine budgets from OP3 campaigns and those reported in the literature.	88
4.1	Kinetic data	120
5.1	Estimated methyl chloride fluxes (Gg yr^{-1}) for 2009 and 2050 from different varieties of rapeseed	165
5.2	Projected methyl bromide fluxes (Gg yr^{-1}) for 2009 and 2050 from different varieties of rapeseed	166
5.3	Projected methyl iodide fluxes (Gg yr^{-1}) for 2009 and 2050 from different varieties of rapeseed	167
5.4	Projected methyl halide fluxes (Gg) for 2050 and 2100 from different varieties of rice	168
5.5	Best estimates for methyl halide fluxes (Gg yr^{-1}) from rapeseed and rice varieties measured in this work	169
5.6	Projected methyl bromide and methyl iodide from rice (Gg yr^{-1}) for a range of climate change scenarios	169

List of Figures

1.1	Temperature-altitude profile of the atmosphere	4
1.2	Evolution of the boundary layer in fair-weather	5
1.3	The general circulation of the Earth's atmosphere.	7
1.4	Atmospheric mixing	8
1.5	Generalised reaction pathway for biogenic VOCs from Atkinson and Arey (2003)	10
1.6	Estimated sources and sinks (Gg/yr) of methyl chloride from Clerbaux et al. (2007)	15
1.7	Changes in stratospheric Br _y from balloon measurements.	19
2.1	The mass spectrometer quadrupole	27
2.2	Signal-to-noise levels for determining LOD.	31
2.3	Location of OP3 measurement sites	35
2.4	The Bukit Atur measurement site.	35
2.5	The BAe-146 aircraft in OP3	37
2.6	All aircraft measurement points, coloured by flight.	37
3.1	Land cover map of Sabah.	43
3.2	Wind rose plots for OP3-I and OP3-III.	48
3.3	Back trajectories: 13 th -22 nd April, OP3-I	49
3.4	Back trajectories: 23 rd April-3 rd May, OP3-I	50
3.5	Back trajectories: 5 th -14 th July, OP3-III	51
3.6	Back trajectories: 15 th -22 nd July, OP3-III	52
3.7	Spatial distribution of methyl chloride over Sabah	54
3.8	Methyl chloride box plots	55
3.9	Spatial distribution of methyl bromide over Sabah	57
3.10	Methyl bromide box plots	58
3.11	Spatial distribution of methyl iodide over Sabah	59
3.12	Methyl iodide box plots	60
3.13	Time series of methyl iodide and methyl bromide for OP3-I and OP3-III	63
3.14	Spatial distribution of bromoform over Sabah	66

3.15 Bromoform box plots	67
3.16 Spatial distribution of dibromomethane over Sabah	68
3.17 Dibromomethane box plots	69
3.18 Correlation plots for ocean flights B389 and B393 for the compounds CHBr_3 and CH_2Br_2	71
3.19 Altitude vs. longitude plot of dibromomethane	72
3.20 Timeseries of CHBr_3 and CH_2Br_2 data for OP3 phase I and OP3 phase III.	73
3.21 Correlation plots for the ground based measurements of CHBr_3 and CH_2Br_2 at Bukit Atur during (a) OP3-I and (b) OP3-III	74
3.22 From Gostlow et al. (2010): CHBr_3 and CH_2Br_2 data (ppt) during OP3-III from the UEA GC-MS and Cambridge University's μDirac instrument. The instrument inlets were situated 18m apart on the GAW tower. Dark symbols denote the μDirac data and light symbols represent the UEA data.	75
3.23 Mean mixing ratios of CHBr_3 and CH_2Br_2 , from OP3-I, in hourly bins.	76
3.24 This figure is adapted from Pearson et al. (2010) who plotted the terrain to show the valley situation of their instrument. The dashed lines represent the nocturnal boundary layer situated below the sampling inlet and the daytime boundary layer above the sampling inlet. Pearson2010 plotted the terrain to convey the gradients involved around Bukit Atur.	79
3.25 Time series of the ratio of bromoform/dibromomethane for OP3-I and OP3-III	81
3.26 Time series of CHCl_2Br , CHBr_2Cl and CH_2BrCl data during OP3-III	83
3.27 Spatial distribution of bromochloromethane over Sabah.	84
3.28 Bromochloromethane box plots	85
3.29 Spatial distribution of dibromochloromethane over Sabah.	86
3.30 Dibromochloromethane box plots	87
3.31 Spatial distribution of chloroform over Sabah.	92
3.32 Chloroform box plots	93
3.33 Spatial distribution of methyl chloroform over Sabah.	94
3.34 Methyl chloroform box plots	95
3.35 Time series of chloroform and methyl chloroform for OP3-I and OP3-III.	97
3.36 Mean value maps for CHBr_3 and CH_2Br_2 during OP3 phase I (top) and III (bottom). The maps were generated using back trajectories calculated through BADC using the ECMWF model.	99
3.37 Mean value maps for methyl iodide (a) and methyl bromide (b) during OP3 phase III. The maps were generated using back trajectories calculated through BADC using the ECMWF model.	99

3.38 Methyl iodide and bromoform data from OP3-III coloured by trajectory classifications defined in Robinson et al. (2011).	101
4.1 NO _x time series for OP3-I	108
4.2 NO _x time series for OP3-III	109
4.3 Spatial distribution of methyl nitrate	111
4.4 Spatial distribution of ethyl nitrate	112
4.5 All aircraft measurements containing 2-C ₃ ONO ₂ (n=344) coloured by 2-C ₃ ONO ₂ concentration. The concentration range has been restricted here to omit outliers for a clearer picture of the distribution	113
4.6 All aircraft measurements containing 2-butyl nitrate (n=290), coloured by 2-C ₄ ONO ₂ concentration. The concentration range has been restricted here to omit outliers for a clearer picture of the distribution.	114
4.7 Methyl nitrate box plots	115
4.8 Ethyl nitrate box plots	116
4.9 2-propyl nitrate box plots	117
4.10 Relationships between various ratios of alkyl nitrates and their parent hydrocarbons for the OP3 aircraft measurements. The points on the model curve that correspond to 1 and 10 days of photochemical processing have been marked.	122
4.11 Time series of the alkyl nitrate data collected at Bukit Atur during OP3 phase 1. Bromoform is shown for reference in the grey trace.	124
4.12 Time series of the alkyl nitrate data collected at Bukit Atur during OP3 phase 3. Bromoform is shown for reference in the grey trace.	125
4.13 Alkane measurements taken at Bukit Atur during OP3 phase 1 on the York GC-MS system	126
4.14 Mean value maps of C ₁ - C ₄ alkyl nitrates from OP3-I	129
4.15 Mean value maps of C ₁ - C ₄ from OP3-III	130
4.16 Back trajectories bringing higher than average (a) & (b) and lower than average concentrations (c) & (d) of C ₂ ONO ₂ to Bukit Atur during OP3-I.	131
5.1 Global rapeseed production	134
5.2 Global rice production	135
5.3 <i>Brassicaceae</i> family tree	137
5.4 <i>Poaceae</i> family tree	138
5.5 Sampling of <i>Arabidopsis thaliana</i> in the Cambridge Laboratory, John Innes Centre	141
5.6 Methyl halides mixing ratios measured in the head space both wild type (WT) <i>Arabidopsis thaliana</i> and the mutant with the HOL gene expressed (hol-1) after 14 hours of enclosure.	142

5.7	Methyl halides mixing ratios with enclosure time. Measured in the head space both wild type (WT) <i>Arabidopsis thaliana</i> and the mutant with the HOL gene	143
5.8	Methyl halides from wild type <i>Arabidopsis thaliana</i> and from the two overexpressor lines 196-9 and 196-11	145
5.9	Plant enclosure sampling setup for <i>Brassica napus</i> field experiment	149
5.10	Mixing ratios of methyl halides from different varieties of rapeseed during telescoping stage of plant development	151
5.11	Methyl halide emissions per minute are plotted against the cumulative leaf length proxy for biomass	152
5.12	Methyl halide fluxes in ng/g/d from <i>Brassica napus</i> varieties	153
5.13	Experimental set up in the greenhouse at JIC for the NaCl <i>Brassica rapa</i> study.	157
5.14	Methyl halide fluxes from adult <i>Brassica rapa</i> plants treated with 0, 100 and 200 mM of NaCl	158
5.15	Fluxes of the methyl halides from different rice varieties	161

Chapter 1

Introduction

In this thesis the atmospheric composition of organohalogenes and alkyl nitrates are presented from field work conducted in the tropics and further organohalogen data is presented from laboratory and field experiments conducted in the UK.

The tropical measurements in this thesis were collected during 2008 in Sabah, Borneo, Southeast Asia. The atmospheric composition in and above the rainforest, oil palm plantations and coastal seas of Sabah, were the focus of this study in the NERC funded project, Oxidant and Particle Photochemical Processes (OP3). The aims of the OP3 project are outlined in Section 1.5 and a description of the measurement sites can be found in Chapter 2. The experimental technique used to analyse the OP3 data has the capability of measuring both the organohalogenes and alkyl nitrates (see Chapter 2 for a full description of the sampling system and analytical setup), this is the primary reason for including both groups of compounds in this thesis as their sources and atmospheric fate generally differ from one another. The organohalogenes are ozone depleting compounds predominantly of biogenic origin (Section 1.3), whereas the alkyl nitrates are formed from their parent hydrocarbons which can be both anthropogenic or natural (Section 1.4). When the alkyl nitrates degrade they release nitrogen oxides back into the atmosphere which can then contribute to tropospheric ozone formation (Section 1.2.1). The chemical species measured and presented in this thesis are influential with ozone chemistry both in the troposphere and stratosphere.

Methyl emissions from crop plants were the subject of a collaborative project between

the University of East Anglia (UEA) and the John Innes Centre (JIC) at Norwich Research Park. Their emission was studied in the model plant *Arabidopsis thaliana* to confirm the gene responsible for their emission, then crop plants from the same plant family were studied. Rapeseed and rice were two of the crop plants used and both are included in the natural sources of methyl halides in the WMO scientific ozone assessment (2011): from the emission data collected in this study, global emission estimates were made for these two crops and compared to the WMO (2011) values (Chapter 5).

This introductory chapter will now provide the reader with an overview of the atmospheric processes, sources of compounds and atmospheric fate of those compounds relevant to the work presented in this thesis.

1.1 Structure of the atmosphere

The Earth's atmosphere reaches to approximately 600 km from the Earth's surface, pressure and temperature define its structure. The pressure declines exponentially with increasing altitude, such that 75% of the total mass of the atmosphere is contained within the lowest region, the troposphere. The temperature-altitude profile of the atmosphere, shown in Figure 1.1, consists of transitions from negative to positive temperature gradients with altitude. These transitions lead to the layering of the atmosphere into the troposphere, stratosphere, mesosphere and thermosphere.

Nearly all atmospheric water vapour or moisture is found in the troposphere and results in almost all weather occurring in this region of the atmosphere. The troposphere is heated by energy radiated from the Earth's surface, causing the temperature to decrease with altitude from the Earth's surface. As a result of this negative lapse rate in temperature the troposphere is characterised by turbulent mixing from convective instability, as described below. The lowest section of the troposphere is known as the 'planetary boundary layer' or 'boundary layer'. The boundary layer consists of inversion layers that restrict the vertical mixing of air in the boundary layer with air in the 'free troposphere' above. The upper boundary of the troposphere, the 'tropopause', is the point where the air ceases to cool with altitude and contains very little moisture. The World Meteorological Organiza-

tion defines the tropopause as the lowest level at which the lapse rate decreases to $2^{\circ}\text{C}/\text{km}$ or less.

The troposphere extends from the Earth's surface to approximately 10-18 km. Its height varies with latitude and season, being highest at the tropics and lowest at the poles during winter. The variation in boundary layer height with latitude is initially a function of the incoming solar radiation and the subsequent heating of the Earth's surface releasing heat back into the atmosphere (Holton, 2004). The change in temperature of a body, such as the Earth's surface, that has not changed phase is termed 'sensible heat'. The sensible heat radiated from the Earth's surface contributes to the vertical convection in the boundary layer: this vertical mixing dictates the height of the boundary layer. As equatorial regions receive more solar radiation than the poles (due to the curvature of the Earth) the boundary layer will extend to a higher altitude near the equator than is possible at the poles.

The boundary layer exhibits a diurnal profile also controlled by the heat energy available. As shown in Figure 1.2, when the sun rises the solar heating causes thermal plumes to rise starting the convective system. Drier air from the free troposphere can penetrate down replacing the rising air parcels: the portion between the highest plume tops and the sinking air from the free troposphere is called the entrainment zone. The degree of turbulence from this convective air motion results in a mixed layer which is defined by approximately constant potential temperature and humidity with height (Garratt, 1994). As the sun sets and the atmosphere cools the boundary layer collapses, becoming the nocturnal boundary layer. The nocturnal boundary layer commonly has a stable layer formed through radiative cooling and surface friction. Above the stable layer, the remnants of the convective boundary layer form a residual layer. The nocturnal layer may also be convective if cold air advects over a warm surface (Piiironen, 1994).

Above the tropopause is the stratosphere which reaches to an altitude of approximately 50 km. It is in the stratosphere that the majority of atmospheric ozone ($\approx 90\%$) resides in what is popularly known as the 'ozone layer'. The ozone layer shields life on Earth from harmful ultraviolet (UV) radiation: without it the increase in UV radiation would

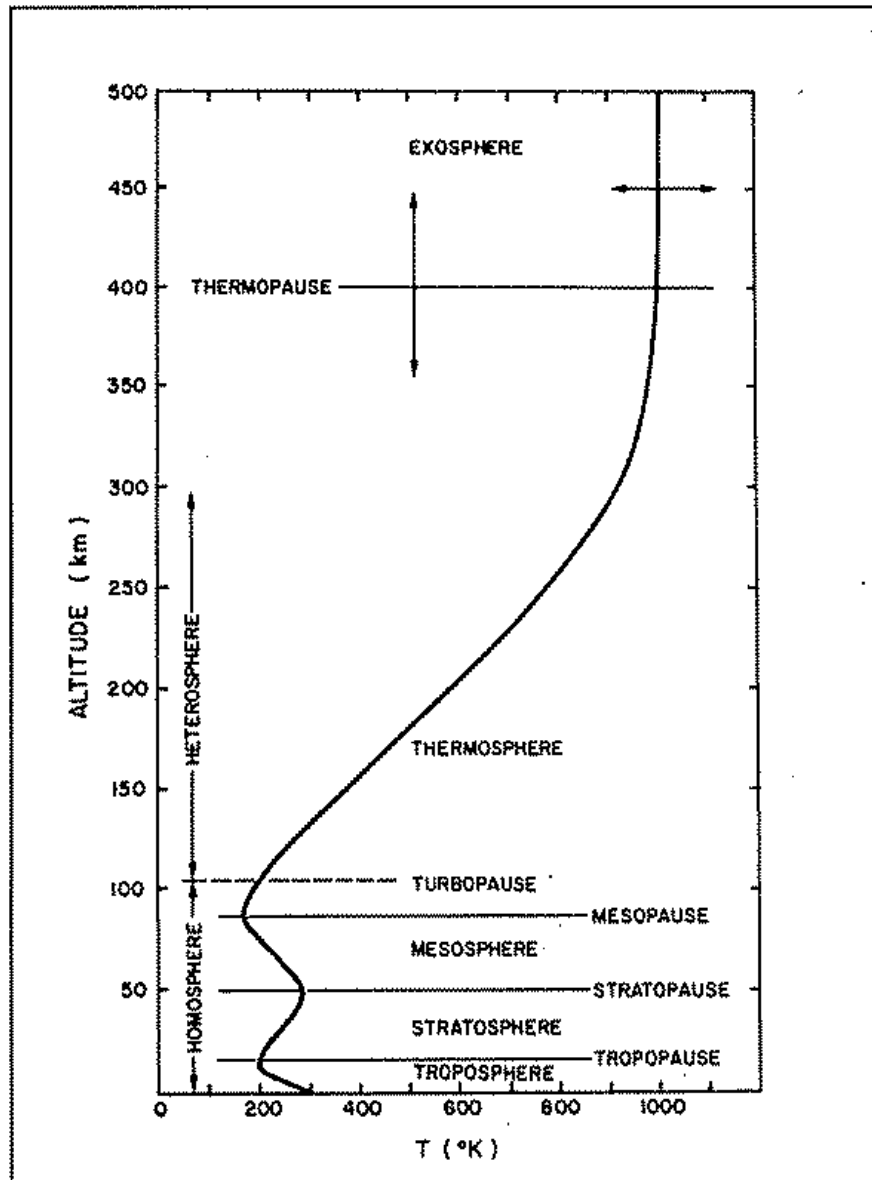


Figure 1.1: Temperature-altitude profile of the atmosphere from Finlayson-Pitts and Pitts (2000)

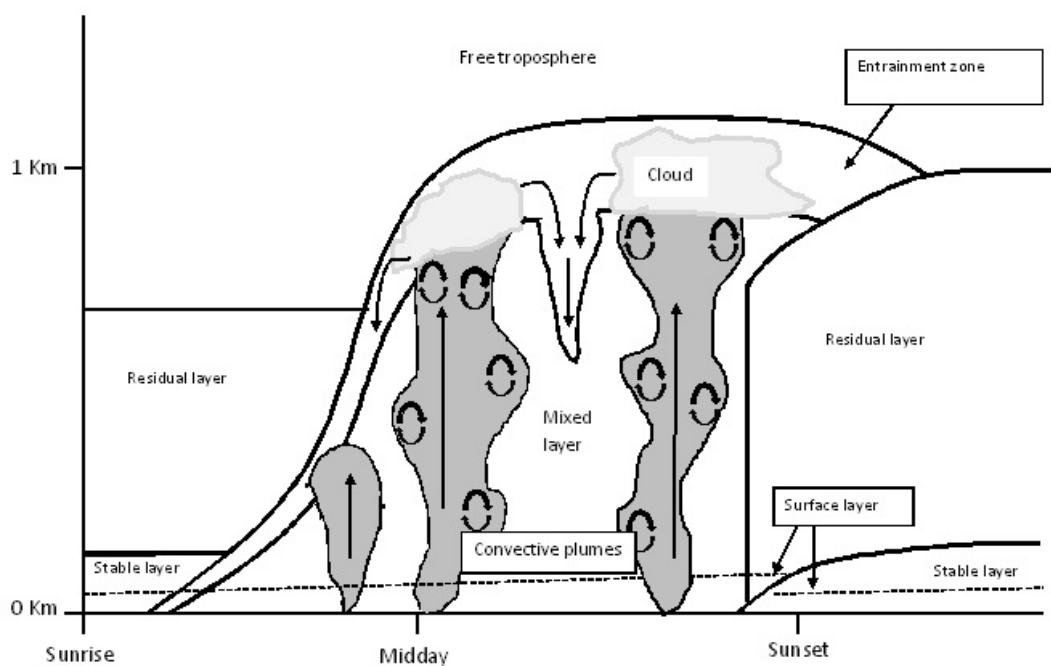


Figure 1.2: This schematic is based on a figure from Piironen (1994) which is designed to show an idealised evolution of the boundary layer throughout the day.

result in an increased incidence of severe sunburn leading to skin cancer (Abarca et al., 2002) and eye cataracts (McMichael et al., 2003), as well as having detrimental effects on plant tissues and oceanic plankton (Smith et al., 1992; Cullen and Neale, 1994). In the mid-1970s it was proposed by Molina and Rowland (1974) that man made substances containing halogens were destroying ozone in the stratosphere, and that these man made substances were exhibiting increasing trends. Farman et al. (1985) provided evidence of a seasonal large ozone losses in Antarctica, supporting the hypothesis of Molina and Rowland (1974). This seasonal ozone depletion event in the southern hemisphere has become commonly known as the ozone 'hole', Manney et al. (2011) described unprecedented stratospheric ozone loss in the Arctic, comparable with that seen in the Antarctic. The mechanism for stratospheric ozone depletion will be discussed in Section 1.2.2 of this Chapter. Beyond the stratosphere, the stratopause separates the stratosphere and the mesosphere.

1.1.1 Atmospheric transport

The Earth is constantly irradiated by short wave ultraviolet radiation from the sun. The distribution of this incoming radiation is not uniform: in the tropics the adsorbed solar radiation exceeds the outgoing infrared radiation while the opposite is true of polar regions. Dynamic transport of heat within the atmosphere and oceans compensates for this latitudinal imbalance in the radiation budget. As a result the Earth's atmosphere is in a constant state of motion in order to redistribute heat: this facilitates the transportation of trace chemical constituents (Finlayson-Pitts and Pitts, 2000).

The general circulation of the atmosphere can be organised into three cells per hemisphere; the Polar Cell, the Ferrel Cell and the Hadley Cell (Figure 1.3). In the tropics of the Hadley cell, hot air rises at the equator and is forced towards the cooler poles due to the higher pressures inherent in higher temperature regions. The Coriolis effect is caused by the rotation of the Earth and the inertia of its mass experiencing that effect. As such the Coriolis effect acts to conserve angular momentum and thus restricts the span of the Hadley Cell stopping it from encompassing an entire hemisphere (Figure 1.3). The air descends in the subtropics and converges again at the equator in the Intertropical Convergence Zone (ITCZ).

The ITCZ is a narrow band along the equator that is characterised by strong vertical motion and heavy rainfall. The intense solar radiation at the equator heats the atmosphere and increases the humidity making the air bouyant. The trade winds of the northern and southern hemisphere come together at the ITCZ and facilitate the bouyant to rise. As the air rises, it cools and expands and the water vapour condenses and is rained our in frequent tropical storms. The ITCZ experiences a seasonal shift in latitude moving north from January to July. Changes in the location of the ITCZ result in wet and dry seasons for many equatorial countries.

Fischer et al. (2003) observed the 'injection' of boundary layer air into the lowermost stratosphere during a strong convective event. Tropical storms are typical in the ITCZ systems and provide excellent mechanisms to penetrate the lower stratosphere with boundary layer air (Fischer et al., 2003). Such systems are of particular interest to the work in this

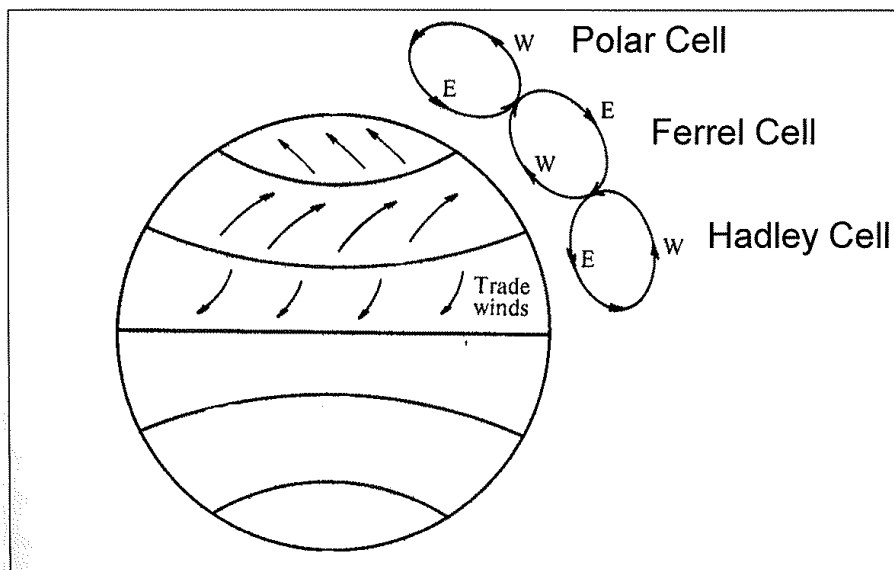


Figure 1.3: The general circulation of the Earth's atmosphere. Illustrating the three circulation cells with each hemisphere (Wayne, 1996).

thesis as they provide a pathway mechanism to transport short lived ozone depleting compounds up into the stratosphere where most of the atmosphere's ozone resides. Once in the stratosphere they can contribute to ozone destruction. This process is important for very short lived compounds that do not have atmospheric residence times long enough to be mixed up into the stratosphere. Figure 1.4 show the average mixing times within the layers of the atmosphere. On average it takes approximately one month for air to mix vertically from the Earth's surface to the tropopause, at around an average altitude of 10 km. Chemical species with lifetimes of approximately one month tend to be well mixed vertically in the troposphere, while species with lifetimes that are shorter than this can show large vertical variations (Jacob, 1999).

1.2 Ozone and climate

1.2.1 Tropospheric ozone

The ability of the atmosphere to cleanse itself of pollutants is often referred to as its oxidizing capacity. There is a direct relationship between tropospheric ozone levels and oxidizing capacity (Lelieveld et al., 2008; Read et al., 2008). Mixing ratios of ozone in the

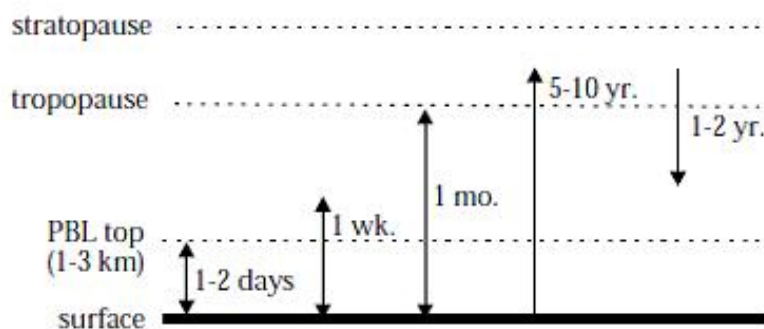
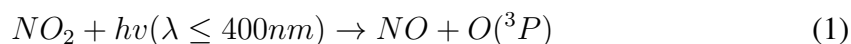


Figure 1.4: Schematic showing mixing times for different atmospheric layers, from Jacob (1999).

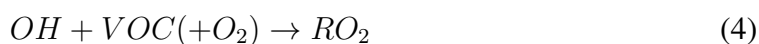
troposphere are not uniform and ozone is largely considered a pollutant due to its ability to damage living tissue and degrade certain materials. Tropospheric ozone is present due to in situ photochemistry involving the oxides of nitrogen (NO_x) and through transport from the stratosphere. The only known pathway to tropospheric ozone formation is shown in Equations 1 - 3. Initially, nitrogen dioxide (NO_2) is photolysed generating ground state atomic oxygen (O^3P). O^3P can then combine with molecular oxygen to generate ozone. The nitrogen monoxide (NO) generated in Equation 1 can be oxidised back to NO_2 by ozone. This cyclical process is known as the 'photostationary state' leading to no net gain of ozone.



Where 'M' = O_2 , N_2 .



There is more ozone in the troposphere than the above reactions can account for. To achieve a net gain in ozone production NO needs to be oxidised back to NO_2 by a peroxy radical such as RO_2 or HO_2 . Equation 4 shows how organic peroxy radicals are formed through reaction with VOCs.



The peroxy radical can then react with NO, NO₂ or other peroxy radicals as shown in Figure 1.5. If the peroxy radical reacts with NO it can form an alkyl nitrate (Equation 5) which will ultimately degrade to release NO₂ back into the atmosphere (Equation 6). The NO₂ can then be photolysed forming O, that can then react with O₂ to form O₃, as in Equations 1 and 2.



As NO_x is required for the formation of tropospheric ozone, the fate and lifetime of NO_x is important to the global distribution of ozone and understanding its precursors Shepson (2007).

1.2.2 Stratospheric ozone depletion

Stratospheric ozone is generated by the 'Chapman cycle' reactions in Equations 7 to 10 below:



Stratospheric ozone is vital to protecting life on Earth. The majority of atmospheric ozone (about 90%) is situated in the stratosphere (WMO, 2010). Situated at high altitudes of 30 to 40 km above the Earth's surface the ozone layer screens harmful ultraviolet radiation (UV) from the Earth's surface. The 1985 discovery by Farman et al. (1985) that the 'ozone hole' was a real phenomenon confirmed the propositions of Molina and Rowland (1974) concerning the damaging impact of anthropogenic halogens on the Earth's protective ozone layer. The ozone hole develops in springtime Antarctic when winds effectively isolate the polar stratosphere and temperatures drop forming ice clouds containing nitric acid (Crutzen and Arnold, 1986). Global atmospheric column ozone amounts decreased over the decades from the 1970s to the 1990s, with a decrease amounting to 3.5% between

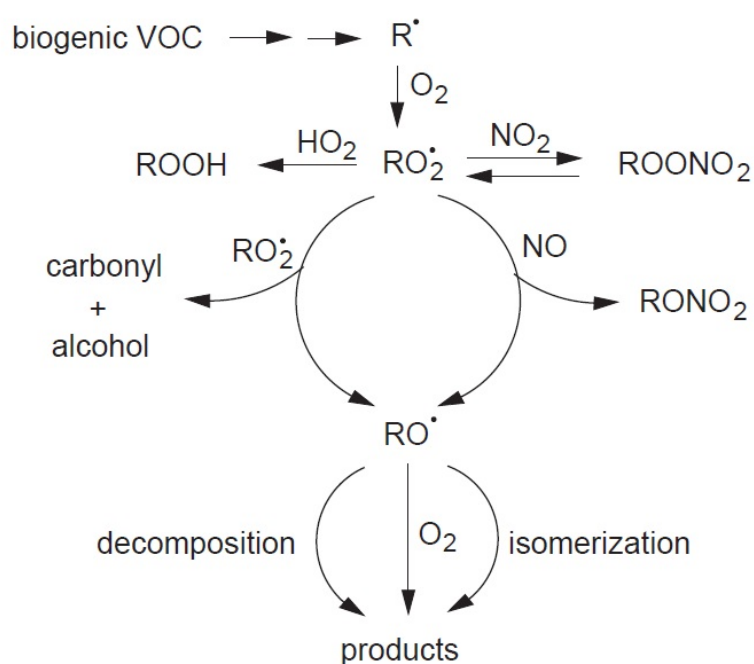


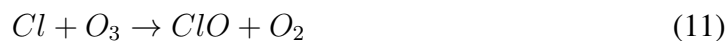
Figure 1.5: Generalised reaction pathway for biogenic VOCs from Atkinson and Arey (2003)

average 1964 to 1980 and 2002 to 2005 values. Springtime Antarctic ozone levels slowly decreased in the 1970s and exhibited rapid decreases in the 1980s and early 1990s. In the Antarctic stratosphere, where most of the ozone resides, virtually all of the ozone is now destroyed every year in the late August to early October period (WMO, 2006).

Crutzen and Arnold (1986) suggest a mechanism for ozone destruction where odd nitrogen is temporarily tied up in reservoir species, resulting in catalytic methane oxidation forming high concentrations of the hydroxyl radical (OH). OH reacts readily with chlorine and bromine containing species producing chlorine monoxide (ClO), bromine monoxide (BrO): ClO, BrO and chlorine and bromine atoms (Cl and Br) are the most reactive ozone depleting gases. Over the course of two to three months, approximately 50% of the total column amount of ozone in the atmosphere disappears. At some levels, the losses approach 90% (WMO, 2007). In spring, temperatures begin to rise, the ice evaporates, and the ozone layer starts to recover (Finlayson-Pitts and Pitts, 2000).

To cause ozone depletion firstly, the halogen containing compound is broken down, then the halogen can engage in catalytic ozone destruction cycles as suggested by Ci-

cerone et al. (1974) for atomic chlorine. Cicerone et al. (1974) hypothesised that if there were sources of atomic chlorine in the stratosphere then the following reactions could occur:

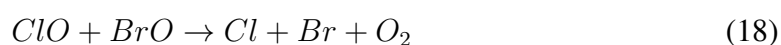


BrO is formed in the same way as above for ClO (Equation 11). The Cl generated in Equation 12 can feed back into Equation 11, as such, one chlorine atom participates in numerous cycles, destroying many ozone molecules (WMO, 2010). A single Cl atom can destroy hundreds of ozone molecules before it reacts with another gas breaking the catalytic cycle, and up to tens of thousands of ozone molecules during its residence time in the stratosphere (Fahey and Hegglin, 2011).

Due to the relatively low abundance of atomic oxygen which limits the rate of ozone loss in Equations 11 and 12, cycles beginning with the self reaction of ClO (Equations 14 to 17) or ClO with BrO (Equations 18 to 22) dominate ozone loss mechanisms. Both cycles involve the destruction of two ozone molecules and the creation of three oxygen molecules.



The cycle involving the reaction of ClO with BrO has two possible pathways: either Equations 18, 21 and 22, or Equations 19 to 22.



Or:



and:



The magnitude of ozone depletion is reduced by conversion of Cl and ClO into reservoir species ClONO₂ and HCl, until these reservoir species react with OH and return to the active species again (O'Doherty, 2007). The reservoir species for bromine compounds are HBr and BrONO₂. These species are more readily photolysed than the chlorine reservoir species and hence bromine has a higher potential to destroy ozone than chlorine by a factor of 45-60.

Solomon et al. (1994) suggest that rapid transport via convective clouds could provide a mechanism for very short lived species such as iodine compounds to be injected into the stratosphere and participate in ozone destruction. They propose that iodine would interact with the ClO cycle in much the same way as BrO. Solomon et al. (1994) also expect BrO-IO cross interactions leading to ozone destruction. They suggest that if 1 pptv of iodine was present in the stratosphere below ≈ 20 Km, then iodine could make a major contribution to ozone destruction.

1.3 Sources of atmospheric organohalogens

The suite of organohalogens presented here in this thesis comprises the methyl halides (CH₃Cl, CH₃Br and CH₃I), bromoform (CHBr₃), dibromomethane (CH₂Br₂), bromochloromethane (CH₂BrCl), dibromochloromethane (CHBr₂Cl), dichlorobromomethane (CHCl₂Br), methylchloroform (CH₃CCl₃) and chloroform (CHCl₃). In Table 1.1 a summary of key attributes of these organohalogens are presented.

Table 1.1: Summary of available observations of VSLS source gases, where MBL = marine boundary layer. Data for the MBL is taken from Law et al. (2007) the remaining data is deemed representative of the troposphere and is from Schauffler et al. (1999) and Montzka et al. (2010).

Compound	Formula	atmospheric lifetime, τ (y= years, d=days)	average mixing ratio (pptv)
Methyl chloride	CH ₃ Cl	1.0 y	550
Methyl bromide	CH ₃ Br	0.7 y	7.6
Methyl iodide	CH ₃ I	0.02 y (3- 7 d)	0.1 - 0.8 (MBL)
Bromoform	CHBr ₃	0.07 y (24 d)	0.5 - 2.4 (MBL)
Dibromomethane	CH ₂ Br ₂	0.3 y (120 d)	0.7 - 1.5 (MBL)
Bromochloromethane	CH ₂ BrCl	137 d	0.4 - 0.6 (MBL)
Dibromochloromethane	CHBr ₂ Cl	59 d	0.1 - 0.8 (MBL)
Dichlorobromomethane	CHBrCl ₂	78 d	0.1 - 0.9 (MBL)
Chloroform	CHCl ₃	149 d	5.2 - 13.1 (MBL)
Methylchloroform	CH ₃ CCl ₃	5.0 y	10.7 - 11.7

Methyl chloride (CH₃Cl) contributes 16% to total chlorine in the troposphere (Montzka et al., 2010). Biomass burning, oceans, and anthropogenic activities are major sources of atmospheric CH₃Cl, as shown in Figure 1.6. It is also produced by vascular plants (Rhew et al., 2010; Saito et al., 2008; Yokouchi et al., 2002, 2007), abiotic release from decaying plant material (Hamilton et al., 2003), coastal salt marshes (Rhew et al., 2000) and emissions from tropical wood-rot (Moore et al., 2005). Currently the known sinks of methyl chloride outweigh the known sources. Recently, Moore (2008) reported a mechanism to produce CH₃Cl through the photochemical reaction of dissolved organic matter in saline waters.

Methyl bromide is a well characterised ozone depleting compound with significant natural and anthropogenic sources. It was used intensively as a fumigant but as its capacity to destroy ozone was understood, its use was phased out. Current estimates of the sources

and sinks of methyl bromide are presented in Table 1.2. Methyl bromide is the single largest carrier of bromine to the stratosphere and like methyl chloride its atmospheric budget suggests that there are missing sources of methyl bromide.

Methyl iodide (CH_3I) is the dominant gaseous organic iodine species in the troposphere. It is predominantly emitted from the ocean, both coastal and open ocean. CH_3I is released by marine macroalgae (Gribble, 2000; Manley and Dastoor, 1988; Peters et al., 2005; Zhou et al., 2005): the study of Manley and Cuesta (1997) observed emission of CH_3I from phytoplankton, and Laturus et al. (1998) and Schall et al. (1994) noted emission of CH_3I from ice algae. CH_3I also has terrestrial sources including rice paddies (Redeker et al., 2000), natural wetland (Dimmer et al., 2001) and biomass burning (Bell et al., 2002). Bell et al. (2002) estimated the terrestrial source of CH_3I to account for 30% of the total budget.

Excluding methyl bromide the bromocarbons of interest in this work are known to be predominantly from oceanic/marine origin. Bromoform and dibromomethane are fairly well characterised in the atmosphere and are observed to correlate well (Yokouchi et al., 2005). Bromoform is the second most abundant 'reactive' organic bromocarbon in the background troposphere (Sturges, 2000), as such it is a potentially significant contributor to reactive bromine in the upper troposphere lower stratosphere as it carries three bromine atoms.

McCulloch (2003) state that 90% of atmospheric chloroform is emitted from natural sources. It has been reported by Khalil et al. (1983, 1999) that the open ocean source predominates, however O'Doherty et al. (2001) questioned these estimates in their modelling study, finding soils to be a larger source and oceans accounting for only 20% of total emissions. McCulloch (2003) infer that human influence and resultant changes in agriculture have lead to increased chloroform emission from soils. Pulp and paper manufacture are another anthropogenic source of chloroform (Keene et al., 1999). Northern hemisphere mixing ratios of chloroform are approximately a factor of two higher than those in the southern hemisphere (O'Doherty, 2007; O'Doherty et al., 2001) and global average mixing ratios range from 10 to 20 pptv (Khalil et al., 1983) and 5 to 13 pptv reported in the

Source or Sink Type	Source or Sink Estimate ^a (Gg/yr)
Sources	
Tropical and subtropical plants	820-8200 ^d
Tropical senescent or dead leaves	30-2500 ^e
Biomass burning	325-1125 ^{d,f}
Oceans	380-500 ^{g,h}
Salt marshes	65-440 ^d
Fungi	43-470 ^d
Wetlands	48 ^j
Rice paddies	2.4-4.9 ^k
Fossil fuel burning	5-205 ^d
Waste incineration	15-75 ^d
Industrial processes	10 ^c
<i>Subtotal</i>	<i>(1743-13,578)</i>
Sinks	
OH ⁻ reaction	3800-4100 ^{h,k}
Loss to stratosphere	100-300 ^d
Cl reaction	180-550 ^d
Soil	100-1600 ^d
Loss to cold waters (polar oceans)	93-145 ^g
<i>Subtotal</i>	<i>(4273-6695)</i>

Figure 1.6: Estimated sources and sinks (Gg/yr) of methyl chloride from Clerbaux et al. (2007)

Table 1.2: Sourced from Montzka et al. (2010): summary of the estimated source and sink strengths (Gg/yr) or methyl bromide for the periods 1996 - 1998 and 2008. n.q. = not quantified. The total burden of methyl bromide is shown as the sinks subtracted from the sources.

	1996 - 1998	Range	2008	Range
SOURCES				
Fumigation-dispersive (soils)	41.5	(28.1 to 55.6)	6.7	(4.6 to 9.0)
Fumigation-quarantine/ pre-shipment	7.9	(7.4 to 8.5)	7.6	(7.1 to 8.1)
Ocean	42	(34 to 49)	42	(34 to 49)
Biomass burning	29	(10 to 40)	29	(10 to 40)
Leaded gasoline	5.7	(4.0 to 7.4)	5.7	
Temperate peatlands	0.6	(-0.1 to 1.3)	0.6	(-0.1 to 1.3)
Rice paddies	0.7	(0.1 to 1.7)	0.7	(0.1 to 1.7)
Coastal salt marshes	7	(0.6 to 14)	7	(0.6 to 14)
Mangroves	1.3	(1.2 to 1.3)	1.3	(1.2 to 1.3)
Shrublands	0.2	(0 to 1)	0.2	(0 to 1)
Rapeseed	4.9	(3.8 to 5.8)	5.1	(4.0 to 6.1)
Fungus (litter decay)	1.7	(0.5 to 5.2)	1.7	(0.5 to 5.2)
Fungus (leaf-cutter ants)	0.5		0.5	
Potential terrestrial sources:				
Tropical trees	n.q.		n.q.	
Temperate woodlands	n.q.		n.q.	
Tropical ferns	n.q.		n.q.	
Abiotic decomposition	n.q.		n.q.	
Subtotal (sources)	143		111.5	
SINKS				
Ocean	56	(49 to 64)	49	(45 to 52)
OH and photolysis	77		63.6	
Soils	40	(23 to 56)	32	(19 to 44)
Subtotal (sinks)	177		147.6	
Total (sources - sinks)	-34		-36.1	

marine boundary layer (Law et al., 2007).

Methylchloroform is used primarily as a cleaner (O'Doherty, 2007), it is a restricted substance under Article 5 of the Montreal Protocol. Production of methylchloroform dropped from 270 Gg/yr in the 1980s to 126 Gg/yr in 1993 (Midgley and McCulloch, 1995) and has continued to decrease WMO. Methylchloroform contributed 13.5 pptv (more than half) of the overall decline observed for total tropospheric Cl in 2003-2004. Globally averaged surface mixing ratios were 22.6 ppt in 2004 versus 46.4 ppt in 2000 (Clerbaux et al., 2007). Montzka et al. (2010) report that by mid-2008 the global surface mean mixing ratio had decreased to about 11 pptv. This decline represents more than a factor of 10 decrease in global surface mixing ratios of methylchloroform since the early 1990s. As its mixing ratios have declined in response to reduced emissions, hemispheric differences have also diminished.

1.3.1 Direct and indirect effects of organohalogens

As previously stated the halogens are ozone depleting compounds. Methods of assessing the environmental effects of halocarbons in the atmosphere have been developed. The two most widely used tools for describing a compounds environmental impact are (i) Ozone Depleting Potential and (ii) Global Warming Potential. The term Ozone Depleting Potentials (ODP) expresses the amount of ozone destroyed by the species of interest relative to the amount of ozone destroyed by the equivalent amount of CFC-11 (CFC13). Global Warming Potential (GWP) is the ratio of the warming caused by a substance to the warming caused by an equivalent mass of carbon dioxide (CO₂) hence the GWP of CO₂ is 1. However, this index is of limited use when applied to the short-lived species discussed here, as these species are not uniformly distributed in the troposphere (O'Doherty, 2007).

Iodine has an even greater efficiency at destroying ozone molecules than bromine, however it is usually present in compounds that have short lifetimes and therefore cannot be successfully transported into the stratosphere by atmospheric mixing alone. It is possible to transport very short lived species (VSLS) such as CH₃I from the surface in the Tropics to the tropical tropopause layer (TTL): for short-lived VSLS (lifetimes of only

hours to days) this is possible if they are emitted directly into the active cell of tropical deep convection (Law et al., 2007; Solomon et al., 1994). Gettelman et al. (2009) predicted higher VSLs concentrations in the TTL in northern hemisphere (NH) winter due to a combination of higher convective cloud tops and higher vertical velocities within the TTL. Some studies have suggested that the northward shift of the deepest convection with the Indian summer monsoon linked with the anticyclonic circulation in the upper troposphere/lower stratosphere (UTLS) could lead to more efficient transport of surface emissions to the TTL in some locations such as the Bay of Bengal and Sea of China (such as James et al. (2008); Randel et al. (2010)). Donner et al. (2007) simulated an enhancement in CH_3I mixing ratios over the Tibetan plateau and the Himalaya during NH summer in the free troposphere showing that short-lived species can be injected into the upper TTL. Ricaud et al. (2007) observed the effect of this pathway noting elevated mixing ratios of methyl iodide in the TTL and stratosphere.

Figure 1.7 shows that 3-7 ppt of bromine are yet to be accounted for in our atmosphere and are expected to be present from VSLs. As mentioned above the tropics provide the ideal meteorological conditions for transport of VSLs from the surface to the UTLS. The brominated VSLs measured in the atmosphere over Borneo in this work could contribute to this missing stratospheric bromine.

1.4 Alkyl nitrates

As described in Section 1.2.1 tropospheric ozone is formed by the oxidation of volatile organic compounds, such as hydrocarbons (RH), in the presence of nitrogen monoxide (NO). Alkyl nitrates are also formed through this process and represent a link between the atmospheric carbon and nitrogen cycles (Equations 4 to 5). When hydrocarbons are oxidised by the hydroxyl radical (OH) alkyl radicals are formed (R) and they can quickly react with O_2 to form alkyl peroxy radicals (RO_2). These then react with nitric oxide (NO) producing either an alkoxy radical (RO) and nitrogen dioxide (NO_2) or an alkyl nitrate (RONO_2). Formation of alkyl nitrates therefore competes with ozone production. Alternative oceanic sources of the shorter chain alkyl nitrates have been proposed by Atlas

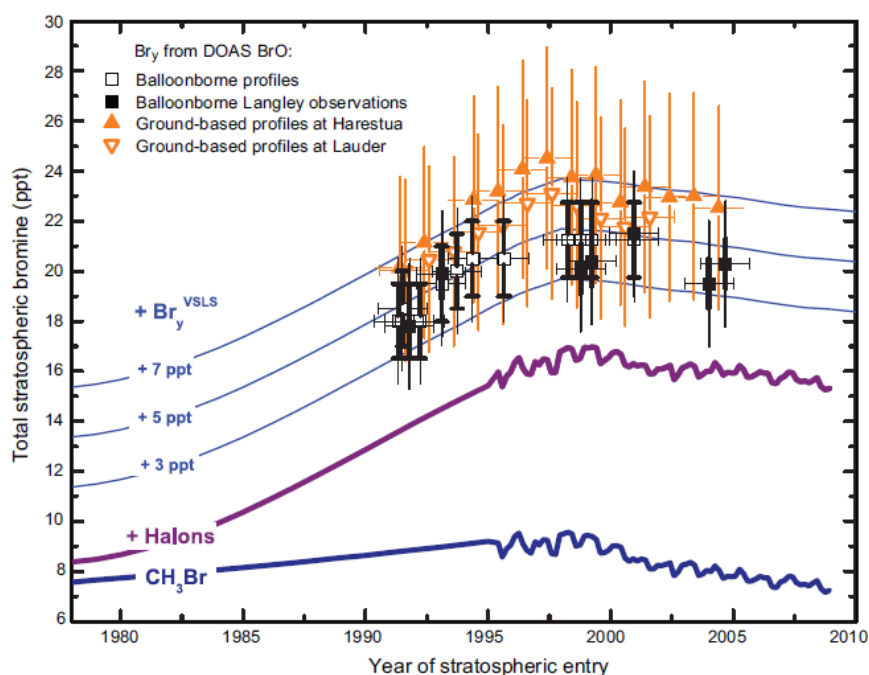


Figure 1.7: Changes in stratospheric Br_y from balloon measurements (squares). Annual mean mixing ratios were calculated from ground-based UV-visible measurements of stratospheric BrO (triangles). Trends of Br at the Earth's surface are shown with thin lines, the trends include an additional constant amounts of Br_y as labelled. The thick blue line represents global tropospheric mixing ratios of bromine from methyl bromide measured in ambient air and firm air with no correction for tropospheric loss of methyl bromide. The purple line represents the global tropospheric bromine from the sum of methyl bromide and the halons. Sourced from Montzka *et al.*, (2011).

et al. (1993); Dahl et al. (2003). Blake et al. (1999); Chuck et al. (2002) and Dahl and Saltzman (2008) support the study of Atlas et al. (1993) observing methyl nitrate to have an oceanic source.

Once nitrogen oxides (NO_x) are tied up in an alkyl nitrates they can be transported much further from source, than as NO or NO_2 , since the alkyl nitrates have longer atmospheric lifetimes ranging from days to weeks. The alkyl nitrates are removed from the reaction through either reaction with OH or via photolysis, degrading to RO and NO_2 . Hence, alkyl nitrates play an important role in the redistribution of NO_x and the global distribution of ozone.

Alkyl nitrates can comprise a significant fraction of odd nitrogen (NO_y) (Reeves et al., 2007), with their greatest contributions to NO_y in air remote from sources (Blake et al., 2003b; Day et al., 2003; Flocke et al., 1991; Shepson et al., 1993). NO_y is the collective term for the reactive atmospheric nitrogen species: peroxyacetyl nitrate, peroxy nitric acid, dinitrogen pentoxide, nitrogen oxides, alkyl nitrate, chlorine nitrate, nitric acid, nitrous acid and aerosol nitrate.

Rainforests are a source of large quantities of biogenic VOCs (Guenther, 1997, 2008; Zimmerman et al., 1988) providing large abundances of peroxy radical which, as discussed above, could react following the pathway that produces alkyl nitrates.

1.5 Aims and objectives

In this Chapter the composition of the background atmosphere was described, the structure of the atmosphere and the general circulation patterns that govern atmospheric transport. The organohalogen and alkyl nitrates were introduced in relation to their atmospheric importance. The methods employed in this work to sample and analyse atmospheric organohalogen and alkyl nitrates are detailed in Chapter 2. Chapters 3 and 4 present and discuss measurements made in a tropical environment as part of the Oxidant and Particle Photochemical Processes (OP3) project in 2008. The aforementioned results chapters discuss ground based and aircraft measurements and provide the major body of this thesis. The aims of the OP3 project are now outlined:

The OP3 project set out to (i) understand how emissions of reactive trace gases from a tropical rain forest mediate the production and processing of oxidants and particles in the troposphere, and (ii) to better understand the impact of these processes on local, regional and global scale atmospheric composition, chemistry and climate. The rationale of the OP3 project is founded on current estimates that equatorial and other tropical forests are estimated to account for almost half of all biogenic reactive volatile organic compound (VOC) emissions into the atmosphere: Guenther (1995) estimate a global total of 1150 Tg C y⁻¹ from forests and they estimate ≈ 500 Tg C y⁻¹ from tropical forests. Tropical forests account for 1.8 billion ha (over half) of the World's forests and are a major contributor of carbon and energy to the troposphere (Hewitt et al., 2010). The study region for the OP3 project was the tropical rain forest of Sabah, in Malaysian Borneo.

The OP3 project aimed to address 5 key questions:

1. What are the rates of transfer and the speciation of organic compounds emitted from this tropical forest region?
2. How are these biogenic reactive compounds chemically processed in the near and intermediate field?
3. How do these emissions contribute to the formation of longer-lived intermediate products?
4. To what extent does the regional biogenic emission control the secondary aerosol budget and its hygroscopic and radiative properties?
5. What are the effects of these biogenic emissions on global chemistry and climate?

OP3 objectives were to investigate the above questions with ground-based and airborne field campaigns measuring surface fluxes and atmospheric composition of reactive trace gases and particles and these measurements integrated into modelling studies of chemical processes in the tropical forest area of Sabah, Borneo. The work covered in this thesis addresses several of the key questions above. The measurement of organohalogenes and alkyl nitrates directly contributes to the speciation of organic compounds in this tropical rainforest region as well as providing data for modelling activities within the

OP3 project. Amongst the organohalogen compounds measured are compounds such as bromoform that are believed to be solely of oceanic origin and by measuring such compounds this work aimed to provide a trace for marine air at a forest measurement site. The impact of biogenic emissions could extend to the upper troposphere and lower stratosphere if the deep convection mechanisms are active: uplifting surface emission of the ozone depleting organohalogen aloft and closer to the stratospheric ozone 'layer'. A further aim of this work was to estimate the amount of bromine available that could be transported to the stratosphere based on the observed data. The organohalogen OP3 data and interpretation is presented in Chapter 3.

The measurement of alkyl nitrates presented in this thesis contribute to the understanding of the oxidative capacity of the rainforest atmosphere. As reservoir species for nitrogen oxides, alkyl nitrates are long-lived intermediate products that can be transported far from where they were formed and ultimately degrade releasing nitrogen oxides which impact the oxidation budget. This work aimed to identify formation regions for the alkyl nitrates. Alkyl nitrate measurements made during OP3 were intended to be used to infer the extent of chemical processing that an air mass has undergone. One of the objectives of collecting the OP3 alkyl nitrate data was to calculate their contribution to the total 'odd' nitrogen budget. The alkyl nitrate measurements from OP3 are discussed in Chapter 4.

Chapter 5 focusses on a group of organohalogen compounds known as the methyl halides. Methyl halide emissions were studied from tropical and temperate crop plants and the results of these studies were used to calculate global estimates of methyl halides from specific crop plants. The aim of this work was initially to confirm the findings of Rhew et al. (2003), who believed they had identified the gene responsible for methyl halide production. This chapter then presents the subsequent experiments that evolved from confirming the work of Rhew et al. (2003). Global emission estimates of methyl halides from crop plants are then calculated based on the method documented in Mead et al. (2008b).

The main findings in this thesis are then summarised in Chapter 6. Appendix A is a published paper which includes a contribution based on the work presented in Chapter 3.

Chapter 2

Experimental methodologies

2.1 Analytical system

The results presented in this thesis are from samples analysed using gas chromatography-mass spectrometry (GC-MS) systems. This analysis technique was used during the Oxidant and Particle Photochemical Processes (OP3) project, April-July 2008, and during the work conducted with the John Innes Centre (JIC) analysed at UEA.

2.1.1 Gas chromatography

Gas chromatography operates on the concept of partition chromatography, by which the various components of an analyte can be individually measured. An analyte in a mobile phase can be separated into its various constituents by interacting with a stationary phase along a column (Skoog et al., 2004). Gas chromatography involves a sample either vapourised or already in the gaseous state, being injected onto the head of a chromatographic column. The sample then flows down the column aided by a chemically inert carrier gas such as helium (He). GC columns are either capillary columns or packed columns. Capillary columns have a thin (several μm) stationary phase chemically bonded to the inside of a silica narrow bore column, known as the film. It is this film that facilitates the adsorption of chemical species in the sample thus separating the chemical components of the sample. It is desirable to have the thinnest film possible combined

with the thinnest bore column to yield the sharpest peaks. Packed columns are generally wider and shorter than capillary columns. They are made of glass or metal tubing densely packed with a uniform, finely divided packing material coated with a thin layer (0.05 to 1 μm) of a stationary liquid phase. The efficiency of a GC column increases significantly with decreasing particle diameter of the packing. However, a lower limit of packing particle size is dictated by the pressure difference required to maintain a reasonable flow rate of carrier gas. Capillary columns offer a number of advantages compared to packed columns; most notable are the reduced analysis times, improved resolution and the flexibility to run smaller sample sizes (Hubschmann, 2009).

GC parameters such as flow rates, column temperature and sample injection are commonly automated functions. The ability to keep these parameters known greatly assists the identification of chromatographic peaks. The He carrier gas keeps the analyte mobile through the GC system. However, the rate at which the analyte migrates through the column is dependent on the retention time of the analyte on the film lining of the column. This retention is determined by the affinity of a particular analyte with the specific film lining and the boiling point of that analyte. The partition between the mobile and stationary phase is described by Equation 23.



The equilibrium constant or partition coefficient (k) for this reaction is described by Equation 24, where C_s is the concentration of the solute A in the stationary phase and C_m is the concentration of solute A in the mobile phase:

$$k = \frac{C_s}{C_m} \quad (24)$$

Different analytes have different partition coefficients, hence separation occurs. The degree of separation between two analytes is dependent on the difference between their partition coefficients; the larger the difference, the greater the separation (Skoog et al., 2004).

The GC column is housed in an insulated oven to provide a controllable column temperature. Varying the temperature of the column throughout a sample run can separate

compounds by their boiling points resulting in a spread of elution times. This is true if the polarity of the stationary phase matches well with the sample components. Polarity is the electrical field effect in the immediate vicinity of a molecule. If a compound has a stronger affinity with the stationary phase, then it will elute later than a compound with a higher boiling point that has a weaker affinity with the stationary phase. A chromatogram from a column set at a relatively low constant temperature of 45°C would likely show a good separation and resolution for the early eluting compounds, but poor for the later ones. Similarly, a column set at a high constant temperature would provide good resolution and separation of later eluting compounds at the expense of the early ones. By ramping up the column temperature throughout a sample run, good separation and resolution can be achieved for all of the analytes.

The separation of components within a sample increases with time and employing a long column facilitates this. Capillary columns are often around 100 m long, whereas packed columns are commonly only up to 6 m long. The separation increases with time spent in the column, as this allows the differences between the partition coefficients of the individual species to become more pronounced. The time it takes for an analyte to migrate through the column can be described by Equation 25, where t_m is the time all components spend in the mobile phase, t_s is the time an analyte has been retained in the stationary phase and t_r is the retention time of that analyte.

$$t_r = t_s + t_m \quad (25)$$

However, increasing time encourages broadening of the peak widths leading to poorer resolution of the individual chemical species. Therefore a balance of flow rate, analysis time and temperature are required to achieve reasonable elution times (2-30 minutes). A longer column allows for a greater number of theoretical plates (Equation 26), and a greater separation of analytes. Theoretical plates are a measure of the peak width broadening that occurs and as a result the column efficiency.

$$N = \frac{L}{H} \quad (26)$$

Here N is the number of theoretical plates, L is the length of the column and H is the plate height. The term 'plates' in a GC column refers to a theoretical version, or an analogy,

of the plates used in a fractional distillation column. The efficiency of a column increases as the number of plates, N , increases and as the plate height, H , decreases. Efficiencies in terms of plate numbers can vary from a few hundred to several hundred thousand; plate heights ranging from a few tenths to one thousandth of a centimeter or less are not uncommon (Skoog et al., 2004).

2.1.2 Mass Spectrometry

The mass spectrometer comprises an ion source, a mass analyser and a detector all of which are operated under high vacuum conditions. The instruments used here were commercially manufactured linear quadrupole mass analysers. The quadrupole is a fused silica tube coated with a thin layer of gold. There are four rods inside that are assembled in line with the tube. Opposing rods are held at opposing potentials created by applying DC and AC voltages to them. As a stable ion enters the quadrupole assembly, periodic forces are exerted on it by the changes in voltage applied to the rods. This results in a resonant ion that is able to traverse the quadrupole assembly without hitting the rods. The voltages of the rods can be tuned to result in a stable trajectory through the quadrupole for specific mass to charge (m/z) ratios, allowing them to pass through and reach the detector (Figure 2.1).

Electron ionisation (EI) is a direct process of energy transfer, where high energy electrons (70 eV) collide with sample molecules. EI is known as a 'hard ionisation' technique as the bombardment of electrons leads to a large degree of observed ion fragmentation (Gross, 2011). The electron beam is produced by a filament (rhenium or tungsten wire) and steered across the source chamber to the electron trap. The source is designed to increase the incident of analyte and electron beam interactions. There are no actual collisions between analyte molecules and electrons; ionisation is caused by electron ejection from the analyte or by analyte decomposition. This primarily produce positive ions through the process of absorption, leading to the formation of a molecular ion M^+ by loss of an electron (Equation 27). The ionization process can either produce the M^+ which will have the same molecular weight and elemental composition of the starting analyte, or it

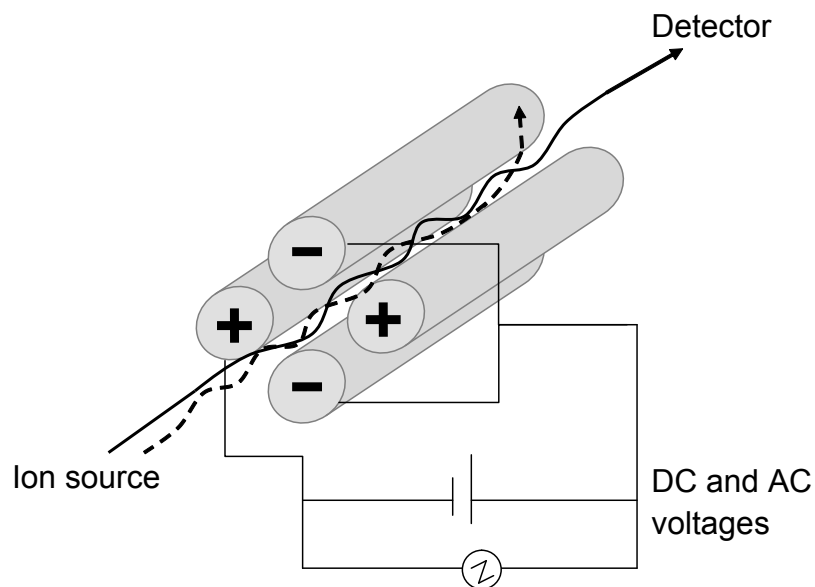
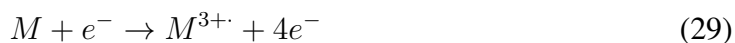


Figure 2.1: Schematic illustrating the pathway through the quadrupole of a resonant ion (solid line) and a non-resonant ion (dashed line) from the ion source to the detector. Adapted from Worton (2005).

can produce a fragment ion which corresponds to a smaller piece of the analyte molecule. The fragmentation of the molecules on ionisation occurs in ways that are predictable as they are structurally specific to the particular analyte (Technologies, 1999).



Depending on the analyte and the electron energy, doubly charged and even triply charged ions may be observed (Equations 28 and 29):



It is this large degree of fragmentation in EI that allows identification of a wide range of compounds. EI mode of operation is less sensitive for compounds such as bromoform (CHBr_3) which have more complex fragmentation patterns, and highly sensitive to compounds with simpler fragmentation patterns such as methyl chloride (CH_3Cl). The

fragmentation process is influenced by the species primary structure, electron energy and ion source temperature. An analyte of low- or medium-polarity is well suited to EI.

Negative chemical ionisation (NI) is a 'softer' mode of ionisation which requires the analyser voltage polarities to be reversed to select negative ions. There are several chemical mechanisms for NI; *electron capture*, *dissociative electron capture*, *ion pair formation* and *ion-molecule reactions*. The method for negative ion requires, in addition to the sample and carrier gas, a reagent gas which is introduced into the ionisation chamber. A common reagent gas is methane (CH_4). The CH_4 is introduced in much larger quantities than the sample gas. Since there is much more CH_4 than sample, most of the emitted electrons react with the reagent gas molecules forming reagent ions (Equation 30). There are of course collisions between the electrons and sample molecules, resulting in sample ions.



The thermal electrons produced in the above reaction have lower energies than the electrons straight from the source filament. It is the thermal electrons which react with the sample molecules. There are no negative reagent gas ions formed in this process; this minimises the level of background noise compared to electron ionisation and so lowers the detection limits in NI. However, sensitivity can drop with prolonged continuous use as the ion source becomes 'clogged' with positive ion fragments. From experience conducting the analysis for this thesis, it was found that the filament of the NI source sagged and became blackened by the inundation of positive fragments. The source chamber itself often appears tarnished and simply cleaning the ion source chamber recovered sensitivity. Obviously the replacement of an NI source filament fully recovers the sensitivity, but it is costly at ≈ 200 per filament.

Electron capture is the primary mechanism of interest in NI. Electron capture provides the high sensitivity for which NI is known: under ideal conditions, electron capture can provide sensitivity as much as 10 to 1000 times that of positive chemical ionisation (Technologies, 1999). Reactions associated with EI will also occur in NI. However, the positive ions formed do not leave the ion source due to the negative polarity. The electron

capture mechanism, described by Equation 31, has the sample molecule 'MX' reacting with a thermal (slow) electron generated by the high energy electron and the reagent gas.

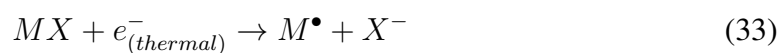


In some instances the $MX^{-\bullet}$ radical anion is not stable, and so the reverse reaction can occur:

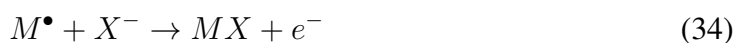


This reverse reaction, often known as the autodetachment reaction, occurs very quickly and so there is little time for the unstable anion to be stabilised through collisions or other reactions. The presence of water, oxygen or other contaminants interfere with the electron-attachment reaction.

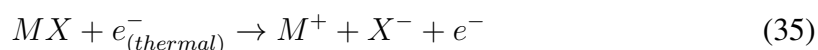
Dissociative electron capture is the dominant mechanism in NI for the species analysed in this thesis, where the sample molecule fragments typically into an anion and a neutral radical (Equation 33). The reaction for dissociative electron capture (Equation 33) does not yield the same sensitivity as electron capture (Equation 31), with the mass spectra generally having lower abundance of the molecular ion.



Sensitivity to one anion and one neutral radical reduces background noise as these are generally the only fragments generated from a particular species. The products with dissociative electron capture are not always stable. The reverse reaction (associative detachment) can sometimes be stable, as described in Equation 34:



Ion pair formation shares similarities with dissociative electron capture, such as the sample molecule fragments. The reaction is shown in Equation 35.



Unlike dissociative electron capture the electron is not captured by the fragments, but the sample molecule fragments in a way that distributes electrons unevenly and positive and negative ions are generated.

The fourth common process to NI is *ion-molecule reactions*. These reactions occur when water, oxygen and other contaminants are present in the ion source. The reactions can be described as:



Here X^{-} is most often a halogen or hydroxyl group created by ionisation of contaminants. Ion-molecule reactions are 2-4 times slower than electron-attachment reactions and do not provide the high sensitivity associated with electron capture reactions (Technologies, 1999). Ion-molecule reactions and electron capture reactions are competing mechanisms of ionisation.

When operating in NI mode the sensitivity to the detection of alkyl nitrates (RONO_2) is vastly improved than that seen in EI on the same system, as there is much less fragmentation. Chlorinated, brominated and iodinated compounds can also be detected in NI mode. The NI process yields halide anions (m/z of 35 and 37 for Cl^{-} , 79 and 81 for Br^{-} and 127 for I^{-}) and the NO_2^{-} fragment ($m/z = 46$).

2.1.3 Sensitivity and detection limits.

The term 'sensitivity' specifies the overall response of an analytical system for a certain analyte when operated under well-defined conditions (Gross, 2011). The sensitivity of an instrumental setup is defined as the slope of a plot of an analyte amount vs. signal strength. As instruments age and equipment undergoes changes in temperature or sustains mechanical stress, performance gradually degrades; this is called drift (Technologies, 1999). Drift cannot be eliminated but it can be detected and quantified through the process of calibration. The GC-MS systems were calibrated against standard reference gases containing known concentrations of analytes to confirm that an instruments were correctly measuring target analytes. Standard reference gases or calibration gases are compared to international standards to provide compatibility of data sets worldwide.

Sensitivity drifts in the data presented were accounted for by linear interpolation of standards and compared with a long-lived compound such as carbon tetrachloride (CCl_4). Data was excluded if the CCl_4 mixing ratios were outside the range 79 - 110 pptv as

it was judged to be a contaminated sample. Calibrations were performed every eight samples using the UEA 2006 Standard reference gas which is calibrated against the 'NOAA 2003' scale for CHBr_3 , CH_2Br_2 and CH_3Br and the 'NOAA 2004' scale for CH_3I (<http://www.esrl.noaa.gov/gmd/ccl/scales.html>).

The terms 'detection limit' or 'limit of detection' (LOD) are often confused with sensitivity: the LOD defines the lowest amount of analyte necessary to obtain a signal that can be distinguished from the background noise. It is common practice to quote the LOD as three times the signal-to-noise ratio, as shown in Figure 2.2, here the signal-to-noise ratio is usually defined as the ratio of the average value of the output signal to its standard deviation. Noise results from the electronics of an instrument, therefore noise is not only

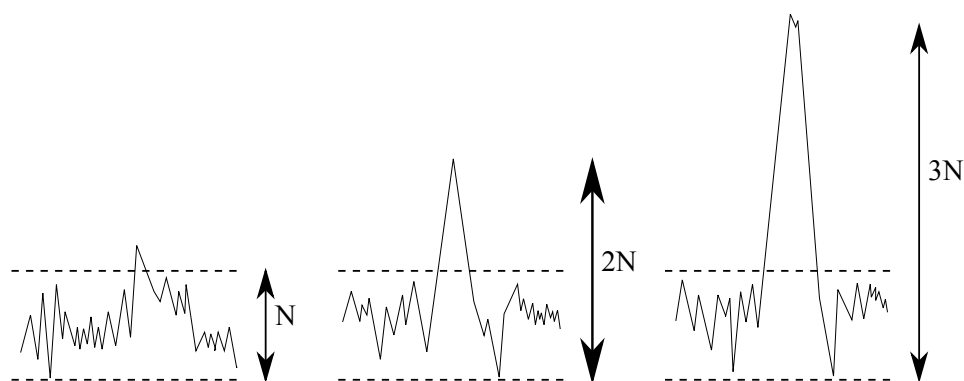


Figure 2.2: Signal-to-noise levels for determining limit of detection. Where 'N' is noise.

present between the signals, but also on the signals. Noise can also be caused by GC column bleed and impurities, appearing in the same way as electrical noise. Signal-to-noise ratios are excellent in NI as the source is negatively charged and so it repels the more abundant positive fragments.

Table 2.1 shows a range of estimated LODs for NI and EI. The compounds shown represent different elution times. LODs were determined based on the aforementioned principle where signal amplitude is three times that of the background noise.

Table 2.1: Determined signal-to-noise estimations of detection limits (ppt) are shown.

Species	NI	EI
Methyl chloride	190	40
Chloroform	0.9	2
Bromoform	0.02	0.04
Methyl iodide	0.06	0.3
2-propyl nitrate	0.04	0.5

2.1.4 OP3 analytical setup

GC-MS analysis during both OP3 campaigns was conducted using an Agilent 6890 GC and the MS5973 N mass spectrometer. All samples were analysed using electron ionisation and negative ion as described above. The GC-MS was coupled to a Markes International UNITY and Online Air Server with a Carbograph B and Carboxen 1000 trap. A pre-purge period of 6 minutes was implemented prior to every sample to clear the system of the previous sample. The trap was also purged prior to each sample for 2 minutes. The trap is held at -10°C for 10 minutes before the trap is rapidly heated to 300°C to desorb all analytes from the trap and the sample injected onto the column via a heated transfer line (150°C). The 502.2 Restek capillary column was used to separate the OP3 sample components. The column is 105 m long and $0.32\ \mu\text{m}$ diameter, with a $1.8\ \mu\text{m}$ film of cross bonded phenyl methyl polysiloxane (5% phenyl) stationary phase chemically bonded to the inside of the silica column. This column is designed by Restek to have excellent separation of trihalomethanes, with the stationary phase having ideal polarity to shift and retain species with lower boiling points, but not too polar that the large polar compounds never come off the column. The length of the column negates any need for cryo-cooling of the sample whilst maintaining the separation of boiling points specific to the analytes of interest.

The GC-MS instrument at Bukit Atur was operated in NI mode, with the ion source being replaced every two weeks of sampling to restrict drift in the mass spectrometer detector. The GC-MS instrument at Kota Kinabalu, for analysis of the aircraft samples, was run in EI to ensure organohalogenes were captured well. Calibration gases were used

to check that the GC-MS systems were accurately measuring target compounds.

The standard gas used at Bukit Atur was from a running standard filled from outside the laboratory into a canister and then cross calibrated against a UEA standard calibrated to the NOAA scale for the organohalogenes and an intercomparison from the International Transport of Ozone and Precursors project (ITOP-UK) providing calibration values for the alkyl nitrates (Worton et al., 2008). The canister air was used to provide a calibration of similar humidity to the sample. At the Kota Kinabalu International Airport (KKIA) site another UEA standard gas calibrated as part of the ITOP comparison was used. The EI and NI data sets were compared by conducting analysis in both modes of the final three flights of aircraft bottle samples. The data sets showed agreement that was good enough to assume that the differences observed in the data are real and not the result of instrumental error. The EI and NI data sets showed agreement of $\pm 7\%$ for CCl_4 .

2.1.5 JIC analytical setup

The JIC samples were analysed for methyl halides and a range of other organohalogenes on a fully automated GC-MS in select ion monitoring electron ionisation mode. A 250 ml sample from each sample flask was processed using the Entech 7100 pre-concentrator system (Entech Instruments Inc.). The sample went through three trapping phases before injection onto the GC column. Firstly, the sample was taken onto a stainless steel trap packed with glass beads and held at $-150\text{ }^\circ\text{C}$ this step removes the water content of the sample. The second trapping phase facilitates the removal of CO_2 from the sample using a stainless steel trap packed with Tenax and held at $-40\text{ }^\circ\text{C}$. The final trapping stage involves cryo-focusing the sample on silica lined stainless steel tubing. The sample is then injected into the GC. The GC column used was a DB-5 capillary column (J&W Scientific) with the dimensions 105 m long, 0.32 mm inner diameter and $1.5\text{ }\mu\text{m}$ film thickness of non-polar phenyl methyl polysiloxane (5% phenyl) stationary phase. This column is suitable for analyses such as the JIC work where not all the analyte components are known. Helium was used as the carrier gas to push the sample through the system.

2.2 Sampling techniques

2.2.1 OP3 project ground based site, Bukit Atur

The GC-MS systems were assembled in situ, firstly at the Global Atmospheric Watch (GAW) site of Bukit Atur the Danum Valley conservation area (4.98°N, 117.8°E) and the second instrument at Kota Kinabalu International Airport (KKIA) (5.93°N, 116.1°E) as shown in Figure 2.3. The work was part of the Oxidant and Particle Photochemical Processes (OP3) project, April-July 2008, there were two four-week ground based measurement campaigns in the rainforest of Sabah, Borneo and an aircraft detachment concordant with the July ground measurement period.

The ground measurements were based at the GAW site of Bukit Atur (Figure 2.4), with two campaigns in April 2008 (OP3 phase 1, OP3-I) and in July of the same year (OP3 phase 3, OP3-III). Figure 2.4 shows the laboratory at Bukit Atur sits in a slight clearing in the forest. The laboratory and the 100 m GAW tower sit atop a 426 m hill. The site is situated in primary rainforest (forest which has not been felled), close to secondary rainforest (felled once, natural regrowth) and within 50 km at the north extensive mature oil palm plantations.

1 litre samples were taken hourly down a 3/8 inch perfluoroalkoxy (PFA) sample line secured at 30 m up the GAW tower. The inlet consisted of a PFA funnel surrounding the end of the PFA sample line. The inlet was orientated facing downwards to reduce exposure. The sample line ran for approximately 80 m from the GAW tower to the laboratory. A pump was fitted to the sample line ensuring that a sample flow rate of 25 ml/min could be maintained. The sample line was flushed prior to the 40 minute sampling period. The sample line ran through a Nafion contra-flow drier outside the laboratory. This measure limited the condensation of the humid tropical air in sample line when it entered the air conditioned laboratory. A second Nafion contra-flow drier was assembled in the sample line inside the laboratory to reduce the risk of water vapour getting onto the GC-MS system.

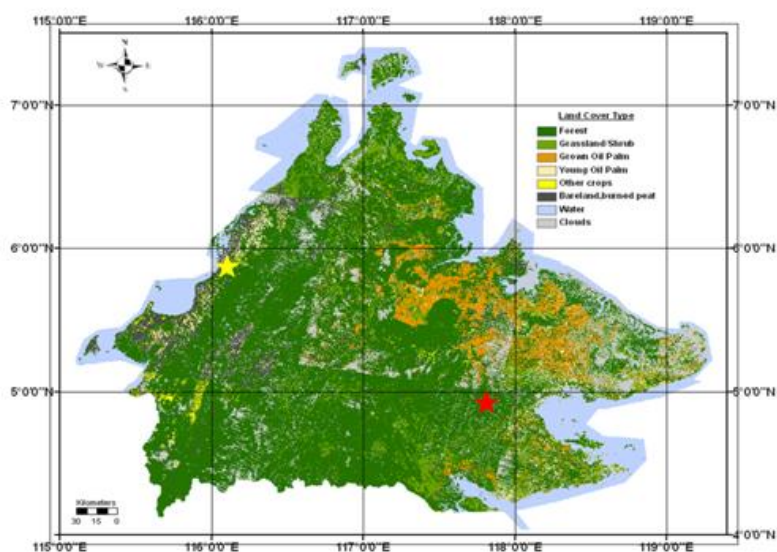


Figure 2.3: Land cover map of Sabah, Borneo. The sites of the UEA GC-MS systems are marked with stars, yellow for the KKIA site (5.93°N, 116.1°E) and red for the Bukit Atur site (4.98°N, 117.8°E). The colours represent different land cover types: Forest (dark green), grassland/shrubs (light green), grown oil palm (orange), young oil palm (beige), other crops (yellow), bareland or burned peat (black), water (blue) and clouds (grey) (Hewitt et al., 2010).



Figure 2.4: The GAW tower, and laboratory at the Bukit Atur site.

2.2.2 OP3 aircraft campaign

During the OP3-III the Facility for Airborne Atmospheric Measurement (FAAM) BAe-146 research aircraft was deployed from Kota Kinabalu International Airport. The FAAM is a collaboration between the Met Office and the Natural Environment Research Council (NERC) and is an established asset of the National Centre for Atmospheric Sciences (NCAS). The aircraft is a modified BAe-146 atmospheric research aircraft owned by BAe Systems and operated for them by Directflight (Figure 2.5).

The BAe-146 was deployed during the July phase of OP3, operating two flights per active day for two consecutive days, before a break on the third day and then resuming flights for a further two days. Whole Air Samples (WAS) were taken using the WAS system fitted to the BAe-146; it consists of 64 silica steel 3 litre cannisters. The cannisters, in packs of eight, nine and fifteen, are fitted to the hold of the aircraft and connected to a bellows pump that draws air from the main sampling manifold (Hopkins et al., 2006). The cannisters were pressurised to a maximum pressure of 47 psi (giving a useable volume of about 9 litres).

There were nine days of flying for OP3 and one day for the NERC Cascade project, whole air samples were also taken on this flight and the measurements included in this thesis as flight B390. Samples were mostly taken at pre-determined locations according to the particular flight plan, with some flexibility for in-flight decisions to take samples at points of interest, determined by the real-time instruments on board. Figure 2.6 shows the spatial distribution of all the whole air samples presented in this thesis. Flight plans for OP3 involved a range of altitude profiles over the landmass and seas of Sabah, focusing on profiles around the Bukit Atur site where the ground measurements for OP3 were taking place.

The WAS samples were analysed in electron ionisation mode on a duplicate of the GC-MS setup for the ground based measurements. The GC-MS system assembled at Kota Kinabalu international airport. The cannister packs were connected to the sampling port of the Unity sampling system on the GC-MS and litre samples were taken.



Figure 2.5: The BAe-146 aircraft being flown during the OP3 campaign, photographed by Martin Irwin from 15 m on the GAW tower, Bukit Atur.

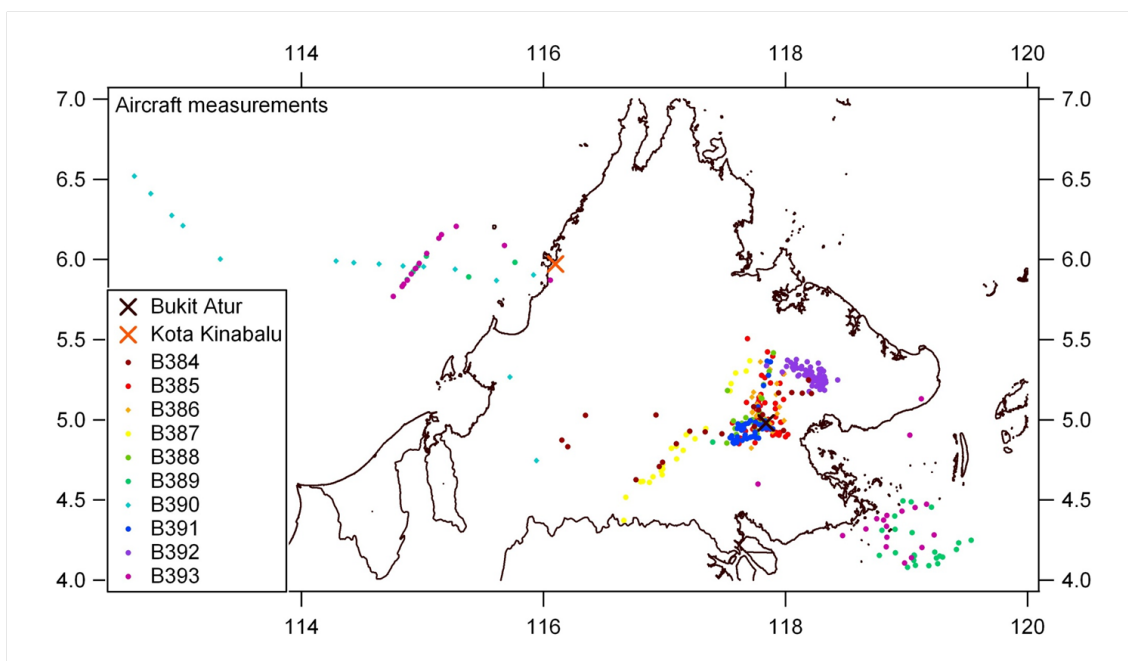


Figure 2.6: All whole air sample measurement points coloured by flight (n=377).

2.2.3 Methyl halide plant emission experiments, John Innes Centre

The work conducted with the crop genetics laboratory at the John Innes Centre (JIC) utilised plant enclosure experiments. Teflon bags were made from Teflon sheet to known volumes. A variety of bag sizes were made depending on the particular experiment ranging from 1.5 litres to 115 litres. In each experiment the Teflon bags were sealed to plant pots, either those the plants were grown in, or for the field experiment the tubing was embedded in the ground around the plants to which the Teflon bags were sealed. Electrical tape, elastic bands and cable ties were used on the outside of the bags to provide an adequate seal. The plants were germinated in agar and grown in grow rooms at the JIC.

The Teflon bags that enclosed the plants had teflon valves fitted to them; this was the port for extracting the sample. Samples were taken into evacuated 1 litre SilcoCans. For the initial experiments conducted with the JIC (Chapter 5, Section 5.2) sampling took place by connecting a piece of Teflon tubing from the valve on the bag to the SilcoCan. Both the valve on the bag and the valve on the cannister were then opened and the negative pressure within the cannister drew in approximately 1 litre of air from the plant's headspace in the bag. This method of sampling was appropriate to these experiments which used the small Teflon bags (1.5 litres). For the larger plants where bigger bags had to be used a battery pump was used to extract the sample from the headspace in the bag. These cannisters were filled to a pressure of 10 psi.

Chapter 3

The atmospheric composition of organohalogens over Borneo

3.1 Introduction

As part of the oxidant and particle photochemical processes project (OP3) campaigns in Sabah, Borneo, organohalogens were measured at the rainforest GAW site of Bukit Atur and from whole air samples (WAS) taken onboard the BAe 146 research aircraft. The suite of organohalogens measured during the OP3 project comprised the methyl halides (CH_3Cl , CH_3Br and CH_3I), bromoform (CHBr_3), dibromomethane (CH_2Br_2), bromochloromethane (CH_2BrCl), dibromochloromethane (CHBr_2Cl), dichlorobromomethane (CHCl_2Br), methylchloroform (CH_3CCl_3) and chloroform (CHCl_3). Ground measurement data collected at the remote rainforest location of Bukit Atur in Danum Valley, Borneo shows the changes observed in the mixing ratios of these organohalogens over time, from April to July 2008. This ground data combined with aircraft measurements taken in July 2008 helps to explore the influence of changing air masses, local mixing, sources and sinks in order to explain the variations observed in the mixing ratios of the organohalogens.

Methyl halides are ozone depleting compounds. Naturally emitted CH_3Cl is currently estimated to account for 16% of chlorine in the troposphere and over half of bromine

in the stratosphere is from natural sources of methyl bromide and other bromocarbons (Montzka et al., 2010). The atmospheric budget of methyl halides is currently unbalanced, with the known sinks outweighing the known sources (Montzka and Fraser, 2003). From current understanding of the sources it has been suggested that terrestrial vegetation may contribute to the 'missing' fraction of the methyl halide budget and research has started to focus on terrestrial plants that emit methyl halides (Blei et al., 2010; Gan et al., 1998; Redeker et al., 2000; Rhew, 2001; Saito et al., 2008; Sive et al., 2007). Tropical vegetation, in particular, has been shown to emit the methyl halides (Lee-Taylor and Redeker, 2005; Yokouchi et al., 2002, 2007). The polybrominated organohalogenes CHBr_3 and CH_2Br_2 are reported to be predominantly of oceanic origin, with macroalgae reported to be responsible for their production (Carpenter et al., 2000; Manley et al., 1992; Sturges and Buckley, 1992). Carpenter and Liss (2000) estimate that 70% of the world's CHBr_3 is produced by macroalgae. Bromoform is known to be a major constituent of seaweeds; 80% of the weight of the edible seaweed 'limu kohu' (*Asparagopsis taxiformis*), which is farmed in tropical waters, is comprised of CHBr_3 (Gribble, 1999).

The purpose of organohalogen production by marine organisms is not yet fully understood. However, some explanation has been offered suggesting that they metabolise halogens for chemical defence (Ohsawa et al., 2001). The prevention of larval settlement, barnacle fouling, and bacterial overgrowth are essential for the survival of marine organisms. The red algae *Corallina pilulifera* is known to 'generate' CHBr_3 to eliminate surface microalgae (Ohsawa et al., 2001).

Although CH_2Br_2 has not been as well characterised as CHBr_3 a good correlation in the emission of the two compounds is often observed in the atmosphere (Butler et al., 2007; Quack et al., 2007; Yokouchi et al., 2005; Zhou et al., 2008).

Measured concentrations of CHBr_3 and dibromomethane will vary with proximity to localised sources. Typical values in the tropical boundary layer are estimated to be 1-2 ppt of CHBr_3 and 1-1.4 ppt of CH_2Br_2 (Quack and Wallace, 2003; Quack et al., 2007). These concentrations will rapidly decrease once in the stratosphere due to photolysis. The marine source of polybromomethanes to the atmosphere is estimated to account for 15%

of stratospheric inorganic bromine which affects the ozone chemistry in the stratosphere (WMO, 2007).

The lifetime of dibromomethane is 69 days (Ko et al., 2003). The lifetime of dichloromethane is 77 days (Ko et al., 2003). The lifetimes of these compounds are so similar that it has been assumed that their seasonality is the same (Worton et al., 2006). The bromocarbons have both OH and photolysis sinks which result in their concentrations in summer conditions being at their lowest. Worton et al. (2006) found that dibromomethane in firm air could be entirely accounted for by natural sources, whereas the other trihalomethanes they studied showed evidence for increases in their atmospheric burdens over the 20th century.

Although the sources of tropospheric inorganic bromine are still poorly understood, organohalogens including CHBr_3 and CH_2Br_2 are known to contribute to the atmospheric bromine budget (von Glasow and Cruzten, 2004). The lifetimes of CHBr_3 and CH_2Br_2 , assuming atmospheric losses via photolysis only, are 36 and 5000 days, respectively, whereas losses via reaction with OH are 100 days and 120 days, respectively (WMO, 2003). Dibromomethane has an average overall atmospheric lifetime of 120 days, whereas CHBr_3 has an average overall atmospheric lifetime of 26 days calculated using both the loss via photolysis and reaction with OH (WMO, 2003).

Currently there is a deficit in the stratospheric organic bromine budget of 3-5 pptv. It is assumed that very short lived substances (VSLS) contribute to this as they are not currently involved in the model simulations, but when they are in the models can recreate the stratospheric organic bromine levels. VSLS are defined by the WMO as trace gases whose lifetimes are comparable to, or shorter than, tropospheric transport timescales, and have non-uniform abundances.

Maximum emissions of natural polybromomethanes are likely to occur near coastlines where macroalgae grow, along with upwelling regions where high densities of chlorophyll can be found (Moore et al., 1996; von Glasow and Cruzten, 2004). Quack and Wallace (2003) discussed the disproportionate emission of organohalogens with regard to the source region; they estimated that 23 % of the sea-to-air flux of CHBr_3 is from coastal

regions (constituting 0.3 % of the ocean surface) whereas the open ocean, representing 88 % of the ocean surface, accounts for only 29 % of the flux. The remaining 48 % is attributed to the continental shelf flux.

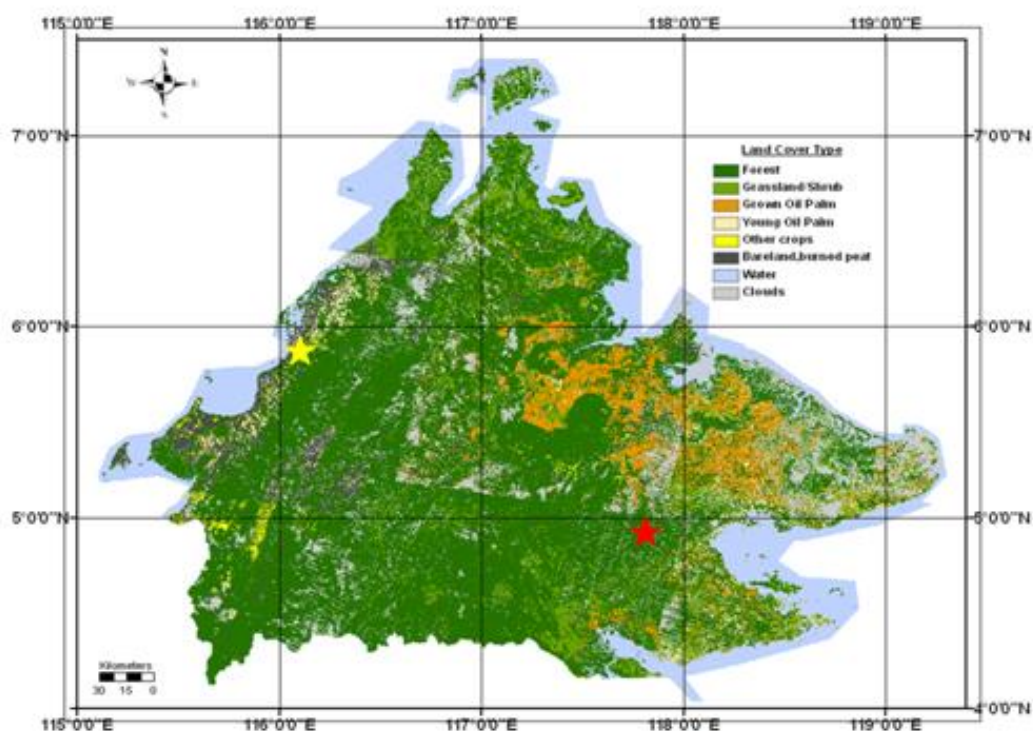
Polybromomethanes such as CHBr_3 and CH_2Br_2 emitted by macroalgae are removed from the atmosphere through photolytic degradation and by reaction with the hydroxyl radical (OH) forming inorganic bromine.

After CH_3Cl , chloroform (CHCl_3) is the second most abundant organic source of natural chlorine to the atmosphere (Montzka et al., 2010). CHCl_3 has sources that are both anthropogenic and natural including the oceans and terrestrial areas. Laturnus et al. (2002) estimated the emissions from anthropogenic sources to account for less than 10% of the estimated total emissions from all sources. The calculated annual biogenic global chloroform emission is 700 Gg, and marine and terrestrial environments are nearly equal contributors (Laturnus et al., 2002). Worton et al. (2006) concludes that anthropogenic sources are responsible for as much as $\approx 50\%$ of the atmospheric CHCl_3 budget. Aucott et al. (1999) breaks down the anthropogenic sources, suggesting that 51% of the 1990 anthropogenic CHCl_3 emissions originated from the manufacture of pulp and paper (34 Gg yr⁻¹), 32% from the chlorination of drinking waters and the chlorination of cooling waters used in power plants (21 Gg yr⁻¹) and 17% from other industrial uses (11 Gg yr⁻¹).

Methyl chloroform (CH_3CCl_3) emissions are predominantly industrial and have declined significantly since the early 1990's. This is because the production of CH_3CCl_3 is now tightly controlled. The result is that stocks of CH_3CCl_3 are thought to be negligible, though some emissions are likely to arise from CH_3CCl_3 use as a feedstock in the production of HCFC-141b and HCFC-142b (Montzka et al., 2010). Biomass burning was thought to play a part in CH_3CCl_3 non-industrial emissions, however, a recent study has reported negligible CH_3CCl_3 in biomass burning (Simpson et al., 2007).

Atmospheric loss processes of CH_3CCl_3 are dominated by oxidation by the hydroxyl radical. Other processes such as photolysis and oceanic removal are substantial sinks for CH_3CCl_3 (Yvon-Lewis and Saltzman, 2009).

3.2 Spatial characterisation of Sabah



Land Cover Type

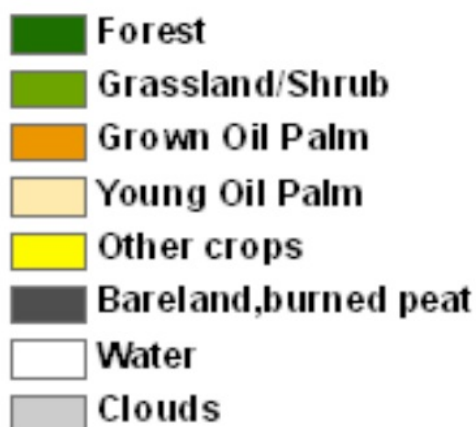


Figure 3.1: Map of Sabah, Borneo, showing land cover data (Hewitt et al., 2009). The colours represent different land cover types as shown in the legend (enlarged). The Bukit Atur ground measurement site (red star) and Kota Kinabalu (yellow star).

The land cover of Sabah is mapped in Figure 3.1, showing the areas oil palm to cover a large area north of the ground measurement site, with the majority of the rest of Sabah currently remaining as rainforest. The aircraft data were split into four categories of landscape: northwest coast, oil palm, rainforest and the southeast coast. The coastal categories were defined by the latitude and longitude that the aircraft measurements were taken (northwest coastal measurements $<116^{\circ}\text{E}$ and $>5.5^{\circ}\text{N}$; southeastern coastal measurements $>118.6^{\circ}\text{E}$ and $<5^{\circ}\text{N}$). The aircraft measurements taken over the landmass of Sabah were categorised as oil palm using a time mask based on the isoprene aircraft data. Isoprene measurements from OP3 found isoprene mixing ratios to be 5 times higher in the oil palm landscapes than those of the rainforest (Hewitt et al., 2009). Isoprene mixing ratios over the rainforest were 1-3 ppbv, whereas, over the oil palm plantations mixing ratios of 5-10 ppbv were observed. When mixing ratios in the latter range were observed the time mask dictates that the aircraft was flying over oil palm landscapes. Using this time mask to ascertain when WAS samples were taken over oil palm landscapes, the remaining aircraft WAS taken over the landmass of Sabah were designated as being representative of a rainforest landscape.

3.3 Wind directions during the OP3 campaigns.

Wind data were collected during OP3 using a Meteorological sensor Vaisala WXT (Hewitt et al., 2010) at 75 m on the GAW tower at Bukit Atur (Chapter 2 Figure 2.4). The wind rose plots in Figure 3.2 show a spread of wind directions during OP3-I, whereas a dominance of southerly sectors during OP3-III. Wind speeds during both campaigns were generally low, at around $\leq 4 \text{ ms}^{-1}$, with some instances of $\geq 6 \text{ ms}^{-1}$: these instances were usually associated with storms.

3.4 Back trajectories for OP3

Five-day back trajectories were run through the British Atmospheric Data Centre (BADC) using the European Centre for Medium-range Weather Forecasting (ECMWF) model.

The trajectories were run for arrival pressure altitude 950 hPa (600 m). As previously stated in Chapter 2, the GAW tower stands 100 m tall at Bukit Atur, which is 426 m above sea level and the UEA GC-MS inlet was located 30 m up the GAW tower. Trajectories were calculated for different arrival times, but no trends were observed for different times of day. Clusters of trajectories were also runs covering arrivals in a slightly broader area ($\pm 0.5^\circ$ of Bukit Atur): this analysis produced trajectories following essentially the same paths. As these variables did not strongly influence the path of the back trajectories single trajectories arriving at Bukit Atur, at 2pm local time, are presented below. It should be noted that the precision and accuracy of the models which derive the back trajectories of air masses are unable to resolve the topographical and meteorological detail of Borneo. The valleys and rapid deep convective systems that characterise these regions environment are not included in the ECMWF model as it operates at a $1.125^\circ \times 1.125^\circ$ resolution (BADC, 2006).

3.4.1 OP3-I

The back trajectories show the air coming to Bukit Atur between the 17th and the 21st April to be predominantly of coastal origin, approaching from low altitudes in the east (Figure 3.3). Air continues to come from the eastern coast of Sabah until the 25th April when the air arrives from the northwest (Figure 3.4). The trajectories for the 13th to the 25th are all low altitudes <1100 m.

The trajectories change direction on the 26th of April when the air starts coming across the land mass of Borneo from the west. The altitude of the trajectory arriving on the 26th increases to a maximum altitude of ≈ 1700 m approximately 48 hours prior to arrival at Bukit Atur, then its altitude drops to <800 m until arrival. The trajectory of the 27th follows a similar pattern, but the altitude decreases approximately 96 hours prior to arrival (Figure 3.4).

The trajectory for the 28th April (Figure 3.4) arrives from the western coast in the area of the capital, Kota Kinabalu, and then the air appears to change direction for a slow approach over the north of Sabah before going further inland to Bukit Atur. The

back trajectory for air arriving at Bukit Atur on the 29th April took a path from the north of Sabah, crossing over Sabah to the sea off the south east coast of Bukit Atur, before spending the final days approach over land to the site. The back trajectory for the air that arrived on the 30th April suggests that it spent the previous 5 days over the land to the north of Bukit Atur. The trajectories for the 1st to the 3th May show air paths predominantly over the landmass of Borneo (Figure 3.4). The trajectory altitudes from the 28th April to the 2nd May remain within a range of 600 - 1200 m (Figure 3.4). The trajectory arriving on the 3rd May starts (120 hours) around 2000 m dropping steadily to around 1000 m 72 hours prior to arrival and remaining around this level until arrival (Figure 3.4).

3.4.2 OP3-III

During OP3 phase III the air masses arrive predominantly from the east and south east of Bukit Atur. The back trajectories for the 5th and 6th of July show air arriving from the west of the site having crossed the landmass of Borneo from the west coast (Figure 3.5): the variable altitudes of these trajectories possibly reflecting the terrain.

From the 7th to the 11th July the air approaches the site from the south to southeast (Figure 3.5). The air arriving at the site on the 7th originated 5 days before from the southern Indonesian province of Kalimantan. When over the land in Kalimantan the altitude of the trajectory elevated from 800 m to 1800 m for a brief period before dropping back to around 400m when the air passed over the sea and remained at low altitudes until arriving at Bukit Atur. The back trajectories arriving between the 6th and the 10th showed low altitude (<1000 m) pathways over the Celebes sea, approaching Bukit Atur from the southeast.

The back trajectory for the 15th July shows a pathway mainly over the Celebes sea to the southeast of Bukit Atur. The trajectory spends time at an altitude of around 1200 m 120 to 72 hours prior to arrival, then the air drops to a altitude of <800 m for the approach to Bukit Atur (Figure 3.3). The pathway for the 16th July changes back to an approach up the east coastline of Borneo. Air arriving at the site on the 17th July follows a similar

pathway to the 16th up the coastline of Borneo, but the air traveled faster beginning its 5 day approach over the southern tip of the island of Celebes. The back trajectories for the 18th and 19th take pathways from the north coast of the island of Celebes, across the Celebes sea to approach Bukit Atur from the east (Figure 3.6). The pathway for air arriving on the 20th July is from the east, approaching over the Semporna peninsula of Sabah to Bukit Atur. The back trajectory for the 21st July spends two and a half days over the sea off the north coast of Sabah, before approaching Bukit Atur from the north. The back trajectories change direction again on the 22nd July when the pathway of air shows an entirely terrestrial 5-day approach from the south over Borneo (Figure 3.3). The trajectories of the 16th to the 22nd July are consistently low altitude pathways of <800 m.

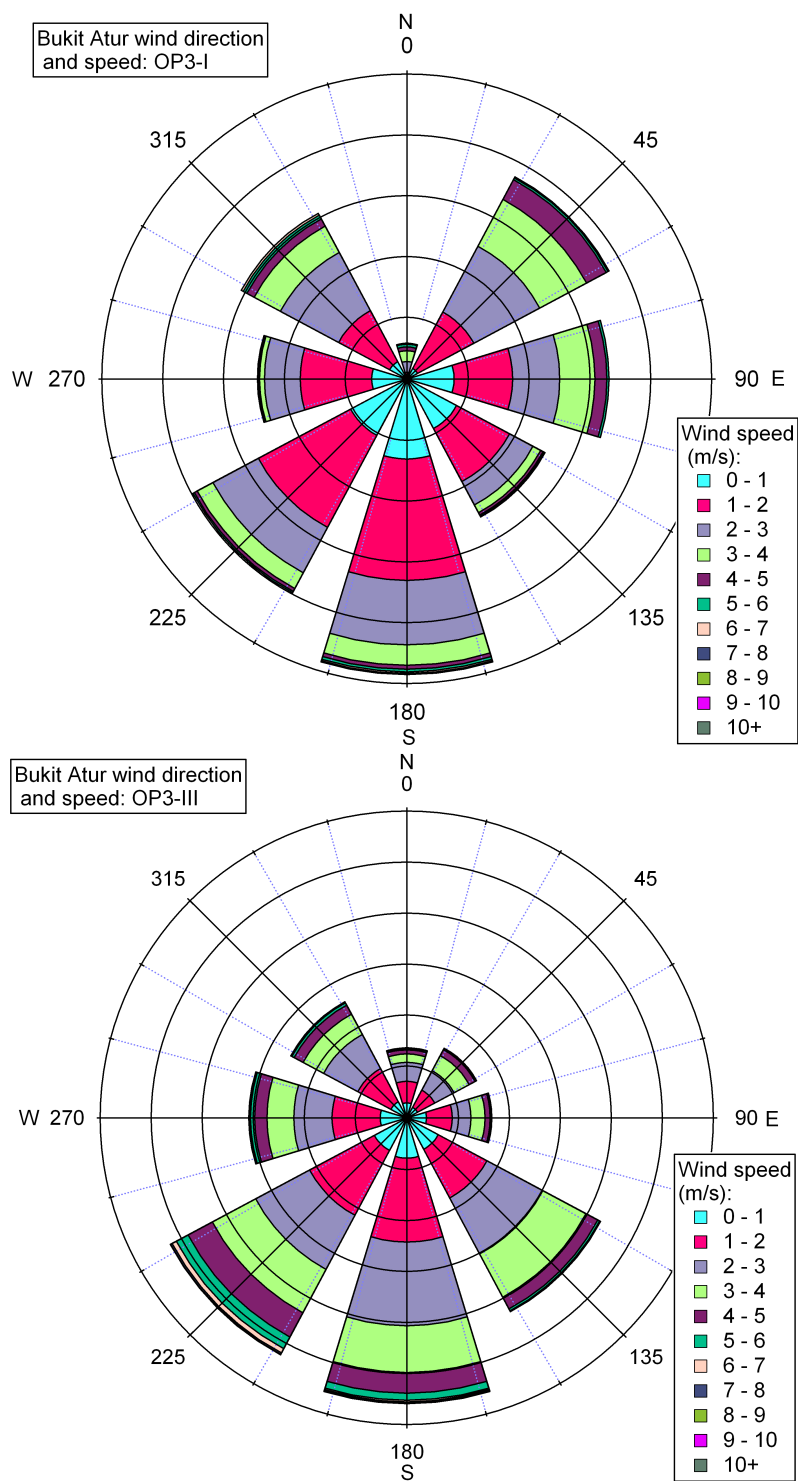


Figure 3.2: Wind rose plots for OP3-I and OP3-III. The first black circle from the centre of the plot represents a 2% of the data, then the following circles represent 4%, 6%, 8%, 10% and 12%.

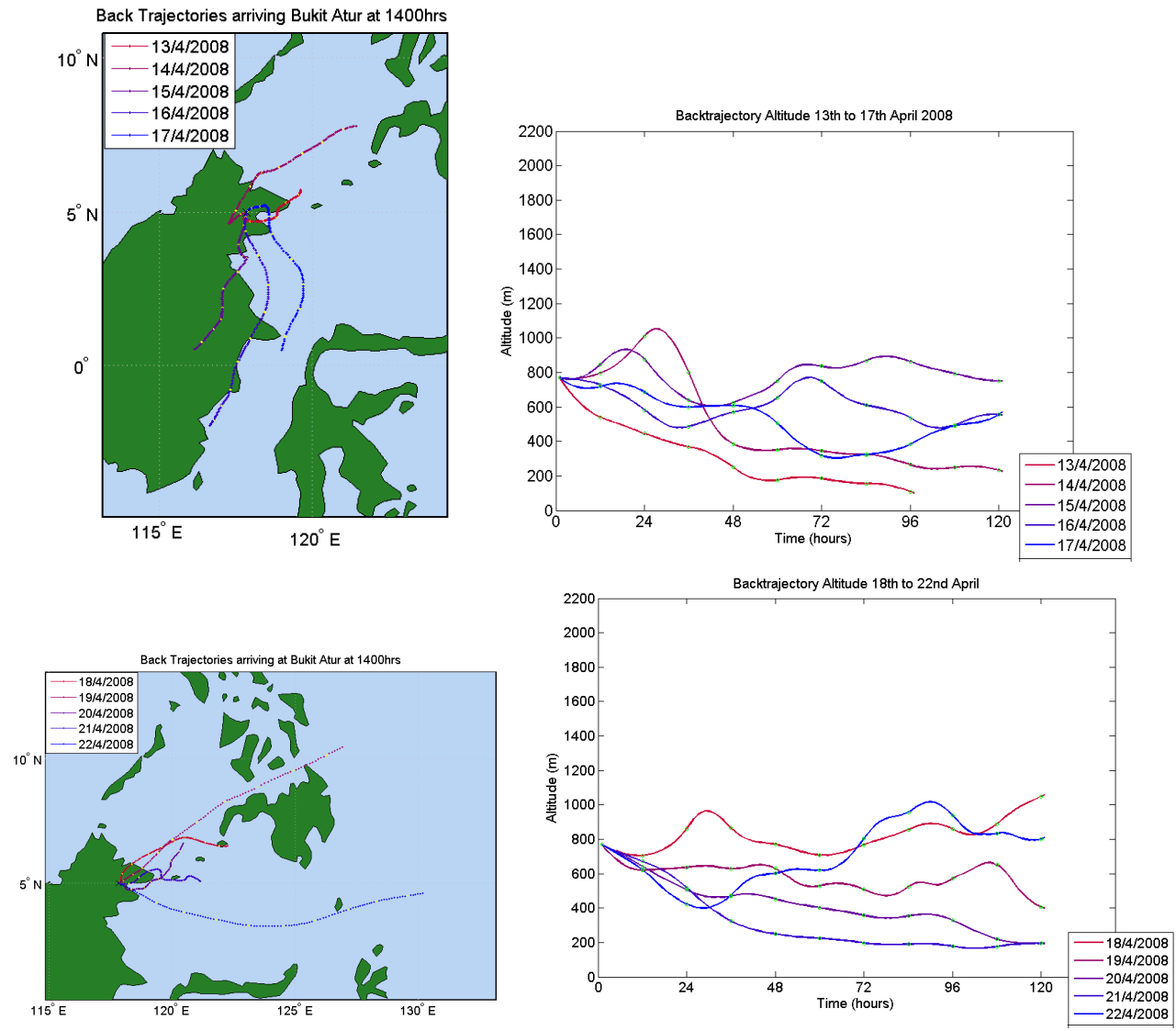


Figure 3.3: Back trajectories for the 13th-22nd April, OP3-I. Yellow/green markers indicate 12 hour periods.

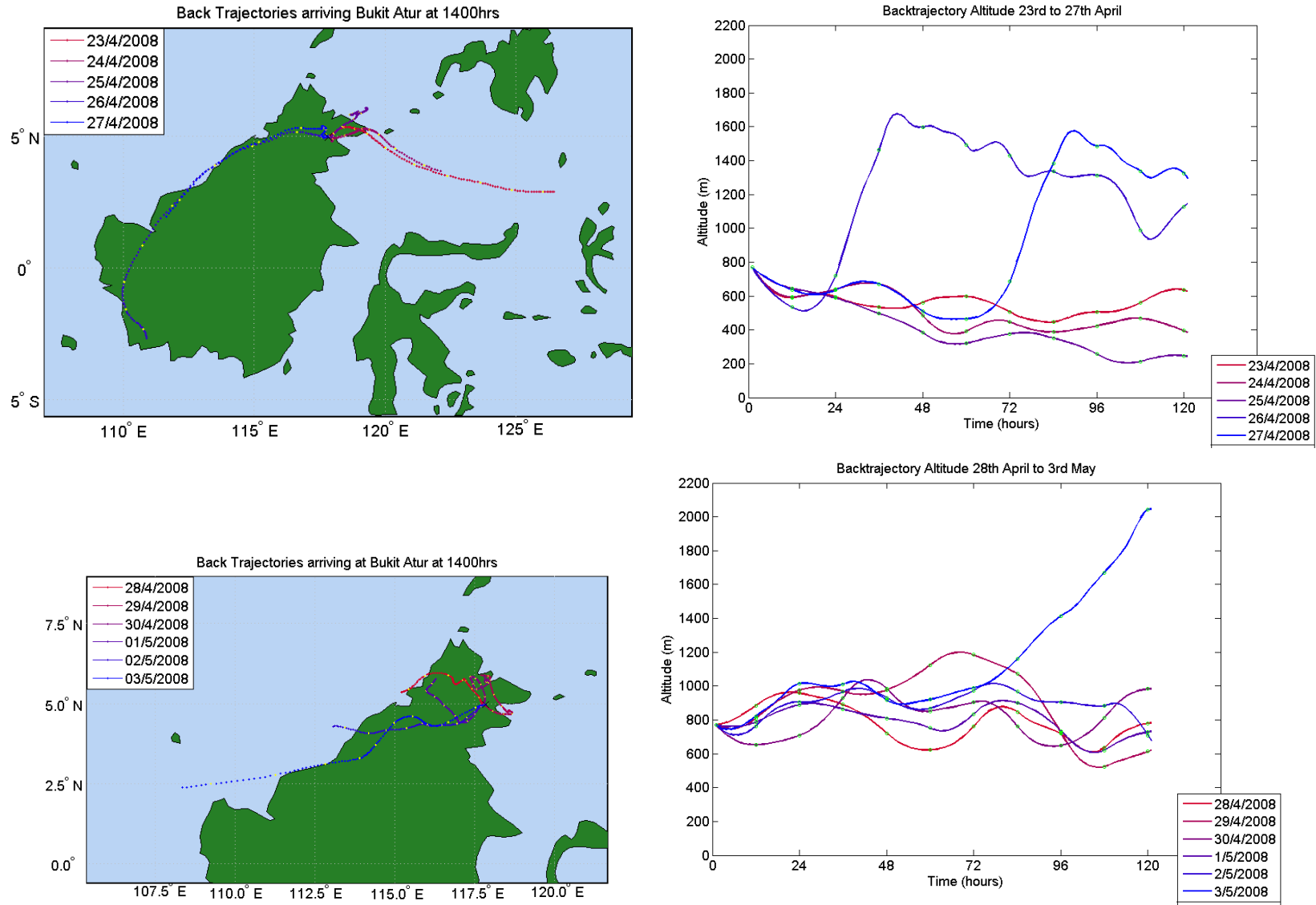


Figure 3.4: Back trajectories for the 23rd April - 3rd May, OP3-I. Yellow/green markers indicate 12 hour periods.

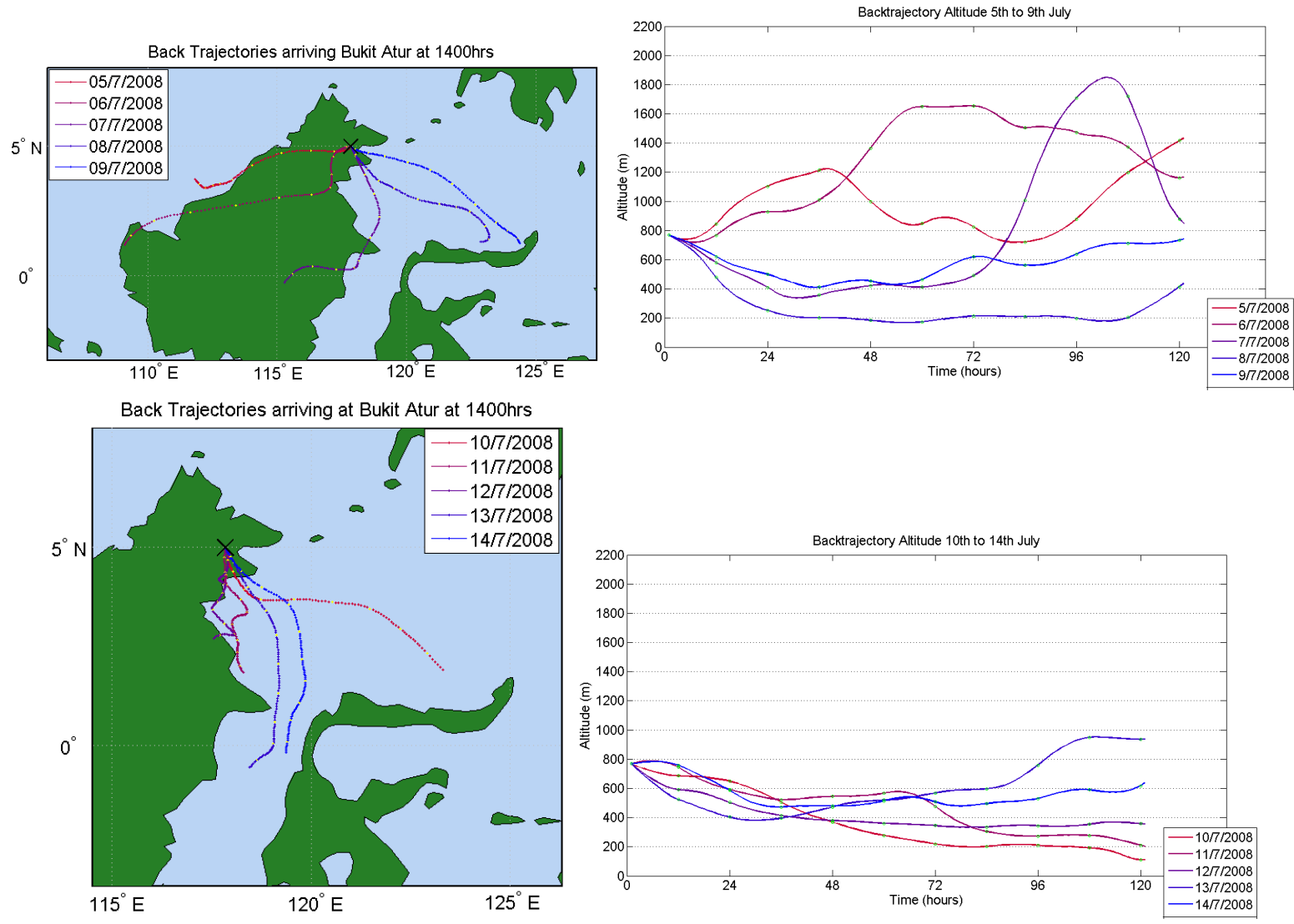
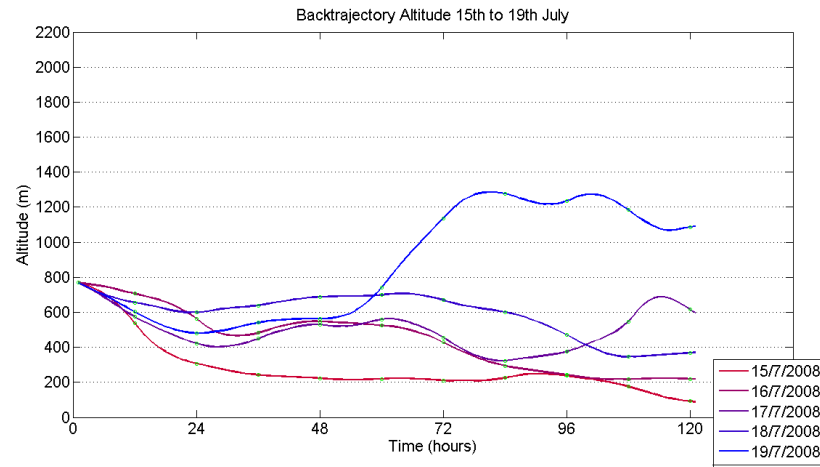
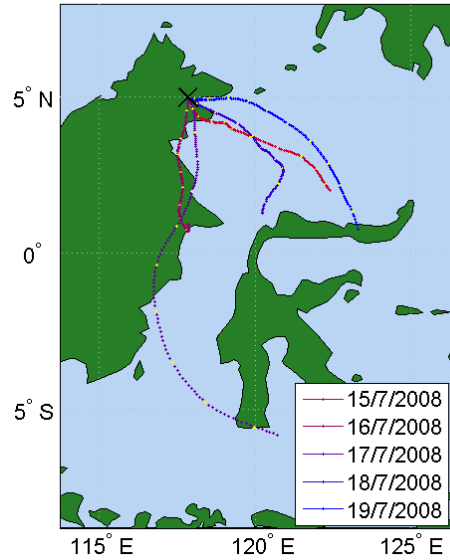
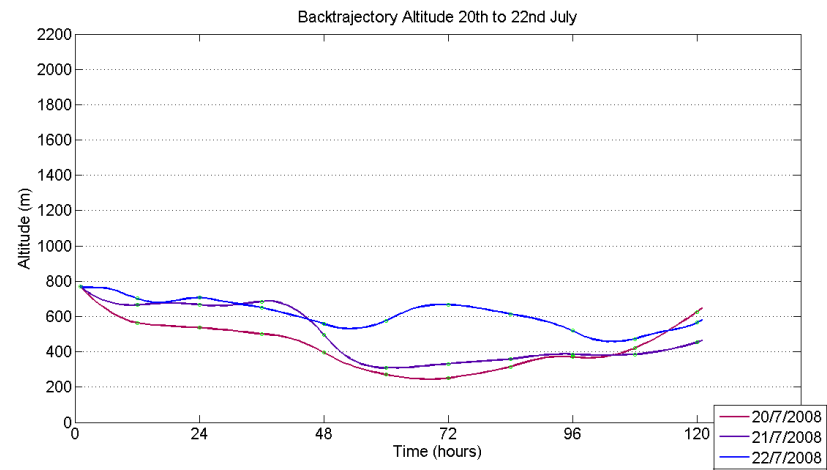
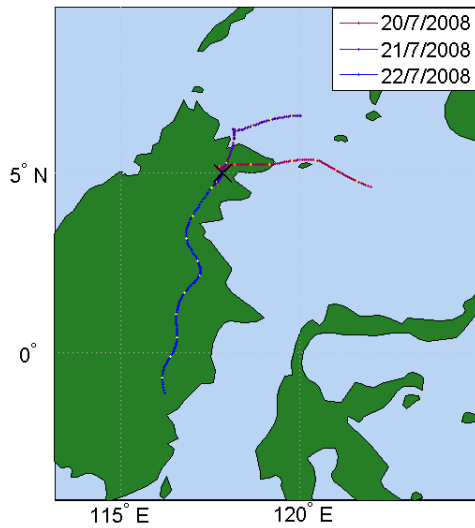


Figure 3.5: Back trajectories for the 5th - 14th July, OP3-III. Yellow/green markers indicate 12 hour periods.

Back Trajectories arriving at Bukit Atur at 1400hrs



Back Trajectories arriving at Bukit Atur at 1400hrs

Figure 3.6: Back trajectories for the 15th-22nd July, OP3-III. Yellow/green markers indicate 12 hour periods.

3.5 Methyl halides

Figure 3.7 shows the spatial distribution of all the methyl chloride (CH_3Cl) aircraft measurements. It is apparent from Figure 3.7 that mixing ratios higher than the average atmospheric background of 550 pptv were observed over both the landmass and seas of Sabah. When looking at the aircraft data overlaid on the land cover map (Figure 3.7(b)) mixing ratios greater than 700 pptv are observed over the landmass.

Employing the landscape categorisations described in Section 3.2 above, the box plots in Figure 3.8 were generated. The upper 75th percentile in the boundary layer over the oil palm plantations was the highest of the CH_3Cl data. Figure 3.8 shows the median of the boundary layer data for the southeast coast, rainforest and oil palm plantations to be higher than the median of the respective free troposphere data. This would be the expected gradient between the two layers, however, the northwest coast yields the same median (660 pptv) for both the boundary layer and free troposphere. High values comparable to those seen in the boundary layer over the oil palm were observed in measurements in the free troposphere off the northwest coast but not in the boundary layer there (Figure 3.8). Given that the prevailing wind direction for the July aircraft detachment was from the south to southeast sector (Figure 3.2), it is possible that the elevated mixing ratios of CH_3Cl seen in the free troposphere off the northwest coast were transported from the oil palm and rainforest regions where mixing ratios in the boundary layer were at their highest.

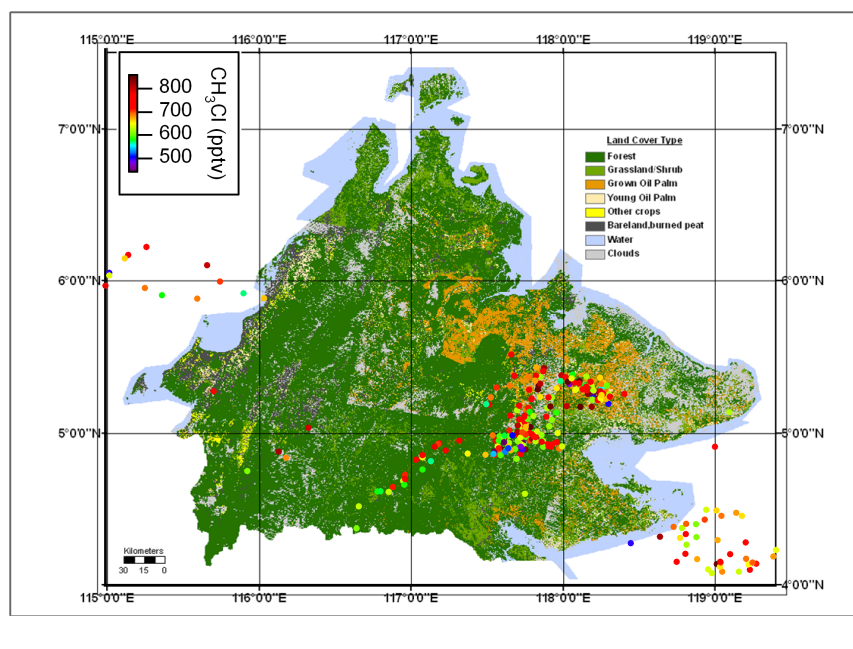
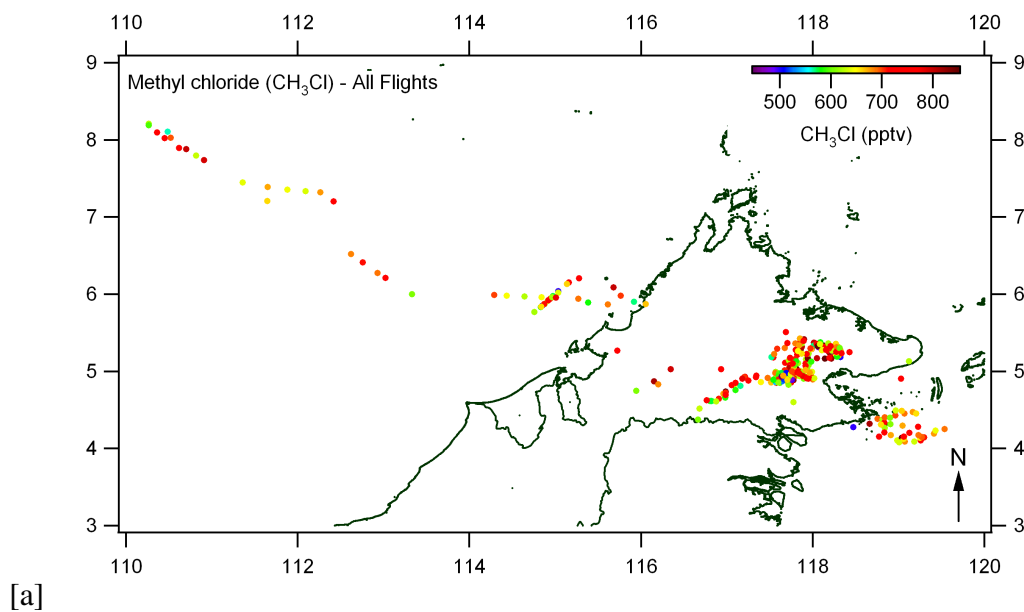


Figure 3.7: (a) Shows a map of methyl chloride mixing ratios measured in the WAS over Sabah and surrounding coast. (b) Land cover map of Sabah with the methyl chloride WAS measurements overlaid. The data points in both plots are coloured by methyl chloride mixing ratios.

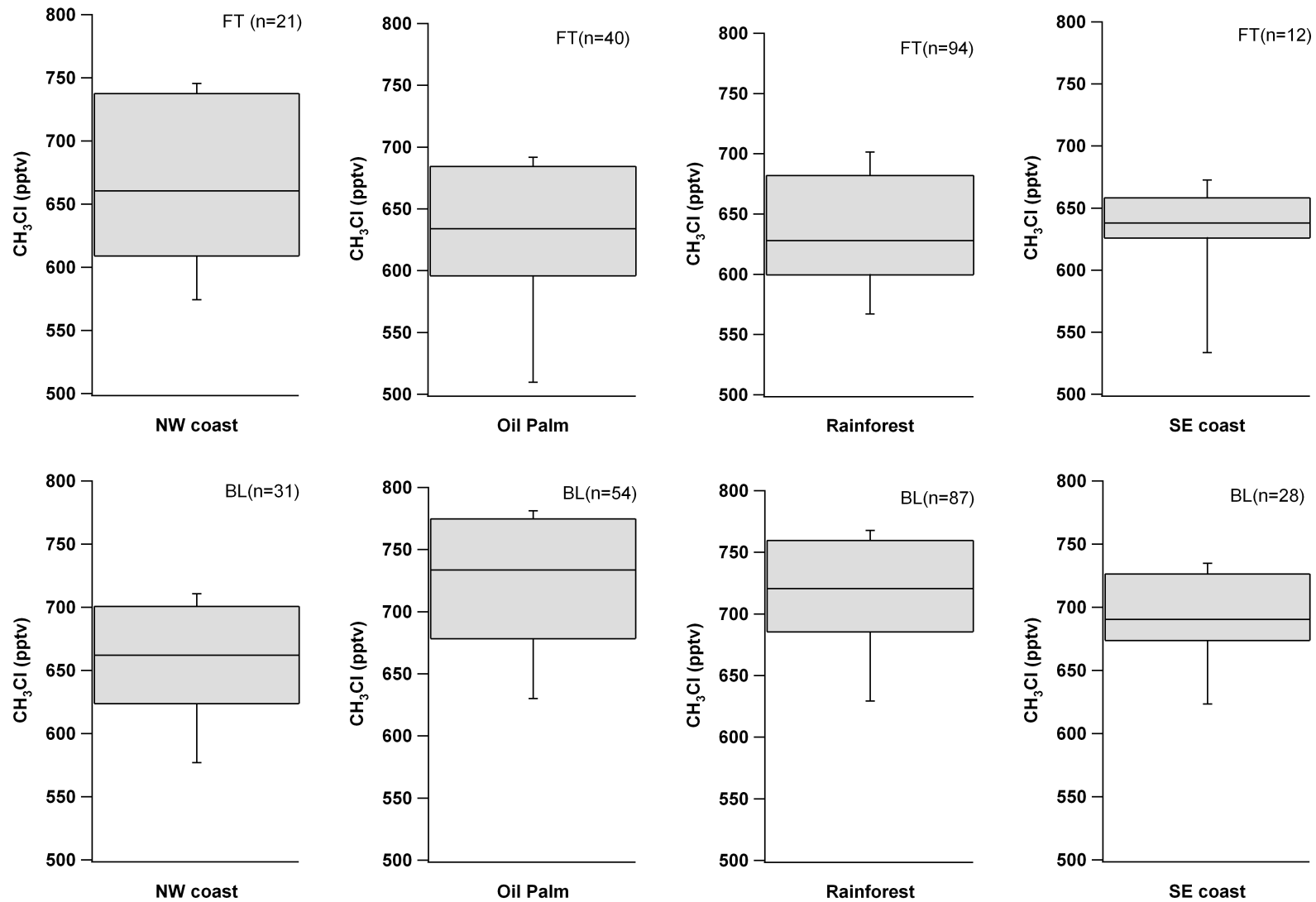


Figure 3.8: Box plots showing the methyl chloride mixing ratios over the different land cover types of Sabah. The line represents median, box top and bottom represent 75th percentile and 25th percentile respectively and the whiskers represent 90% and 10% of the data. FT= free troposphere; BL= boundary layer.

The methyl bromide (CH_3Br) measurements show reduced overall variability in their mixing ratios compared to those of methyl chloride. There is a scattering of high measurements across all areas, with an increased occurrence of values greater than 8 pptv in the samples taken over the Danum valley area and the southeast coast (Figure 3.9).

The box plots for the CH_3Br data, shown in Figure 3.10, identify the highest absolute values (75th percentile at 9.3 pptv) and median (7.8 pptv) to be over the southeast coast in the boundary layer. The boundary layer data for the northwest coast, oil palm and rainforest all shared a median value of 7.5 pptv and an upper quartile value of approximately 8 pptv. The medians for the rainforest and oil palm are higher in the free troposphere than the boundary layer: this could suggest transport of the higher CH_3Br mixing ratios seen off the southeast coast up into the free troposphere and over the landmass (Figure 3.10).

The spatial distribution of methyl iodide (CH_3I), shown in Figure 3.11, shows the southeast coast of Sabah to yield the highest mixing ratios of CH_3I . When the methyl iodide data are presented in box plots (Figure 3.12) it can be seen that the highest median and upper quartile of the data is over the southeast coast in the boundary layer. With CH_3I having known oceanic sources, this data could suggest the southeast coast as a source region of CH_3I , or closer to a source region of CH_3I when the prevailing wind direction is from the southeast. While the southeast coast appears to be a source, the northwest coast does not exhibit this behaviour to the same extent. When flying over these two separate areas, it was visible that the sea off the southeast coast was far shallower than the areas off the northwest coast, this may be of relevance to a macroalgae source that is depth-dependant. CH_3I has a short atmospheric lifetime of ≈ 3 days which would be enough time to transport mixing ratios from the southeast coast further inland (using the mean wind speed for OP3-III, a transport time of 10 hours is calculated from the nearest coastal point - Bukit Atur), however, this source region does not appear to show any influence on the measurements taken over the landmass.

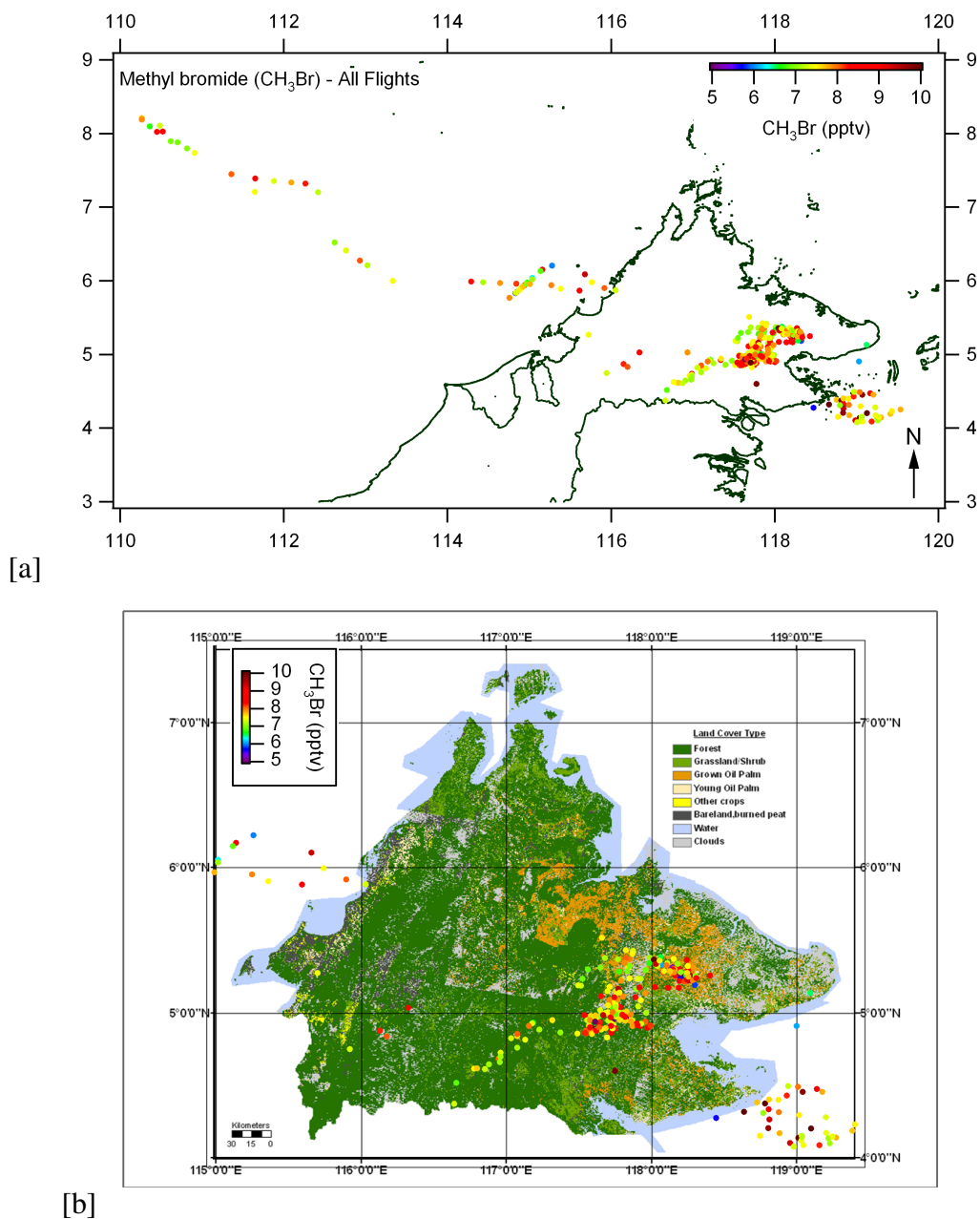


Figure 3.9: (a) Shows a map of methyl bromide mixing ratios measured in the WAS over Sabah and surrounding coast. (b) Land cover map of Sabah with the methyl bromide WAS measurements overlaid. The data points in both plots are coloured by methyl bromide mixing ratio.

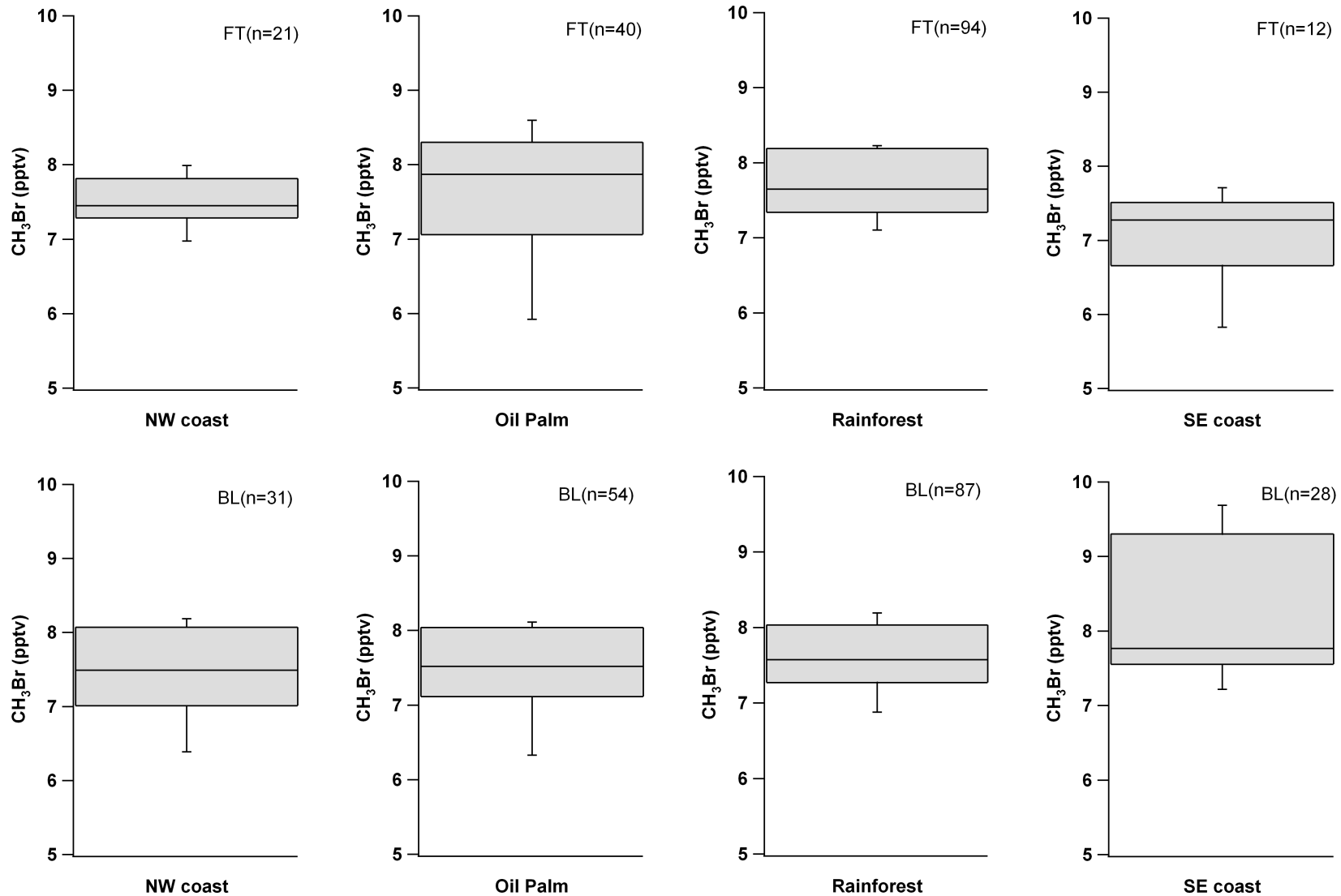


Figure 3.10: Box plots showing the methyl bromide mixing ratios over the different land cover types of Sabah. The line represents median, box top and bottom represent 75th percentile and 25th percentile respectively and the whiskers represent 90% and 10% of the data. FT= free troposphere; BL= boundary layer.

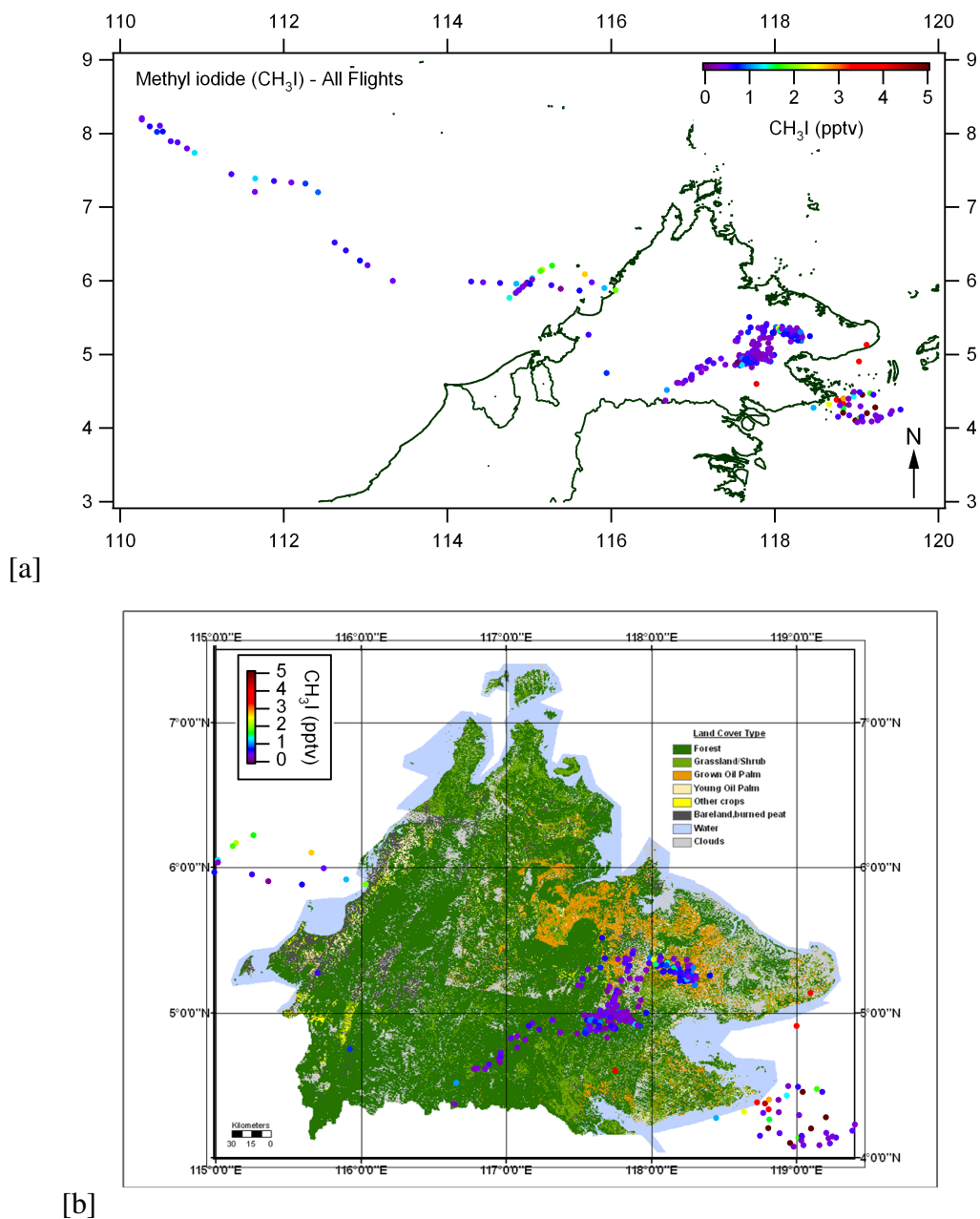


Figure 3.11: (a) Shows a map of methyl iodide mixing ratios measured in the WAS over Sabah and surrounding coast. (b) Land cover map of Sabah with the methyl iodide WAS measurements overlaid. The data points in both plots are coloured by methyl iodide mixing ratio.

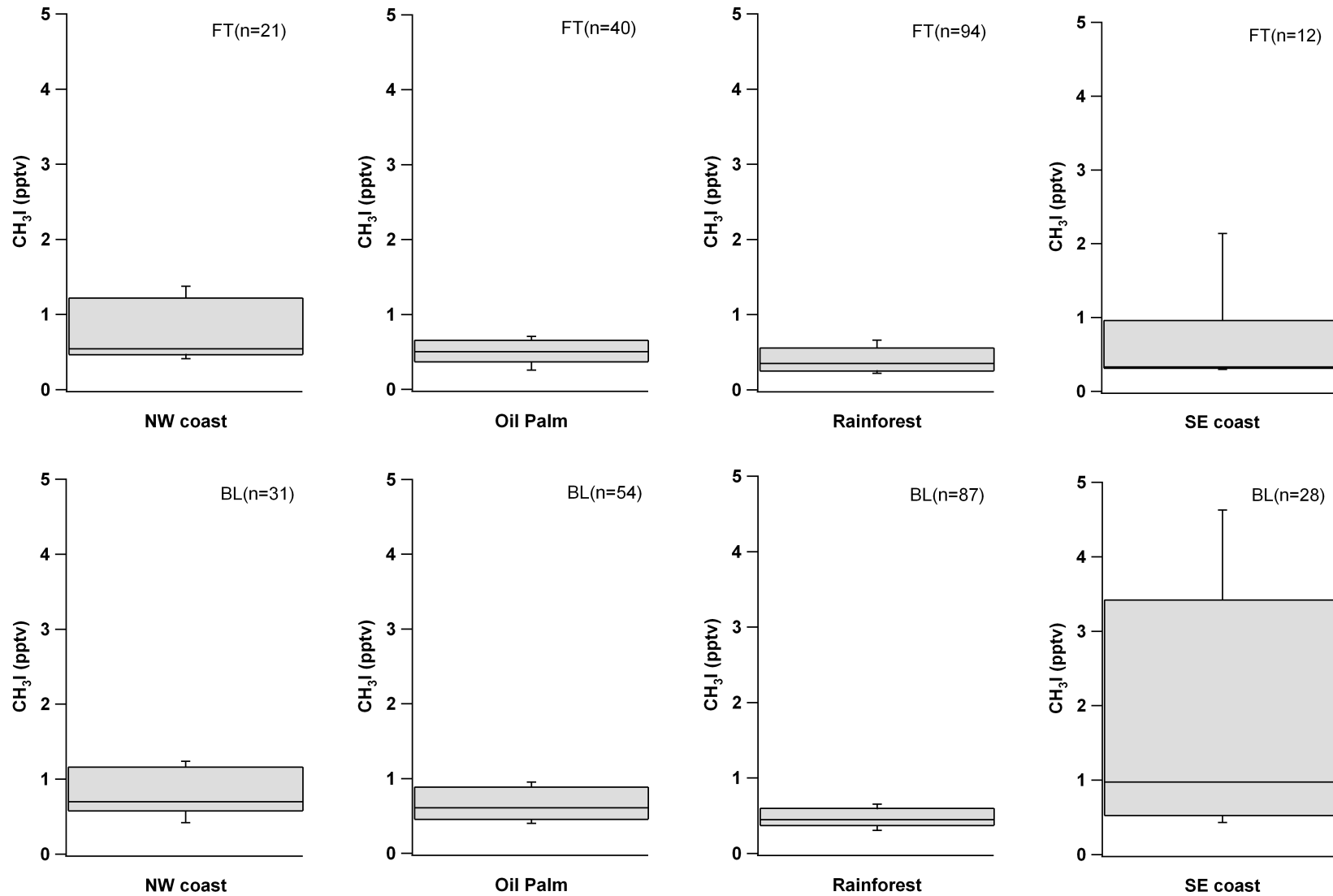


Figure 3.12: Box plots showing the methyl iodide mixing ratios over the different land cover types of Sabah. The line represents median, box top and bottom represent 75th percentile and 25th percentile respectively and the whiskers represent 90% and 10% of the data. FT= free troposphere; BL= boundary layer.

Unfortunately the CH₃Cl measurement in negative ion mode on the GC-MS is not as reliable as in EI mode as other chloride fragments can be detected, introducing noise and error in the CH₃Cl signal. As the ground site measurements were in negative ion (Chapter 2), the CH₃Cl data from the ground-based site will not be presented.

The time series of CH₃Br and CH₃I data for OP3-I and OP3-III are shown in Figure 3.13(a). During OP3-I the methyl halides show a great deal of variation in their time series, this reflects the changes in wind direction during this measurement period. The CH₃Br data shows elevations (≥ 16 pptv) from the mean of 11.5 ± 2.2 pptv on the 18th and 19th when air masses approached the site from the northeast (Figure 3.3). CH₃Br then shows a downwards trend as the air masses shift to come across from the west of Borneo, until the 28th when a small period of elevation in mixing ratios is observed. From the 1st to the 3rd variations within 24 hour periods are visible in the CH₃Br data, however, there is considerable scatter.

The CH₃I data for OP3-I (Figure 3.13(a)) shows a downward trend throughout the measurement period. Initially mixing ratios around 2 pptv are observed decreasing to 1.25 pptv by the end of the campaign. Some variations in the time series are observed, but with little correlation with the CH₃Br data.

The time series for OP3-III by contrast shows very little variation in the data for the methyl halides and mixing ratios far lower than OP3-I. This may be due to the predominance of air masses from south of the site. The CH₃Br data for OP3-III has a mean of 6.8 ± 1.3 pptv which is a considerable drop from OP3-I, and slightly lower than the median of the aircraft data in the boundary layer over the rainforest (7.5 pptv, Figure 3.10). The CH₃I data, shown in Figure 3.13, has a mean of 1.1 ± 0.2 pptv which is comparable with the median of the aircraft data in the boundary layer over the southeast coast. However, the upper quartile value for the southeast boundary layer CH₃I aircraft data is 3.5 pptv which is not reflected in the OP3-III ground-based time series. This is somewhat surprising given the prevailing wind directions for this period were from the south sector (Figure 3.2). Although the southeast coast of Sabah exhibits high mixing ratios of CH₃I, further down the coast of Borneo on this eastern side may not. If this is the case, then the wind

direction with respect to Bukit Atur would need to be easterly to reflect the high mixing ratios seen in the boundary layer over the southeast coast of Sabah.

Blei et al. (2010) measured CH_3Cl and CH_3Br via branch enclosures in conjunction with OP3 phase III, their findings agree with the Yokouchi et al. (2002) study, suggesting that tropical vegetation is a strong source of CH_3Cl to the atmosphere. Blei et al. (2010) report mean emission of $19 \text{ ng h}^{-1}\text{g}^{-1}$ of CH_3Cl from Malaysian trees, and they also report to be a mean emission of $0.4 \text{ ng h}^{-1}\text{g}^{-1}$ of CH_3Br . Some of the samples collected by Blei et al. (2010) were analysed in situ on the UEA GC-MS in NI. This CH_3Br signal at the leaf level is all but lost in the ground based measurements presented here which represent the canopy. This loss of signal suggests that there are complex relationships in the mixed vegetation environment of a tropical forest. The purpose of methyl halide emissions from plants is not yet fully understood and it is possible that the emission of methyl halides from these tropical plants serves some purpose to another organism in the forest system, which could be why this strong emission is not observed close to and above the canopy.

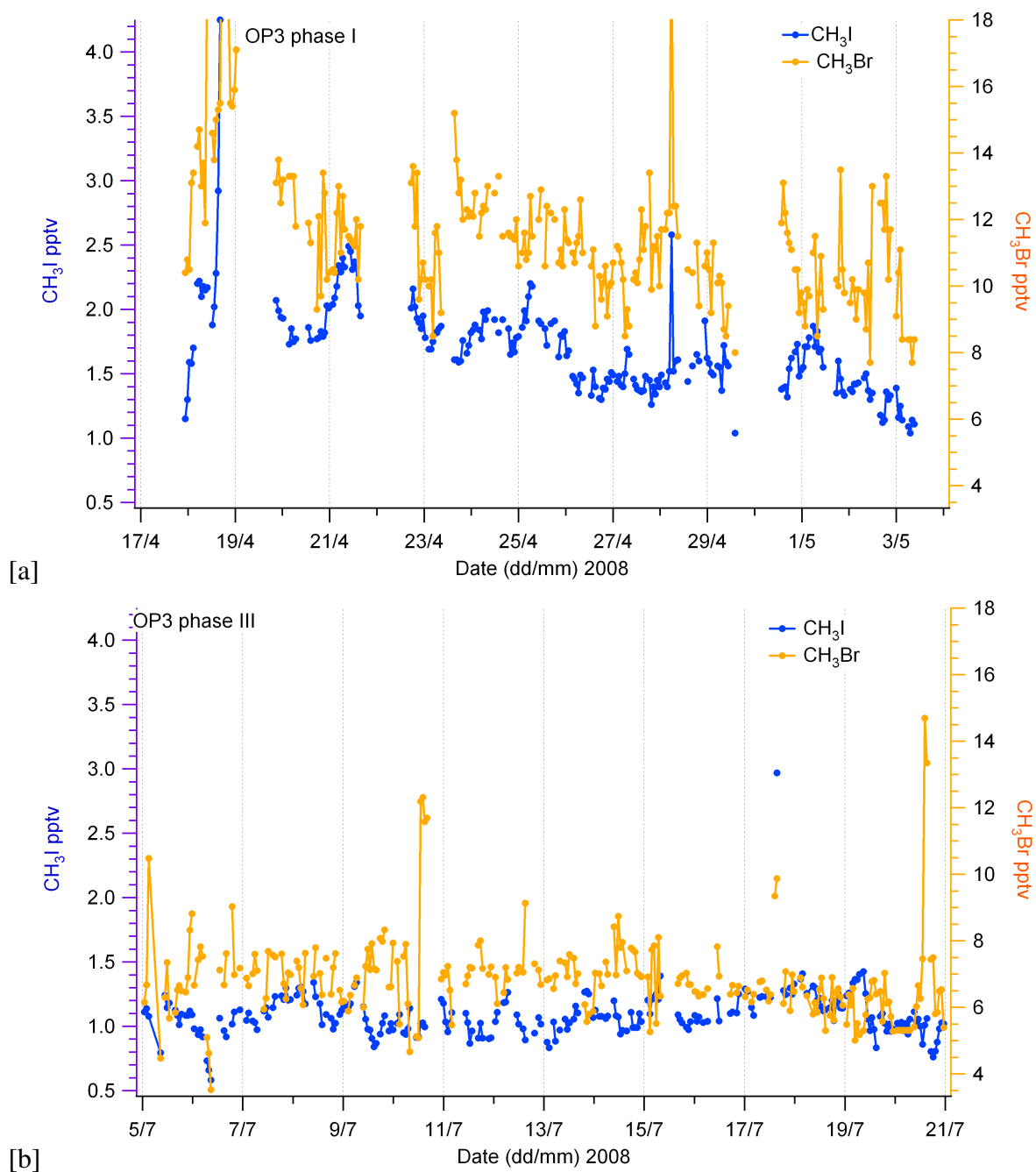


Figure 3.13: Time series data of methyl iodide (blue) and methyl bromide (orange) for OP3 phase I (a) and III (b). All mixing ratios are in parts per trillion by volume, measured in negative ion mode on the GC-MS system.

3.6 Short lived bromocarbons

Figures 3.14(a) and (b) show all the bromoform (CHBr_3) aircraft measurements mapped over the landmass of Sabah and its surrounding seas. There are clear areas where higher mixing ratios were seen, most obvious from figure 3.14 is the area off the southeast coast of Sabah where mixing ratios of >2 pptv CHBr_3 were observed. Figure 3.15 shows the box plots of the CHBr_3 aircraft data. The boundary layer data shows the southeast coast to have the highest range of mixing ratios, with a median of 2.4 pptv, compared to medians of 1.6 pptv over the rainforest and oil palm, and 1.5 pptv over the northwest coast. The free troposphere data tells a different story, with the upper quartile over the northwest coast being the highest. The values in the 75th percentile of the free tropospheric data and that of the boundary layer data over the northwest coast are directly comparable. The higher mixing ratios that represent 90% of the data in the free troposphere off the northwest are difficult to explain with the boundary layer data, possibly uplift of air from a surface region of higher mixing ratios not measured. The southeast coast has a median of 1.25 pptv in the free troposphere, which is comparable with those over the oil palm and northwest coast, although higher than that of the rainforest (≈ 1 pptv).

The dibromomethane (CH_2Br_2) aircraft data shown mapped in Figure 3.16 shows a spread of mixing ratios ≥ 1 pptv. The box plots for CH_2Br_2 (Figure 3.17) show the highest median (1 pptv) and upper quartile (1.12 pptv) in the boundary layer data over the southeast coast. The median is slightly lower than the median for the marine boundary layer reported by Law et al. (2007) which was 1.1 pptv, but the data is within their reported range of 0.7 - 1.5 pptv. The boundary layer data of the northwest coast has the lowest of the medians and upper quartiles. However, like the CHBr_3 data, the free troposphere data for the northwest coast has the highest median and upper quartile of the free tropospheric data. When looking at the CH_2Br_2 in context of the altitude of the samples and the longitude, in Figure 3.19, high values of CH_2Br_2 can be seen at altitudes of 6,500 m off the northwest coast of Sabah. These measurements were from two different flights: B389 and B393.

Cluster back trajectories run for these samples (not shown) indicate different pathways

for the different flights. The 2 samples from flight B389 suggest the air is to have traveled from 134°E and 2°N, over the Celebes Sea and across Sabah to the northwest coast. The altitude of this path initiated at $\approx 4,000$ m gradually increasing to 5,000 m 48 hours prior to arriving over the northwest coast, then in the final 48 hours the air is uplifted to 6,500 m. When crossing Borneo the air must negotiate mount Kinabalu, a 4 km mountain near Kota Kinabalu, this topographic obstacle may influence the uplift observed. Samples from flight B393 (n=3) have 5-day back trajectories beginning $\approx 124 - 125^\circ\text{E}$ and $\approx 7^\circ\text{N}$ at altitudes of $\leq 2,500$ m passing over the sea to the north of Borneo, before heading down the northwest coast of Borneo over the China sea. In the final 24 hours before arriving at the WAS sample location, the trajectory doubles back on itself slightly whilst considerable uplift takes place taking the air from $\leq 2,500$ m to the measurement altitude of 6,500 m. Satellite images of this region on the day of flight B393 show convection building in this region. Convective events were a daily occurrence at Bukit Atur ground measurement site, with the period of intense convective activity within the boundary layer occurring between 09:00 and 15:00 local time (Pearson et al., 2010).

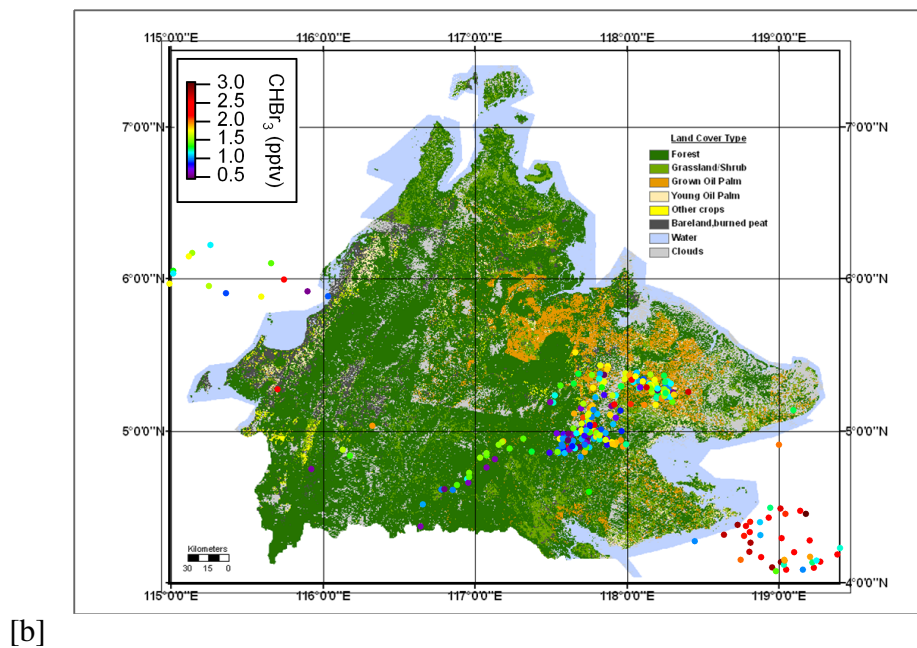
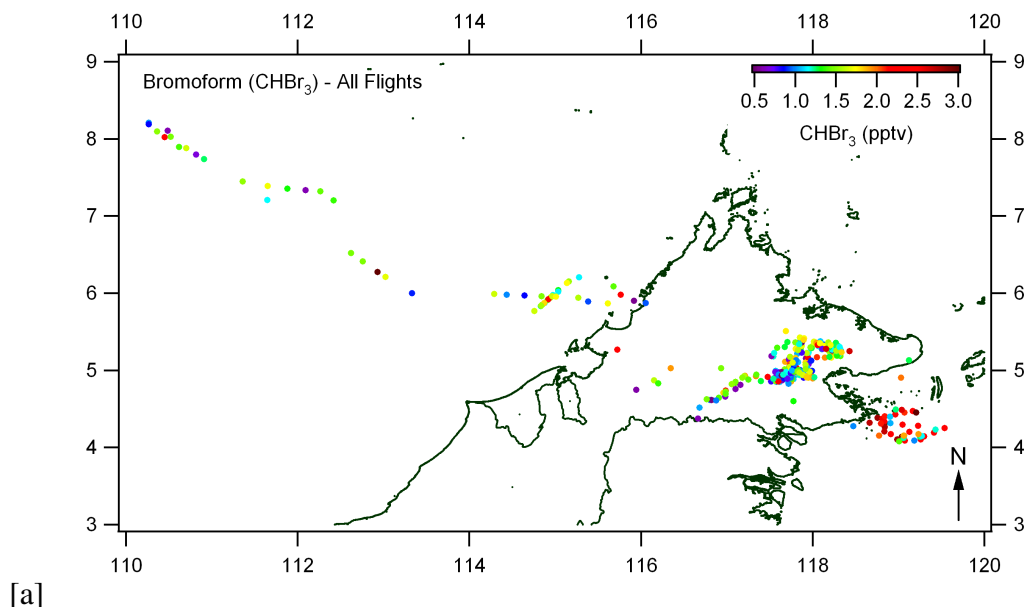


Figure 3.14: (a) Shows a map of CHBr_3 mixing ratios measured in the WAS over Sabah and surrounding coast. (b) Land cover map of Sabah with the CHBr_3 WAS measurements overlaid. The data points in both plots are coloured by CHBr_3 mixing ratio.

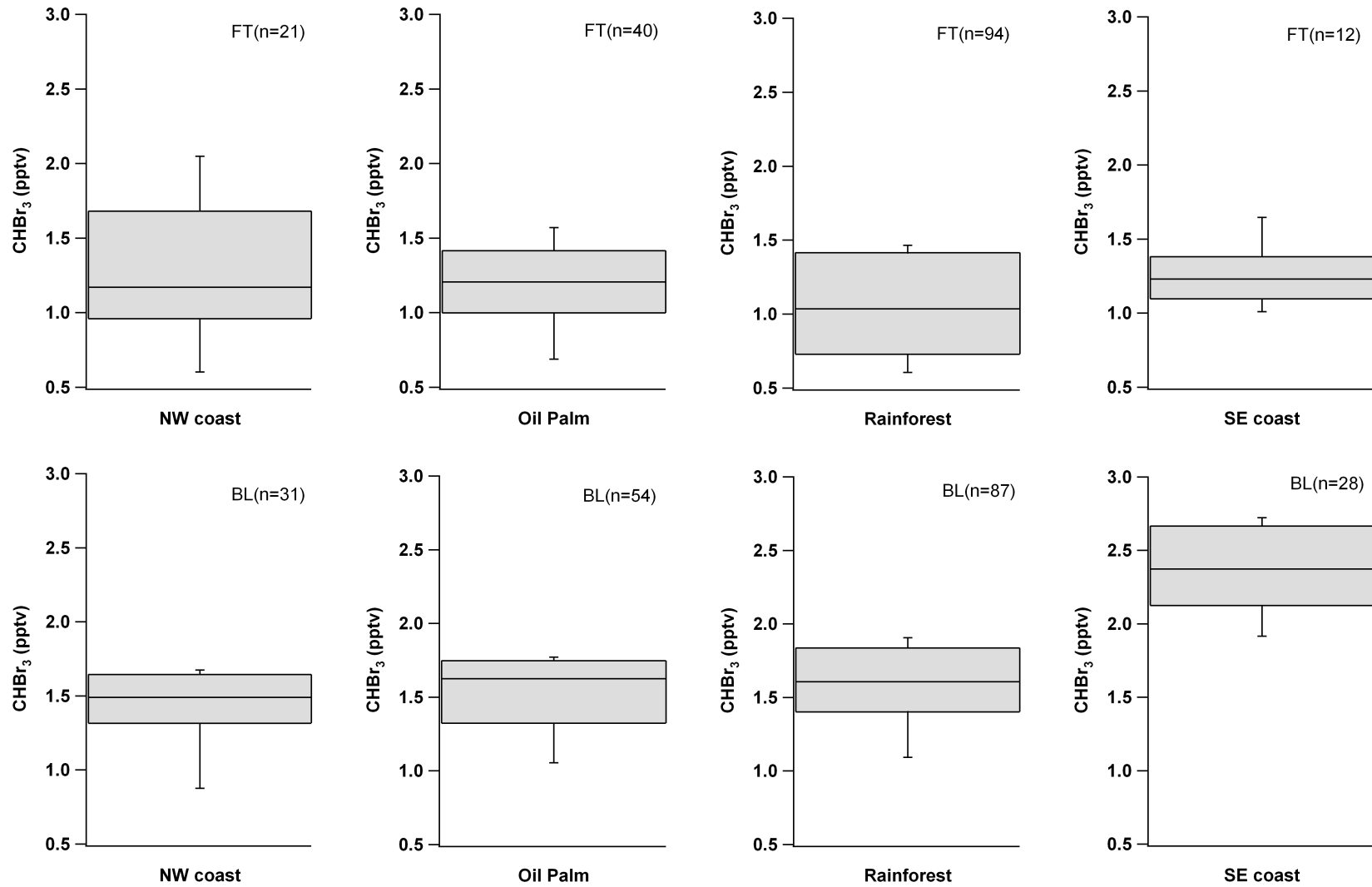
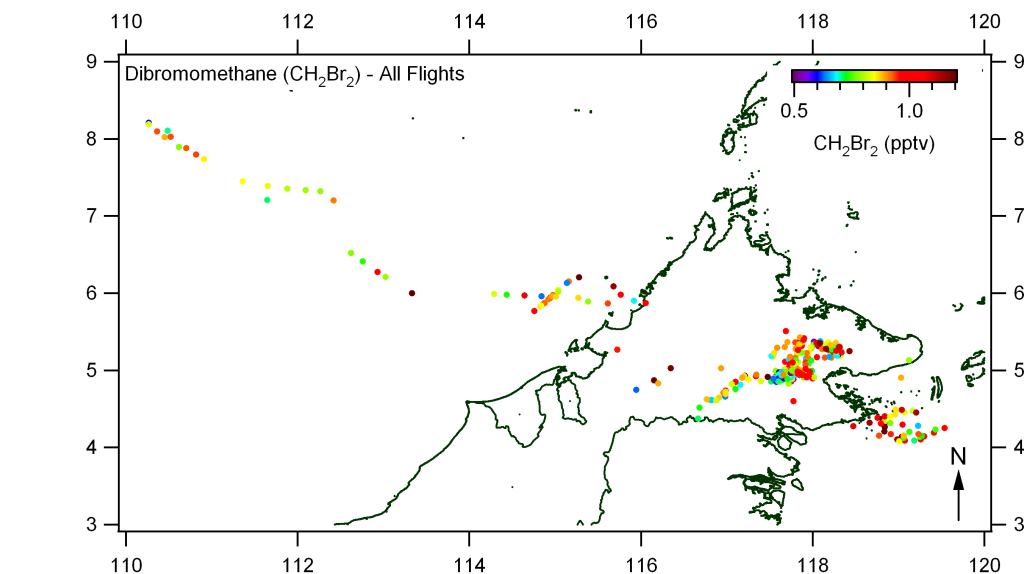
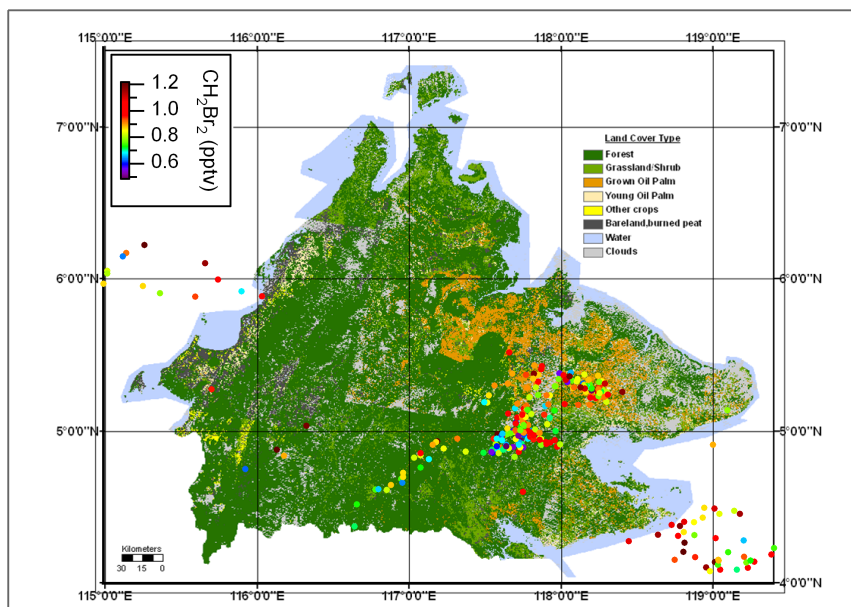


Figure 3.15: Box plots showing the bromoform mixing ratios over the oil palm plantations and the northwest coast off Sabah. The line represents median, box top and bottom represent 75th percentile and 25th percentile respectively and the whiskers represent 90% and 10% of the data. FT= free troposphere; BL= boundary layer.



[a]



[b]

Figure 3.16: (a) Shows a map of CH_2Br_2 mixing ratios measured in the WAS over Sabah and surrounding coast. (b) Land cover map of Sabah with the CH_2Br_2 WAS measurements overlaid. The data points in both plots are coloured by CH_2Br_2 mixing ratio.

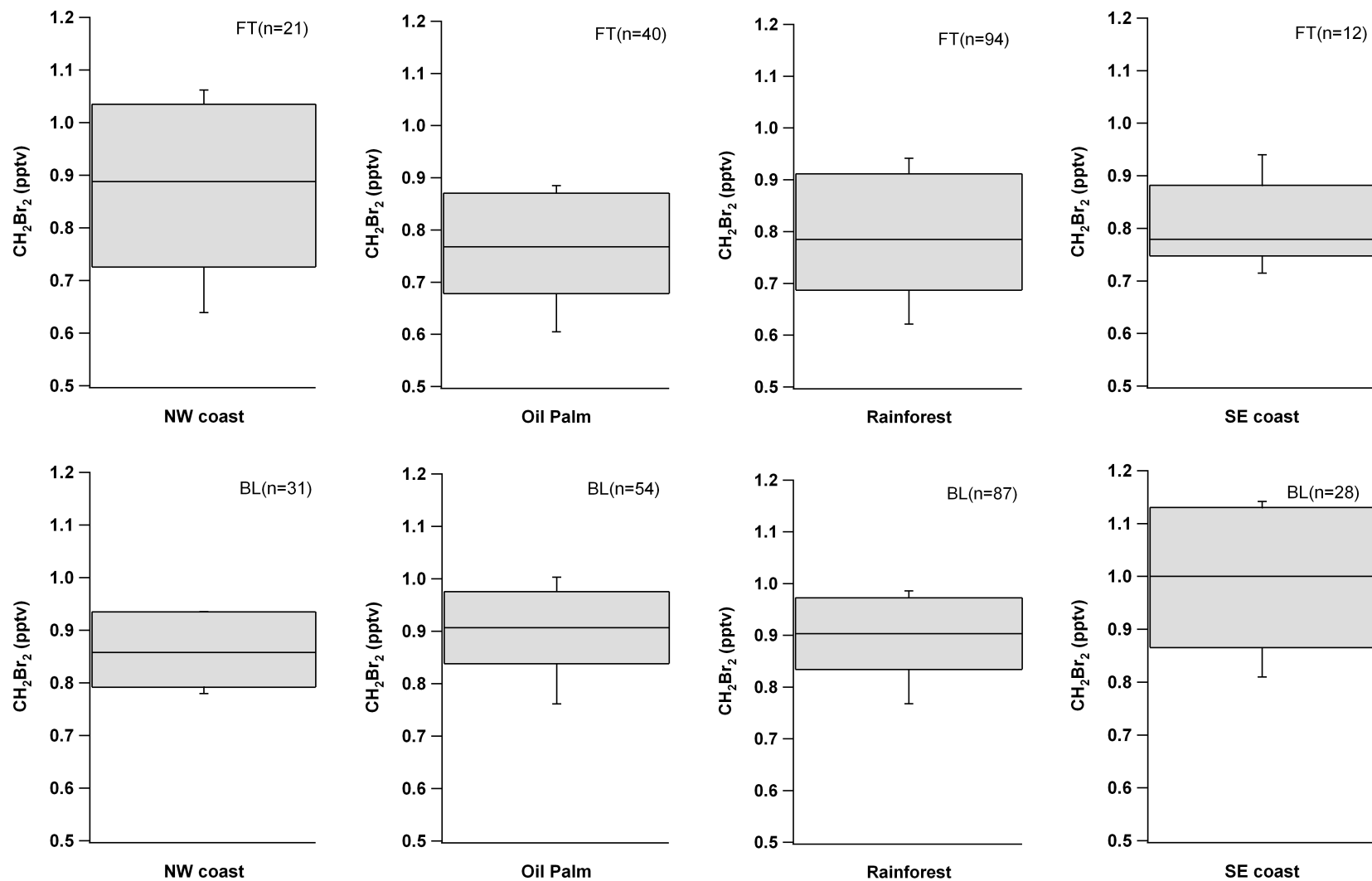
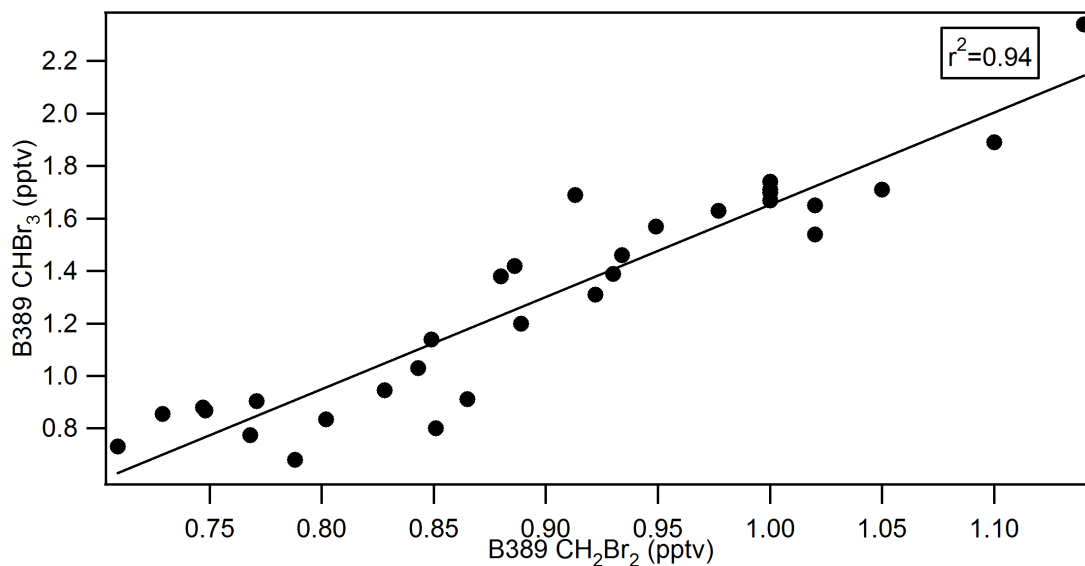


Figure 3.17: Box plots showing the dibromomethane mixing ratios over the oil palm plantations and the northwest coast off Sabah. The line represents median, box top and bottom represent 75th percentile and 25th percentile respectively and the whiskers represent 90% and 10% of the data. FT= free troposphere; BL= boundary layer.

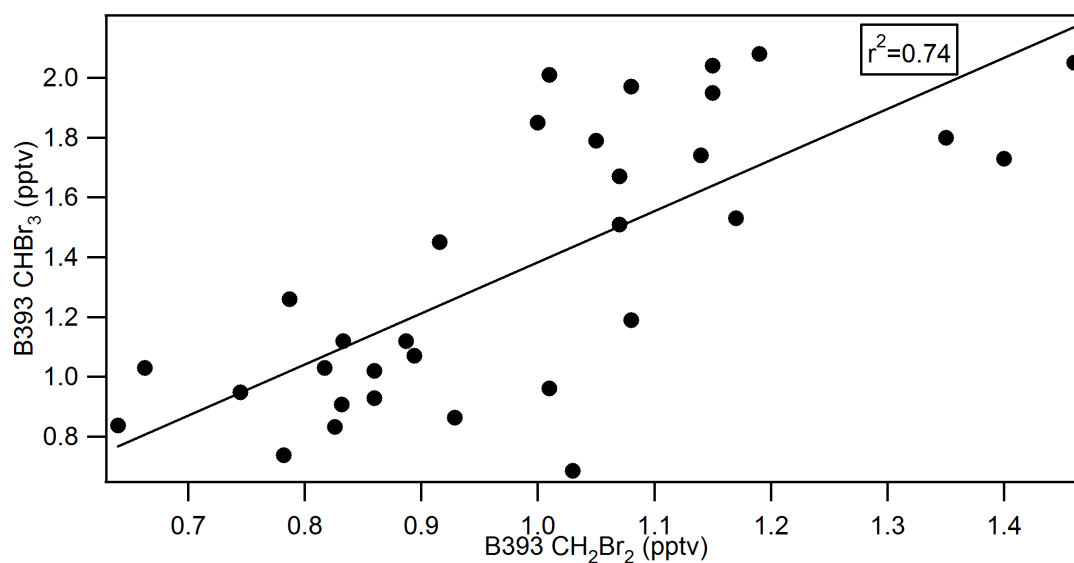
Aircraft measurements from the flights over the seas off the southeast coast of Sabah show particularly good correlations for the two compounds, with r^2 values 0.74 and above (Figure 3.18). Consistently high mixing ratios of CHBr_3 and CH_2Br_2 were seen over the southeast coastal waters of Sabah, an area known to be cultivating seaweed as a crop. In this south-eastern region the sea appeared shallow and several offshore seaweed farms on raised sandbars were observed from the aircraft.

Throughout the two measurement periods at Bukit Atur, CHBr_3 and CH_2Br_2 followed similar patterns and features (Figure 3.20), indicating that they share a common source. This supports the work of Yokouchi et al. (2005) who found CHBr_3 and CH_2Br_2 to be well correlated in the atmosphere. There are, however, some periods during OP3-I where CHBr_3 is seen in elevated mixing ratios with respect to CH_2Br_2 . Of particular note in OP3-I is the enhancement 'event' on the 28th April where elevated mixing ratios were maintained for approximately 24 hours. The time series for OP3-III (Figure 3.20) shows a relatively steady increase in mixing ratios of both compounds up to the 11th July where there is an enhancement in mixing ratios followed by a small drop in CHBr_3 and CH_2Br_2 , then the increasing trends picks up again until the 19th July, after which there is a rapid decrease in mixing ratios for the final 3 days of measurements. CHBr_3 and CH_2Br_2 are shown to exhibit consistently good correlation during OP3-III, both at Bukit Atur and in the aircraft data. The rainforest measurements at Bukit Atur were particularly well correlated with an r^2 value of 0.88 for OP3 phase III (Figure 3.21). The correlation for OP3-I is not as strong (r^2 of 0.64) owing to the relative enhancements of CHBr_3 to CH_2Br_2 in the time series as shown in Figure 3.25.

The features of the CHBr_3 and CH_2Br_2 time series for OP3-I show daily variations without the regularity of a diurnal pattern (Figure 3.23). The daily variations observed during OP3-I were at their peak mixing ratios during night time/early morning hours, 2-5am. The daily variations in mixing ratios in the OP3-III time series are less apparent than in OP3-I (Figure 3.20). This suggests that there must be something different in the emission of CHBr_3 and CH_2Br_2 , their transport to Bukit Atur, or their atmospheric loss processes. CH_2Br_2 and CHBr_3 still show good agreement in features, so they still appear



[a]



[b]

Figure 3.18: Correlation plots for ocean flights B389 and B393 for the compounds CHBr₃ and CH₂Br₂. B389 was solely over the southeast coast, flight B393 includes measurements from both the southeast coast and the northwest coast. Regression lines and values are shown on each plot.

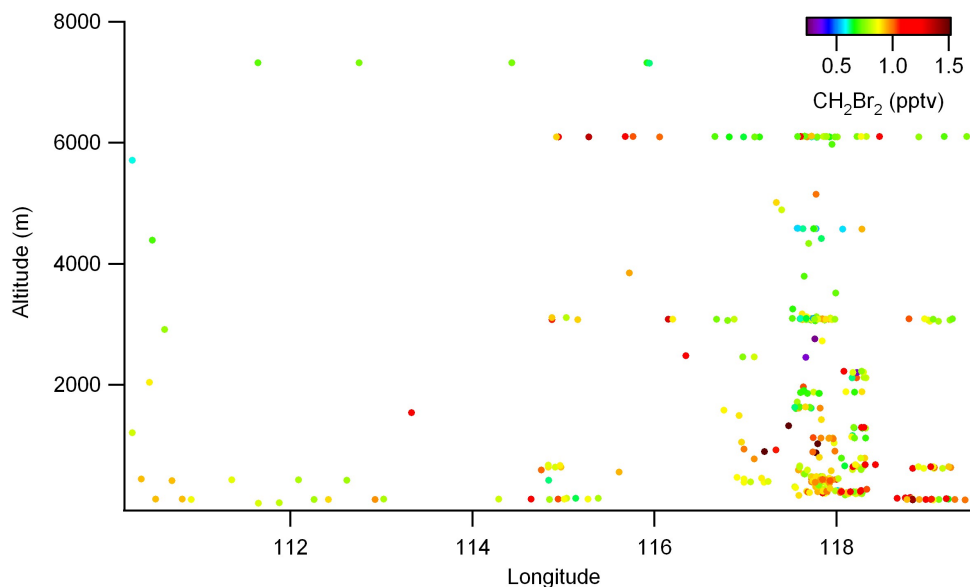


Figure 3.19: A longitude plot of all aircraft measurements showing the altitude of the sample on the y axis and the CH_2Br_2 mixing ratio of the samples using the colourscale.

to share a common source throughout OP3-III.

Cambridge University also measured organohalogens on their μDirac GC-ECD (Gas Chromatography - Electron Capture Detector) instrument (Gostlow et al., 2010) at Bukit Atur, the μDirac inlet was at 12 m on the GAW tower (UEA inlet at 30 m). Both the mixing ratios and the trend for OP3-III in the CHBr_3 data were very well correlated between the μDirac and the UEA GC-MS system (Figure 3.22). However, the μDirac CH_2Br_2 mixing ratios were lower than those in the UEA data, but the trend remained comparable (Figure 3.22). Gostlow et al. (2010) go into greater detail regarding the disparity in the UEA and μDirac CH_2Br_2 data, discussing the co-elution of CH_2Br_2 and dichlorobromomethane (CHBrCl_2) in the μDirac chromatograms. Gostlow et al. (2010) observe that the co-elution of CH_2Br_2 and CHBrCl_2 makes the lower mixing ratios in the μDirac CH_2Br_2 even more surprising and go on to suggest that the disparity may be a result of changes in the calibration gas standard used for the μDirac instrument.

The daily variations in the $\text{CHBr}_3:\text{CH}_2\text{Br}_2$ ratio, in Figure 3.25, show some periods of clear anti-correlation with the temperature time series. Unfortunately, the instrument recording temperature at the site was only operational until the 28th April 2008, which misses the period of elevated mixing ratios seen in the CHBr_3 and CH_2Br_2 data. The

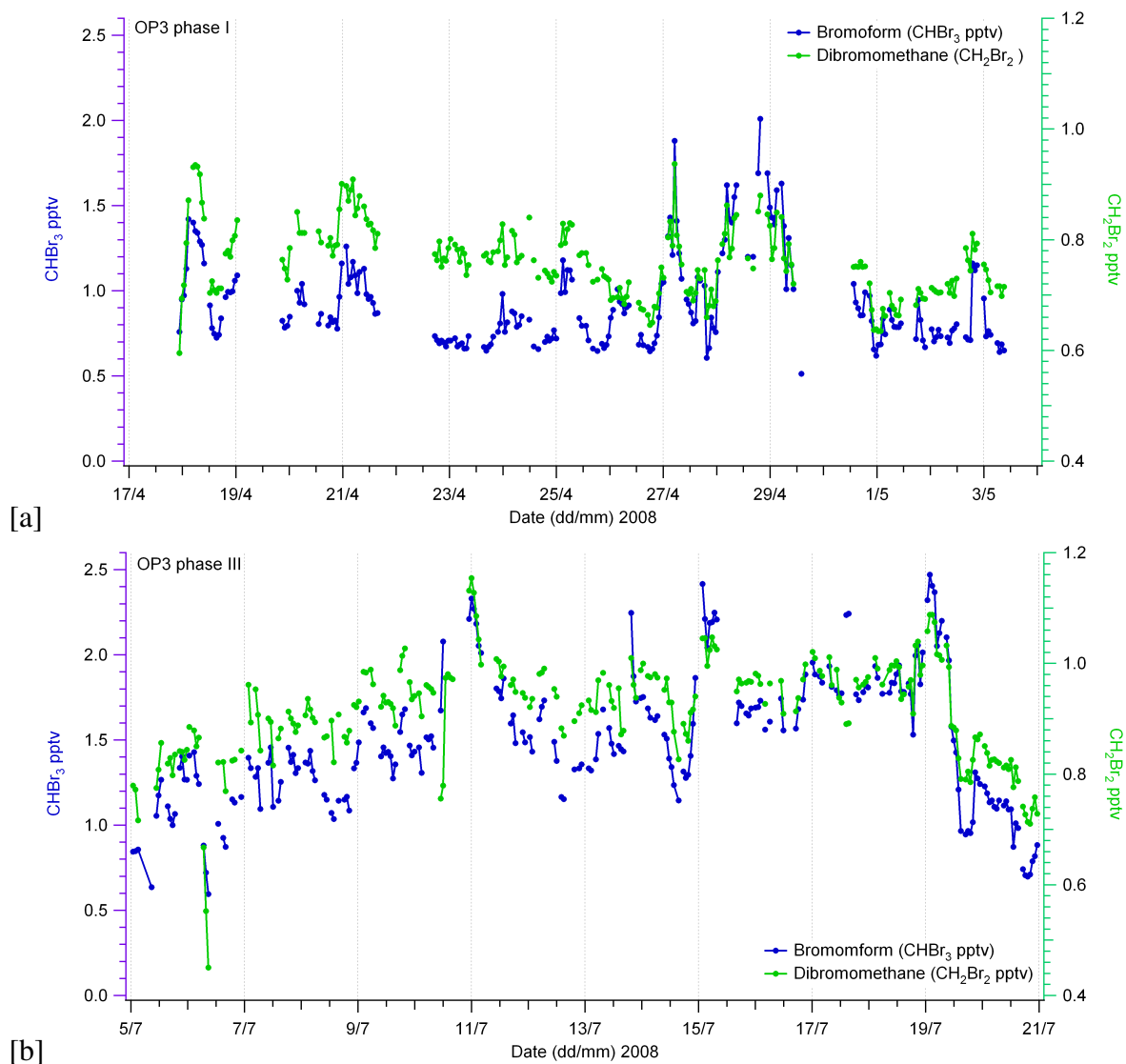


Figure 3.20: Timeseries of CHBr_3 (blue) and CH_2Br_2 (green) data for OP3 phase I (a) and OP3 phase III (b). All mixing ratios are in parts per trillion by volume, measured on a GC-MS in negative ion mode.

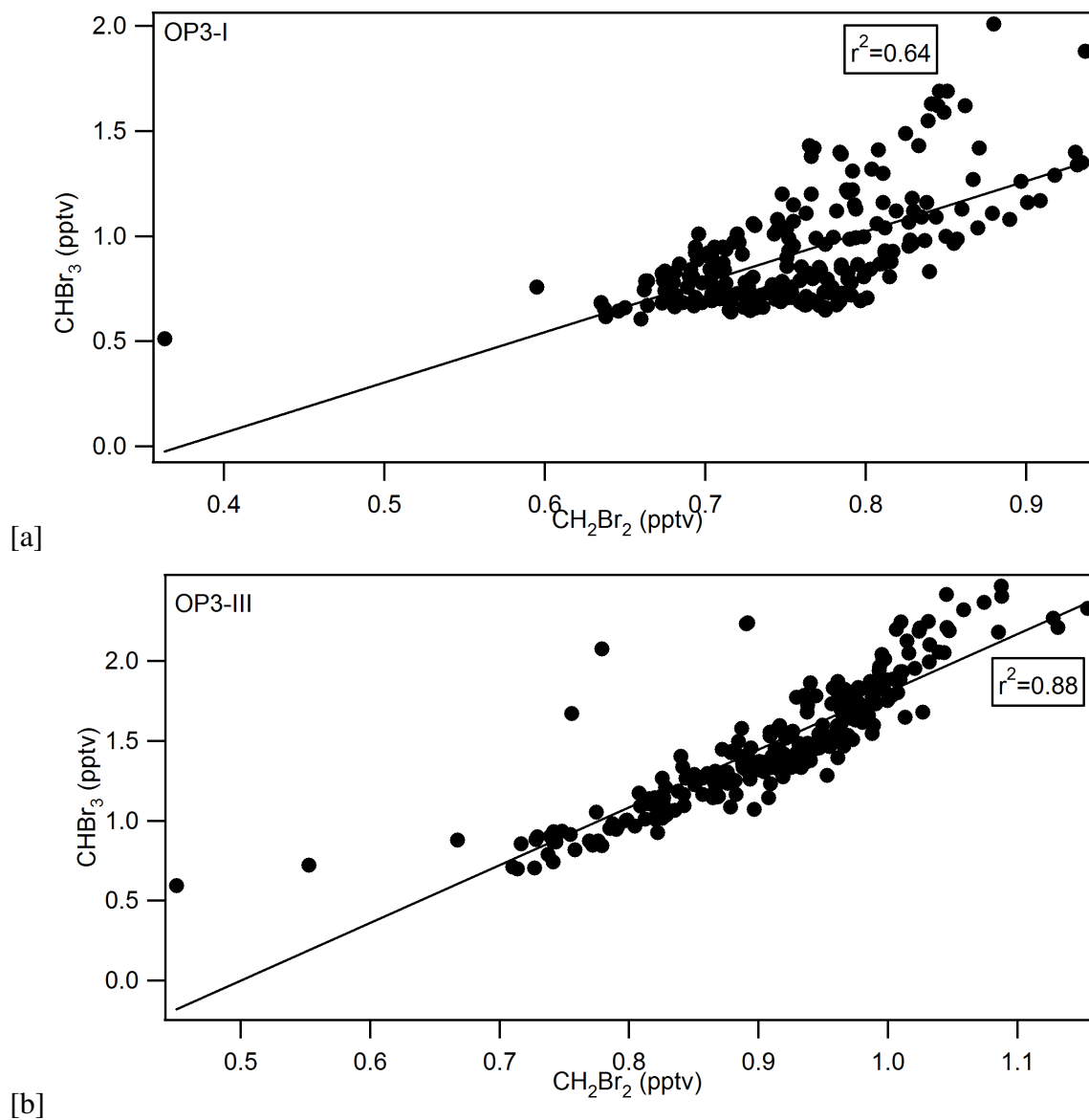


Figure 3.21: Correlation plots for the ground based measurements of CHBr_3 and CH_2Br_2 at Bukit Atur during (a) OP3-I and (b) OP3-III

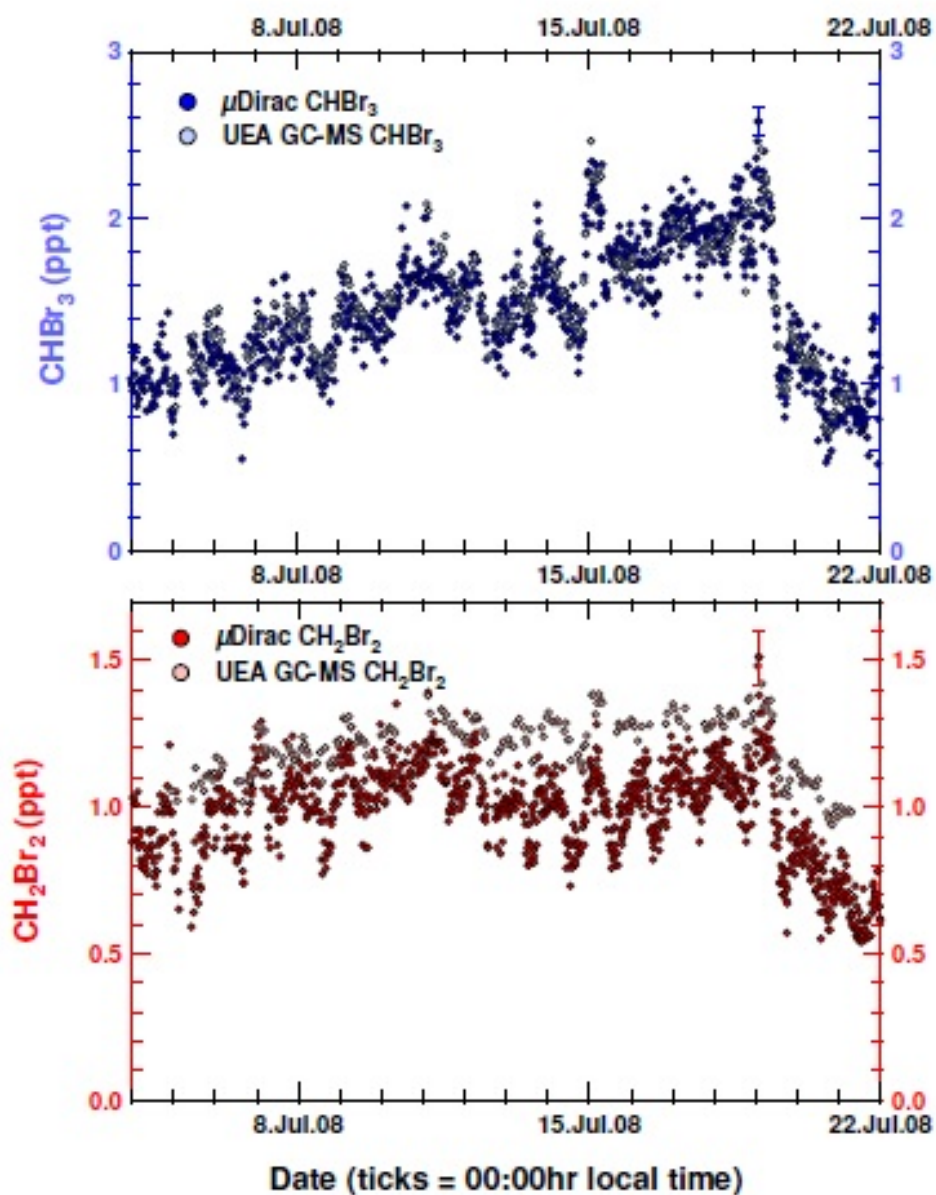


Figure 3.22: From Gostlow et al. (2010): CHBr_3 and CH_2Br_2 data (ppt) during OP3-III from the UEA GC-MS and Cambridge University's μDirac instrument. The instrument inlets were situated 18m apart on the GAW tower. Dark symbols denote the μDirac data and light symbols represent the UEA data.

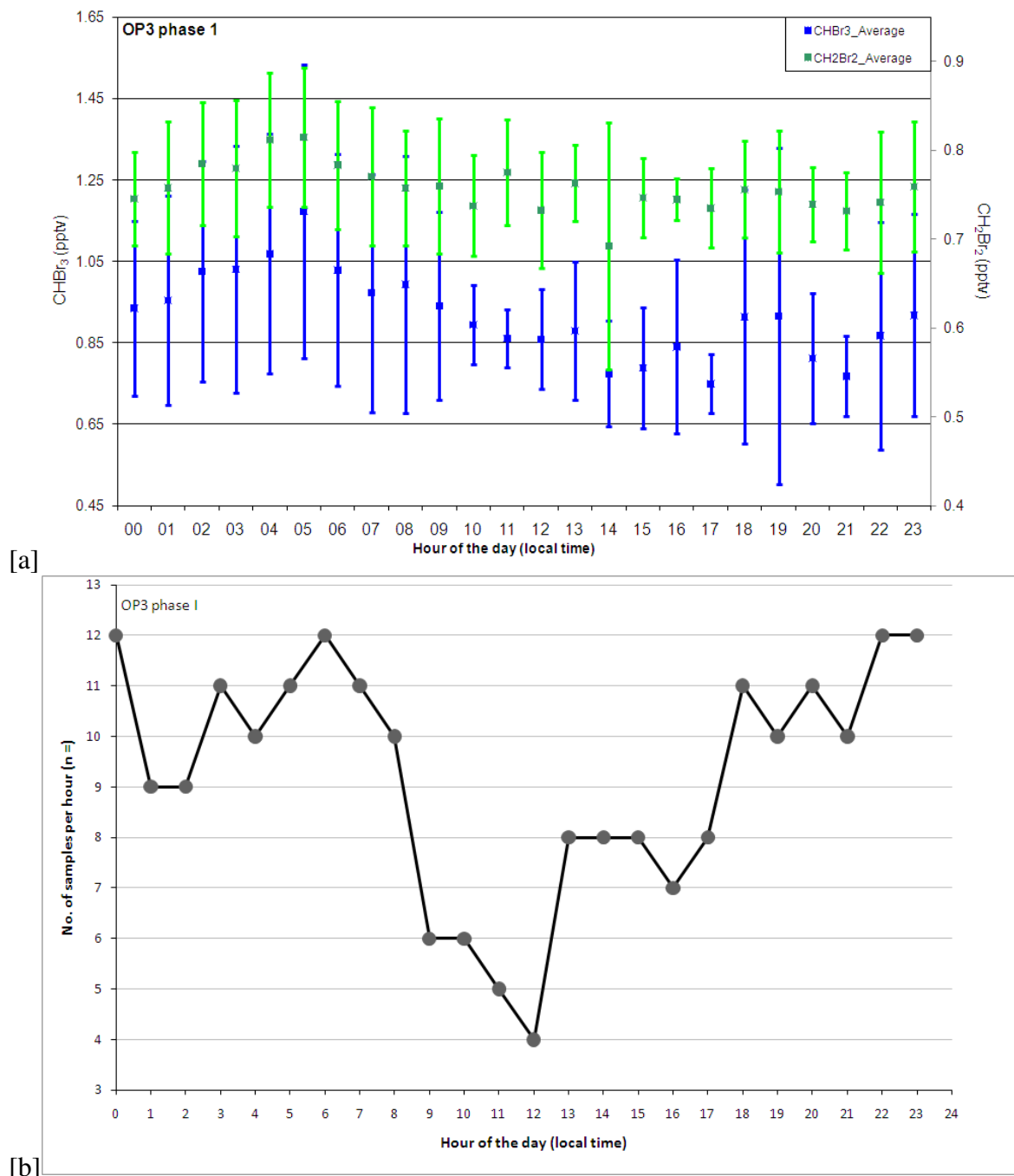


Figure 3.23: Plot (a) shows the mean mixing ratios of CHBr_3 (blue) and CH_2Br_2 (green) from OP3-I, averaged in hourly bins. Error bars represent 1 standard deviation from the mean. The number of samples per hourly bin are shown in plot (b).

anti correlations observed suggest that the processes that drive diurnal emissions are not responsible for the variations observed here. Diurnal patterns show differences between day and night, such patterns are observed in the data series of compounds emitted from forest vegetation, such as isoprene, following the photosynthetic cycle of the emitting plant. Photosynthesis, being light and temperature dependent, typically results in peak emissions observed during the warmest and brightest hours of the day (Muller et al., 2008; Lerdau and Throop, 2000).

The μ Dirac data shows daily variations in OP3-III, with average amplitude of 0.18 pptv for CHBr_3 , compared to 0.14 pptv seen in the UEA data for the same period. The Cambridge μ Dirac samples were collected at more frequent intervals than the UEA GCMS which may explain why these variations are more pronounced in the Cambridge data, but are not as clear in the UEA data. A coastal diurnal source could explain the variations seen in the UEA and Cambridge data. Cambridge made halocarbon measurements at the coastal location of Kunak, on the southeast coast, where the background mixing ratio of CHBr_3 was 2-5 pptv (Pyle et al., 2011). Pyle et al. (2011) used the NAME mode (a Lagrangian air parcel dispersion model) to reproduce the variability in the OP3 and coastal bromoform data. Their analysis with the NAME model confirms that the air parcels during OP3-III had crossed potentially rich oceanic and, especially, coastal regions prior to measurement at Bukit Atur. Pyle et al. (2011) also conclude with NAME that when the coastal measurement variability being dominated by local emissions, gradients in the mixing ratios between the coast and Bukit Atur can be expected for bromoform (despite the lifetime of bromoform: ≈ 14 days in the tropics).

Another possible explanation of the daily variations is that the height of the GC-MS inlet on the GAW tower, at 30 m, was within the boundary layer during the day and above it at night. If the boundary layer collapsed below the measurement inlet it may have been in contact with more marine influenced air in the free troposphere. In the early mornings clouds were often observed in the valleys beneath Bukit Atur (426m asl), this is a physical indicator that the site was above the boundary layer at night. If this is the case then the inlet would be in contact with air from aloft which is highly likely to have a

marine influence, and therefore contain more CHBr_3 and CH_2Br_2 . With this hypothesis it is difficult to explain why there is little marine influence in the canopy air, as Bukit Atur is situated approximately 50 km inland from the coast and the compounds have relatively long atmospheric lifetimes (14 days for CHBr_3 and 120 days for CH_2Br_2). While the rainforest may provide some sheer slowing down the movement of air from the coast, it would seem unlikely that with the influence of tropical storms the forest air could remain stagnant. However, very low wind speeds were recorded in the canopy relative to the cloud movement aloft.

NO_x measurements taken at Bukit Atur also suggest that the GAW tower was disconnected from the canopy at night (discussed further in Chapter 4, Section 4.3), but indicate that Bukit Atur lies above the nocturnal boundary layer in the residual layer (Pearson et al., 2010). A schematic representing this change in the boundary layer relative to the sampling site is presented in Figure 3.24. Pearson et al. (2010) observed a diurnal pattern in convective updrafts where an intense period of convective activity can be seen to exist between 09:00 and 15:00 local time, with a peak updraft velocity of $2.5 - 3 \text{ ms}^{-1}$.

Alternatively, a diurnal coastal source could produce the variations observed. As mentioned in Section 3.5 the transport time from the coast would be ≈ 10 hours: with a diurnal signal this would result in an anti-phase diurnal pattern, such as that seen in the CHBr_3 and CH_2Br_2 OP3-I data. The μDirac was running for a short period at the southeast coast, however, no diurnal pattern was reported. A diurnal coastal source provides a plausible explanation, but there is little evidence here to support this theory. Diurnal variations in CHBr_3 have been observed in subtropical and temperate macroalgae, with maximum release rates at midday: CHBr_3 production is generally reported to increase with irradiance (Carpenter et al., 2000; Goodwin et al., 1997).

As the daily variations of CHBr_3 and CH_2Br_2 during OP3-III are different to OP3-I, in the context of this hypothesis it would mean that either the boundary layer is no longer dropping below the inlet at night, which is unlikely, or there is a greater degree of mixing in general to result in the loss of daily variations that were seen in OP3 phase I. If the latter were the case then it may be that the drop off seen after the 19th July was a return

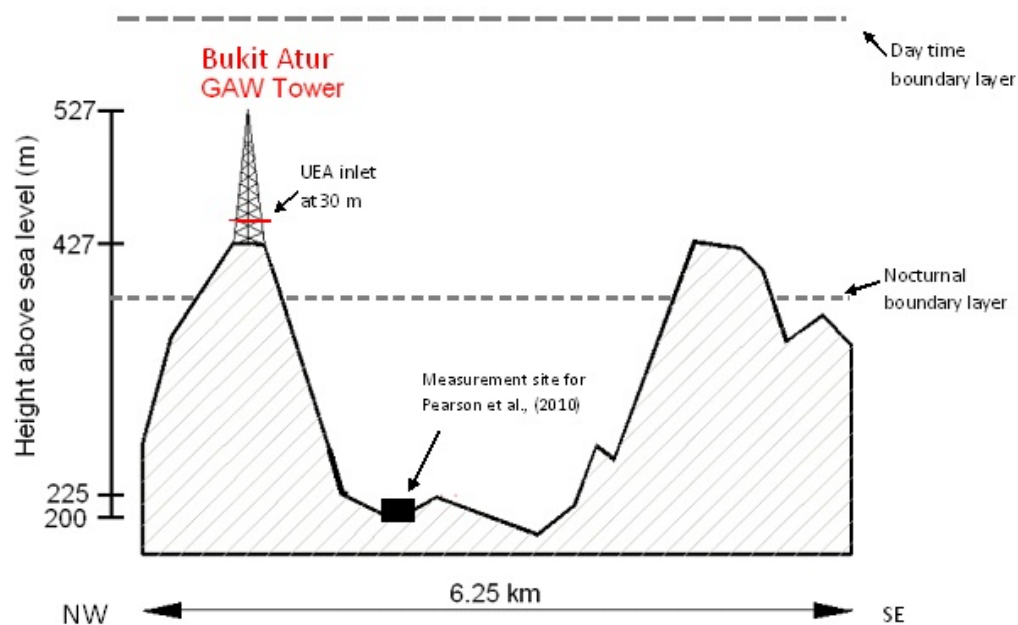


Figure 3.24: This figure is adapted from Pearson et al. (2010) who plotted the terrain to show the valley situation of their instrument. The dashed lines represent the nocturnal boundary layer situated below the sampling inlet and the daytime boundary layer above the sampling inlet. Pearson2010 plotted the terrain to convey the gradients involved around Bukit Atur.

to a more stratified atmosphere, or a result of the changes in wind direction.

The polybrominated compounds bromochloromethane (CH_2BrCl), dibromochloromethane (CHBr_2Cl), and dichlorobromomethane (CHCl_2Br) were included in the analysis at Bukit Atur during OP3-III. Figure 3.26 shows their time series for OP3-III. Both CHBr_2Cl and CHCl_2Br show the same decrease in mixing ratios after the 19th July that the CHBr_3 and CH_2Br_2 data exhibit. This correlation in the short lived brominated species supports the hypothesis of a change in air mass.

To investigate the enhancement 'events' in the data the ratio of the shorter lived CHBr_3 to the longer lived CH_2Br_2 has been plotted and shows an increase in CHBr_3 relative to CH_2Br_2 during this 'event' on the 28th April (Figure 3.25(a)), possibly reflecting an air mass which has been in more recent contact with a source of CHBr_3 (McKeen et al., 1990; McKeen and Liu, 1993; Yokouchi et al., 2005).

Transport time from sources will affect the measured mixing ratios, considering this the ratio of the shorter-lived CHBr_3 ($\tau \approx 14$ days) to CH_2Br_2 ($\tau \approx 120$ days) showed CHBr_3 to be elevated with respect to CH_2Br_2 . This is unlikely to be a result of the proximity of the measurement site to the known and shared macro algae source in the coastal waters, however, the rate at which the compounds are emitted from that source could be contributing to the relative elevation of CHBr_3 mixing ratios. It is reasonable to suggest that air measured on the 28th April was in recent contact with a different source of CHBr_3 . The mean mixing ratios for CHBr_3 and CH_2Br_2 are shown in Table 3.1 and compared to recent studies in Southeast Asia. Java Island, just south of Borneo, shows atmospheric mixing ratios of CHBr_3 similar to those seen in April-May in Borneo. The CH_2Br_2 mixing ratios Yokouchi et al. (2005) measured in Java in January are more comparable with OP3 measurements in July. The OP3 aircraft measurements averages for these polybromomethanes are similar to the ranges considered typical for the tropical boundary layer (Law et al., 2007).

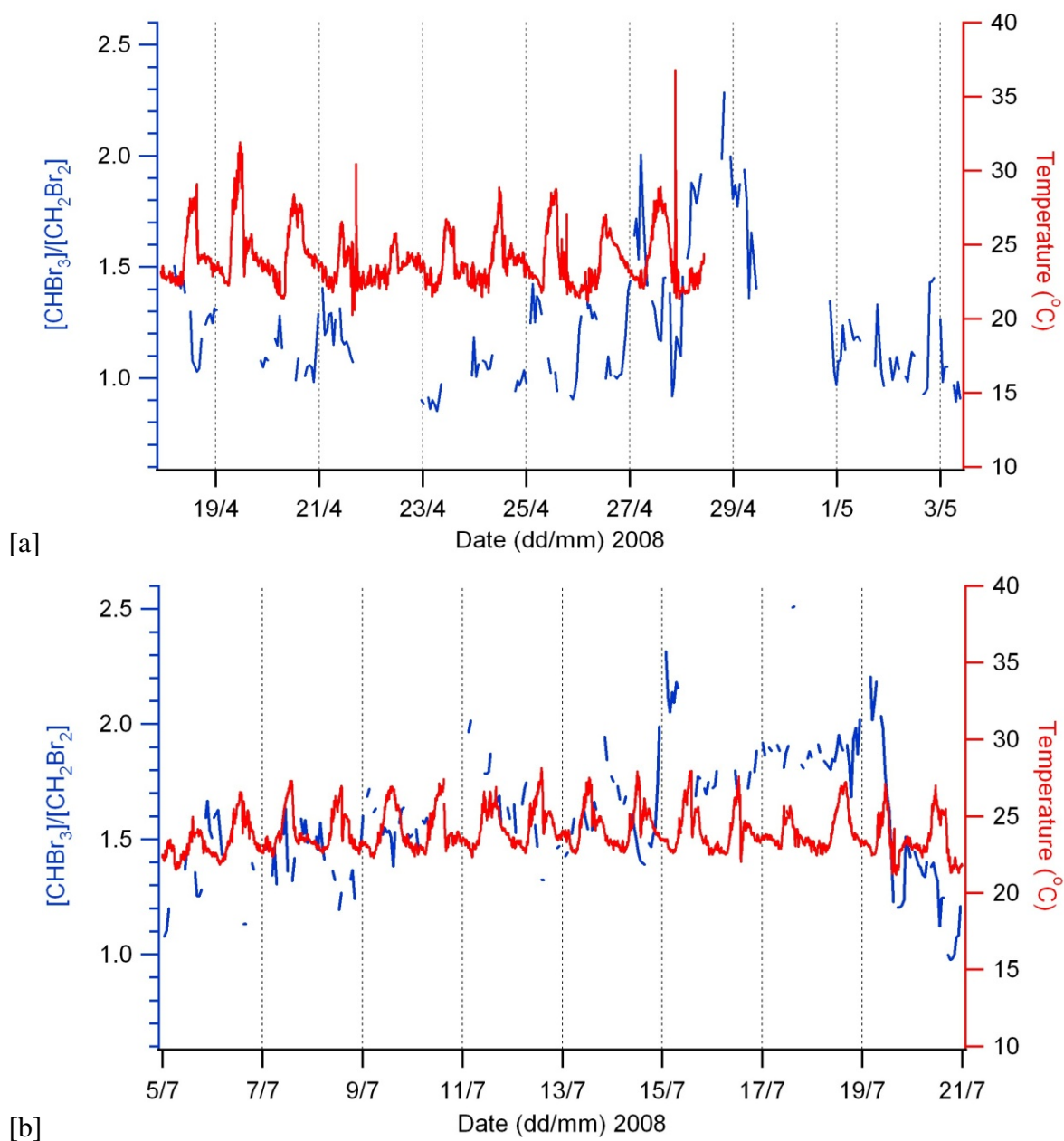


Figure 3.25: The time series of the ratio of bromform/dibromomethane $[\text{CHBr}_3]/[\text{CH}_2\text{Br}_2]$ for OP3 phase I (a) and OP3 phase III (b). Temperature data from 30 m on the tower shown as the red trace as a proxy for time of day.

Table 3.1: Mean mixing ratios (pptv) \pm 1 standard deviation from the mean from OP3-I and OP3-III ground based and aircraft campaigns and compared to the literature.

	CHBr ₃	CH ₂ Br ₂
	Mean \pm SD	Mean \pm SD
OP3-I, Bukit Atur	0.94 \pm 0.27	0.76 \pm 0.07
OP3-III, Bukit Atur	1.46 \pm 0.36	0.92 \pm 0.09
Java Island, Jan 2003 (Yokouchi et al., 2005)	0.9 \pm 0.4	0.9 \pm 0.2
Western Pacific, Jan-Dec 2003 (Yokouchi et al., 2005)	1.1 \pm 0.6	1.0 \pm 0.3
OP3-III, aircraft	1.43 \pm 0.53	0.89 \pm 0.41
mixing ratios considered typical for the tropical boundary layer (Law et al., 2007)	1.1-1.83	1.07-1.33

The spatial distribution of bromochloromethane (CH₂BrCl), shown in Figure 3.27, indicates mixing ratios \geq 0.6 over the landmass of Sabah and off the northwest coast. Figure 3.28 gives a clearer picture of the CH₂BrCl aircraft data. For the boundary layer measurements, the highest median and upper quartile of the data was observed in the samples over the northwest coast. The medians for the other three land cover types were \approx 0.5 pptv, which is the median value held to typically represent the marine boundary layer (Law et al., 2007). The CH₂BrCl data for the free troposphere again shows the northwest coast to yield the highest median of the data, but the data over the oil palm plantations produced the highest upper quartile and 90% outlier. The boundary layer data over the oil palm has a higher median than that of the free troposphere, but a slightly

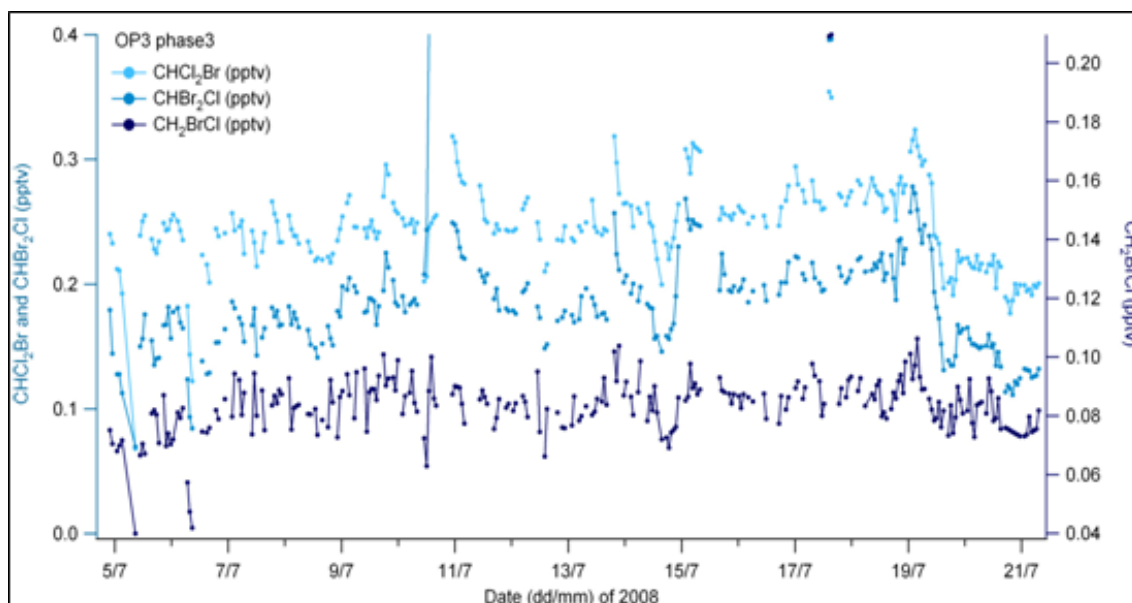


Figure 3.26: OP3-III time series of CHCl_2Br (light blue), CHBr_2Cl (mid blue) and CH_2BrCl (dark blue).

lower upper quartile value. The oil palm upper quartile value is more representative of the upper quartile in the northwest coast boundary layer data: possibly the air is being uplifted from the northwest coast to the free troposphere over the landmass. However, the back trajectories for samples ≥ 0.6 pptv in the free troposphere over the oil palm (not shown) approach predominantly from the south and the east of Sabah. This suggests a source region to the east or south of Sabah in a local where data was not collected.

Figure 3.29 shows that the data collected over the areas of oil palm and the southeast coast yielded the highest mixing ratios of dibromochloromethane (CHBr_2Cl). The box plots for the CHBr_2Cl data confirm this: in the boundary layer the highest medians are observed in the oil palm and southeast coast data. In some of the boundary layer measurements over the coasts the CHBr_2Cl was below the limit of detection (0.08 pptv). The CHBr_2Cl data over the oil palm had the highest upper quartile of the boundary layer data. The medians of the CHBr_2Cl data are below the typical median of CHBr_2Cl in the marine boundary layer (Law et al., 2007). The interquartile range for CHBr_2Cl over the oil palm is comparable in the boundary layer and above it in the free troposphere.

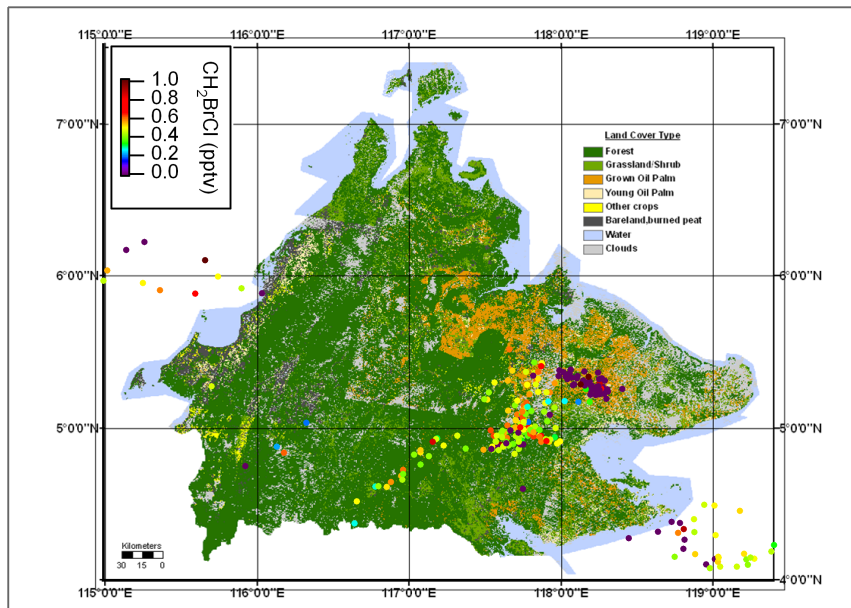
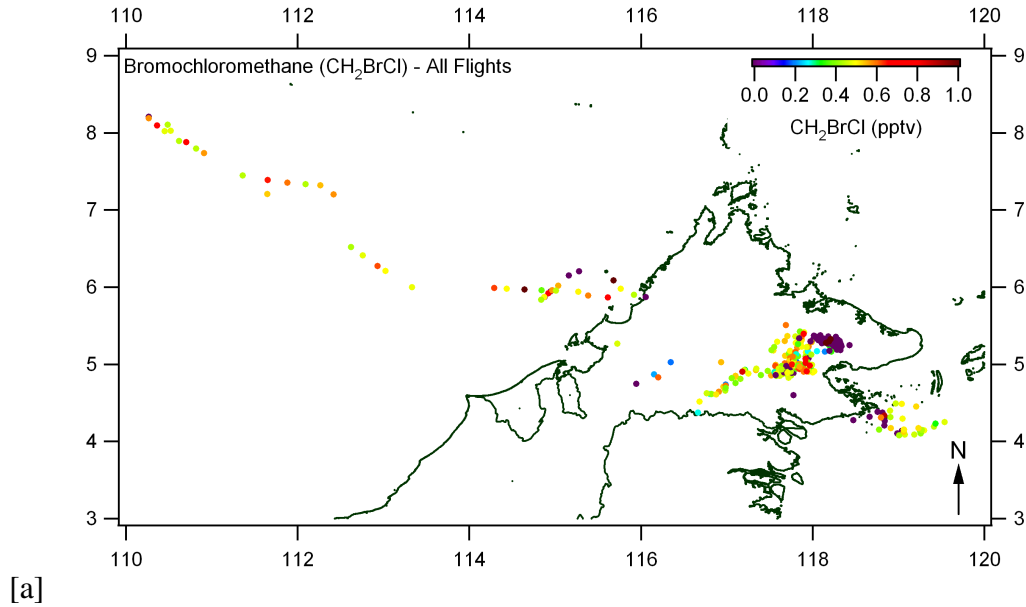


Figure 3.27: (a) Shows a map of bromochloromethane mixing ratios measured in the WAS over Sabah and surrounding coast. (b) Land cover map of Sabah with the bromochloromethane WAS measurements overlaid. The data points in both plots are coloured by bromochloromethane mixing ratios.

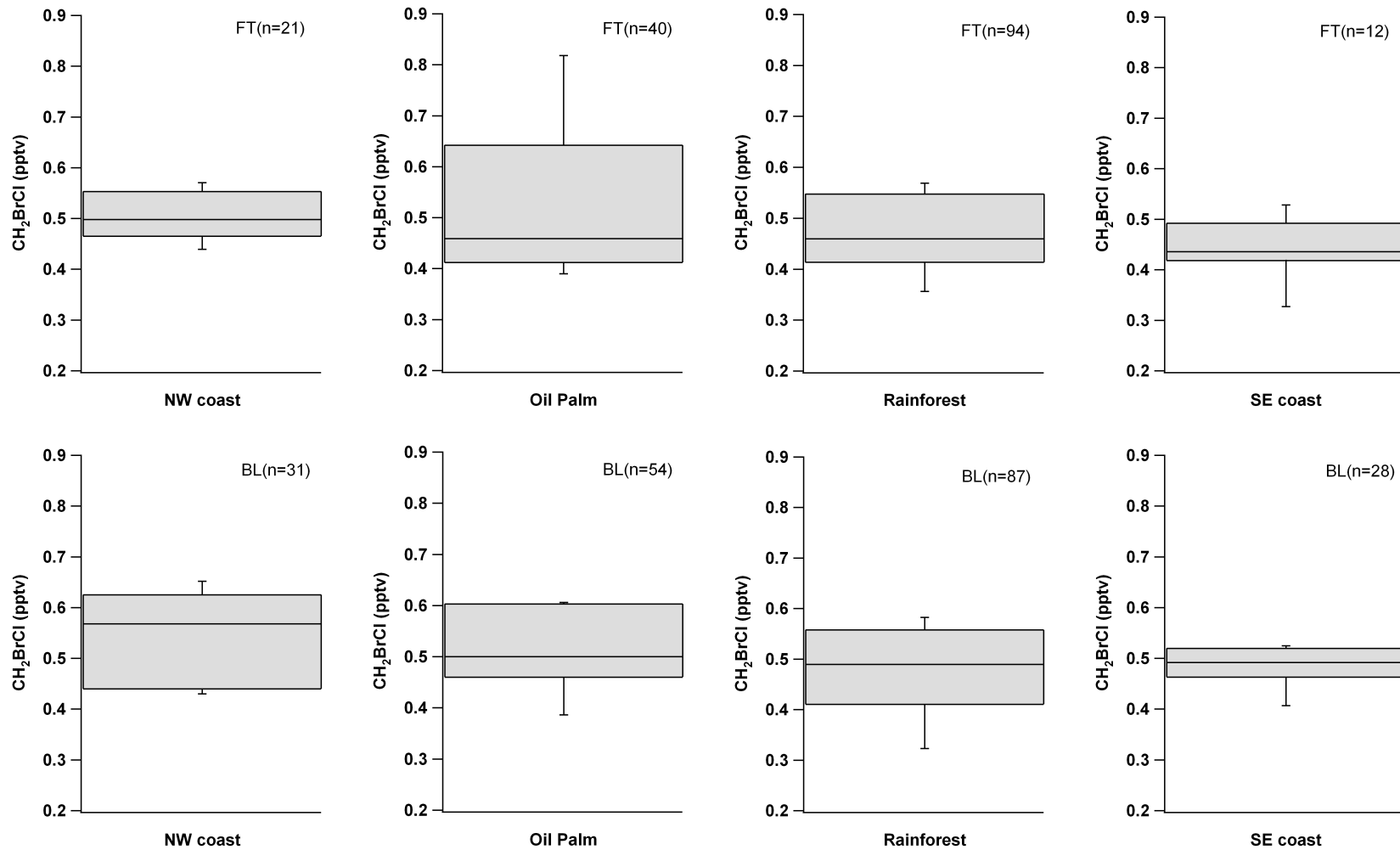


Figure 3.28: Box plots showing the bromochloromethane mixing ratios over the oil palm plantations and the northwest coast off Sabah. The line represents median, box top and bottom represent 75th percentile and 25th percentile respectively and the whiskers represent 90% and 10% of the data. FT= free troposphere; BL= boundary layer.

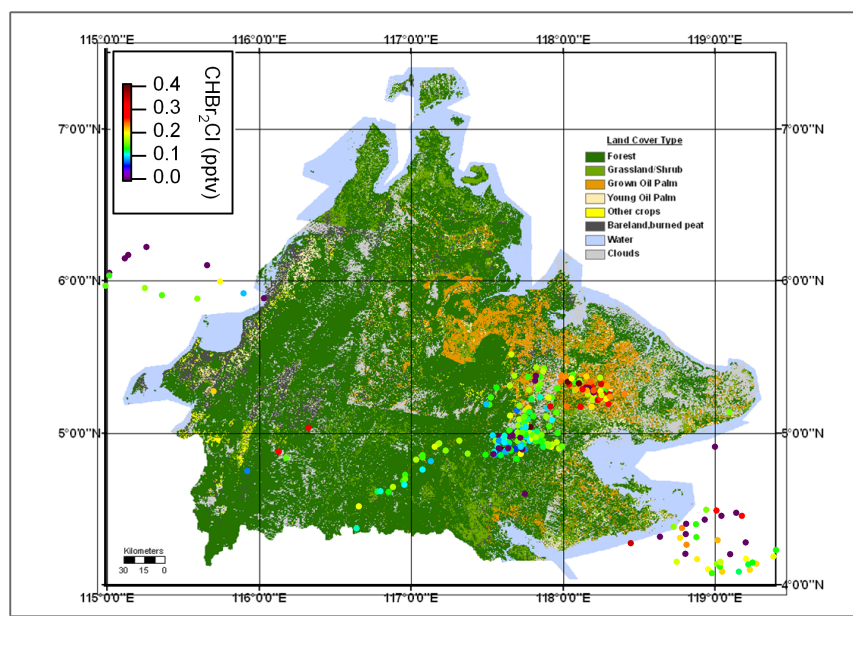
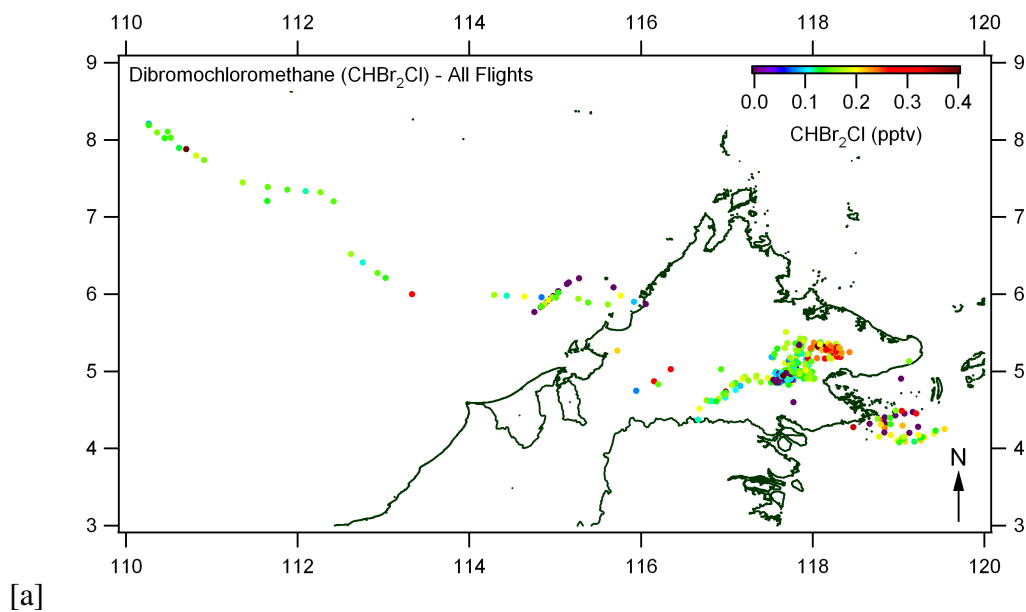


Figure 3.29: (a) Shows a map of dibromochloromethane mixing ratios measured in the WAS over Sabah and surrounding coast. (b) Land cover map of Sabah with the dibromochloromethane WAS measurements overlaid. The data points in both plots are coloured by dibromochloromethane mixing ratios.

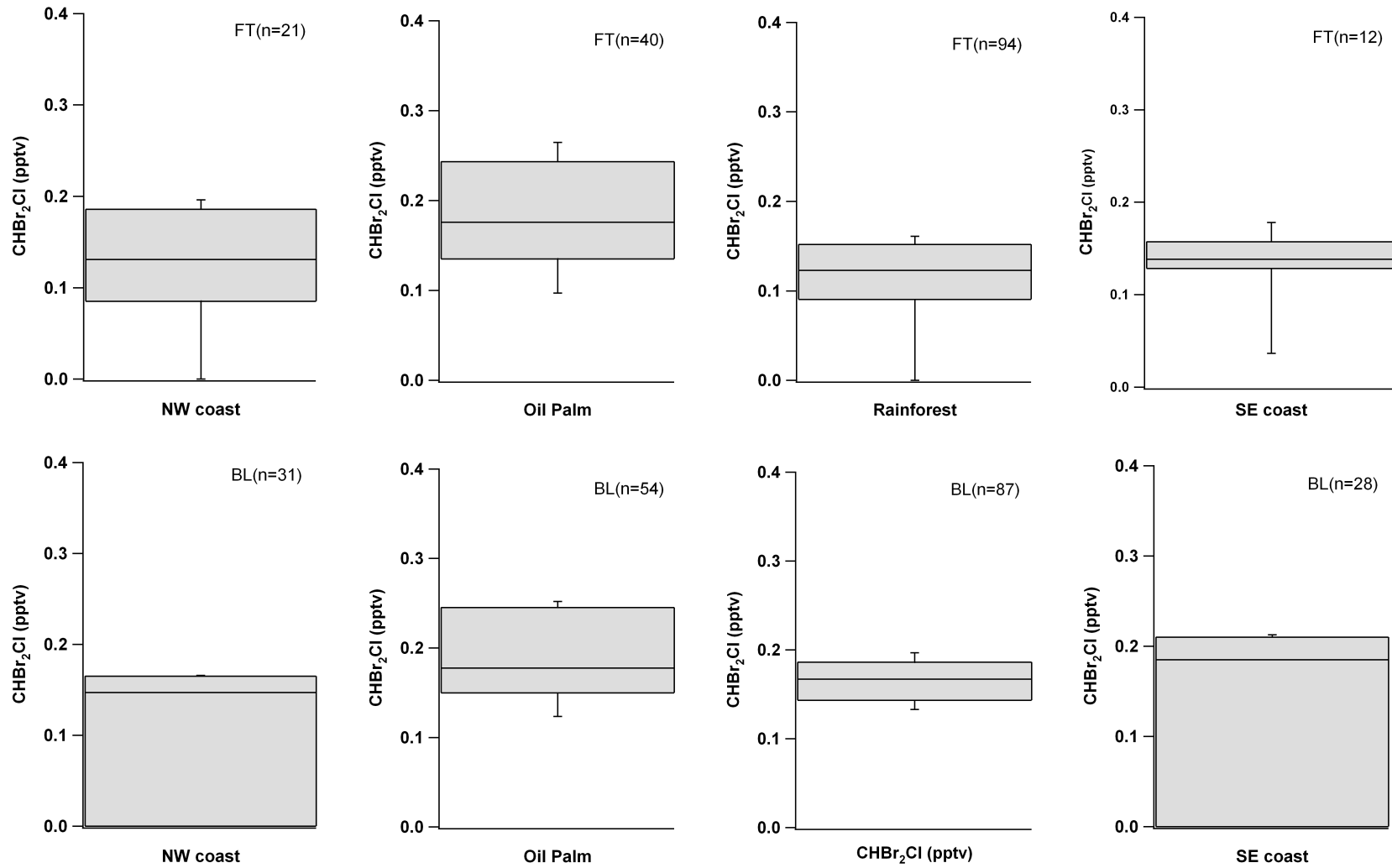


Figure 3.30: Box plots showing the dibromochloromethane mixing ratios over the oil palm plantations and the northwest coast off Sabah. The line represents median, box top and bottom represent 75th percentile and 25th percentile respectively and the whiskers represent 90% and 10% of the data. FT= free troposphere; BL= boundary layer.

3.6.1 Bromine budget

Table 3.2: Break down of the bromine budget for the OP3 campaigns. Mean mixing ratios in pptv are presented, with their percentage contribution to the bromine budget for that measurement period in parentheses. The total bromine from the short lived brominated species (excluding CH₃Br) is presented in the bottom row. The tropospheric range of CH₃Br is included for comparison, from the AGAGE, NOAA and SOGE networks as reported in Montzka et al. (2010). The ranges of tropospheric mixing ratios for CH₂Br₂, CHBr₃ and CHCl₂Br are from Law et al. (2007).

	Bukit Atur, OP3-I	Bukit Atur, OP3-III	Aircraft WAS, OP3-III	Range from literature
CH ₃ Br	11.5 (86%)	6.8 (72%)	7.7 (55%)	7.3-8.1
CH ₂ Br ₂	0.76 (6%)	0.91 (10%)	1.78 (13%)	0.8-3.4
CHBr ₃	0.94 (7%)	1.5 (16%)	4.2 (14%)	0.6-3.0
CHCl ₂ Br	0.21 (1%)	0.25 (2%)	0.23 (2%)	0.12-0.6
Sum of obs. Br excluding CH ₃ Br	6.2	6.6	7.2	

Table 3.2 contains a break down of the brominated species measured in all three OP3 campaigns. Methyl bromide dominated the bromine budget, this is to be expected with its varied sources and long atmospheric residence time of 0.7 years. Out of the short lived bromocarbons measured during OP3, bromoform contributed to the greatest degree. These short lived bromocarbons constitute 14% of the bromine budget in OP3-I, but their contribution is doubled in the ground based OP3-III campaign. The ground based and aircraft measurements of OP3-III show a similarly apportioned bromine budget.

The organic bromine budgets calculated in Table 3.2 represent the bromine available that could potentially contribute to the stratospheric deficit of 3-5 pptv Br. The budgets calculated fall within the reported mixing ratios of organic bromine from the short lived compounds are (1.77-4 pptv) in the tropical upper troposphere (1012 km), with a mean

reported as 3.5 pptv (Montzka et al., 2010). The organic bromine from short lived compounds reported by Montzka et al. (2010) consists mostly of CH_2Br_2 and CHBr_3 with smaller amounts of bromochloromethanes: this is supported by the budgets presented here from OP3 data.

3.7 Chloroform and methyl chloroform

Figure 3.31 shows the chloroform (CHCl_3) data mapped over Borneo. From this plot the highest mixing ratios of CHCl_3 are apparent over the landmass of Sabah, in particular the oil palm region to the north of Bukit Atur. When the CHCl_3 data is categorised in the box plots in Figure 3.32 it can be seen that the oil palm plantation yields the highest median (9 pptv) and upper quartile (10.2 pptv) of the boundary layer data. The medians of the coast CHCl_3 data were lower than either terrestrial category. The northwest coast data in the boundary layer shows a median of ≈ 7 pptv compared to ≈ 8 pptv for the southeast coast. The CHCl_3 measurements from the free troposphere off the northwest coast contained higher mixing ratios in the 75th percentile (≈ 7.8 pptv) than the boundary layer measurements, though the medians of the boundary layer and free troposphere were comparable at ≈ 7 pptv. This suggests CHCl_3 from the oil palm and terrestrial regions might have been transported aloft. The back trajectories and wind direction during OP3-III (predominantly from the east and south east) support this uplift hypothesis.

Laternus et al. (2002) report forests as contributing to the release of CHCl_3 into the environment. Forests are only a minor source in the total biogenic flux of CHCl_3 , contributing less than 1% to the annual global atmospheric input (Laternus et al., 2002). However, it should be noted that these conclusions are based on data from Northern temperate forests only. The large tropical forest areas may provide an input of CHCl_3 to the atmosphere (Laternus et al., 2002). A subsequent study reported CHCl_3 fluxes from tropical vegetation (Gebhardt et al., 2008), but the contribution has not been quantified in a global context as yet. The elevated mixing ratios seen over the terrestrial regions of Sabah, support and develop the work of Laternus et al. (2002) and Gebhardt et al. (2008), by suggesting that the oil palm plantations, and to a lesser extent the rainforest, of Sabah are source regions of chloroform.

The methyl chloroform (CH_3CCl_3) data (Figure 3.33) shows a spread of high mixing ratios across most regions of sampling. Figure 3.34 shows the medians for all four categories both boundary layer and free troposphere to be similar. The upper quartile of the boundary layer oil palm data is very slightly higher than the other categories, but the dif-

ference is not significant. The CH_3CCl_3 in the free troposphere over the northwest coast has the highest median and upper quartile, but again the difference is very slight.

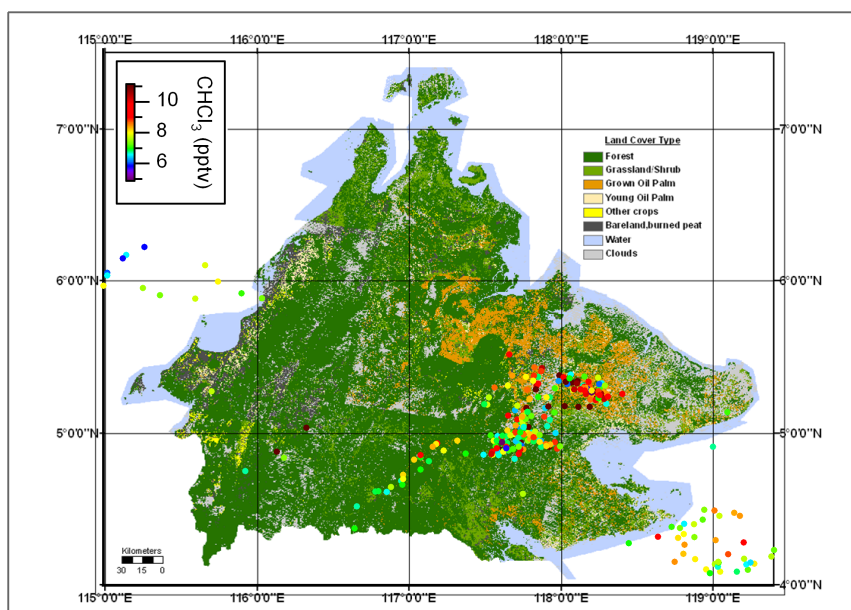
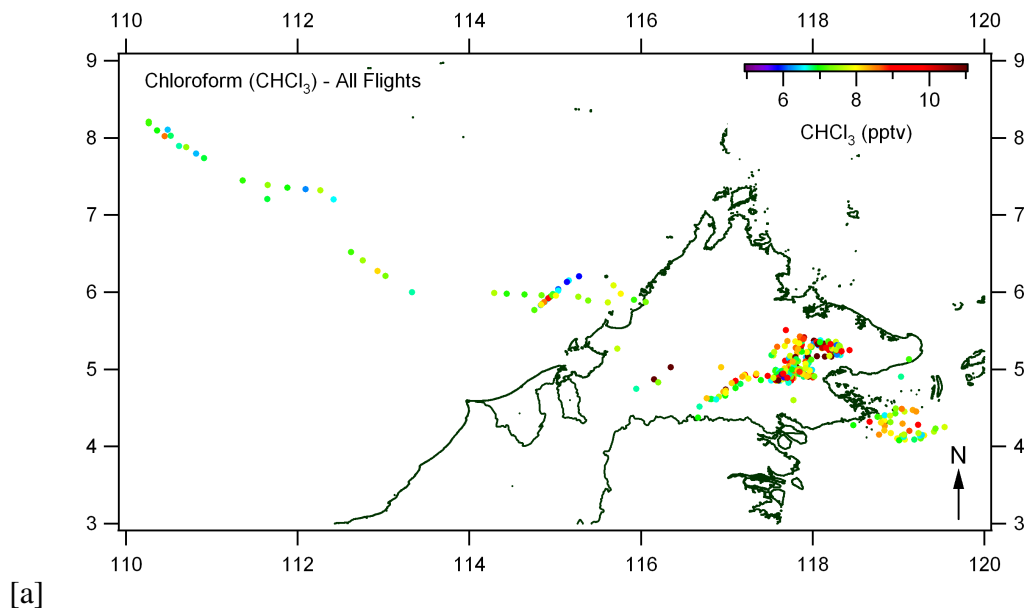


Figure 3.31: (a) Shows a map of chloroform mixing ratios measured in the WAS over Sabah and surrounding coast. (b) Land cover map of Sabah with the chloroform WAS measurements overlaid. The data points in both plots are coloured by chloroform mixing ratios.

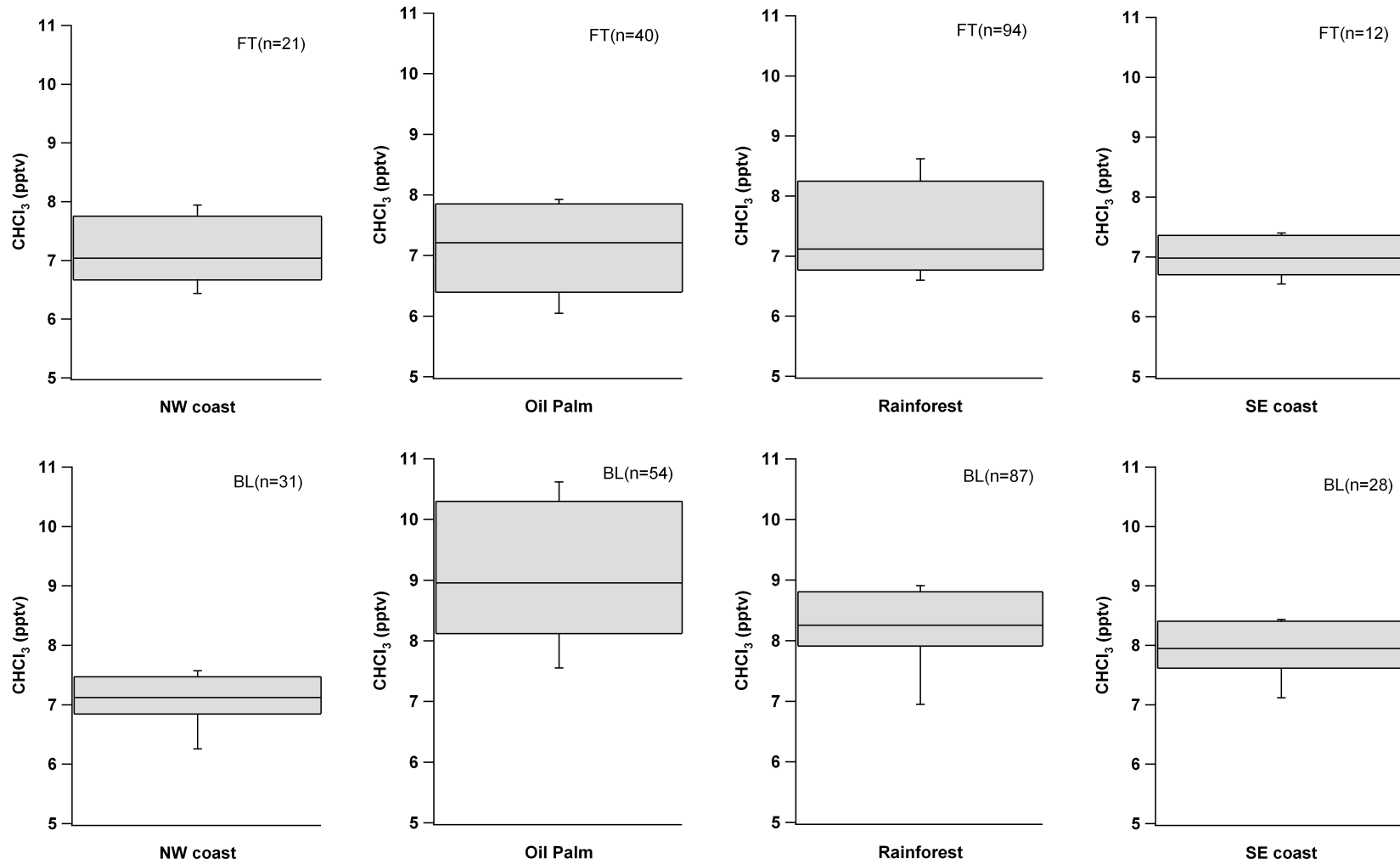


Figure 3.32: Box plots showing the chloroform mixing ratios over the oil palm plantations and the northwest coast off Sabah. The line represents median, box top and bottom represent 75th percentile and 25th percentile respectively and the whiskers represent 90% and 10% of the data. FT= free troposphere; BL= boundary layer.

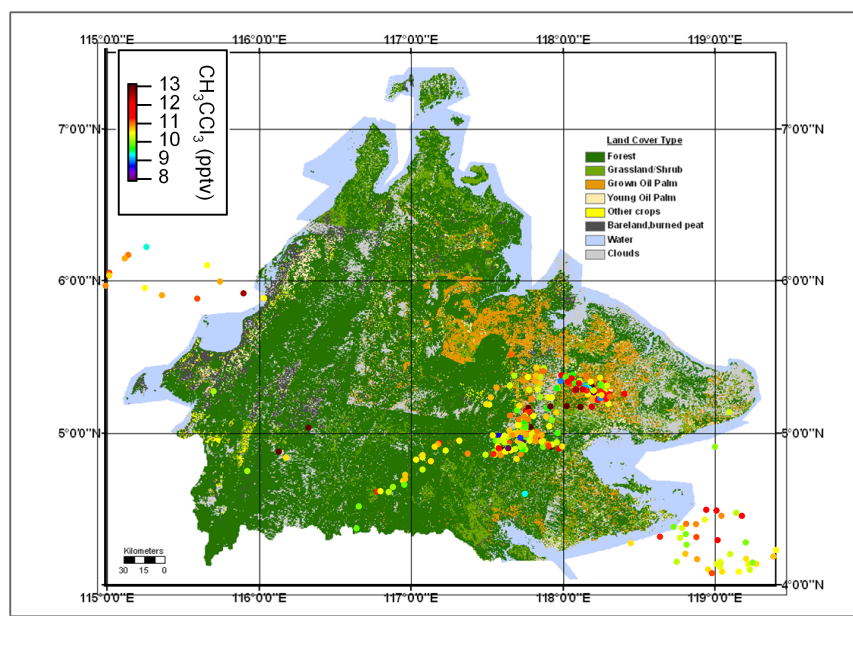
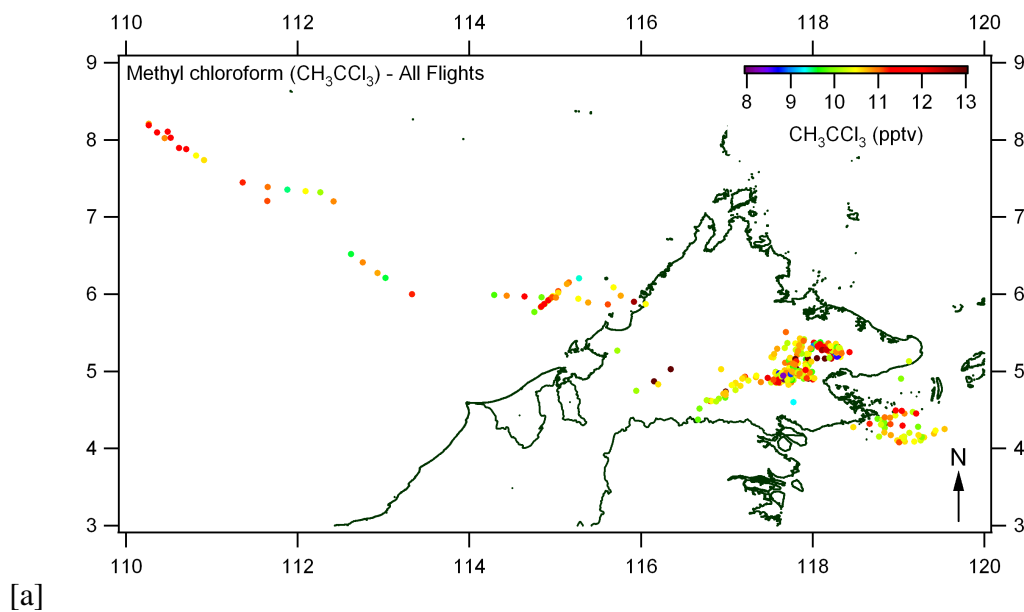


Figure 3.33: (a) Shows a map of methyl chloroform mixing ratios measured in the WAS over Sabah and surrounding coast. (b) Land cover map of Sabah with the methyl chloroform WAS measurements overlaid. The data points in both plots are coloured by methyl chloroform mixing ratios.

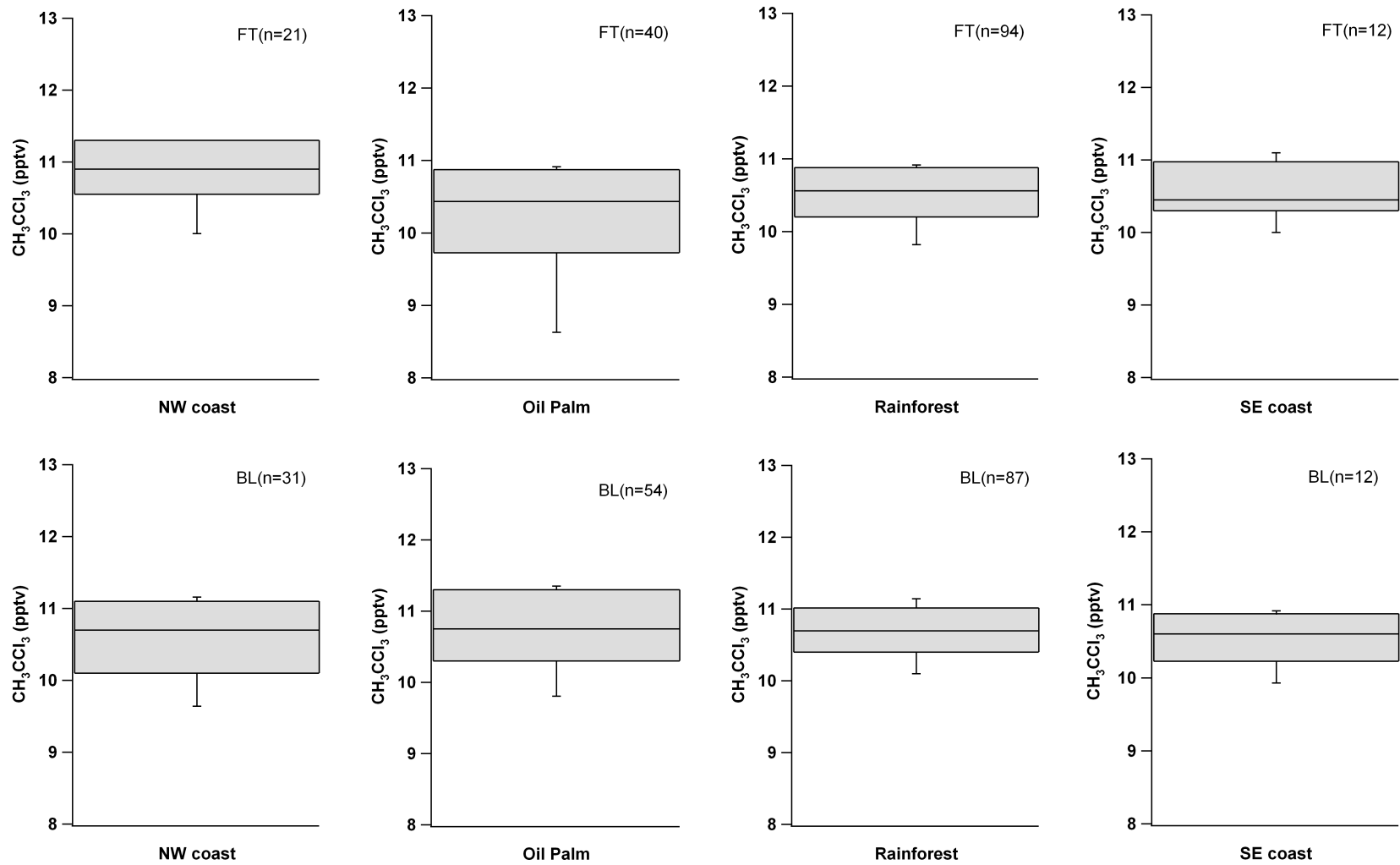


Figure 3.34: Box plots showing the methyl chloroform mixing ratios over the oil palm plantations and the northwest coast off Sabah. The line represents median, box top and bottom represent 75th percentile and 25th percentile respectively and the whiskers represent 90% and 10% of the data. FT= free troposphere; BL= boundary layer.

The time series data for CHCl_3 begins part way throughout OP3-I due to an error in the mass spectrometry method that was rectified on the 24th April 2008. The CHCl_3 mixing ratios are slightly lower in OP3-III than OP3-I and remain lower than the values observed in the aircraft data (Figure 3.31). During the first campaign the ground measurement site was influenced by air masses from a variety of directions, however, in OP3-III the wind arrived at Bukit Atur predominantly from an east and southeast direction (Section 3.3). It seems likely that during OP3-I Bukit Atur was being influenced by air masses that had passed over the oil palm plantation. The 10% outlier of the CHCl_3 aircraft data in Figure 3.32 is more comparable with the ground site data. As suggested earlier with reference to CHBr_3 , there may be a shear effect of the forest. Assuming that the oil palm is a source region of CHCl_3 , the forest may prevent the CHCl_3 signal from the oil palm getting to the Bukit atur ground site.

The mixing ratios of CH_3CCl_3 during OP3-I (11.8 ± 0.9 pptv) are also higher than those in OP3-III (10.6 ± 0.7 pptv). The mean of the CH_3CCl_3 data from OP3-III is comparable with the medians of the aircraft data (Figures 3.33 and 3.34). It appears that during OP3-III CH_3CCl_3 was fairly ubiquitous. The mean mixing ratios from OP3 are comparable with the the range of 10.7-11.7 pptv CH_3CCl_3 from ground based measurements reported in Montzka et al. (2010).

Neither the CH_3CCl_3 or CHCl_3 data for OP3-I share the enhancement 'events' seen in the time series of the brominated compounds: notably the 'event' on the 28th is absent from these time series. However, the CHCl_3 time series for OP3-III seems to exhibit the drop off in mixing ratios observed in the brominated compounds around the 19th July.

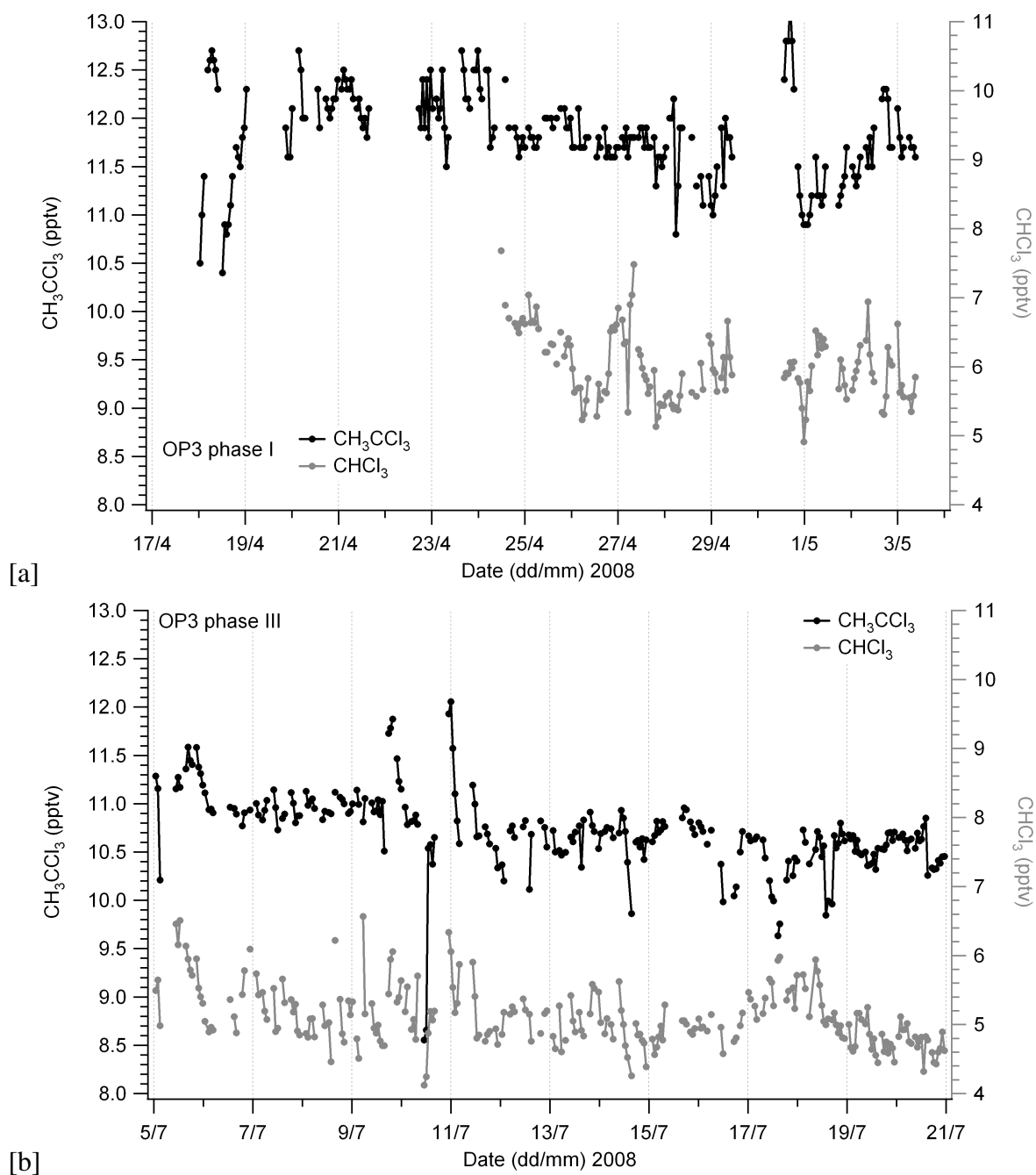


Figure 3.35: Time series of chloroform (grey) and methyl chloroform (black) data for OP3 phase I (a) and OP3 phase III (b). All mixing ratios are in parts per trillion by volume, measured on a GC-MS in negative ion mode.

3.8 Back trajectories and source attribution analysis of select halocarbons

In this section the result of some collaborative work with the University of Manchester is presented. A type of back trajectory analysis was performed, generating figures such as Figures 3.36 and 3.37. The method described in Robinson et al. (2011) (see Appendix) assesses the dependence of a species on air mass history. These figures are generated for a given measurement, by constructing a geographical grid using a cell size of $0.1^\circ \times 0.1^\circ$. The measured value at Bukit Atur at the time of arrival of a given trajectory is added to the grid cell that contains each trajectory point. Doing this for all trajectories and dividing by the total number of trajectory points in each cell gives the mean value measured at the ground site for an air mass that has passed over that cell. These plots are referred to as mean value maps.

The CHBr_3 (Figure 3.36) and CH_2Br_2 mean value maps show similar profiles ($r^2 = 0.90$) confirming that these compounds are well correlated in the atmosphere as previously shown by Butler et al. (2007), Yokouchi et al. (2005) and Zhou et al. (2008). CHBr_3 and CH_2Br_2 show elevated levels over coastal and marine regions, this is consistent with other studies which have shown CHBr_3 and CH_2Br_2 to be produced by macro-algae (Carpenter et al., 2000; Goodwin et al., 1997; Quack et al., 2007). The region of seaweed cultivation in the southeast coast is reflected in the high mixing ratios seen in air masses from this region.

The methyl iodide mean value map (Figure 3.37(a)) is similar to those of the poly-brominated compounds (Figures 3.36), although, there are some differences in features (mean value map correlations of $r^2 = 0.65$ and $r^2 = 0.64$ for CHBr_3 and CH_2Br_2 respectively). The methyl iodide map shows high values to be predominantly attributable to a marine source. By classifying the trajectories used to generate these mean value maps into marine, terrestrial and north-easterly etc. it has been established that the marine cluster yields the highest mean methyl iodide values (Figure 3.38). This is consistent with whole air samples collected in the boundary layer during the OP3 flight campaign (Figure

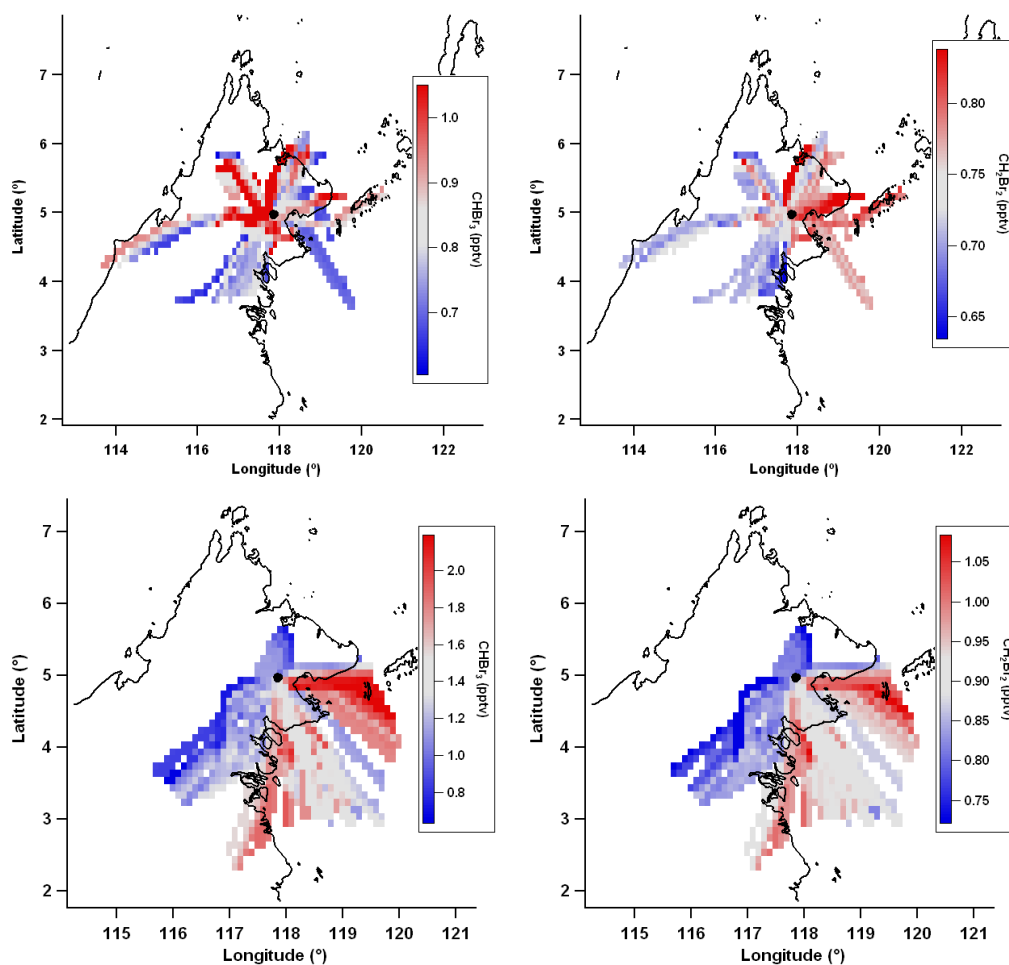


Figure 3.36: Mean value maps for CHBr_3 and CH_2Br_2 during OP3 phase I (top) and III (bottom). The maps were generated using back trajectories calculated through BADC using the ECMWF model.

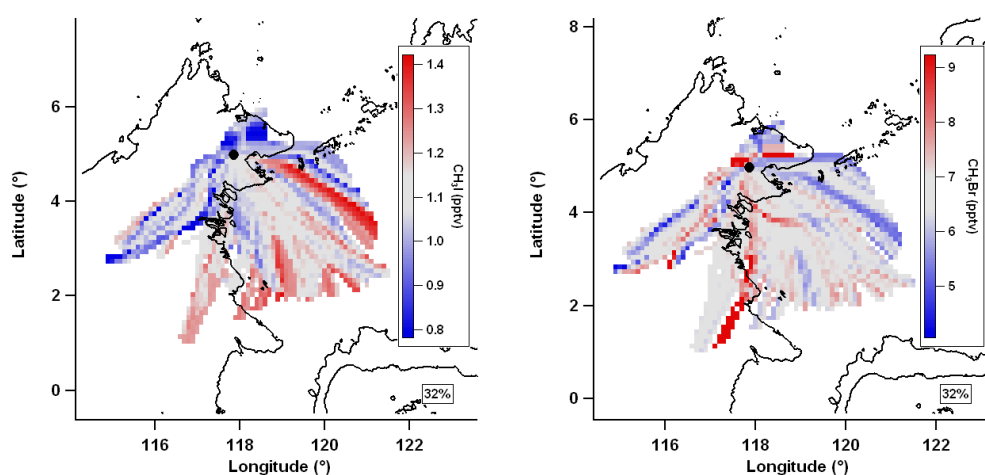


Figure 3.37: Mean value maps for methyl iodide (a) and methyl bromide (b) during OP3 phase III. The maps were generated using back trajectories calculated through BADC using the ECMWF model.

3.11). The pattern of high values seen over the sea in the methyl iodide mean value map is similar to that seen in the polybrominated compound mean value maps. In particular the methyl iodide and polybrominated mean value maps both show a region of high values off the coast to the immediate east of Bukit Atur. This feature extends east out to the southern tip of Bongao island (5 °N, 120 °E) where it broadens off to the south east. This shared feature suggests a co-located source of methyl iodide and the polybrominated compounds, possibly even the same source. The most likely source would be macro algae which has been shown to produce all three of these compounds (Carpenter et al., 2000; Manley et al., 1992). Another study observed correlations between methyl iodide and these polybrominated compounds, but noted the inconsistency of their correlation, suggesting different production mechanisms for the methyl iodide and polybrominated compounds (Butler et al., 2007). There is a small feature of high values to the south west of Bukit Atur (approx. 3-4 °N, 115.5-116.5 °E), which is not shared with the polybrominated compounds. This feature is unlikely to be transported from a marine source, therefore suggesting a terrestrial input from that region. This is plausible as methyl iodide is known to have a mixture of marine and terrestrial sources (Bell et al., 2002; Sive et al., 2007; Smythe-Wright et al., 2006). Methyl iodide has also been reported to have biomass burning sources (Cox et al., 2005; Mead et al., 2008a) which may contribute to the signal seen in that area. Although MODIS fire count plots do not support this (not shown), small fires and smoke plumes were observed from the FAAM BAe-146 during the OP3 aircraft campaign which are not shown in the MODIS plots, therefore a small scale biomass burning event cannot be ruled out as having been responsible for the signal to the south west of Bukit Atur.

In contrast to methyl iodide and the other brominated halocarbons presented here the waters immediately east of Bukit Atur and to the south east of Bongao island do not appear to be a productive region for methyl bromide (Figure 3.37(b)). There is clearly some marine contribution, predominantly from the coastal zone south of Sabah included in the extent of these maps, which is consistent with known marine sources of methyl bromide such as macro algae (Baker et al., 2001; Cox et al., 2005). Higher values (8-9 pptv) are

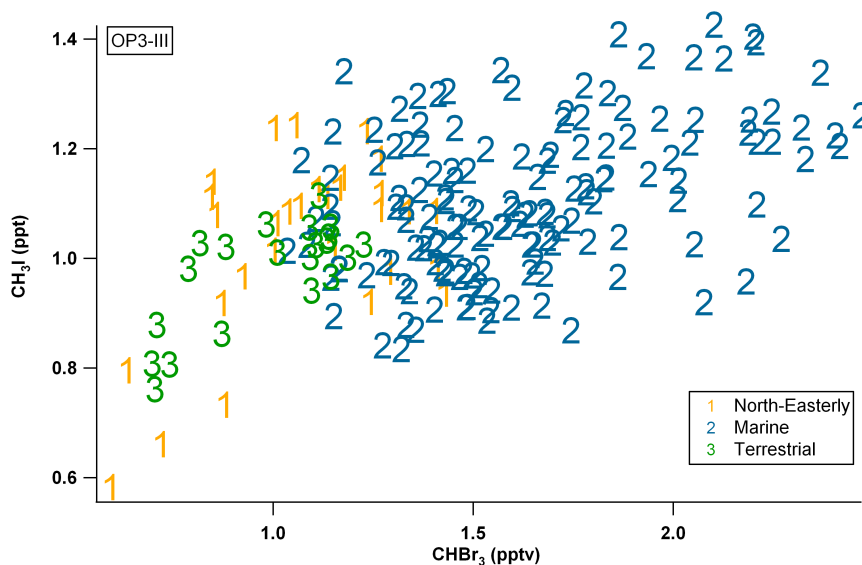


Figure 3.38: Methyl iodide and bromoform data from OP3-III coloured by trajectory classifications defined in Robinson et al. (2011).

seen over an area to the north of Bukit Atur (5.4-6 °N) covering both land and coastal areas: this is by far the strongest source region for CH₃Br under this analysis, this finding would warrant a further focussed study. As it is currently unknown whether oil palm is a source of methyl bromide, associated activities within the oil palm plantations such as biomass burning, a known source of methyl bromide, may contribute to the localised high values. That said, a coastal source cannot be discounted as responsible for this feature, possibly a macro algae source.

3.9 Conclusions

After Yokouchi et al. (2002) measured methyl chloride at leaf level (0.9 Tg yr^{-1}) and ambient mixing ratios (1,000 - 3,500 pptv) in the tropical vegetation section of the Tropical Rainforest Glasshouse in Tsukuba Botanical Gardens and found the tropical vegetation to be an apparent strong source of methyl chloride, it was expected that similar findings would be observed in real tropical forest environments. While the findings from OP3 show higher than the atmospheric background levels of methyl chloride, neither the mixing ratios from Bukit Atur nor the aircraft are comparable with those seen by Yokouchi et al. (2002) or Blei et al. (2010) who report $19 \text{ ng h}^{-1}\text{g}^{-1} \text{ CH}_3\text{Cl}$ and $0.4 \text{ ng h}^{-1}\text{g}^{-1} \text{ CH}_3\text{Br}$ from Malaysian trees. This discrepancy between leaf-level measurements and canopy-level measurements suggests that the methyl chloride is being used up by some other organism in the rainforest environment or that branch enclosure/ chamber techniques do not provide a sufficient representation of the natural environment. Greater understanding of why plants emit methyl halides could also assist our understanding of what is happening to the methyl chloride in the rainforest and why the signal is lost above it.

The organic bromine budgets calculated in Table 3.2 show that there is 6-7 pptv organic Br available in addition to methyl bromide, in the atmosphere over the landmass and seas of Sabah, to potentially contribute to the missing 3-5 ppt stratospheric Br.

The southeast coast appears to be a source region for methyl bromide, methyl iodide and the short lived bromocarbons. The seaweed farms of the southeast coast are likely to be the source, supporting the work of Baker et al. (2001), Yokouchi et al. (2005) amongst others, who reported high mixing ratios of these compounds from macroalgae.

Data collected in the boundary layer over the oil palm plantations show the highest mixing ratios of methyl chloride and chloroform. As the oil palm fluxes are unknown, it is difficult to state what contribution the oil palm itself has to the observed mixing ratios of methyl chloride and chloroform. If the oil palm plantations are a source region for methyl chloride and chloroform there is further difficulty in saying what portion of that source is from natural sources within the oil palm plantations and what portion of these mixing ratios is attributable to anthropogenic activities within the oil palm plantations. It may be

the case that these sources are mutually exclusive.

The daily variations in the OP3-I time series data could be explained by a diurnal coastal source, however, in the absence of data to support that hypothesis the position of the boundary layer relative to the sampling point may be the predominant influence creating the observed variations in mixing ratios.

Periods of elevation, greater than the daily variations were found to be associated with air mass changes. Both the event on the 28th April in OP3-I and the decline in mixing ratios after the 19th in OP3-III were evident in the time series of the brominated halocarbons.

The oil palm plantations showed the highest mixing ratios of chloroform in the upper quartile (9-10 pptv). The methyl chloroform measurements in the aircraft data were consistently lower quartile at ≈ 10 pptv and the upper quartile at ≈ 11 pptv. The time series for methyl chloroform also showed little variation in the values measured.

In summary, the main factors affecting the variations observed at Bukit Atur are the nature and location of compound sources and how the meteorology changes influencing the site with air masses from source rich or depleted regions. The physical properties of the boundary layer also play a key part in understanding the data at this site as the GAW tower at Bukit Atur remains above the nocturnal boundary layer and so is disconnected from the residual layer. The complexity of the mountainous and forest environment complicate the interpretation of the data, but the influence of the above factors remain and are likely to be applicable to other compounds measured in the OP3 periods.

3.10 Further work

An underlying problem here is that the apparent marine source(s) cannot be definitively pinpointed. Concurrent measurements, for a period of weeks, at a range of coastal sites would improve understanding of the supposed marine source. Likewise, measurements in an oil palm plantation would be greatly beneficial. In this way rough calculations could be done to appoint source contributions.

Comprehensive mapping of the macroalgae source regions would be a great asset to

studies of this kind where the predominant known source is macro algae. The current seaweed maps of Malaysia are very poor in detail and undoubtedly do not cover all the seaweed farming sites and naturally occurring seaweed areas.

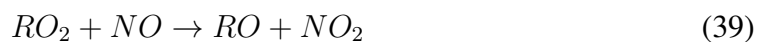
Chapter 4

C₁-C₄ Alkyl nitrate atmospheric composition over Borneo

4.1 Introduction

4.1.1 Formation of alkyl nitrates

Alkyl nitrates are secondary products of hydrocarbon (RH) oxidation. Whereby hydrocarbons are oxidised by the hydroxyl radical (OH), forming organic peroxy radicals, which can then react in the presence of nitrogen oxides (NO_x=NO+NO₂) to produce alkyl nitrates (Equations 37 to 40).



or



The production of alkyl nitrates from their 'parent' hydrocarbons has been well studied and their relationship used to indicate air mass age (Bertman et al., 1995; Blake et al., 2003a; Reeves et al., 2007; Simpson et al., 2003; Worton et al., 2010). Atlas

et al. (1993) proposed an alternative source to the breakdown of parent hydrocarbons, an oceanic source of alkyl nitrates to the atmosphere. Subsequent studies have supported this idea finding C₁ONO₂ to have a significant oceanic source (Blake et al., 1999; Chuck et al., 2002; Dahl and Saltzman, 2008). Currently there is no known biological mechanism for the production of alkyl nitrates in aquatic systems, although it has been proposed that the free radical reaction of organic peroxy radicals and NO could form alkyl nitrates in aqueous phase (Dahl et al., 2003; Moore and Blough, 2002).

Atmospheric C₁ONO₂ and C₂ONO₂ are frequently well correlated with marine halo-carbons such as bromoform and thus they have been concluded to have a marine source. Chuck et al. (2002) suggested bacterial and/or algal processes produce C₁ONO₂ and C₂ONO₂ as their alkyl nitrate observations coincided with the chlorophyll maximum in seawater depth profiles. Similarities were also observed in the profiles of C₂ONO₂ and the dissolved nutrient NO₃⁻ which may indicate a role for NO₃⁻ in the production of C₂ONO₂. Worton et al. (2010) hypothesised a nighttime source of C₁ONO₂ from NO₃ chemistry in the residual layer based on their observations of a morning maximum in the diurnal profile of C₁ONO₂.

Alkyl nitrates are a component of the "odd nitrogen" reservoir. "Odd nitrogen" is the collective term for peroxyacetyl nitrate (PAN, CH₃C(O)OONO₂), peroxyntic acid (HOONO), dinitrogen pentoxide (N₂O₅), alkyl nitrate (RONO₂), chlorine nitrate (ClONO₂), nitric acid (HNO₃), nitrous acid (HNO₂), the oxides of nitrogen (NO_x) and aerosol nitrate (NO₃) represented as "NO_y". Estimates of the alkyl nitrate contribution to NO_y have been reported as high as 80% in the equatorial marine boundary layer (Blake et al., 1999, 2003b), whereas their contribution to NO_y in continental regions is more like 10% owing to close proximity of primary NO_x emissions (Flocke et al., 1998; Shepson et al., 1993; Simpson et al., 2006). As a 'reservoir' species for NO_x, alkyl nitrates have been concluded to play an important role in regulating tropospheric ozone levels in remote marine regions (Atlas et al., 1993).



The primary removal mechanisms from the atmosphere are photolysis and reaction with OH. Photolysis is the dominant destructive process for the shorter-chain (C_1 - C_3) alkyl nitrates while OH oxidation is the more important loss process for the larger alkyl nitrates (Clemitshaw et al., 1997; Flocke et al., 1998; Roberts, 1990). Chuck et al. (2002) calculated atmospheric residence times for methyl and ethyl nitrates using sea-to-air flux data and atmospheric measurements giving C_1ONO_2 an atmospheric residence time of 4.5 to 25 days and 5 to 10 days for C_2ONO_2 . Worton (2005) calculated atmospheric residence times for summer at $45^\circ N$ suggesting atmospheric lifetimes of 1-3 days for $2C_3ONO_2$, 1-2 days for 1-propyl nitrate, 1-1.2 days for 2-butyl nitrate and ≤ 1 day for 1-butyl nitrate.

4.1.2 NO_x observations during OP3

The oxides of nitrogen (NO and NO_2 , collectively termed NO_x) have a mixture of sources, including both biogenic (e.g. from soils) and anthropogenic agricultural activities (e.g. in vehicle exhaust and from fertilizer applications). In the absence of sources NO_x is known to exhibit diurnal variations where mixing ratios follow an expected pattern where shortly after sunrise NO mixing ratios would increase due to the onset of photochemical reactions converting NO_2 to NO, with a peak around solar noon followed by a decrease to zero at sunset.

Moller (2010) used the OP3 ground based NO_x measurements to indicate whether Bukit Atur could be said to represent the forest canopy or boundary layer air by comparing the canopy site (not presented here) and Bukit Atur. NO mixing ratios were higher at the canopy site than at Bukit Atur, the lack of similarity between the NO_x data sets at the canopy site and Bukit Atur show that the measurements at Bukit Atur are not representative of those seen under the rainforest canopy, suggesting that the site can be classified as above the canopy. NO_x measurements were also used from the aircraft to help classify Bukit Atur as being in the boundary layer or free troposphere. Concentrations in the free troposphere of both NO and NO_2 were considerably lower than those measured in the boundary layer and those measured at Bukit Atur. Therefore, Bukit Atur can be classified as an above canopy boundary layer site (Moller, 2010).

The characteristics of Sabah are a consideration in interpreting both the ground-based and aircraft alkyl nitrate measurements as land use is an important factor in assessing anthropogenic precursor emissions such as hydrocarbons and NO_x. From looking at the landuse map (Figure 3.1) the proximity of the oil palm plantations to Bukit Atur makes it likely that there will be higher concentrations of anthropogenic precursors in air masses that have passed over the oil palm plantation. To the west of Bukit Atur the land coverage is largely rainforest (Figure 3.1), whereas the east has more oil palm plantations and coastal settlements which will have associated anthropogenic NO_x sources. Tawau to the south east of the site has a population of 354,243 people and Sandakan to the north of the site has a population of 453,759 people, both towns are ports and house some industrial activity, Lahad Datu, to the west of the site, is a coastal settlement slightly smaller than Tawau, however, it has a very small airstrip and airport which receives daily internal flights with their associated NO_x emissions from the aircraft.

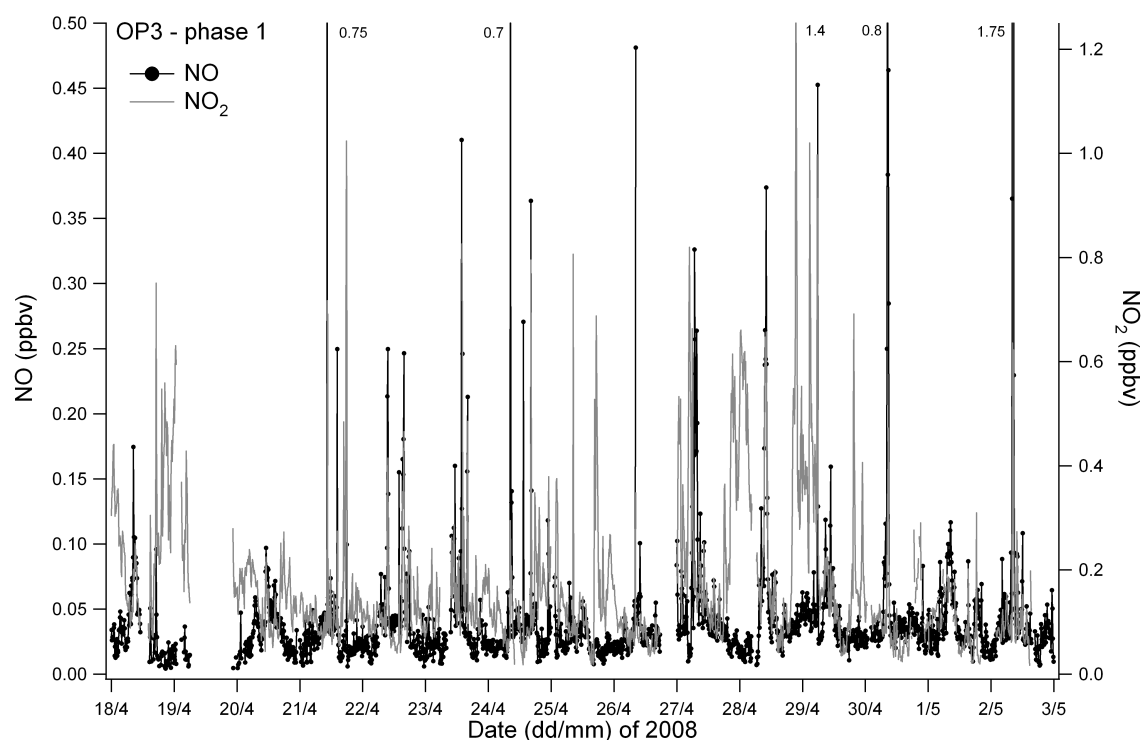


Figure 4.1: Nitrogen monoxide (NO) and nitrogen dioxide (NO₂) data for OP3-I. The data was measured on the University of York's NO_x instrument.

Back trajectory analysis of the OP3 NO_x revealed a predominant east/west divide rather than identifying attributable sources (Moller, 2010). However, the analysis showed

that there were much higher mixing ratios of NO_x seen in air masses from the east compared to air masses from the west. A consideration with any back trajectory analysis of the data is the 'snapshot' period that OP3 took place in, although both campaigns were over one month in duration, the wind directions within these periods did not encompass all of Sabah, this is a limit in attempting source attribution of this kind. For instance the capital of Sabah, Kota Kinabalu, lies on the western coast of Sabah with a population of 617,972 people and an international airport, presumably a significant source of NO_x however, very few trajectories passed over Kota Kinabalu before arriving at Bukit Atur.

The time series for the NO_x data for OP3-I at Bukit Atur (Figure 4.1) shows several period of elevated mixing ratios. Those in the NO_2 trace track particularly well with those seen in the bromocarbon data (Chapter 3). The NO_x data for OP3-III (Figure 4.2 shows higher mixing ratios of NO_2 and much higher mixing ratios of NO than during OP3-I. During OP3-I NO_x average mixing ratios were 0.23 ± 0.5 ppb increasing to 0.79 ± 0.5 ppb during OP3-III. The average boundary layer mixing ratio of NO_x from the aircraft measurements was 0.19 ± 0.1 ppb.

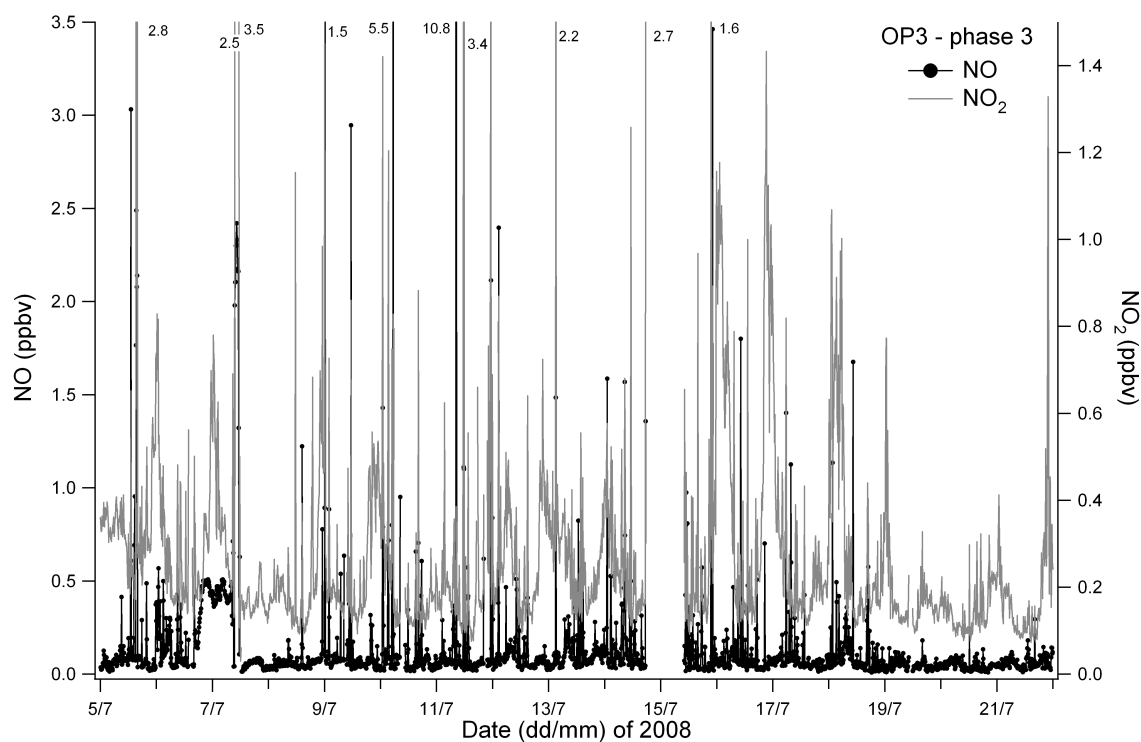


Figure 4.2: Nitrogen monoxide (NO) and nitrogen dioxide (NO_2) data for OP3-III. The data was measured on the University of York's NO_x instrument.

4.2 Spatial observations of alkyl nitrates over Borneo

The whole air samples collected on board the BAe146 FAAM aircraft were also analysed in E.I. (Chapter 2) for alkyl nitrates (RONO₂). As explained in the experimental methodologies Chapter E.I. mode is much less sensitive to alkyl nitrates than negative ion mode, so a more limited selection of the alkyl nitrates will be discussed here (C₁ONO₂, C₂ONO₂, 2-C₃ONO₂ and 2-C₄ONO₂). The sum of the means of the alkyl nitrates measured in the whole air samples was 13.6 pptv.

C₁ONO₂ and C₂ONO₂ are known to have marine sources (Chuck et al., 2002) and often observed to correlate well with marine halocarbons (Atlas et al., 1993; Blake et al., 1999). However, from immediately looking at the aircraft measurements of methyl and C₂ONO₂ plotted spatially over Sabah, it can be seen that the highest mixing ratios (>8 pptv) are not seen over the seas but over Bukit Atur and the region slightly to the north where the oil palm plantations lie (Figures 4.3 and 4.4). The C₁ONO₂ aircraft data ranges between 2-14 pptv. Values between 3-6 pptv of C₁ONO₂ were common over the ocean, with some higher mixing ratios seen off the Semporna peninsula over the Celebes Sea. This range of mixing ratios observed fits within the wide range of mixing ratios reported in the literature. Reeves et al. (2007) report slightly lower mixing ratios of C₁ONO₂ (~1-5 pptv) during the ITOP campaign over the North Atlantic Ocean, whereas Chuck et al. (2002) observed mixing ratios of 10-20 pptv over the equatorial waters of the Eastern Atlantic Ocean. C₁ONO₂ contributed 44% to the total alkyl nitrates observed in the aircraft measurements of the OP3 project.

C₂ONO₂ aircraft measurements were in the range 0.5-14.9 pptv however, the majority of the data fell between 0.5-5 pptv. This is the range used to colour the whole air samples in Figure 4.4. Again, higher ranges of mixing ratios were seen over Bukit Atur and the oil palm plantation (2-5 pptv) and some high points were seen off the south east coast of Sabah. The mixing ratios of C₂ONO₂ recorded over the oceans were in the 0.5-1.5 pptv range. This is in keeping with equatorial atmospheric measurements taken by Chuck et al. (2002) over the Western Atlantic ocean and not dissimilar to the mixing ratios recorded during the NAMBLEX project at Mace Head (Worton, 2005). Simpson et al.

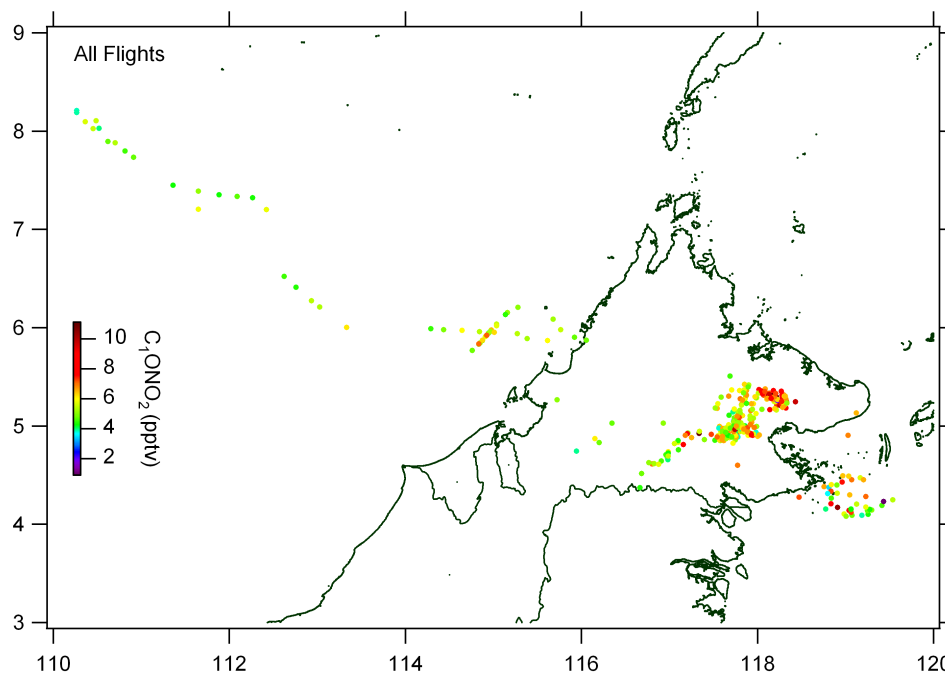


Figure 4.3: All aircraft measurements containing C_1ONO_2 ($n=375$), coloured by C_1ONO_2 concentration.

(2002) reported high mixing ratios of C_1 to C_4 nitrates from biomass burning in Australia, with the highest mixing ratios (122 ± 46 pptv) observed during the 'smoldering' stage, the mixing ratios observed at the Karachi city site (11.8 ± 2.2 pptv), reported in the same paper, are more comparable with the OP3 aircraft C_2ONO_2 measurements. However, the oil palm processing mills in situ with the plantations may mimic the atmospheric signature of biomass burning to some extent.

$2-C_3ONO_2$ shows a range of 0.2-49.5 pptv, with a mean of 3 pptv which contributes 21.8% to the sum of alkyl nitrates measured in the aircraft samples. The majority of the $2-C_3ONO_2$ data falls between 0.2-10 pptv, therefore, for clarity this is the colour scale that has been used in Figure 4.5. Figure 4.5 shows that the higher values of $2-C_3ONO_2$ were seen over the landmass of Sabah, in particular over the oil palm plantation area to the north west of Bukit Atur. Mixing ratios of 70 ± 27 pptv of $2C_3ONO_2$ were reported during the flaming stage of bushfires in Australia (Simpson et al., 2002), the maximum concentration recorded during OP3 aircraft detachment was 49.5 pptv of propyl nitrate. The OP3 aircraft data fits within the range of 1.9-53.2 pptv recorded in whole air samples at a river delta in southeast China (Simpson et al., 2006), these measurements were recorded at a coastal

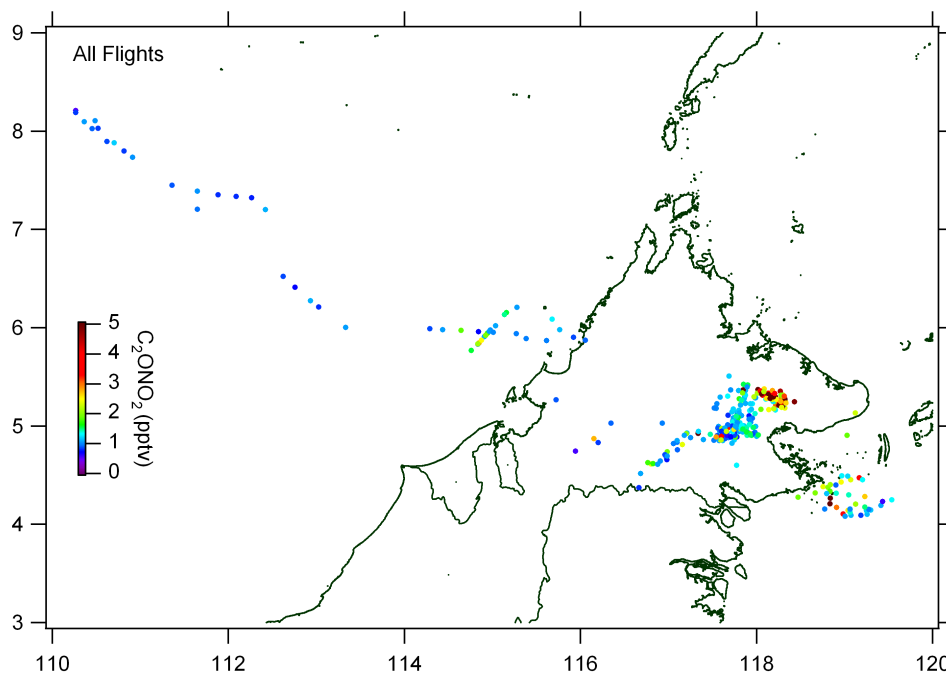


Figure 4.4: All aircraft measurements containing C₂ONO₂ (n=370), coloured by C₂ONO₂ concentration. The concentration range has been restricted here to omit outliers for a clearer picture of the distribution

site which was frequently impacted from urban pollution plumes.

In keeping with the other alkyl nitrate maps, 2-C₄ONO₂ also shows its most elevated values over the area of oil palm to the north of Bukit Atur. The data ranges from 0.1-37.3 pptv with the majority of the data within 0.1-3 pptv (the range used in Figure 4.6), similar mixing ratios of 2-C₄ONO₂ have recently been reported in marine air masses during the TORCH campaigns (Worton et al., 2010) and a range of ~3.6-6.5 pptv were observed at a seacoast site in New Hampshire (Russo et al., 2010).

1-C₃ONO₂ and 1-C₄ONO₂ were not present in all of the whole air samples analysed. The chromatogram peaks for both of these compounds are very small due to the reduced sensitivity to the alkyl nitrate fragments when the GCMS is operating in EI mode (Chapter 2). As a result both species were below the limit of their detection in many of the whole air samples. The spatial plots for 1-C₃ONO₂ and 1-C₄ONO₂ appear with this reduced number of data points, n=142 and n=51 respectively (not shown). The distribution of 1-C₃ONO₂ and 1-C₄ONO₂ both show their maximum mixing ratios over the land mass in the region of oil palm plantations.

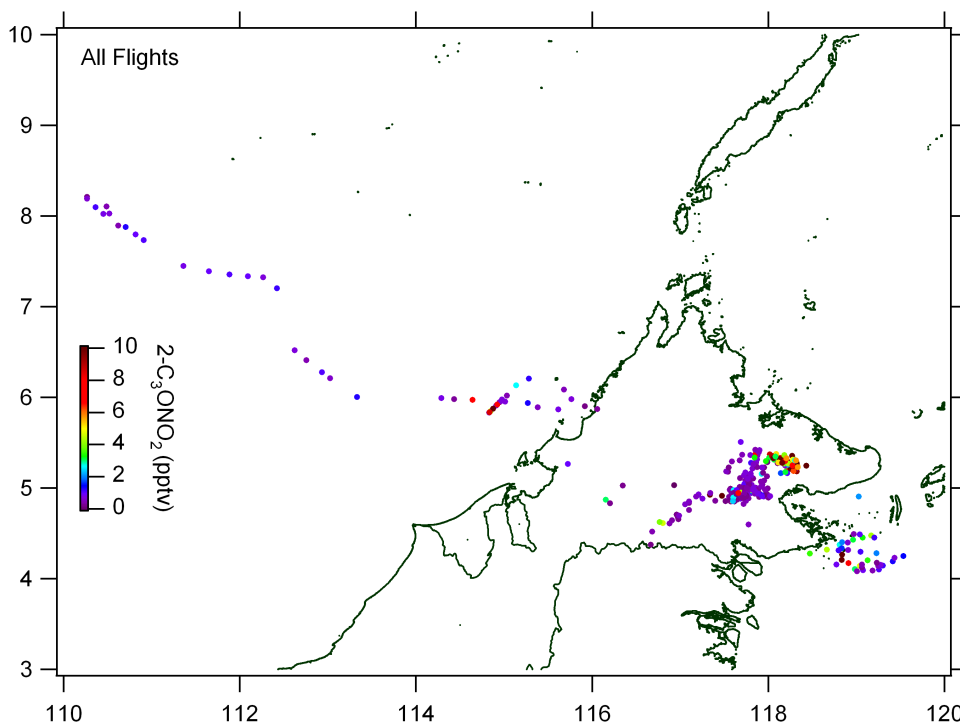


Figure 4.5: All aircraft measurements containing 2-C₃ONO₂ (n=344) coloured by 2-C₃ONO₂ concentration. The concentration range has been restricted here to omit outliers for a clearer picture of the distribution

Correlations between the alkyl nitrates over different land uses show methyl and C₂ONO₂ to have weak relationship for the whole aircraft data set. Methyl and ethyl nitrates show a reasonable correlation in whole air samples over the marine environment (r^2 of ≥ 0.5), with this exception C₁ONO₂ does not correlate well with the other alkyl nitrates or with the biogenically produced marine bromocarbons. C₂ONO₂, propyl nitrates and the butyl nitrates show very good correlations with each other in the samples over the marine environment. In particular for flight B389 where the whole air samples were collected almost entirely over the sea off the Semporna peninsula the correlations between the C₂-C₄ nitrates were showing r^2 values of ≥ 0.8 , but their absolute concentrations were lower than for C₁ONO₂ indicating that the C₁ONO₂ was experiencing the addition of a marine source.

The maps of aircraft measurements appear to show higher concentrations of alkyl nitrates over the oil palm, the box plots in Figures 4.7, 4.8 and 4.9 confirm that there is a quantitative difference between the two land types. For C₁ONO₂ the difference is less

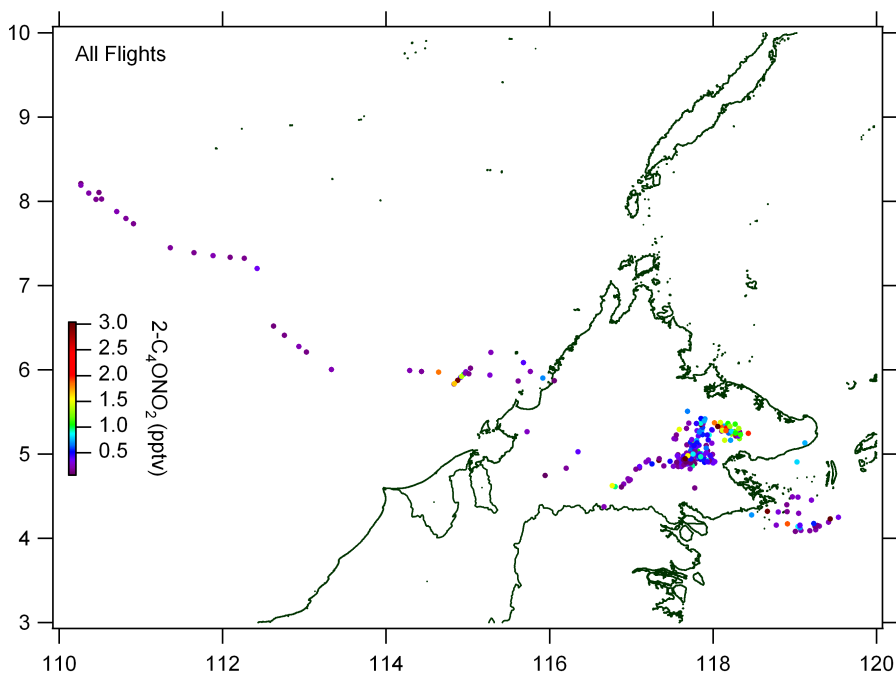


Figure 4.6: All aircraft measurements containing 2-butyl nitrate (n=290), coloured by 2-C₄ONO₂ concentration. The concentration range has been restricted here to omit outliers for a clearer picture of the distribution.

dramatic as for 2C₃ONO₂, this will in part be due to C₁ONO₂ having the additional marine source raising the perceived 'background' level of C₁ONO₂. The highest medians and upper quartiles for C₁ONO₂ in both the boundary layer data and the free troposphere data are over the oil palm plantations (Figure 4.7). For methyl and ethyl nitrates the box plots show that the measurements taken off the southeast coast exhibit higher concentrations of the alkyl nitrates than the northwest coast, this may be a result of the oil palm plantations that fringe the coastline on the southeast of Sabah, or more likely, as this behaviour does not extend to 2C₃ONO₂, that the marine source of these alkyl nitrates is stronger from the south east compared to the north west coast. This conclusion also ties in with the southeasterly winds during the OP3-III period.

The oil palm plantations of Sabah seem to be a source region for the alkyl nitrates reported here (Figures 4.7, 4.8 and 4.9). Box plots for the NO and NO₂ measurements in the boundary layer and free troposphere over the oil palm plantation show much higher concentrations in the boundary layer over the oil palm than the rainforest (Hewitt et al., 2009).

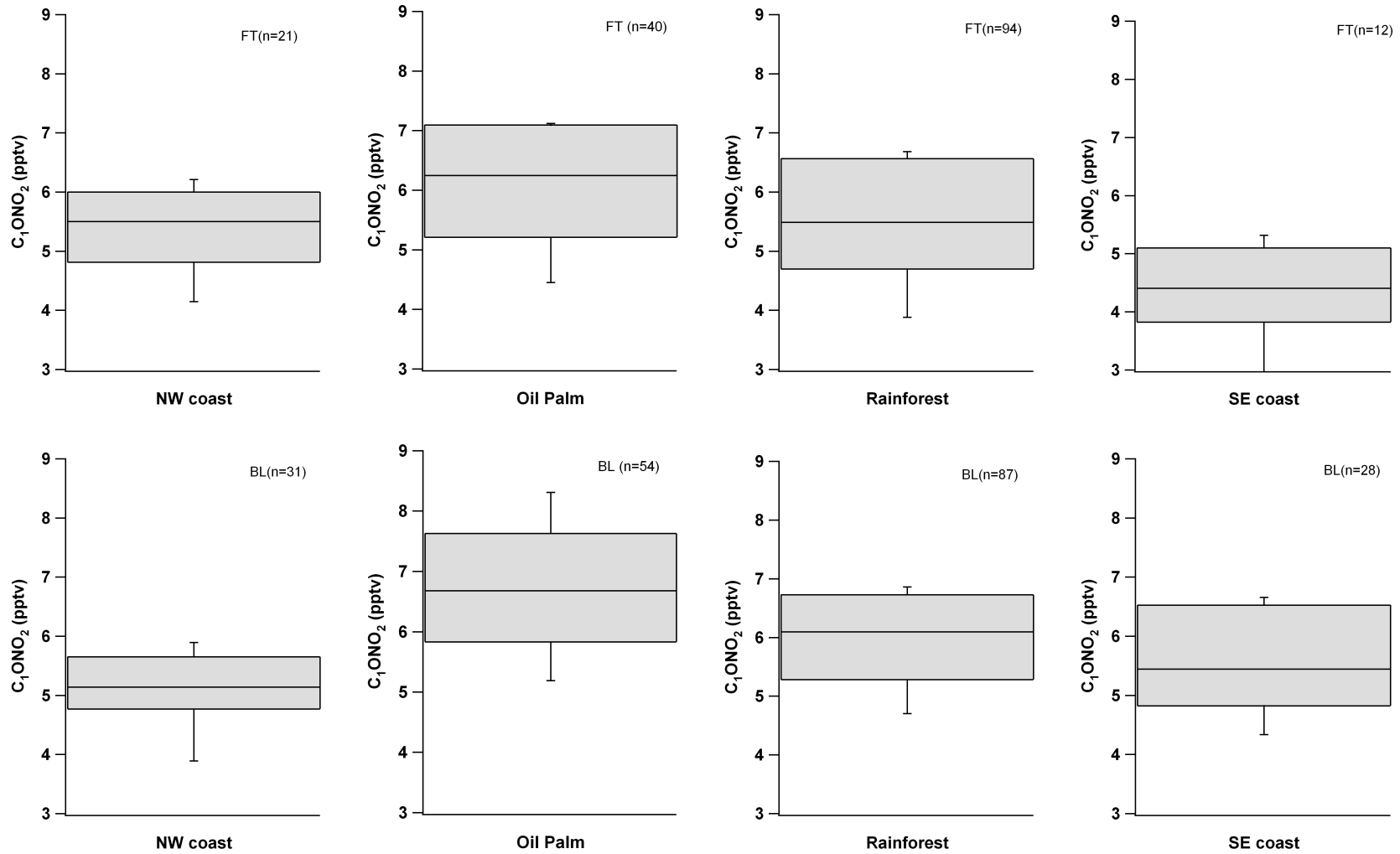


Figure 4.7: Box plots showing the methyl nitrate mixing ratios over the different land cover types of Sabah. The line represents median, box top and bottom represent 75th percentile and 25th percentile respectively and the whiskers represent 90% and 10% of the data. FT= free troposphere; BL= boundary layer.

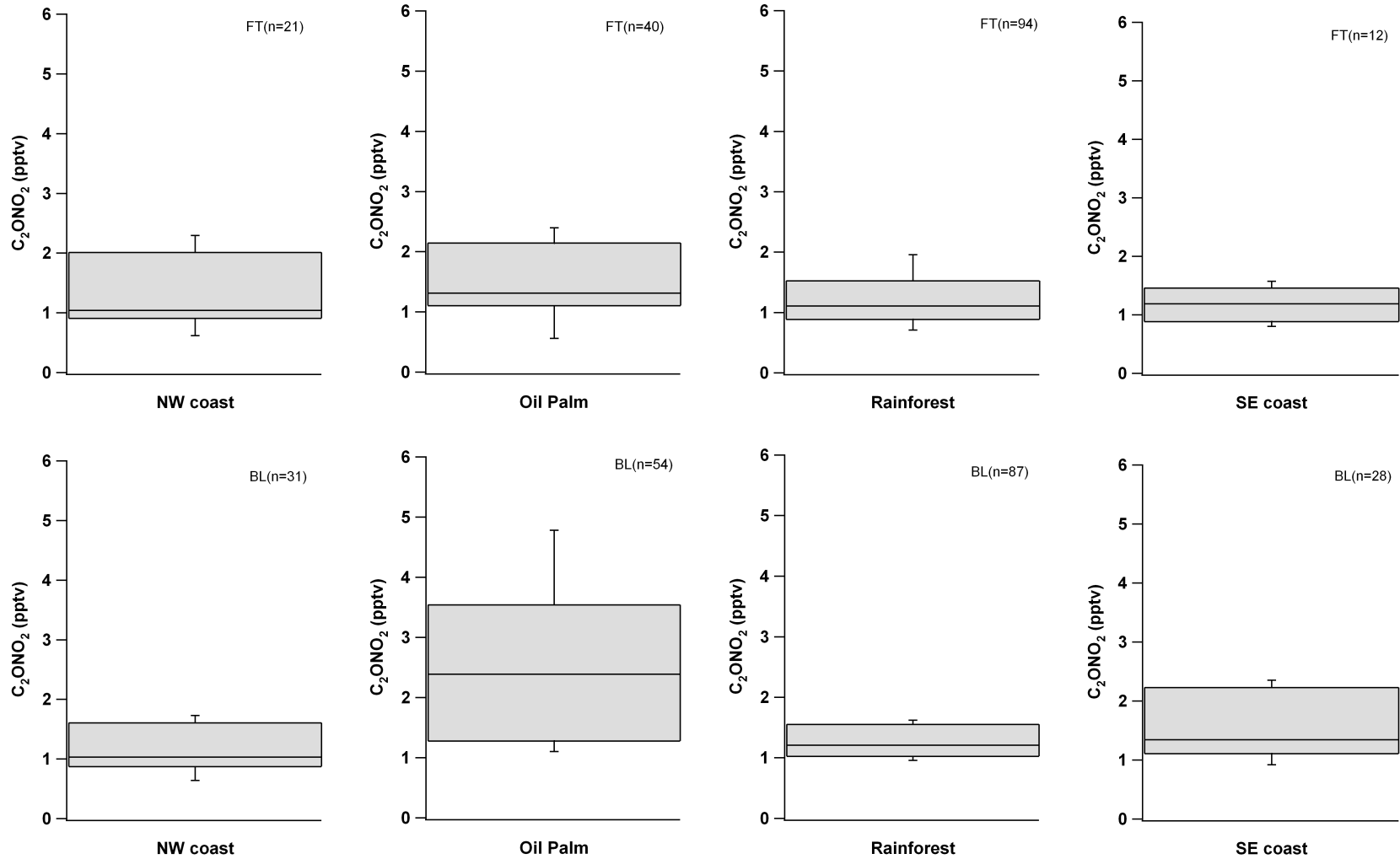


Figure 4.8: Box plots showing the ethyl nitrate mixing ratios over the different land cover types of Sabah. The line represents median, box top and bottom represent 75th percentile and 25th percentile respectively and the whiskers represent 90% and 10% of the data. FT= free troposphere; BL= boundary layer.

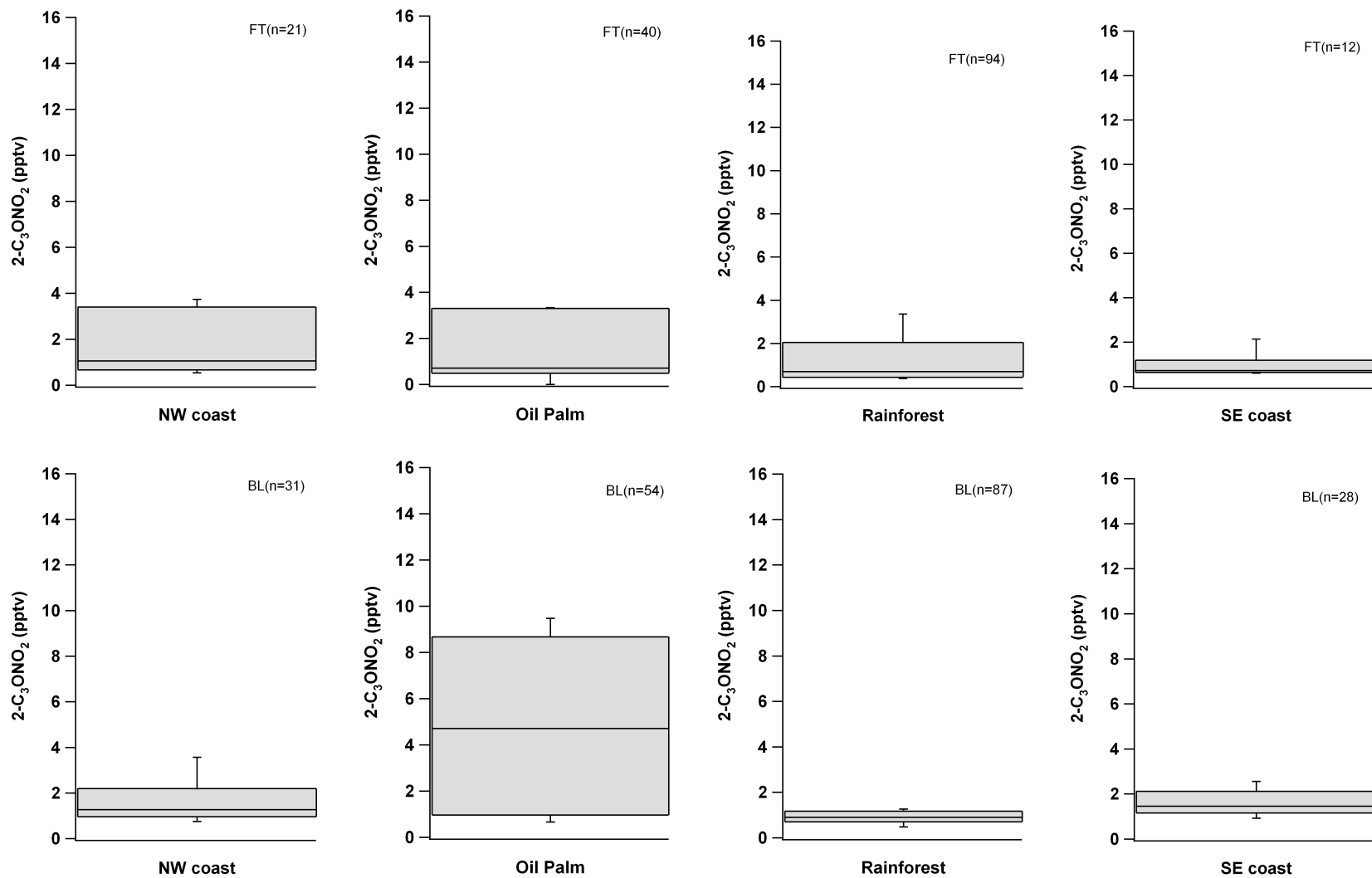


Figure 4.9: Box plots showing the 2-propyl nitrate mixing ratios over the different land cover types of Sabah. The line represents median, box top and bottom represent 75th percentile and 25th percentile respectively and the whiskers represent 90% and 10% of the data. FT= free troposphere; BL= boundary layer.

As previously stated the FAAM BAe 146 aircraft flew over several of the oil palm plantations of Sabah. There was the expectation that the NO_x levels would be of interest as well as the isoprene measurements. The isoprene concentrations in the boundary layer over the oil palm plantations were observed at levels 2-5 times that seen in the boundary layer over the rainforest (Hewitt et al., 2010). Hewitt et al. (2009) projected that the NO_x levels could potentially cause significant ozone production. The sources of nitrogen are mixed but the soil source within the oil palm plantations, coupled with the intense fertiliser regime that is in place whereby a hole is drilled adjacent to the trunk of the plant and a large quantity of nitrogen-rich fertiliser is introduced in this way. The vehicles used to transport the oil palm fruit from the plantation to the processor plant and to distribute the final product are often old and inefficient vehicles, Hewitt et al. (2009) suggest that simple measures such as the fitting of catalytic converters could substantially reduce the emission of NO_x from transport in and around the plantations. There is also the issue of the processor plants themselves which are commonly co-located with the oil palm plantations. Measures to manage the nitrogen from these sources could improve the local air quality in the oil palm plantations of Sabah, both from an environmental perspective and a human health perspective. Ozone is a well known atmospheric pollutant that attacks and can destroy soft tissue such as those found in the human respiratory system as well as the soft tissue of new growth on plants. Ozone stresses plants and it has been shown that it significantly reduces crop productivity. For this reason nitrogen management and VOC management in oil palm plantations is also important from an economic perspective (Hewitt et al., 2009). The relatively long lifetimes of these alkyl nitrates mean that some of this signal could plausibly come from neighbouring land in the Celebes sea or South China sea. To explore this further back trajectory analysis was employed to establish any consistency in noticeably high/low concentrations and the origin of that air mass. Source attribution using this method has been implemented with the halocarbons in (Chapter 3).

4.2.1 Relationship between alkyl nitrates and their parent hydrocarbons in the OP3-III aircraft data

The alkane aircraft data shows the areas over oil palm plantations to have the highest mixing ratios of ethane and propane and n-butane shows equally high values in the whole air samples over Bukit Atur and the oil palm plantations. As described earlier alkyl nitrates can be formed during the breakdown of their parent alkanes (equations 43 and 44). Ratios have been calculated here to show the relationships between the alkyl nitrate and parent hydrocarbon, using the relationship originally defined by Bertman et al. (1995). This method assumes no other source of alkyl nitrates other than their parent hydrocarbon and that the reaction with OH is the rate determining step in the formation of the alkyl nitrate. A high NO environment is also assumed, such that no peroxy radical self reactions take place. Given these assumptions the rate of formation and loss of the alkyl nitrates can be described as follows:



The reaction in Equation 43 occurs at the rate βk_A where $k_A = k_1[OH]$ and $\beta = \alpha_1 \cdot \alpha_3$. The rate of reaction of RH with OH (Equation 37) is represented by k_1 , α_1 represents the proportion of RH that forms the particular alkoxy isomer, $[OH]$ is the molecular density of OH, and α_3 is the branching ratio of the reaction of the alkyl peroxy radical with NO (Equations 39 and 40).



The reaction in Equation 44 occurs at the rate k_B where $k_B = j_4 + k_5[OH]$

Here j_4 is the photolytic loss rate of the $RONO_2$ and k_5 is the rate of reaction of the alkyl nitrate reacting with OH (Equation 42).

To calculate the relationship between $RONO_2$ and the parent alkane concentration as a function of time (t) the relationship defined by Bertman et al. (1995) can be used:

$$[RONO_2]/[RH] = \beta k_A / (k_B - k_A) \cdot (1 - e^{-(k_A - k_B)t}) + [RONO_2]_0 / [RH]_0 \cdot e^{-(k_A - k_B)t} \quad (45)$$

The simplified relationship between RONO₂ and the parent alkane is shown below (Equation 46) where initial concentrations of zero are assumed (i.e. no direct emissions). Generally previous studies have also assumed that the initial alkyl nitrate mixing ratio is zero (Bertman et al., 1995; Roberts et al., 1998; Stroud et al., 2001; Simpson et al., 2003), though the analysis by Reeves et al. (2007) included non-zero initial ratios and analysis of alkyl nitrates by Sommariva et al. (2008) attempted to quantify the influence of additional precursors.

$$[RONO_2]/[RH] = \beta k_A / (k_B - k_A) \cdot (1 - e^{-(k_A - k_B)t}) \quad (46)$$

The above formula creates an idealised curve that describes the ratio of alkyl nitrate to parent hydrocarbon exclusive of atmospheric mixing. Using the kinetic data in Table 4.1, the ratio between the parent hydrocarbons and alkyl nitrates were calculated as in Equation 46 for various times assuming the average concentration of OH to be 2×10^6 molecules cm⁻³: based on OP3 OH data. Through plotting pairings of these ratios against one another the observed data can be compared to the values calculated from the kinetic data (Figure 4.10). Photochemical processing times shift along the kinetic or modelled curve, though is not sensitive to the value of OH.

Figure 4.10 displays the ratios of the alkyl nitrates to their parent hydrocarbons. The mean NO concentration observed during OP3 was 33 ± 41 pptv which is sufficient for the reaction with NO to be the dominant pathway for RO₂ radicals (Roberts et al., 1998). The points on the modelled curve that represent 1 day and 10 days of t are marked in each

Table 4.1: Kinetic data

RH	k_1 ($\times 10^{-12}$ cm ³ molecule ⁻¹ s ⁻¹)	RO ₂	α_1	α_3	k_5 ($\times 10^{-12}$ cm ³ molecule ⁻¹ s ⁻¹)	j_4 ($\times 10^{-6}$ s ⁻¹)
Ethane	0.248	ethyl	1	0.014	0.018	0.73
Propane	1.09	2-propyl	0.727	0.042	0.29	1.10
Propane	1.09	1-propyl	0.272	0.02	0.58	0.77
n-butane	2.36	2-butyl	0.855	0.084	0.86	0.91

Kinetic data from Reeves et al. (2007) and references therein.

plot.

The ratios of alkyl nitrates to parent hydrocarbon shown in Figure 4.10 give an indication of air mass age that the samples were taken in. Figure 4.10(a) showing the C_2ONO_2 /ethane ratio plotted against the butyl nitrate/n-butane ratio to be above the kinetic curve which is indicative of less photochemically processed air (Bertman et al., 1995; Stroud et al., 2001), suggesting that a source other than the parent hydrocarbons is contributing to the alkyl nitrate. C_2ONO_2 is known to have marine sources which may be a contributing source, also the breakdown of a longer chained hydrocarbon into a number of smaller peroxy radicals and therefore smaller chain alkyl nitrates could provide an alternative source as Reeves et al. (2007) concluded for C_1ONO_2 .

Figure 4.10(b) 1-propyl nitrate/propane and 2-butyl nitrate/n-butane shows some evidence of two 'populations' of data: one within 1-10days of photochemical processing and several points of high alkyl nitrate to parent hydrocarbon ratio indicating photochemically older air. Interestingly once the C_2ONO_2 /ethane and 1-propyl nitrate/propane ratios are no longer constrained by the 2-butyl nitrate/n-butane ratio the observed ratio of these species agrees reasonably well with the calculated curve (figure 4.10(c)). The ratio of $2C_3ONO_2$ /propane against butyl nitrate/n-butane also exhibits a divide into two 'populations' (Figure 4.10(d)), in this instance with several points relatively close to the calculated curve and indicating that they represent air that has been recently polluted and experience less than one day of photochemical processing. The limit of detection of the alkyl nitrates (<0.04 pptv) and the parent hydrocarbons (1-9 pptv Hopkins et al. (2011)) are to be considered when viewing these plots, as a small error in the integration of either peak in the chromatogram as a result of the signal to noise count being reduced near the limit of detection, may result in an erroneous point that appears to represent a high alkyl nitrate to alkane ratio.

4.3 Temporal trends in alkyl nitrate observations

The time series data for the alkyl nitrates collected at Bukit Atur were analysed in negative ion mode (Chapter 2) which is very sensitive to the alkyl nitrates so here C_1 - C_4 nitrates

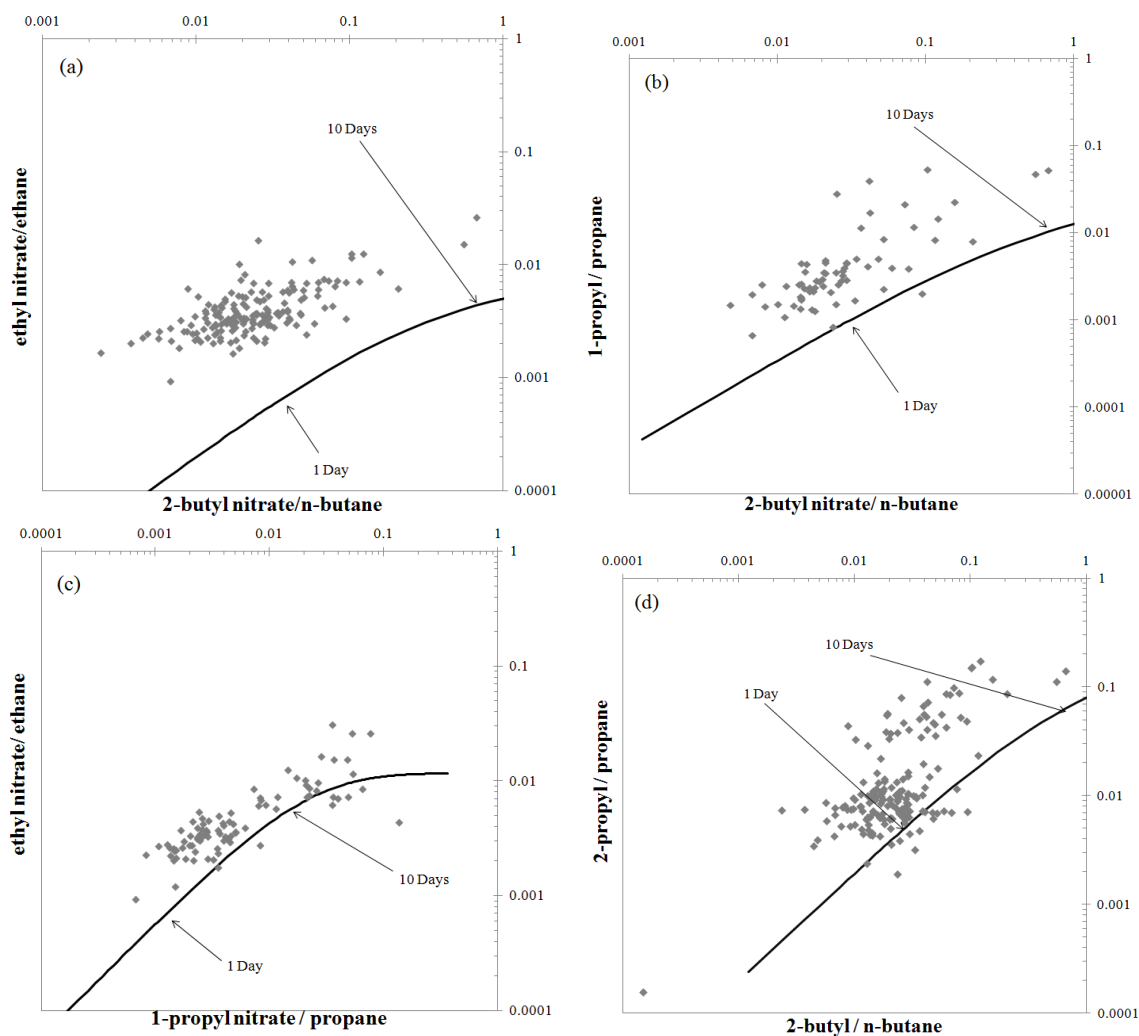


Figure 4.10: Relationships between various ratios of alkyl nitrates and their parent hydrocarbons for the OP3 aircraft measurements. The points on the model curve that correspond to 1 and 10 days of photochemical processing have been marked.

can be discussed. In the first instance looking at the time series for OP3-I it is apparent that the propyl and butyl nitrates follow a very similar pattern as the bromocarbons (here using bromoform as a comparison in the grey trace) Figure 4.11. Methyl and C_2ONO_2 show some variations that are independent of the higher (C_3 - C_4) nitrates and the bromocarbons. This is most likely attributable to additional marine sources of these nitrates, an observation that supports past studies.

Some diurnal variation can be seen in the time series for OP3-I (Figure 4.11) but it is not consistent, peaking at varying times in the early hours of the morning, as discussed in Chapter 3 this is most likely linked to the position of the inlet in relation to the nocturnal boundary layer at Bukit Atur (we measured at 30m on the GAW tower, i.e. above the nocturnal BL). The presence of cloud cover below the Bukit Atur site before sunrise implies that Bukit Atur is above the nocturnal boundary layer. Doppler lidar measurements were made in the valley close by to Bukit Atur, these measurements give an indication of the mixed layer height and support the suggestion that Bukit Atur lies above the nocturnal boundary layer in the residual layer and therefore separated from the canopy emissions in the valley below (Pearson et al., 2010). During the OP3-I measurement period there was an 'event' on the 28th April where elevated the concentrations of the propyl and butyl nitrates were seen, and to a lesser extent C_2ONO_2 , with no apparent impact on the C_1ONO_2 concentrations observed. The variations observed in the alkyl nitrates during OP3-I track the variations seen in the time series of the brominated compounds reasonably well, suggesting the variation most likely reflect changes in air mass.

OP3-III shows predominantly lower concentrations of the propyl and butyl nitrates, which all exhibit a slight downwards trend throughout the campaign. C_1ONO_2 however shows the opposite increasing from ~ 2 -3 pptv to ~ 7 -8 pptv by the end of OP3-III. C_2ONO_2 seems to show a slight increase from ~ 0.8 pptv to ~ 1.4 pptv around 12th/13th July before decreasing gradually back to 0.8 pptv over the remainder of the measurement period.

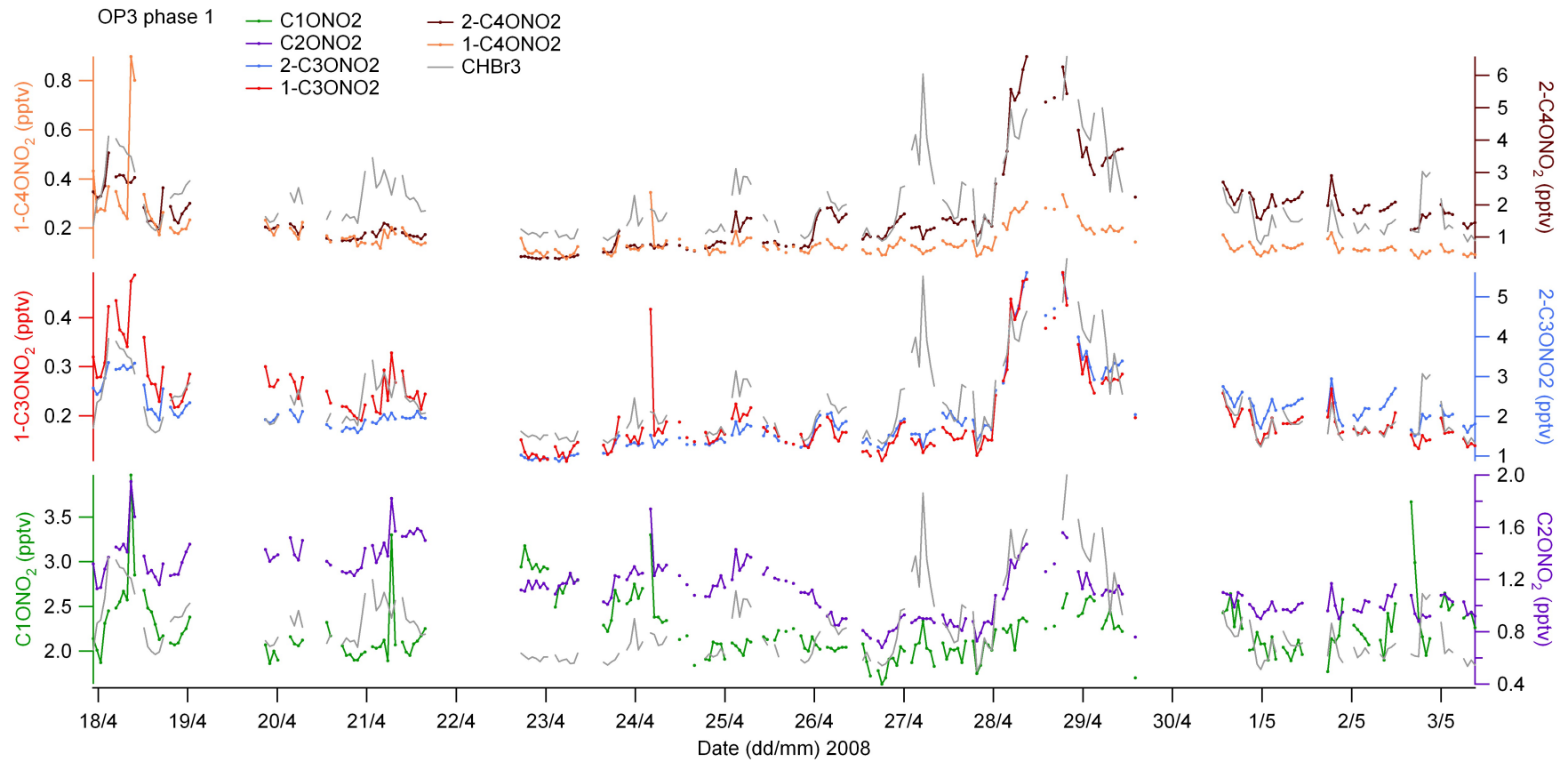


Figure 4.11: Time series of the alkyl nitrate data collected at Bukit Atur during OP3 phase 1. Bromoform is shown for reference in the grey trace.

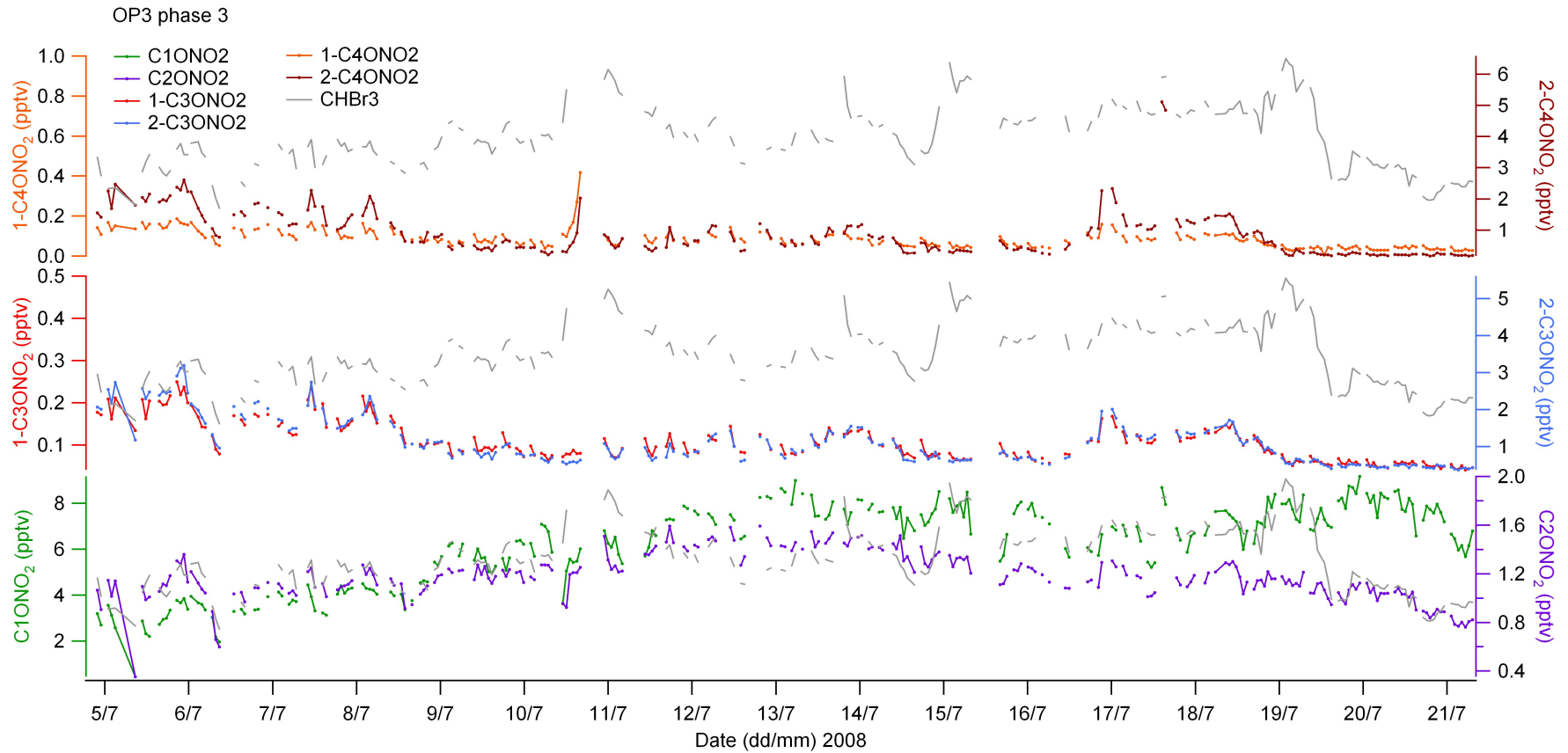


Figure 4.12: Time series of the alkyl nitrate data collected at Bukit Atur during OP3 phase 3. Bromoform is shown for reference in the grey trace.

When comparing the OP3-I alkyl nitrate time series with the alkane time series for that same period it is noticeable that ethane, propane, n- and iso-butane exhibit similar variations, showing the period of elevated concentrations on the 28th/29th April. This supports the conclusion that this period of elevated concentrations is attributable to the path of the air mass prior to passing over Bukit Atur. For this period the back trajectories show a change in their direction of approach to Bukit Atur which was further discussed in Chapter 3.

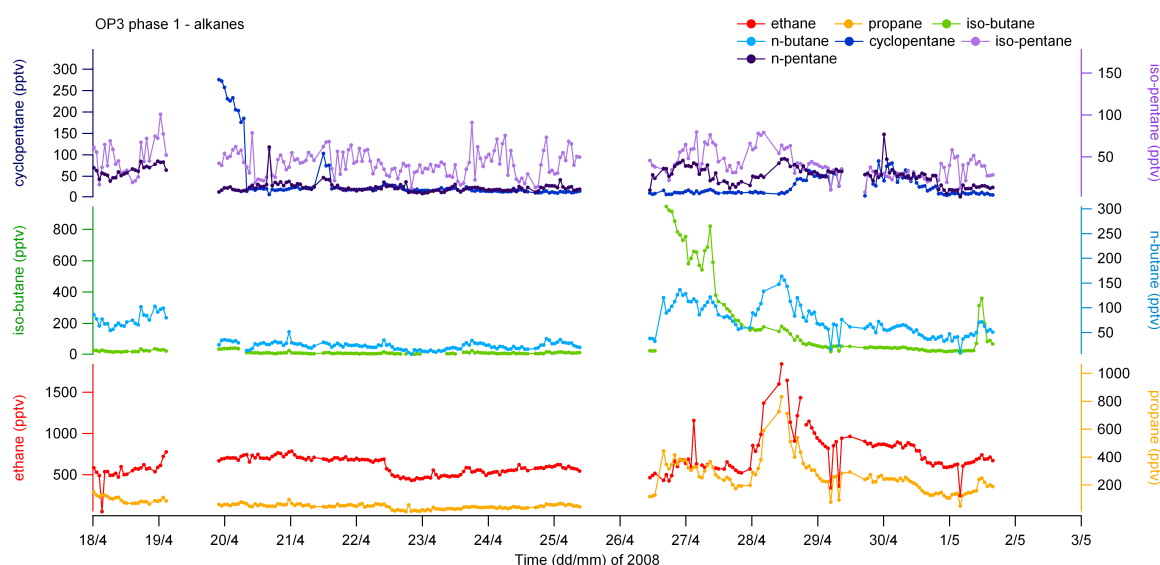


Figure 4.13: Alkane measurements taken at Bukit Atur during OP3 phase 1 on the York GC-MS system

The alkane data for OP3-III is very patchy and does not cover a great deal of the period that the alkyl nitrates were measured in. Ethane and propane are available for the OP3-III period and they exhibit the same downward trend from the 19th July seen in the propyl to butyl nitrates and the bromocarbons. There is a period of sustained enhancement in the ethane and propane measurements from the 17th July, before this drop on the 19th July. This enhancement feature is also apparent in the propyl and butyl nitrates (Figure 4.12) and the NO_x time series shows large enhancements on the 17th July and the 19th July, but they are not sustained and the concentrations fall between the two days.

The average total alkyl nitrates measured during OP3-I was 9.1 ± 3.2 ppt, increasing to 10.9 ± 3.1 ppt measured at the ground site during OP3-III and the average sum of total alkyl nitrates for all flight samples was 12.3 ± 2.1 ppt. The total alkyl nitrates for OP3-I

made up 3% of NO_y and although total alkyl nitrate mixing ratios were higher during OP3-III at the ground site the increase in other nitrogen species mean that total alkyl nitrates contributed 2% to NO_y .

These contributions to the NO_y budget are similar to those reported in the literature. O'Brien et al. (1995) measured C_3 - C_6 alkyl nitrates at a rural site in Ontario and found them to contribute 0.5 - 3% to NO_y , Russo et al. (2010) measured C_1 - C_5 alkyl nitrates on the mainland and off the coast of New Hampshire finding them to contribute $\leq 1\%$ NO_y , and Flocke et al. (1998) found an average contribution of 3% to NO_y from the C_1 - C_8 alkyl nitrates they measured at the Schauinsland station in the Black Forest. Higher contributions to NO_y have been reported for rural sites, such as the study by Day et al. (2003) who report total alkyl nitrates to account for 10-20% of NO_y at a rural site in California.

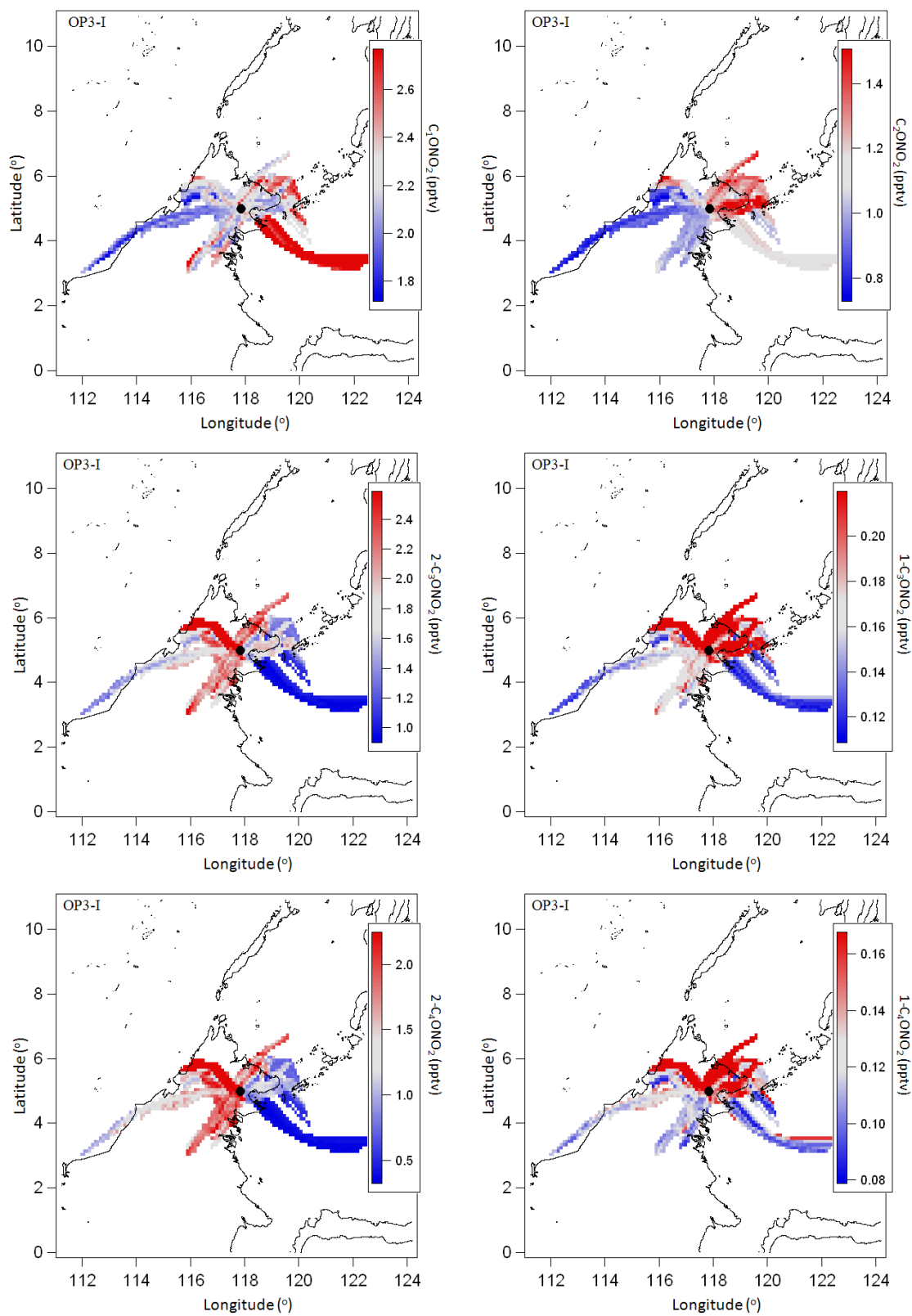
4.3.1 Back trajectory analysis of alkyl nitrates from measurements at Bukit Atur

Using the back trajectory analysis of Robinson et al. (2011) mean value maps for the alkyl nitrates have been generated. Details of how the maps are generated can be found in Chapter 3 where they were first discussed. The mean value maps for OP3-I support the lack of correlation seen between C_1ONO_2 and the other alkyl nitrates through clearly showing that the origin of air masses yielding high concentrations of C_1ONO_2 are not shared with those bringing in the higher values for the larger alkyl nitrates. Most striking is the marine air mass approaching Bukit Atur passed the end of the Semporna peninsula off the south east coast of Sabah (Figure 4.14(a)), this particular air mass is responsible for the lower than average concentrations for the propyl and butyl nitrates (Figures 4.14(c)-(f)). C_2ONO_2 shows the north eastern sector to be attributable for delivering concentrations higher than the mean to Bukit Atur (Figure 4.14(b)), 1-propyl nitrate shows a similar pattern as does 1-butyl nitrate. Both 2-propyl and 2-butyl nitrate exhibit a similar pattern in the mean value maps, with the air masses contributing most to their high concentrations arriving from the same directions as one another excluding the north east to south east

sector which does not seem to have passed over a source region.

The mean value maps for the OP3-III tell a different story for the alkyl nitrates, skewed by the wind directions predominantly approaching from the south and south east and the absolute concentrations for the propyl to butyl nitrates having dropped in this measurement period at Bukit Atur. As before C₁ONO₂ does not correlate well with the other alkyl nitrates, its mean value map indicates that air masses from the east and north of the site are responsible for the higher concentrations seen in the OP3-III Bukit Atur data (Figure 4.15(a)). The propyl and butyl alkyl nitrates show their highest concentrations to be from air approaching Bukit Atur from across the landmass of Borneo from the south west of the site (Figure 4.15 (c)-(f)). The air masses that approach along the east coast of Borneo to the south of Bukit Atur also seem to contribute high concentrations of ethyl to butyl nitrates. C₂ONO₂ is neither correlated or anti correlated with the other alkyl nitrates (Figure 4.15(b)), there seems to be an area of exclusion to the north of Bukit Atur where air from this direction brings lower concentrations and the west coastline to the south of the site seems to bring higher concentrations in, but there is not a strong dependence on wind direction exhibited for C₂ONO₂ during OP3-III.

The time series data for Bukit Atur show some daily variations, most notably in OP3-I (Figure 4.11), it is possible that the high and low areas of the mean value maps above are simply reflecting a diurnal pattern in air mass movement. By looking at the individual trajectories it allows us to dissect the mean value maps to see if this is the case. Figure 4.16 is an example of this analysis, showing the spatial nature of the trajectories split onto two separate maps: for those with concentrations higher than the mean measured at Bukit Atur and those bringing in concentrations lower than the mean. Two further plots illustrate the pressure height of the trajectories approaching Bukit Atur with time. This analysis has been completed for all C₁-C₄ alkyl nitrate measurements at Bukit Atur from both OP3-I and OP3-III. This break-down of the trajectories shows that the time that the trajectory arrived at Bukit Atur is not a common influence on the concentration of the alkyl nitrates seen, suggesting the mean value maps are a useful qualitative tool in attributing source regions for the alkyl nitrate measurements.

Figure 4.14: Mean value maps of C_1 - C_4 alkyl nitrates from OP3-I

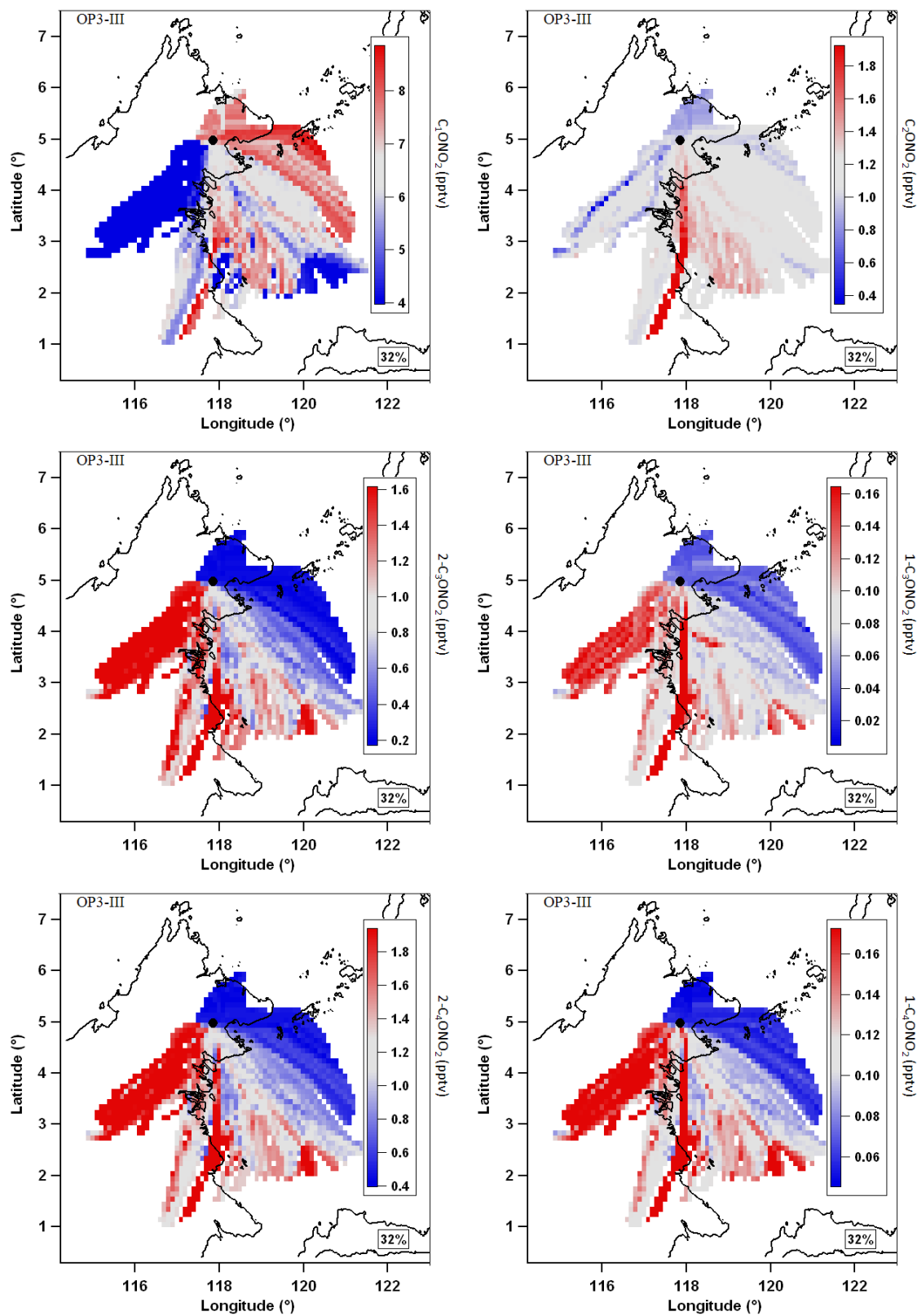


Figure 4.15: Mean value maps of C₁- C₄ from OP3-III

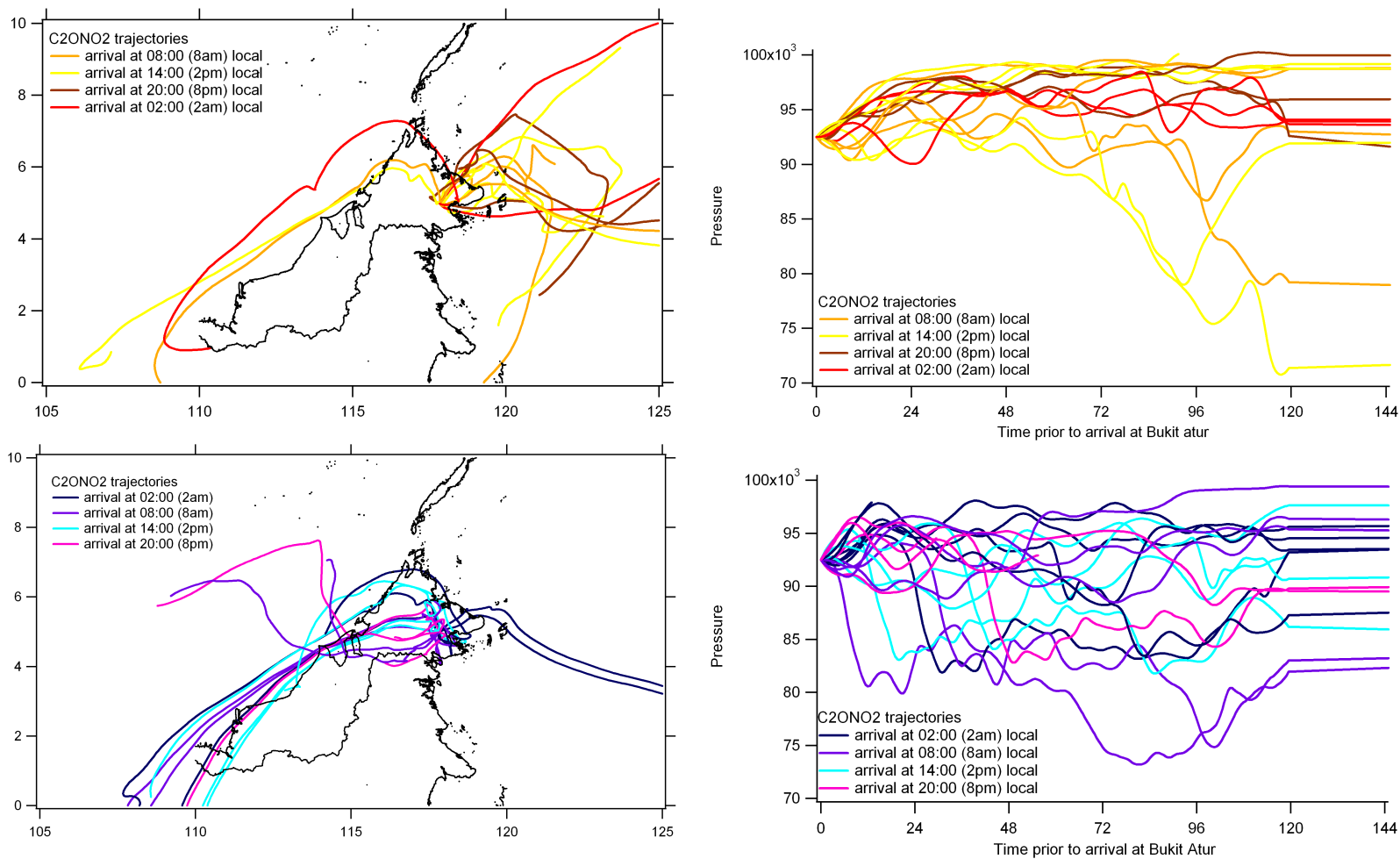


Figure 4.16: Back trajectories bringing higher than average (a) & (b) and lower than average concentrations (c) & (d) of C_2ONO_2 to Bukit Atur during OP3-I.

4.4 Summary

C₁ONO₂ contributed 44% to the total alkyl nitrates observed in the aircraft measurements, 24% for OP3-I and 61% for OP3-III making it the most dominant of the alkyl nitrates observed during the whole of the OP3 project. The mean concentration of C₁ONO₂ increases from 2.22 pptv during OP3-I to 6.24 pptv during OP3-III at Bukit Atur and a comparable 6.02 pptv for the aircraft measurements during OP3-III. However, the propyl and butyl nitrates show a decrease in their means between the two ground based periods of measurement. Despite this the sum of the alkyl nitrates measured at Bukit Atur increases from 9.2 pptv during OP3-I to 10.2 pptv for OP3-III.

Total alkyl nitrates made a small contribution to the local NO_y: 3% during OP3-I, decreasing to 2% during OP3-III at Bukit Atur. This suggests that the alkyl nitrates are having little influence on local O₃ and NO_y budgets. These values are in keeping with figures from the literature in other remote environments, such as the studies by O'Brien et al. (1995) and Russo et al. (2010).

The oil palm plantations of Sabah appear to be a source of the propyl and butyl nitrates reported here. The average concentration of 2C₃ONO₂ was 3 pptv in the aircraft measurements and 1.1 pptv at Bukit Atur during OP3-III. The air during the OP3-III period approached Bukit Atur predominantly from the south and south east of the site where little to no oil palm plantations are located. One of the limitations with back trajectory analysis concerns the relatively long atmospheric residence of the alkyl nitrates with respect to the 5 day back trajectories used: this complicates the allocation of source regions for the alkyl nitrates.

Looking at the ratios between the parent alkanes and the alkyl nitrates it is evident that the degradation of the parent alkanes cannot account for the range of mixing ratios observed. C₁ONO₂ and C₂ONO₂ both show evidence of an alternative source besides their parent hydrocarbons. These species show some high values in the marine boundary layer off the Semporna peninsula and even higher concentrations were observed in the boundary layer over the oil palm plantations, suggesting that these regions are providing additional sources.

Chapter 5

Methyl halide emissions from crop plants

5.1 Introduction

Methyl halides are ozone depleting compounds. Currently it is estimated that 16% of chlorine in the troposphere is derived from naturally emitted methyl chloride and over half of bromine in the stratosphere is from natural sources of methyl bromide and other bromocarbons (Montzka et al., 2010). However, the atmospheric budget of methyl halides is currently unbalanced, with the known sinks outweighing the known sources (Montzka and Fraser, 2003). From current understanding of the sources it has been suggested that terrestrial vegetation may contribute to the 'missing' sources and research has begun to focus on terrestrial plants that emit methyl halides (Blei et al., 2010; Gan et al., 1998; Redeker et al., 2000; Rhew, 2001; Saito et al., 2008; Yokouchi et al., 2002, 2007). In areas of natural mixed vegetation e.g. forests, the high concentrations of methyl halides measured at the leaf or branch level in some of these studies, such as Blei et al. (2010) and *et al.*(2002), are not always observed at the canopy level or above the canopy (Chapter 3 contemporary measurements to Blei *et al.*(2010)).

It is possible that complex chemical or biological mechanisms and/or dynamics in mixed vegetation environments result in the loss of signal above the canopy, however,

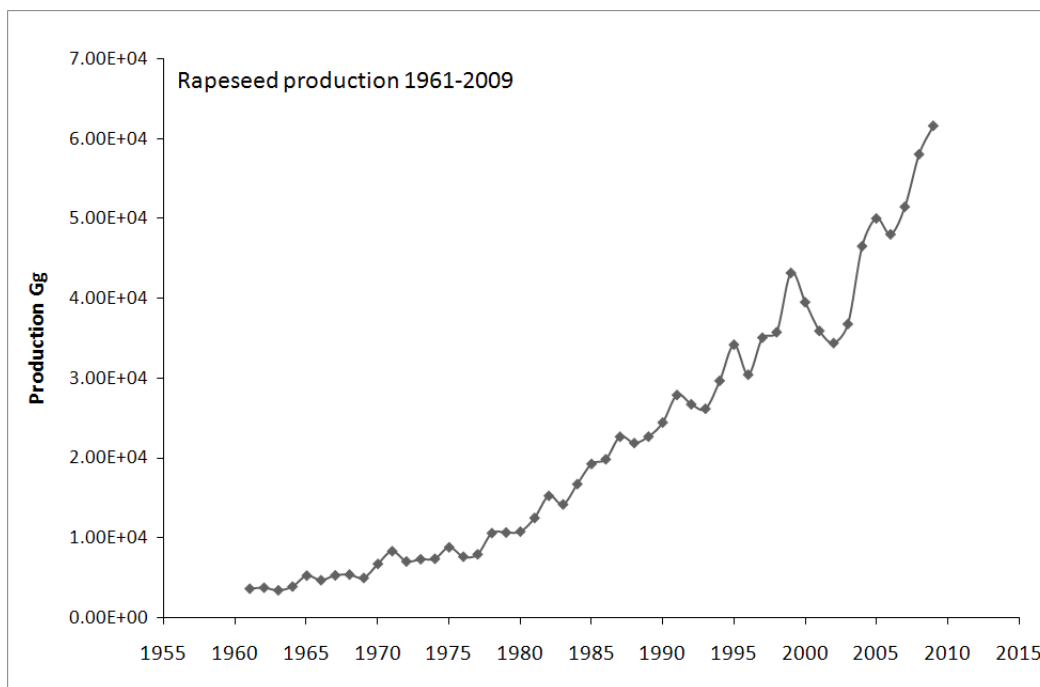


Figure 5.1: Global rapeseed production in gigagrams (Gg) from 1961-2009. (FAOSTAT, 2011)

where a large area of only one species is present its emissions will dictate the atmospheric composition above it. In this chapter the focus is not on naturally occurring vegetation but crop plants. In a world experiencing continued expansion of agriculture and increasing global population, the pressure to feed that population and meet the fuel demands of the developed world are high. Rapeseed (*Brassica napus*) is a widely grown crop in the northern hemisphere with uses from cooking oils to biofuel and it is a known emitter of methyl halides (Mead et al., 2008b). With the biofuel industry set to rise, the production of rapeseed will undoubtedly rise too, leading to an increase in methyl halide emissions: quantifying this emission is important to guide the industry as to which varieties of rapeseed should be grown and whether genetically modified cultivars should be used to suppress the emission of these ozone depleting compounds. Other widely grown crops have the potential to impact the atmosphere, rice (*Oryza sativa*) is a key example as it is central to food security the world over, providing the main source of calorie intake for approximately half the World's population (FAOSTAT, 2011).

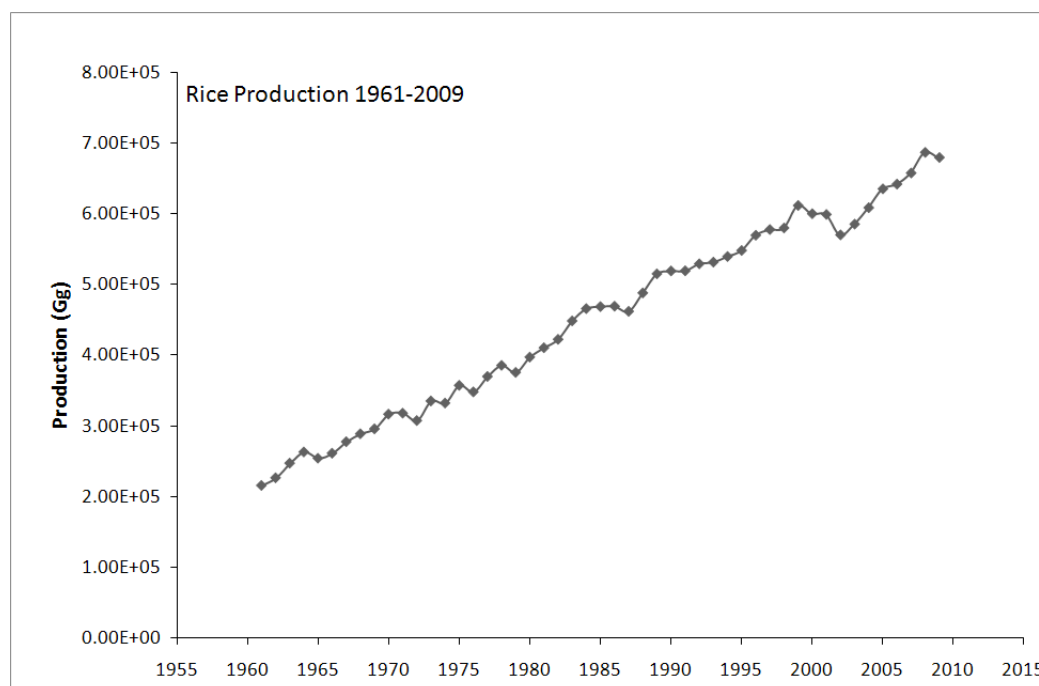


Figure 5.2: Global rice production in gigagrams (Gg) from 1961-2009. (FAOSTAT, 2011)

Studies into the emissions from rice have shown that methyl halides, and in particular methyl iodide, are emitted from rice cultivation (Muramatsu and Yoshida, 1995; Redeker et al., 2000, 2002; Redeker and Cicerone, 2004; Lee-Taylor and Redeker, 2005). There is a drive to increase the global production of rice to reduce poverty. The Bill & Melinda Gates Foundation funded the International Rice Research Institute (IRRI) to develop 'heartier' varieties of rice and deliver them to 400,000 farmers in Africa and Asia to increase their yields and incomes. In this case the Gates Foundation met their goal of doubling rice yields for these 400,000 farm households by 2010 (Bill & Melinda Gates Foundation, 2010). The economic and social drivers for increasing agriculture have spurred the increasing production trends in these two important crops, rapeseed production has increased twenty-fold from 3.6×10^3 Gg in 1961 to 61.6×10^3 Gg in 2009 (Figure 5.1) and rice has more than trebled from 1961 production of 21.6×10^4 Gg to 67.9×10^4 Gg reported in 2009 (Figure 5.2).

5.1.1 The methylation process and the HOL gene

Gan *et al.* (1998) observed that *Brassica* plants can take up Br^- from soil, produce methyl bromide (CH_3Br) and release it into the air. Br^- has a ubiquitous presence in soils, with soil containing an average of 1.0 mg/kg Br^- (Flury and Papritz, 1993; Yuita, 1994). Gan *et al.* reported that the emission of methyl bromide from *Brassica* plants increased proportionally with the level of Br^- level in the soil. In their experiments no methyl bromide was reported in the Br^- treated soils without plants or from the Br^- soils containing only plant roots, thus it was concluded that methyl bromide was produced by and released from the above ground part of the plant. Plant Br^- uptake and soil Br^- were found to be linearly correlated with an R^2 of 0.96, which also coincided with a linear relationship between the methyl bromide production rates and the plant Br^- contents.

Arabidopsis thaliana is a member of the *Brassicaceae* family of which several members have been shown to emit methyl halides (Gan *et al.*, 1998). Crop geneticists such as Attieh *et al.* (1995) and Rhew *et al.* (2003) have studied the methylation process in plants which results in the emission of methyl halides into the atmosphere. Methyltransferases are the enzymes responsible for the methylation of chloride, bromide and iodide within plants. Rhew *et al.* (2003) demonstrated that the model plant *Arabidopsis thaliana* produces and emits methyl halides and that the enzyme responsible for the production is encoded by the HARMLESS TO OZONE LAYER (HOL) gene. The gene was named 'HOL' based on its expected effect when it is disrupted and its function is lost. The protein encoded by *HOL* is capable of catalysing the S-adenosyl-L-methionine (SAM)-dependant methylation of halide ions to produce methyl halides (Attieh *et al.*, 1995; Saxena *et al.*, 1998; Wuosmaa and Hager, 1990). In mutant plants (where the HOL gene is disrupted), the methyl halide production has been shown to be largely eliminated (Rhew *et al.*, 2003), however, few studies have focused on this.

Rhew *et al.* (2003) showed that the *HOL mRNA* was found in all above ground tissues, the expression in the juvenile plants was considerably higher than in tissues from the adult plants. Ribonucleic acid (RNA) is one of three known macromolecules along with DNA and proteins that are essential for all known forms of life. Messenger RNA

(mRNA) is used to carry genetic information that directs the synthesis of proteins. Unpublished studies conducted at the John Innes Centre have shown that the HOL gene seems to be expressed very early in plant development, as early as germination. Two-week old seedling roots have high expression of the HOL gene and when developed the anther (pollen production zone in the flower) also exhibits some expression of the HOL gene.

5.1.2 Plant varieties studied here

Plants from two different families were studied as part of this thesis work: the *Brassicaceae* family (Figure 5.3) and the *Poaceae* family (Figure 5.4).

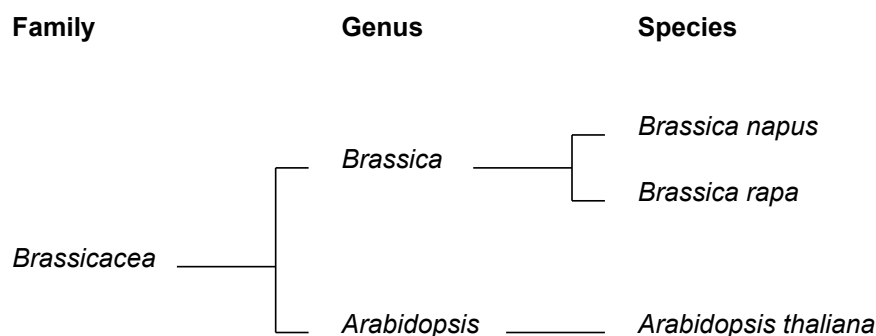


Figure 5.3: Brassicaceae family tree, illustrating genetic link between *Brassica* species and *Arabidopsis thaliana* studied in this thesis.

The *Brassicaceae* family contains many plants of economic importance such as *Brassica oleracea* (broccoli, cabbage, and cauliflower), *Brassica rapa* (turnip), *Brassica napus* (rapeseed), *Raphanus sativus* (common radish), and *Arabidopsis thaliana* (thale cress). The *Brassica* plants investigated in this thesis were *Arabidopsis thaliana*, *Brassica napus* and *Brassica rapa*. Firstly (Section 5.2) the 'model' plant *Arabidopsis thaliana* was used to identify the trait for emission of methyl halides. *Arabidopsis thaliana* is extremely well studied and its biology well understood. Prior unpublished work by the John Innes Centre identified this genomic trait for methyl halide emission in plants among the *Brassicaceae* family, therefore, findings in *Arabidopsis thaliana* plants may be analogous to other plants in the *Brassicaceae* family.

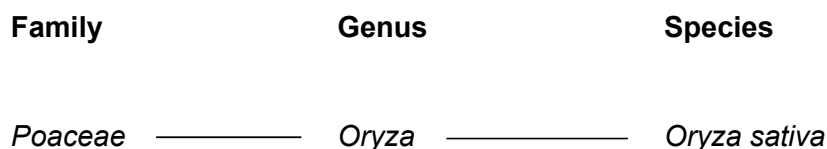


Figure 5.4: Poacea family tree for species *Oryza sativa* studied here.

Plants in the *Poaceae* family are commonly known as grasses. The genus *Oryza* of the *Poaceae* family is native to tropical and subtropical regions of Asia, Northern Australia and Africa. The species of *Oryza* studied in this thesis, *Oryza sativa*, is commonly known as Asian rice. It has the smallest cereal genome of the *Oryza* genus. This small genome makes its biology well understood and easy to genetically modify. Previous studies by Redeker *et al.* (2000), Lee-Taylor & Redeker (2005) and Redeker & Cicerone (2004) showed methyl halide emissions from rice paddies.

The work presented here in this chapter is the result of an Earth and Life Systems Alliance (ELSA) funded collaboration between the UEA Trace Gas Laboratory and the Crop Genetics group at the John Innes Centre (JIC). This collaboration initially set out to confirm that the *HOL* gene is responsible for the emission of methyl halides (Section 5.2) by measuring the emissions from plants with and without this gene function. The success of the initial experiment enabled the emissions of methyl halides to be studied from plants with the *HOL* gene overexpressed (Section 5.2.4), where the expectation was to see an increase in methyl halide emission. Once the sampling design and analysis was validated in the first two laboratory studies there was the opportunity to study the emissions from rape-seed in a field environment (Section 5.3). This field experiment provided the framework to observe methyl halide emission at different stages of plant development and focus on a widely grown crop plant. Agricultural environments with increasing salinity were then focussed on by conducting an experiment where turnip plants were treated with a saline solution during watering (Section 5.4). The final experiment presented here was intended as the first in series of experiments with rice plants. This experiment aimed to ascertain whether rice plants grown in soil (i.e. not in a paddy field) emit methyl halides (Section 5.5). In all experiments samples were taken in to cannisters and so the number of samples

were limited by the number of cannisters available. The findings of these experiments are then used to estimate global emissions from these crop plants within different scenarios (Section 5.6).

5.2 Pilot study of methyl halide emissions from *Arabidopsis thaliana*

5.2.1 Hypothesis 1

Arabidopsis thaliana seedlings without the 'HARMLESS TO THE OZONE LAYER' gene (HOL) emit less methyl halides (CH₃Cl, CH₃Br and CH₃I) than the wild type *Arabidopsis thaliana* seedlings.

5.2.2 Methodology

Rhew et al. (2003) found the expression of the HOL mRNA to be noticeably higher in the tissues of juvenile plants (5 day old seedlings) compared to adult plants (4 week old). Based on these findings, this experiment used juvenile *Arabidopsis thaliana* seedlings. The seedlings were germinated and grown in Petri dishes with an agar substrate. Twenty days after germination separate Petri dishes of the juvenile plants were enclosed in Teflon bags of approximately 1.5 litre capacity at 14, 6, 3 and 1 hours prior to sampling and at the time of sampling. The plants were enclosed in Teflon bags at these recorded times prior to sampling to ascertain the optimal enclosure time. Samples were taken into evacuated 1 litre SilcoCans, connecting the SilcoCans via Teflon tubing to the Teflon bag over the seedlings. Then once connected, the Teflon valve attached to the bag was opened and the SilcoCan valve opened to draw in approximately 1 litre of the enclosed air (Figure 5.5). Blanks were also sampled, the blanks were an enclosed petri dish containing the agar substrate. 200 ml of each sample was analysed for methyl halides and also screened for other organohalogens, on an Entech GCMS system at UEA (Chapter 2).

5.2.3 Results from HOL vs. wild type experiment

In all cases the sample taken after 14 hours of enclosure showed the highest concentrations of methyl halides and the mutant plant sample without a functional *HOL* gene are lower than the wild type samples (Figure 5.6), this supports our hypothesis 5.2.1. The



Figure 5.5: Sampling of *Arabidopsis thaliana* in the Cambridge Laboratory, John Innes Centre

blanks are high compared to expected background atmospheric concentrations, however the composition of the agar contains high halide concentrations as it is a derivative of seaweed. There did not appear to be any consistent emission of other organohalogens from *Arabidopsis thaliana*.

Figure 5.7 shows elevated mixing ratios of the methyl halides from the wild type after just 1 hour of enclosure. The wild type exhibits high mixing ratios of the methyl halides relative to their average background atmospheric mixing ratios ($\text{CH}_3\text{Cl} \approx 550$ pptv (AGAGE, 2010); $\text{CH}_3\text{Br} \approx 7.5$ pptv (Montzka et al., 2010); $\text{CH}_3\text{I} \approx 1.2$ pptv (Bell et al., 2002)). From these results, it was concluded that an enclosure time of around 3 hours would be appropriate to ensure seeing the methyl halide emissions without prolonging the plant's enclosure. Enclosure experiments will always create an artificial and stressful environment for the plant, with more sophisticated experimental set-up these stresses can be reduced but never eliminated (Blei et al., 2010; Owen and Hewitt, 2000).

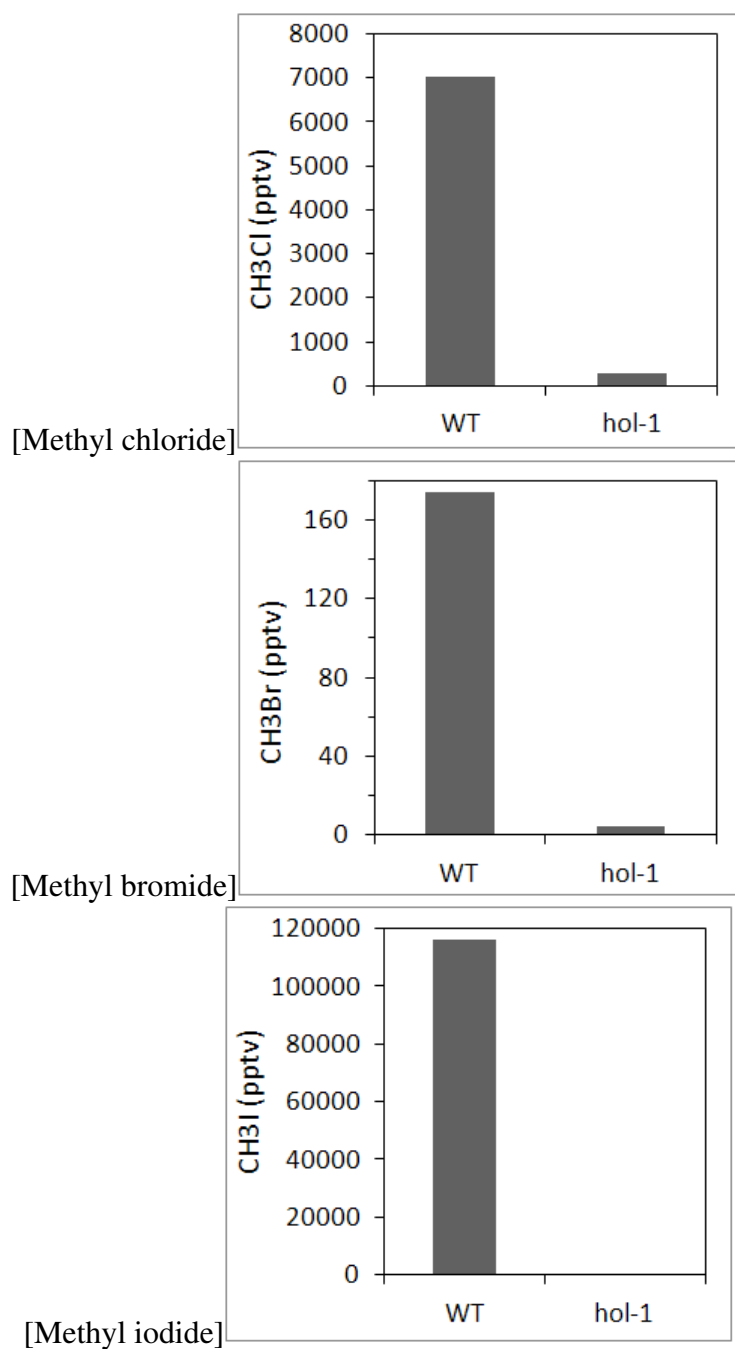


Figure 5.6: Methyl halides mixing ratios measured in the head space both wild type (WT) *Arabidopsis thaliana* and the mutant with the HOL gene expressed (hol-1) after 14 hours of enclosure.

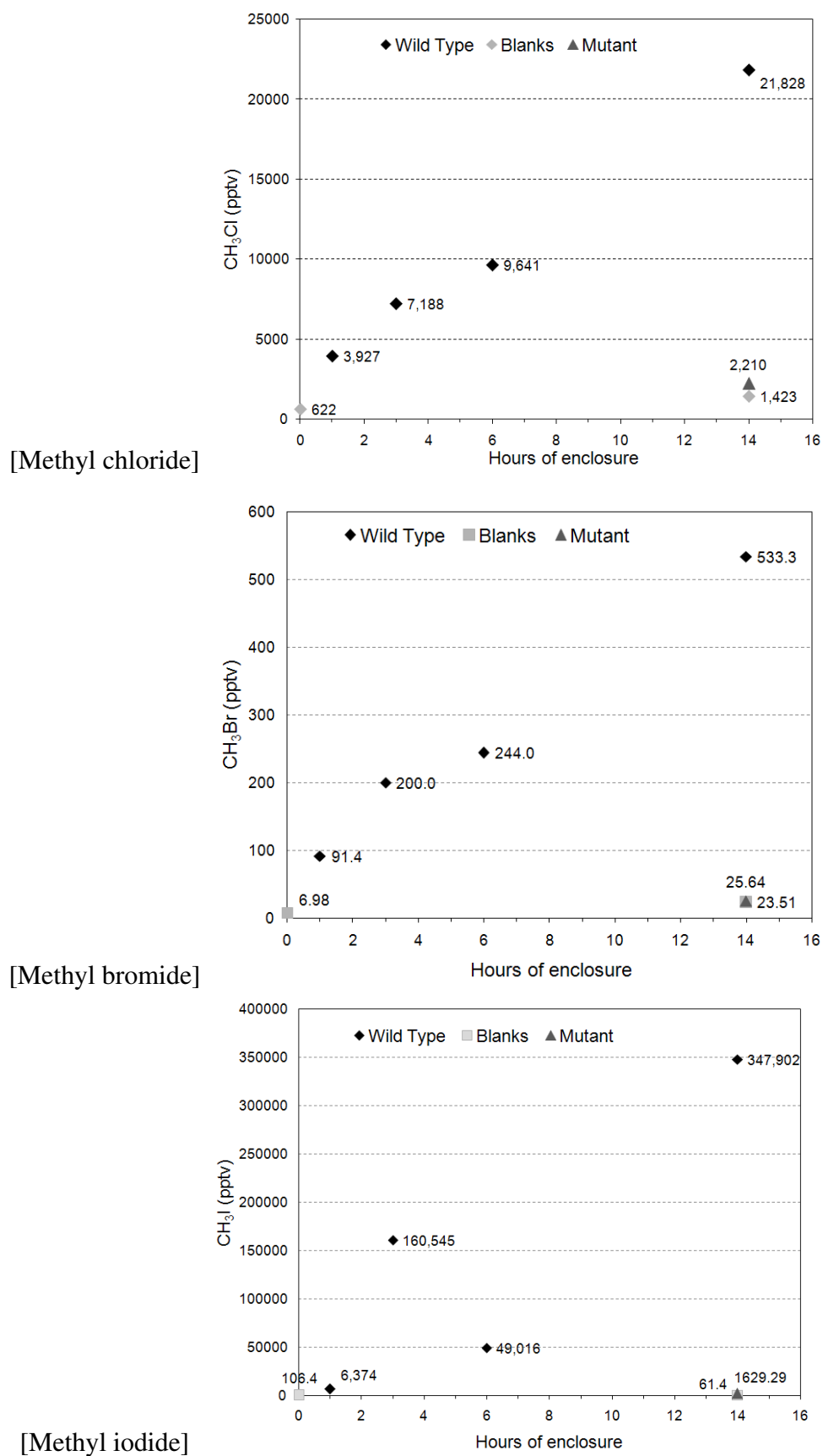


Figure 5.7: Methyl halides mixing ratios with enclosure time. Measured in the head space both wild type (WT) *Arabidopsis thaliana* and the mutant with the HOL gene and a blank.

5.2.4 Hypothesis 2

Overexpressor lines of *Arabidopsis thaliana* seedlings will emit more methyl halides (CH_3Cl , CH_3Br and CH_3I) than the wild type *Arabidopsis thaliana* seedlings.

5.2.5 Methodology

A subsequent study was conducted looking at the lines over expressing the *HOL* gene in *Arabidopsis thaliana* namely 196-9 and 196-11 lines. The seedlings were grown in the same material and were exposed to the same growing conditions as in the initial wild type vs. *HOL* experiment (Subsection 5.2.2). Mutant seedlings (*hol*) were also grown for this overexpressor experiment, however, the results have not been presented here for clarity, the *hol* mutants exhibited lower emissions of methyl halides than the wild type as found in the results of the *HOL* vs. wild type experiment above (subsection 5.2.3). The plants were harvested at the end of this experiment to provide biomass values.

5.2.6 Results of overexpressor experiment

It was expected that these lines would exhibit more methyltransferase activity and therefore more methyl halide emissions than the wild type. As expected, the lines 196-9 and 196-11 over expressing the *HOL* gene showed greater fluxes than the wild type *Arabidopsis thaliana*. The line 196-11 exhibited the highest emission of both methyl chloride and methyl bromide. Methyl iodide fluxes however, were highest for the other over expressor line 196-9.

5.2.7 Summary of *Arabidopsis thaliana* experiments

These experiments confirm that when plants have the *HOL* gene 'deactivated' their emission of methyl halides is suppressed. In plants where the methyltransferase trait is over-expressed the emissions of methyl halides are observed to be higher than wild type *Arabidopsis thaliana*, confirming that the emission of methyl halides is controlled by methyltransferase activity in the plant. In the wild type the observed emission of methyl iodide

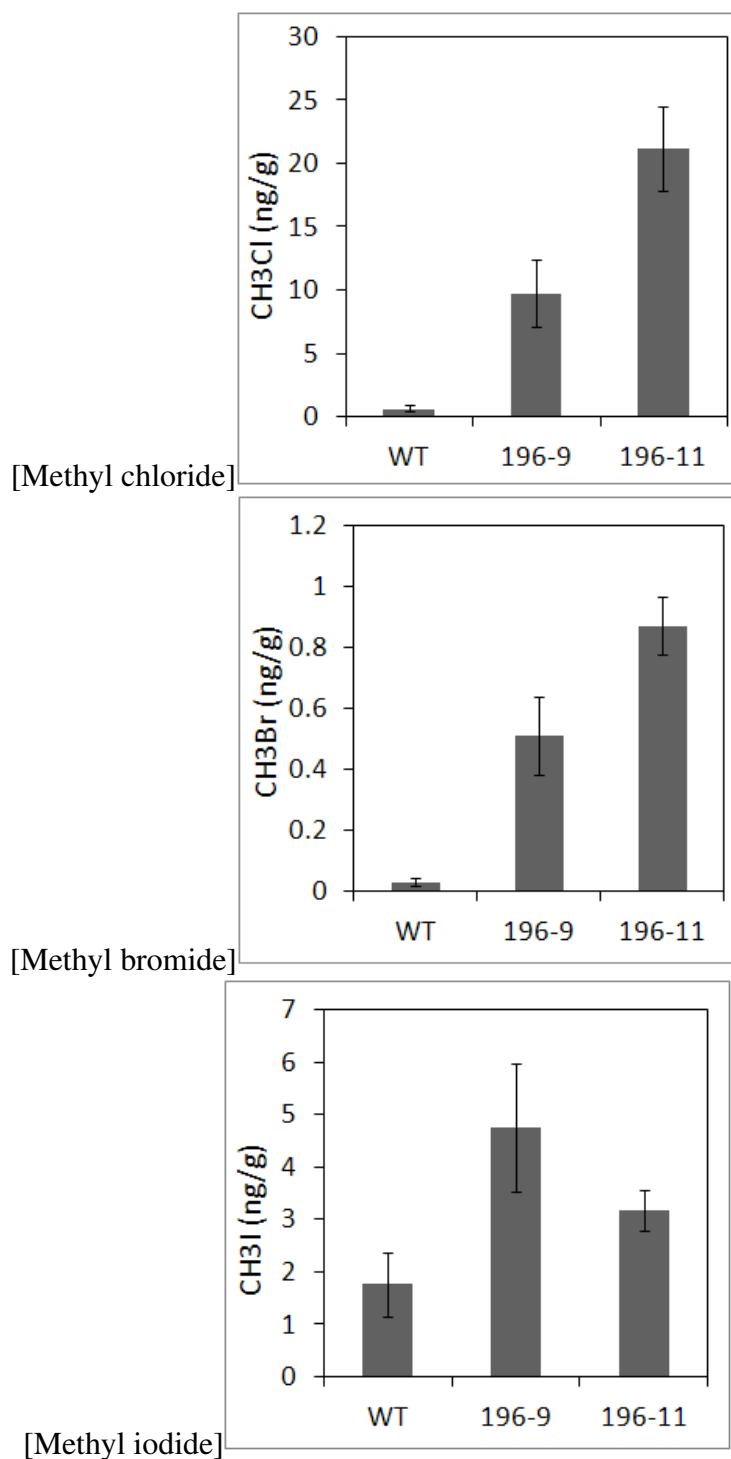


Figure 5.8: Methyl halides from wild type *Arabidopsis thaliana* and from the two overexpressor lines 196-9 and 196-11, shown here as means in nanogram per gram (ng/g) fresh weight \pm SE (n=3).

was the greatest of the three methyl halides, this supports the findings of Rhew et al. (2003). These findings confirm the involvement of the *HOL* gene in the emission of methyl halides. It is reasonable to hypothesise that the emission of methyl halides in other plants of the *Brassicaceae* family is also attributable to the *HOL* gene.

There is the possibility that the seedling emissions are due to the agar medium composition they were grown in. Sterilised agar was used as the growth medium for the germination of seeds and growth of seedlings. Agar is made from a seaweed derivative and as such is highly likely to contain high levels of halide ions. A sample of the agar used by the JIC in the above experiments was analysed by the UEA Chromatography Laboratory using a Dionex instrument. Chloride and bromide were measured successfully, however, despite several runs iodide was not successfully analysed in the samples. The agar used at the JIC contained 97.6 ± 30 mg/l chloride and 44.5 ± 21 mg/l of bromide. When the agar is prepared a formulation of nutrients is added to the agar. At the JIC the Murashige and Skoog (MS) plant growth salts are added. These salts contained 332.16 mg/l calcium chloride (CaCl_2), 0.83 mg/l of potassium iodide (KI), but no bromine containing compounds. It would be desirable to repeat these experiments in the future with *Arabidopsis thaliana* seedlings grown in soil as it is currently unknown how much of this 'artificial' halide content is available for the plant to use in the methylation process.

The relationship between the halide content of a substrate and the emission of methyl halides from a plant grown on that substrate is poorly known. Mead et al. (2008b) stated from a personal communication from Gan that a linear relationship was assumed between the halide content in soil and the methyl halide emissions from the *Brassicaceae* plants studied. However, this linear relationship is not defined in either the Gan et al. (1998) paper or the subsequent modelling of those experimental results in the 2008 paper by Mead et al. (2008b).

5.3 *Brassica napus* field experiment

5.3.1 Hypothesis 3

Different varieties of rapeseed (*Brassica napus*) emit different amounts of methyl halides and these emissions are influenced by the developmental stage of the plant.

5.3.2 Methodology

Manley et al. (2006) suggested that there was developmental regulation of methyl halide emission from certain salt marsh species of the Brassicaceae family, peaking during the flowering stage of the plants. In this experiment emission of the methyl halides were measured at two developmental stages in the life cycle of *Brassica napus* plants. Firstly, at the teloscopying stage (104 days after sowing when the stem starts growing, also known as 'bolting') and secondly at the flowering stage of the plants (118 days after sowing). Ten different varieties of rapeseed were studied. These ten varieties included the genetic pairs Tapidor and Ning You, Tapidor and Q14, Tapidor and Q57, Capitol and Rocket, Grizzley and Verona, and DK142 and Apex. These ten varieties have been used by the Brassica research community to generate genetic linkage maps (Armeanu-D'Souza, 2009). Such linkage maps can be used in combination with knowledge of specific traits, to identify genomic regions that are involved in regulating such traits. In this pilot experiment, the interest was in identifying if methyl halide emissions could be measured from these varieties for future detailed linkage map analysis. Conclusions of Brassica linkage map analysis will not be presented in this thesis.

Single measurements were made of the ten different varieties of rapeseed at the teloscopying stage, again using a whole plant enclosure technique similar to that used in the *Arabidopsis thaliana* experiments. The plants were grown in a growth room at the JIC and planted out in one of the study fields at the JIC two weeks prior to the first sampling taking place. The plants were enclosed in 115 litre Teflon bags for 3 hours prior to sampling (Figure 5.9). To seal the Teflon bags around plants, plastic pipes of 16 cm di-

ameter were placed in the soil around each plant, extending 4-8 cm above the soil surface. The headspace of four soil blanks was also sampled at this stage, these were spatially distributed throughout the plants being sampled. All samples were collected into 1 litre evacuated SilcoCans using a battery pump, filling the SilcoCans to a positive pressure of 10 psi. The air samples were analysed on the UEA Entech GCMS system (Chapter 2), where 200 ml of each air sample was used in analysis.

Based on the results of the first round of sampling during the telescoping stage, the two pairs Ning You and Tapidor, and Capitol and Rocket were selected to be studied when flowering. These four varieties were then subjected to the same enclosure and sampling set-up, to observe if the differences between varieties remained similar in the plants at a later stage of development. Triplicate measurements of these varieties of rapeseed were used for this second field experiment at the JIC. The headspace of three soil blanks were also taken and again all samples were analysed on the UEA Entech GCMS system (Chapter 2), where 200 ml of each air sample was used in analysis. In order to get an estimate of biomass during the telescoping stage, whilst avoiding destroying the plant, total plant leaf area was estimated from the sum of recorded leaf lengths per plant, referred to as cumulative leaf length (Armeanu-D'Souza, 2009). As the second sampling, during flowering, was the final measurement of the experiment the biomass of the plants could be obtained when harvesting the plants. Whilst the cumulative leaf length provides a proxy for biomass, it is difficult to say how comparable it is with the actual weight of the plant. Harvest weight used here is fresh weight as the global production figures available from FAO are also fresh harvest weight.

5.3.3 Results and Discussion

The soil blanks in each experiment suggested uptake of methyl chloride with mixing ratios approximately half that of the average atmospheric background. The JIC does not have stocks of methyl bromide and laboratory air analysed contemporary to the field experiment contained typical background mixing ratios of the methyl halides. Methyl bromide was also approximately half that of the expected background in the first experiment sug-

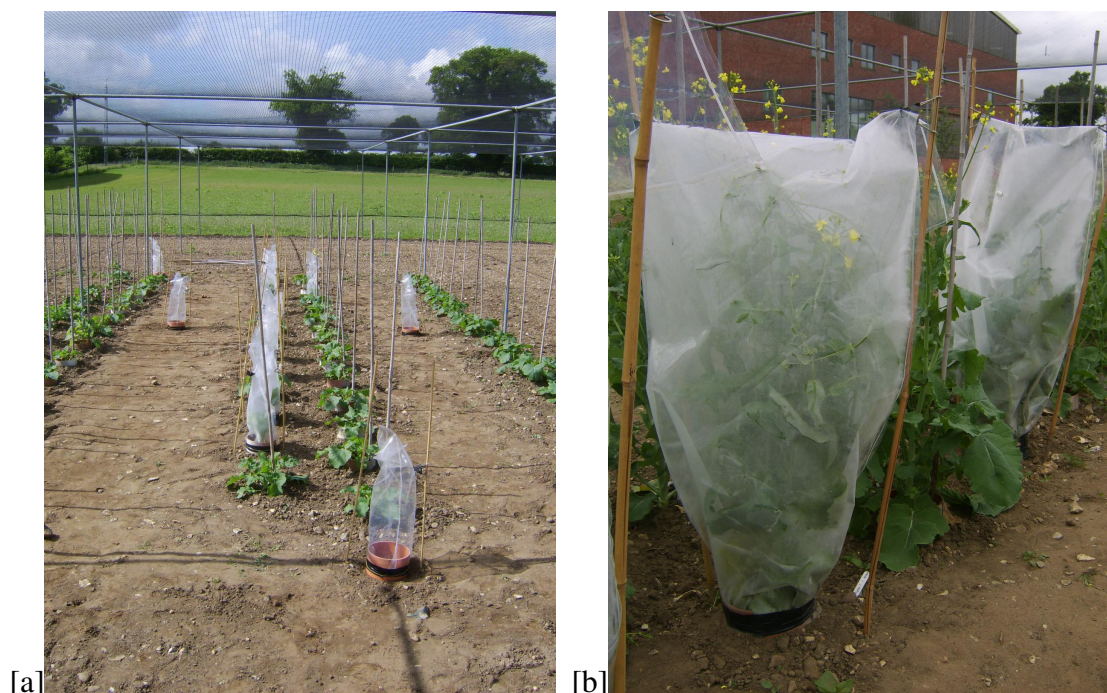


Figure 5.9: Plant enclosure sampling setup for *Brassica napus* field experiment. (a) Sampling at 104 days and (b) Sampling at 118 days.

gesting soil uptake of methyl bromide, however, in the second stage of the experiment the average of the soil blanks were slightly elevated above atmospheric background at a mean of 9.9 pptv. The methyl iodide mixing ratios in the soil blanks were considerably higher than the atmospheric background for both measurement stage one and two, at 12 pptv and 9 pptv respectively. The absolute mixing ratios from the different varieties measured here show the variety Ning You to exhibit the highest emission of the methyl halides, however, its partner Tapidor does not share this behaviour, showing some of the lowest emissions of methyl halides (Figure 5.10). This difference in emissions between the genetic pair, makes the Tapidor-NingYou mapping population particular well-suited for future analysis.

In an attempt to normalise these emissions by biomass, the methyl halide emission over time from each of the ten varieties of rapeseed have been plotted against their cumulative leaf length to identify whether the methyl halide emission would increase with increasing leaf length (Figure 5.11). When presented in this way, the emission of methyl halides from varieties Capitol and Rocket shows a fairly consistent emission for all three methyl halides where the variety Rocket is greater than or equal to the emission of methy

halides from Capitol. Figure 5.11 appears to show no correlation between the emission and the cumulative leaf length, but with one group of plants (Grizzley, Ning You and Verona) exhibiting higher emissions. Ning You consistently emits the most methyl halides of all the varieties. In contrast, its genetic partner Tapidor is consistently amongst the lowest emitting varieties. The pairs Ning You and Tapidor and, Capitol and Rocket were selected for further study in the second phase of the field experiment, to observe if the differences in emission between the varieties remains the same at a later stage of plant development.

The second phase of measurement during the flowering stage of the rapeseed plants found that all four varieties consistently emitted the methyl halides in the preferential order of methyl chloride > methyl bromide > methyl iodide (Figure 5.12). Ning You showed the highest methyl chloride flux of the four varieties with an average of 35 ng/g/d, however a large variance was observed among the three replicates of Ning You. One of the Ning You replicates was a replacement for a plant that had not survived the transition from the grow room to the study field, this particular plant had been grown in a reserve population and the stress of the introduction into the field set-up resulted in accelerated development and it was fruiting at the time of sampling when the other plants were flowering. This individual had a particularly large methyl chloride flux compared to the other two replicates, suggesting that the fruiting stage of development incurs large fluxes of methyl chloride into the atmosphere. The methyl bromide flux from Tapidor was the lowest of the four varieties, however, the pair showed similar methyl iodide fluxes. Consistently higher fluxes of the methyl halides from Capitol were observed compared to the Rocket variety.

In this experiment the fluxes of methyl bromide were higher (mean 98.7 ± 15 ng/g/d dry weight) than those reported in the Gan et al. (1998) study of rapeseed, where a flux of 25 ng/g/d (dry weight) was reported. However, to scale up these fluxes to a global emission from rapeseed the fluxes need to be in ng/g/d fresh weight to be comparable with the FAO rapeseed harvest statistics. Gan et al. (1998) use their dry weight flux multiplied by the FAO crop stats and as a result they calculate a disproportionately large

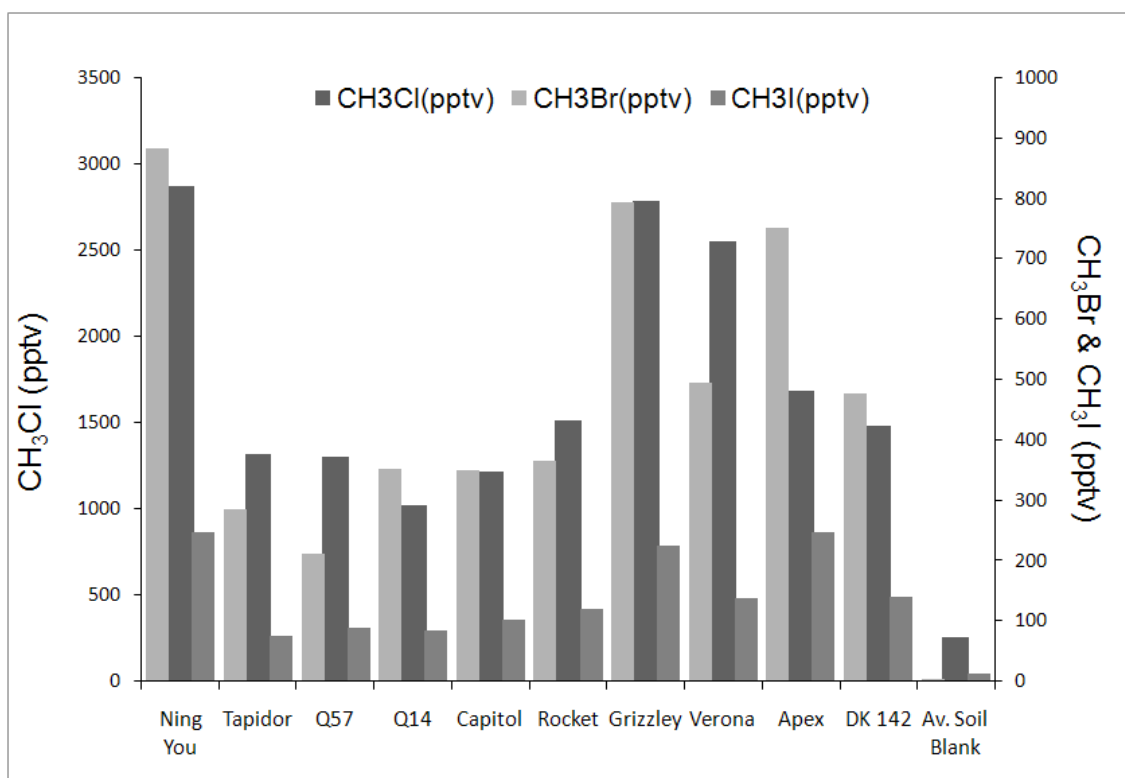


Figure 5.10: Mixing ratios of methyl halides from different varieties of rapeseed during telescoping stage of plant development. The mean of the soil blanks taken (n=4) is also represented in this figure.

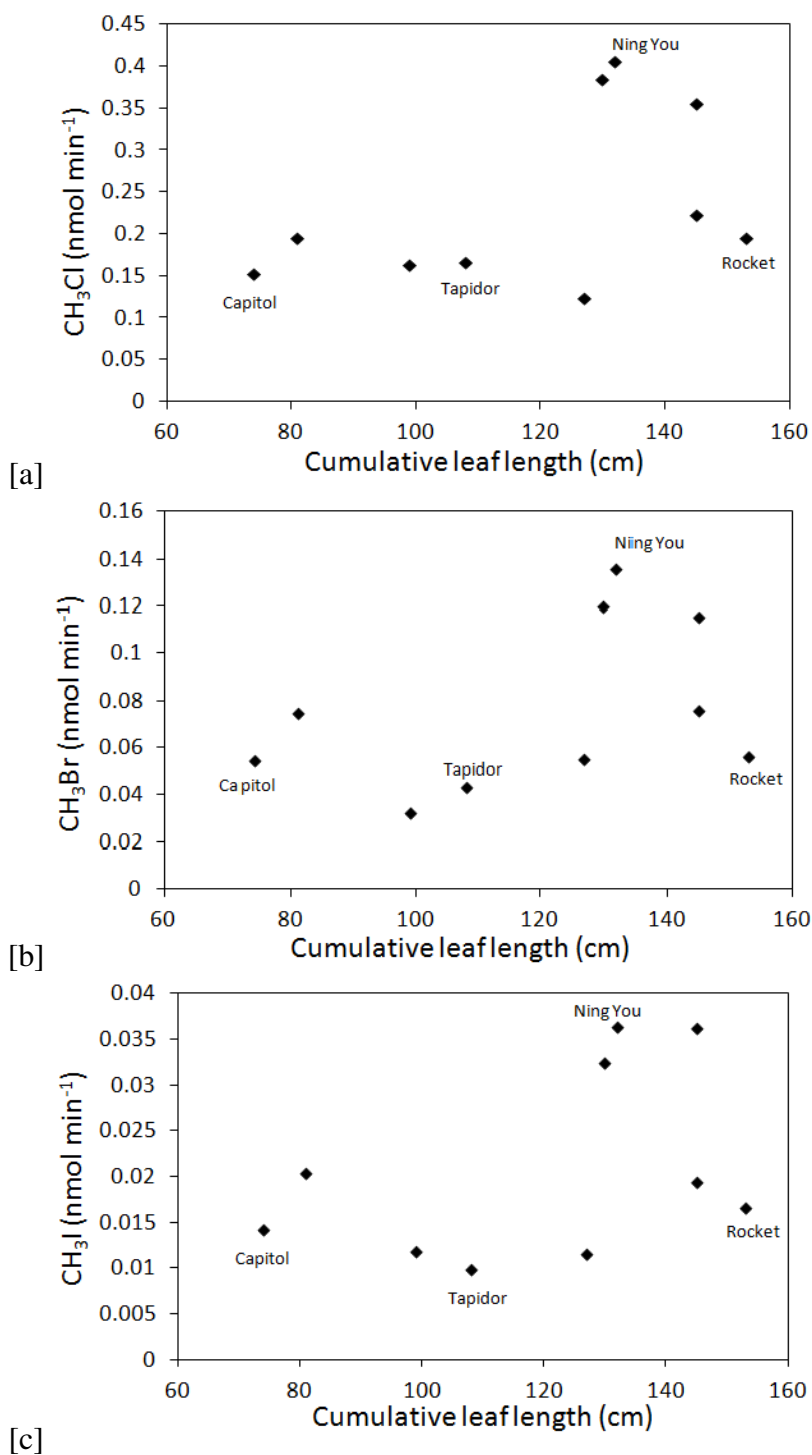


Figure 5.11: Methyl halide emissions per minute are plotted against the cumulative leaf length proxy for biomass. (a) Methyl chloride, (b) methyl bromide and (c) methyl iodide. The four varieties of rapeseed that were studied in the flowering stage are annotated in each plot.

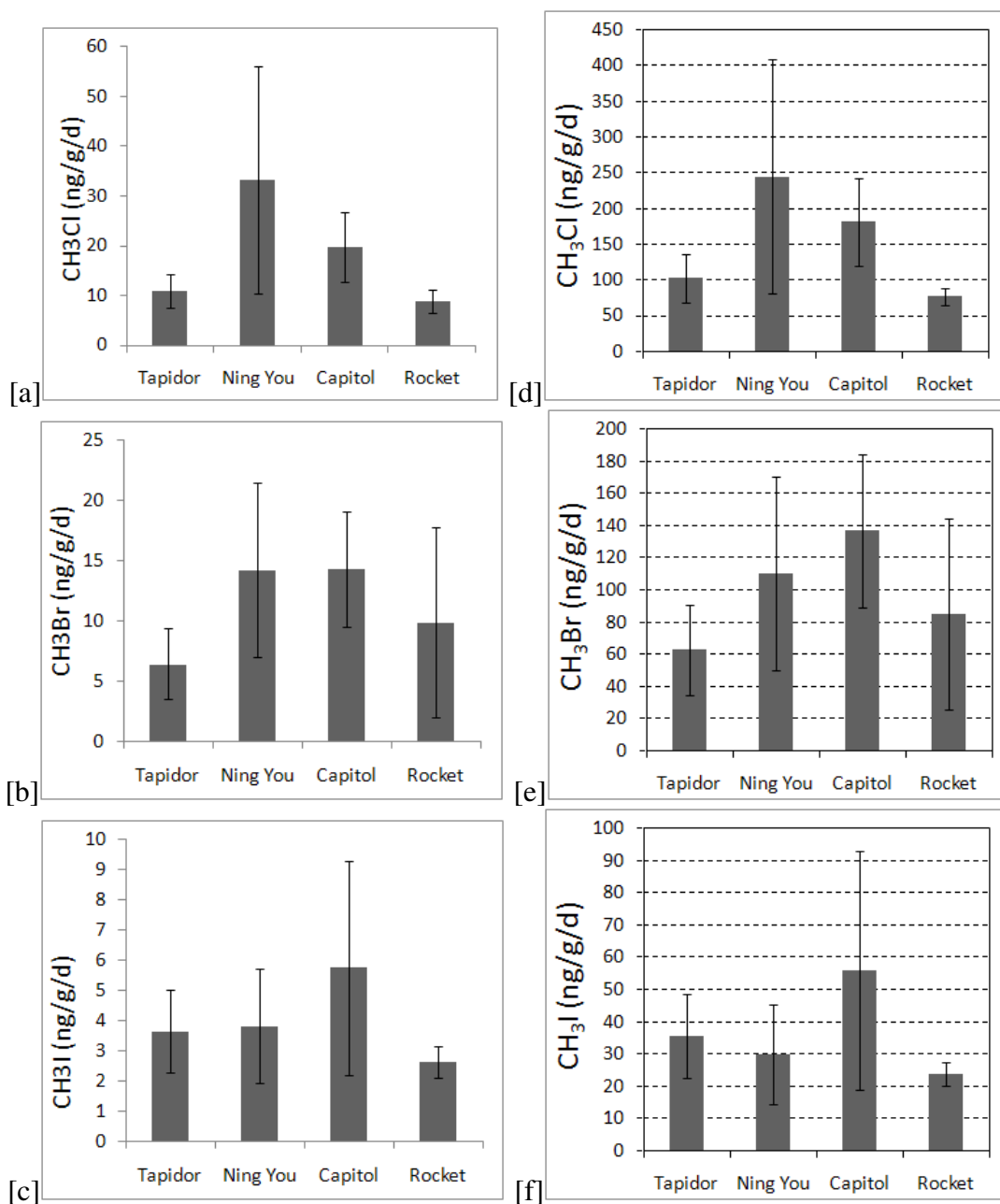


Figure 5.12: Methyl halide fluxes in ng/g/d from *Brassica napus* varieties Tapidor, Ning You, Capitol and Rocket. Shown in ng/g/d fresh weight (a) Methyl chloride, (b) methyl bromide and (c) methyl iodide and by ng/g/d dry weight (d) Methyl chloride, (e) methyl bromide and (f) methyl iodide. Data are means \pm SD (n=3).

global production of methyl bromide (6.6 Gg/yr) from *Brassica napus*. In this thesis fresh weight is reported so that the fluxes can be used to estimate global emissions using the FAO reported fresh weight biomass of the crop at harvest, this will be further covered in Section 5.6.

The correlation between the fluxes of methyl chloride and methyl bromide among the pair Tapidor and Ning You was $R^2 = 0.60$, whereas for the pair Capitol and Rocket the correlation between the methyl chloride and methyl bromide fluxes was $R^2 = 0.47$. Figure 5.12 shows a similarity between the methyl iodide fluxes for Tapidor and Ning You confirmed with an R^2 value of 0.71. Fluxes of methyl chloride and methyl iodide were poorly correlated for all four varieties.

5.3.4 Summary of *Brassica napus* field experiment

The measurements presented here from the 104 day old plants show that the *Brassica napus* variety Ning You emits the highest mixing ratios of all three methyl halides during the telescoping stage. Its genetic partner Tapidor is, contrastingly, a low emitter of all three methyl halides. The preferential order of emission of the methyl halides from *Brassica napus* at both stages of development, in the varieties analysed here, shows methyl chloride to be the dominant emission, followed by methyl bromide, with the least prevalent being methyl iodide emission. This is consistent with the approximate ratio between average concentrations of halogens in some soils, which have been reported to range from 56-1800, 0.5-6.0 and <0.5-6.0 ppm (dry weight) for chlorine, bromine and iodine respectively (Redeker et al., 2000).

The absolute mixing ratios at the telescoping stage were lower than those measured during the flowering stages of the plants. The Ning You mean flux for the flowering stage was skewed by one of the plants which had progressed on to the fruiting stage and exhibited very high emissions. Overall, the flux data appeared to show lower emissions of the methyl halides during the telescoping stage than the flowering stage, however, the comparison of biomass is complicated by the cumulative leaf length being the best available proxy for biomass at that stage. Further experiments would be necessary with a

large enough population of plants to destructively harvest plants at both stages, enabling fluxes in ng/g/d to be consistently reported. Or alternatively if cumulative leaf length were measured at the final stage prior to the destructive harvest, some relationship between the two parameters could be eluded to.

5.4 Effect of NaCl salinity on emission of methyl halides from *Brassica rapa*

5.4.1 Hypothesis 4

Sodium chloride (NaCl) salt stress effects the emission of methyl halides from *Brassica rapa* plants.

5.4.2 Rationale

This experiment focused on the effect of sodium chloride (NaCl) salinity on the methyl halide emissions from *Brassica rapa* (turnip) plants, also a member of the Brassicaceae family. Emission of methyl chloride and methyl bromide have been reported from saline environments such as coastal salt marshes (Rhew et al., 2000) and from coastal land (Yokouchi et al., 2000).

There is evidence that the process of methyltransferase is influenced by halide substrate exhibiting a preference for iodide > bromide > chloride (Attieh et al., 1995). The work of Attieh et al. (1995) also demonstrated an affinity of the methyltransferase to bisulphide (HS^-) to a similar magnitude as iodide and subsequent study showed that the highest affinity of the methyltransferase process was to thiocyanate (CNS^-) (Attieh et al., 2000). Thiocyanate and bisulphide are toxic to insects, therefore Attieh et al. (2000) suggested that the purpose of halide or bisulphide methyl transferase is to protect the plant by emitting a 'pesticide'.

5.4.3 Methodology for NaCl *Brassica rapa* experiment

This experiment was conducted in one of the greenhouses at the JIC. The plants were all grown in soil, three were control plants where no NaCl was added and three plants that were treated with 100 mM NaCl and another three plants treated with 200 mM NaCl. Salinity treatments were administered with a saline solution when watering and began 22 days after sowing, the treatments continued for 15 days, then the sampling took place. To

sample the emissions the whole plants were again enclosed in Teflon bags sealed to the plant pots three hours prior to sampling (Figure 5.13). Sampling took 1 litre into evacuated SilcoCans using a battery pump. All samples were analysed on the UEA Entech GCMS system.



Figure 5.13: Experimental set up in the greenhouse at JIC for the NaCl *Brassica rapa* study.

5.4.4 Results of NaCl treatment experiment

Methyl chloride fluxes dominated the emissions in the untreated, 100 mM and 200 mM NaCl treatments (Figure 5.14). Methyl bromide fluxes decreased dramatically, but not significantly, with increasing NaCl salinity treatment. The methyl iodide emission is very low throughout, though it does seem to exhibit a 2-fold increase in methyl iodide emission in the 100 mM treated plant compared to the control, however, the variability between the triplicate measurements is not significant. The 200 mM treated plants show similar emission to the control for methyl iodide. The reproducibility of the methyl iodide flux in the control plants and 200 mM treated plants were poor, with one point skewing the mean

of the data considerably.

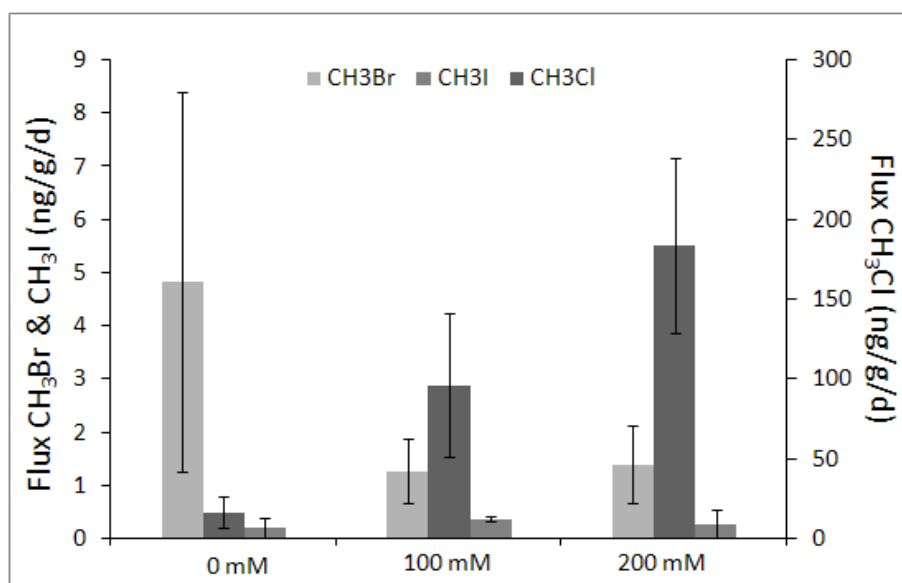


Figure 5.14: Methyl halide fluxes (ng/g/d fresh weight) from adult *Brassica rapa* plants treated with 0, 100 and 200 mM of NaCl. Data are means \pm SD (n=3).

The methyl bromide emissions decrease with NaCl treatment by 75% from the control to the 100 mM, the emission remains suppressed to the same degree for the 200 mM NaCl treated plant. A previous study conducting similar experiments, but using sodium bromide (NaBr), also showed an increase in emission of the halide that was introduced and a reduction in the emission of the other two methyl halides (Rhew et al., 2003). This supports the findings presented in this section and suggests that the plant system emits methyl halides to remove the excess halide from the plant system, as here an 11-fold increase of methyl chloride emission from the 200 mM compared to the control plant, and a 2-fold increase between the methyl chloride emission from the 100mM treated plant and the 200 mM treated plant.

5.4.5 Conclusions of NaCl treatment experiment.

Emissions of methyl chloride dominated the fluxes from the control plants and those under both NaCl treatments. The addition of the chloride in the form of NaCl appears to suppress the methyltransferase of the other halides and focus on removing the excess

chloride in the plant system. A further study developing this experiment with more replicate measurements would distinguish anomalous results and reduce their influence on the mean of the data.

5.5 Methyl halide emissions from rice, *Oryza sativa*

5.5.1 Hypothesis 5

Methyl halides are emitted from rice plants when grown in soil.

5.5.2 Methodology

Methyl halides emissions have been observed from rice paddies (Lee-Taylor and Redeker, 2005; Muramatsu and Yoshida, 1995; Redeker et al., 2002), the separation of plant and growth medium, i.e. paddy field have not been isolated, here methyl halide emissions from rice plants grown in soil are studied. Emissions of methyl halides from four different varieties of rice were measured. This was achieved by growing four different varieties of rice in a soil medium in a grow room at the JIC. The varieties grown were CO39, Yashiro Mochi, Bala and Nipponbare. The same plant enclosure technique as with the previous experiments was employed and analysis was again undertaken on the UEA Entech GCMS.

5.5.3 Results from rice experiment

The results of this experiment with rice (Figure 5.14) exhibit the similar preferential order of methyl halide emission with the experiments using members of the *Brassicaceae* family (methyl chloride > methyl bromide > methyl iodide). The methyl bromide flux was the highest from variety CO39. The variety Yashiro Mochi had to be discarded from interpretation as either the plant enclosure or the sampling canister were contaminated, therefore only CO39, Bala and Nipponbare will be discussed here. Bala exhibited higher fluxes of methyl bromide and iodide than the variety Nipponbare, however, Nipponbare showed a higher average flux for methyl chloride than that of Bala. Differences between the varieties Bala and Nipponbare were not significant. There was a large variation amongst the CO39 replicate fluxes of methyl chloride. The methyl bromide average flux from CO39 replicates were significantly higher than the other two varieties.

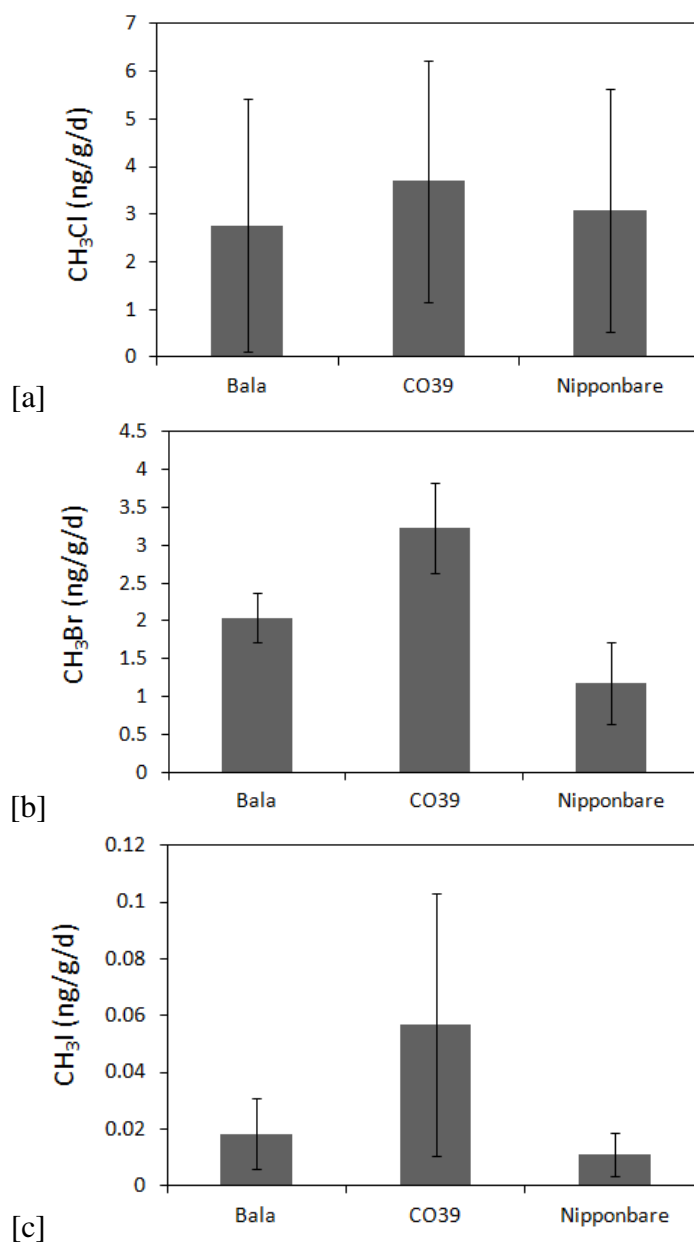


Figure 5.15: Fluxes of the methyl halides from the rice varieties Bala, CO39 and Nipponbare (ng/g/d fresh weight). Data are means \pm SD (n=3).

5.6 Global emission estimates based on the plant varieties measured

It is useful to consider the results presented in this chapter in a wider context, and compare the extrapolation of these results to global emission estimates from other studies. The World Meteorological Organization publish current estimates of the atmospheric budget of ozone depleting compounds in their scientific assessment of ozone pollution, currently rapeseed is attributed to 5% of the natural sources of methyl bromide to the atmosphere and rice is estimated to account for 1%. Rough estimates of the global production of methyl halides from the varieties of rapeseed and rice measured in these studies are presented here.

Gan et al. (1998) estimated the global production of methyl bromide from rapeseed (*Brassica napus*) alone to be 6.6 ± 1.6 Gg/yr. Since this study this high value has not been replicated, Mead et al. (2008b) found that a similar value to this can only be reached when modelling emissions for a short growing season and where the production figures only represent 25% of the actual biomass. Gan et al. (1998) arrive at this value by extrapolating their observed flux based on an undisclosed linear relationship between the soil halide content and the methyl halide emission, in the 1998 study the soil halide levels are deemed lower than the global average and so based on this undisclosed linear relationship the observed flux of 25 ng/g/d is scaled up to 515 ng/g/d (presumably dry weight) which yields 6.6 Gg yr⁻¹. Here using latest annual estimates of rapeseed (61.6×10^3 Gg yr⁻¹) and rice (67.9×10^3 Gg yr⁻¹) production values (FAOSTAT, 2011) the emission estimates below were calculated. Calculations made in this chapter will use a flux per fresh weight of plant which can be more directly compared with the FAO harvest figures.

A consideration with calculations such as these, particularly in the case of rapeseed, is the growing season of the crop. Unless the crop can be grown year round the production reported by the FAO is the total harvest gathered that year, however, this crop may only have been growing for several months of the year. Hence, the process of multiplying the flux calculated from our studies, by the FAO reported annual production of the crop may

introduce a large error in annual emission of methyl halides into the atmosphere from these more seasonal crops. Rapeseed has two main varieties: winter rapeseed and spring rapeseed. In our studies with the John Innes Centre winter rapeseed was used. Spring rapeseed varieties with a shorter growing season are grown in Canada and China where they plant in March/April and harvest in July/August. In the UK and other European countries winter rapeseed is planted in early September and harvested in July.

Another assumption with this technique is that the emission rate is constant throughout the plants life cycle. Although the *Brassica napus* field experiment had two sampling stages, at only one of those could a fresh weight be determined due to the destructive nature of the process. The cumulative leaf length was used as a proxy for biomass, however, there are various uncertainties with this method and it cannot be quantitatively used as a comparison with fresh or dry weight.

The FAO crop statistics only consider the portion of the plant which is of economic value i.e. it does not consider the portion of the crop left standing in the field after harvest. To account for this several studies have implemented a 'Harvest Index' to adjust the value to one more representative of the whole biomass of the plant (Diepenbrock, 2000; Gunasekera et al., 2001; Mead et al., 2008b). Mead et al. (2008b) used scenarios, for rapeseed, of 'low harvest index' where only 25% of the actual biomass is presumed to be harvested and a 'high harvest index' where 35% of the actual biomass is harvested. Harvest indexes have also been defined for rice with a high harvest index where estimated 55% of the plants biomass is harvested and a low harvest index where an estimated 45% of the plants biomass is harvested (Alam et al., 2009; Prasad et al., 2006; Yoshida, 1981). These scenarios are used in this thesis to further constrain the rapeseed and rice flux estimates from the studies described above.

The 1961-2009 rapeseed production trend fits an exponential fit with an R^2 of 0.98, though it is unrealistic that this will be the actual trend in rapeseed production, it can be used to calculate estimates of production over the next half century. Beyond that the area of land required to grow rapeseed, given an exponential trend, is unrealistic. For example, to reach a 2100 modelled emission 6 billion hectares of the Earth's land surface (14.8

billion Ha) would need to be cultivated for rapeseed crops. Extrapolating production rates using the aforementioned exponential fit of the current rapeseed data has been employed to estimate future global emissions of methyl halides from rapeseed (Tables 5.1, 5.2, 5.3).

5.6.1 Emission calculations

The emission estimates presented below were calculated in the following way. The Ideal Gas Law (Equation 47) can be utilised to calculate the number of moles of the methyl halide (Equation 48). Firstly, the raw mixing ratio data in pptv (i.e. $\times 10^{-12}$) minus the blank is multiplied by the volume of the bag enclosure (in m^3) giving the term 'V' for Equation 48.

$$pV = nRT \quad (47)$$

Where p = absolute pressure (95000 Nm^{-2}), V = volume, n = number of moles, R = universal gas constant ($8.3143 \text{ J K}^{-1} \text{ mol}^{-1}$) and T = temperature (290 K). This can be rearranged to give the number of moles by:

$$n = \frac{pV}{RT} \quad (48)$$

Then the number of moles calculated can be multiplied by the relative molecular mass (RMM) of the compound ($\text{CH}_3\text{Cl} = 50.5 \text{ g}$; $\text{CH}_3\text{Br} = 94.9 \text{ g}$; $\text{CH}_3\text{I} = 142 \text{ g}$) to yield the mass (g) of compound present. This mass should then be multiplied by the biomass (fresh weight) to yield g/g of the methyl halide. This should be divided by the period of enclosure to provide a flux in g/g/d. This flux (in g/g/d) is then multiplied by the growing season (in days) and the total rapeseed production for that year to yield g yr^{-1} . This annual emission can then be converted to the commonly used Gg yr^{-1} unit.

Currently it is estimated that 5% of the total methyl bromide emissions are from rapeseed and 1% from rice paddies (WMO, 2010). However, the value for rapeseed from Mead et al. (2008b), is modeled on the experimental work of Gan et al. (1998), who used dry weight which will have introduced error into the calculations. The work conducted with the JIC suggests that the current value included in the WMO ozone assessments for rapeseed contribution to the natural sources of methyl bromide is too high. The combined

Table 5.1: Estimated methyl chloride fluxes (Gg yr^{-1}) for 2009 and 2050 from different varieties of rapeseed. The 2009 values are based on the measurements reported in this chapter, the 2050 estimates are based on a continuation of the trend in global rapeseed production. Averages are also shown \pm standard deviation.

Variety of rapeseed	LS HHI	LS LHI	SS HHI	SS LHI	Average by variety
2009					
Tapidor	0.34	0.41	0.29	0.35	0.35 ± 0.05
Ning You	1.04	1.25	0.90	1.08	1.07 ± 0.14
Capitol	0.62	0.74	0.53	0.64	0.63 ± 0.09
Rocket	0.28	0.33	0.24	0.29	0.28 ± 0.04
Average by growing conditions	0.57 ± 0.34	0.68 ± 0.42	0.49 ± 0.30	0.59 ± 0.36	0.58 ± 0.24
2050					
Tapidor	3.68	4.42	3.18	3.81	3.77 ± 0.51
Ning You	11.3	13.5	9.71	11.7	11.5 ± 1.56
Capitol	6.65	7.98	5.74	6.88	6.81 ± 0.92
Rocket	2.99	3.59	2.58	3.10	3.07 ± 0.42
Average by growing conditions	6.15 ± 3.8	7.37 ± 4.5	5.30 ± 3.2	6.36 ± 3.9	6.29 ± 2.6

LHI, low harvest index; HHI, high harvest index; SS, short season; LS, long season (Mead et al., 2008b)

average of all rapeseed varieties measured and the different possible growing conditions produces a figure of 0.36 Gg yr^{-1} (Table 5.2) which is 0.3 % of methyl bromide sources, compared to the figure of 5.1 Gg yr^{-1} currently used in WMO 2010. Increasing cultivation could result in rapeseed contributing 4.3% of the natural methyl bromide budget by the year 2050.

Rice production for the same period has a linear upwards trend with a linear trendline matching the data with a R^2 value of 0.99, again using this projection of future rice yields global estimates of the methyl halide emissions have been calculated (Table 5.4). The figure currently used in the WMO ozone assessment is 0.7 Gg yr^{-1} which is 0.8% of natural methyl bromide sources, this is slightly lower than the estimates calculated here. From the rice varieties measured here values of $0.97 - 1.18 \text{ Gg yr}^{-1}$ were calculated, this is 1 - 1.3 % natural methyl bromide flux.

Table 5.2: Projected methyl bromide fluxes (Gg yr^{-1}) for 2009 and 2050 from different varieties of rapeseed. The 2009 values are based on the measurements reported in this chapter, the 2050 estimates are based on a continuation of the trend in global rapeseed production. Averages are also shown \pm standard deviation.

Variety of rapeseed	LS HHI	LS LHI	SS HHI	SS LHI	Average by variety
2009					
Tapidor	0.20	0.24	0.18	0.21	0.21 ± 0.03
Ning You	0.45	0.54	0.39	0.46	0.46 ± 0.06
Capitol	0.45	0.54	0.39	0.47	0.46 ± 0.06
Rocket	0.31	0.37	0.27	0.32	0.32 ± 0.04
Average by growing conditions	0.35 ± 0.1	0.42 ± 0.1	0.30 ± 0.1	0.37 ± 0.1	0.36 ± 0.9
2050					
Tapidor	2.19	2.63	1.89	2.27	2.24 ± 0.30
Ning You	4.83	5.80	4.17	5.00	4.95 ± 0.67
Capitol	4.85	5.82	4.19	5.02	4.97 ± 0.67
Rocket	3.36	4.03	2.90	3.47	3.44 ± 0.47
Average by growing conditions	3.81 ± 1.3	4.57 ± 1.5	3.28 ± 1.1	3.94 ± 1.3	3.9 ± 0.9

LHI, low harvest index; HHI, high harvest index; SS, short season; LS, long season (Mead et al., 2008b)

Lee-Taylor and Redeker (2005) modelled methyl halide emissions from rice paddies, estimating $2.4\text{-}4.9 \pm 73\% \text{Gg yr}^{-1}$ of methyl chloride, $0.5\text{-}0.9 \pm 87\% \text{Gg yr}^{-1}$ methyl bromide and $16\text{-}29 \pm 75\% \text{Gg yr}^{-1}$ of methyl iodide. Methyl bromide emissions from the rice varieties measured here are comparable with the Lee-Taylor and Redeker (2005) study, at $1.08 \pm 0.5 \text{Gg yr}^{-1}$. The rice varieties measured here exhibit lower emissions of methyl chloride ($1.59 \pm 0.3 \text{Gg yr}^{-1}$) and methyl iodide at least three orders of magnitude lower ($0.014 \pm 0.011 \text{Gg yr}^{-1}$) than the range suggested by Lee-Taylor and Redeker (2005) (Table 5.5). It is possible that in saturated rice paddy fields algae in the water are producing methyl iodide thus contributing to the high mixing ratios observed in the Lee-Taylor and Redeker (2005) study.

Table 5.3: Projected methyl iodide fluxes (Gg yr^{-1}) for 2009 and 2050 from different varieties of rapeseed. The 2009 values are based on the measurements reported in this chapter, the 2050 estimates are based on a continuation of the trend in global rapeseed production. Averages are also shown \pm standard deviation.

Variety of rapeseed	LS HHI	LS LHI	SS HHI	SS LHI	Average by variety
2009					
Tapidor	0.12	0.14	0.10	0.12	0.12 ± 0.02
Ning You	0.12	0.15	0.10	0.13	0.12 ± 0.02
Capitol	0.18	0.22	0.16	0.19	0.19 ± 0.03
Rocket	0.08	0.10	0.07	0.09	0.09 ± 0.01
Average by growing conditions	0.12 ± 0.04	0.15 ± 0.05	0.11 ± 0.04	0.13 ± 0.04	0.13 ± 0.03
2050					
Tapidor	1.24	1.49	1.07	1.29	1.27 ± 0.17
Ning You	1.30	1.56	1.12	1.34	1.34 ± 0.18
Capitol	1.95	2.34	1.68	2.02	2.00 ± 0.27
Rocket	0.90	1.07	0.77	0.93	0.92 ± 0.12
Average by growing conditions	1.35 ± 0.4	1.62 ± 0.5	1.16 ± 0.4	1.40 ± 0.5	1.38 ± 0.3

LHI, low harvest index; HHI, high harvest index; SS, short season; LS, long season (Mead et al., 2008b)

Table 5.4: Projected methyl halide fluxes (Gg) for 2050 and 2100 from different varieties of rice. The 2009 values are based on the measurements reported in this chapter, the 2050 and 2100 values are based on a continuation of the trend in global production.

Variety of rice	HHI			LHI		
	CH ₃ Cl	CH ₃ Br	CH ₃ I	CH ₃ Cl	CH ₃ Br	CH ₃ I
2009						
Bala	1.24	0.92	0.008	1.52	1.12	0.010
CO39	1.67	1.46	0.026	2.04	1.78	0.031
Nipponbare	1.39	0.53	0.005	1.70	0.65	0.006
Average by growing conditions	1.45±0.2	0.97±0.5	0.013±0.01	1.75±0.3	1.18±0.6	0.016±0.01
2050						
Bala	2.02	1.49	0.013	2.47	1.82	0.016
CO39	2.70	2.36	0.042	3.30	2.88	0.051
Nipponbare	2.26	0.86	0.008	2.76	1.05	0.010
Average by growing conditions	2.32±0.4	1.57±0.8	0.021±0.02	2.84±0.42	1.92±0.9	0.026±0.02
2100						
Bala	2.93	2.17	0.019	3.59	2.65	0.024
CO39	3.93	3.43	0.060	4.80	4.19	0.074
Nipponbare	3.28	1.25	0.012	4.01	1.53	0.014
Average by growing conditions	3.38±0.5	2.28±1.1	0.030±0.03	4.13±0.62	2.79±1.3	0.037±0.03

HHI, high harvest index where and estimated 55% of the plants biomass is harvested; LHI, low harvest index where and estimated 45% of the plants biomass is harvested (Alam et al., 2009; Prasad et al., 2006; Yoshida, 1981).

Model results obtained by Lee-Taylor and Redeker (2005) found that each increase of 1°C in ambient temperature resulted in a 10% increase in methyl bromide and methyl iodide emission from rice. Projections of the methyl bromide and methyl iodide emission from rice have been calculated here for future climate scenarios where the ambient temperature is increased by, 1, 2, 3 and 4°C. According to the IPCC Fourth Assessment Report surface temperature could increase up to 4°C over Europe by 2100 (Meehl et al., 2007), using the range of temperatures from this IPCC report and the projected methyl chloride emission for rice (Table 5.5), the values in Table 5.6 have been calculated. Temperature increases of up to 3°C are suggested in the IPCC report for mid 21st century.

Table 5.5: Best estimates for methyl halide fluxes (Gg yr^{-1}) from rapeseed and rice varieties measured in this work. The estimates are the means of all scenarios. Values are shown \pm standard deviation (n=3).

	Methyl chloride	Methyl bromide	Methyl iodide
Rapeseed	0.58 ± 0.24	0.36 ± 0.09	0.13 ± 0.03
Rice	1.59 ± 0.3	1.08 ± 0.5	0.014 ± 0.011

Table 5.6: Projected methyl bromide and methyl iodide from rice (Gg yr^{-1}) for a range of climate change scenarios. The values are calculated using the average methyl bromide and methyl iodide emissions from the rice varieties reported in this chapter. The different harvest index scenarios are shown as increases in rice harvest from the 2009 values of $\text{HHI} = 1.2 \times 10^6 \text{ Gg}$ and $\text{LHI} = 1.5 \times 10^6 \text{ Gg}$.

Harvest Index	Methyl bromide				Methyl iodide			
	+1°C	+2°C	+3°C	+4°C	+1°C	+2°C	+3°C	+4°C
HHI ($+0.8 \times 10^6$)	1.73	1.88	2.04	2.20	0.023	0.025	0.027	0.029
LHI ($+0.9 \times 10^6$)	2.11	2.30	2.49	2.69	0.028	0.031	0.033	0.036
HHI ($+1.7 \times 10^6$)	2.51	2.74	3.30	3.64	0.034	0.037	0.040	0.043
LHI ($+2.0 \times 10^6$)	3.07	3.35	3.80	4.14	0.041	0.045	0.048	0.052

HHI, high harvest index where and estimated 55% of the plants biomass is harvested; LHI, low harvest index where and estimated 45% of the plants biomass is harvested (Alam et al., 2009; Prasad et al., 2006; Yoshida, 1981).

Assuming the rest of the natural sources of methyl bromide remain fixed at their current known values, Table 5.6 shows that a temperature increase of just +1°C by 2050, com-

bined with a high harvest index, could increase the methyl bromide emission from rice by almost doubling its contribution to the natural methyl bromide budget. The methyl iodide figures calculated in Table 5.6 show that for these climate change scenarios the methyl iodide emission from rice remains well below that reported from rice paddies by Lee-Taylor and Redeker (2005).

5.7 Conclusions

The hypotheses investigating the *hol* gene in *Arabidopsis thaliana* plants were both confirmed: The *hol* gene has been shown to be responsible for methyl halide emission in *Arabidopsis thaliana*, supporting the work of Rhew et al. (2003). The lines over-expressing the gene, where it is deemed 'over active', displayed an expected increase in methyl halide emission.

Hypothesis 3 (Section 5.3) was partially confirmed with the *Brassica napus* field experiment showing Ning You to be the highest emitter of methyl halides from the rapeseed varieties studied, however, the extent to which development of the plant affects the methyl halide emission was not ascertained. Both the rapeseed experiment and the *Arabidopsis thaliana* experiment showed the same preferential order of methyl halide emission suggesting that this is a common trait of the Brassica family of plants.

It is clear that constancy in the reported biomass as fresh weight is an important factor when scaling up fluxes from the plant level to global emissions. Although there is clearly huge uncertainty with scaling up such small pilot studies, consistency in units will help reduce that error. This study suggests that the current value included in the WMO ozone assessments for rapeseed contribution to the natural sources of methyl bromide is too high at 5% compared to a contribution of 0.3% calculated in this work. However, if rapeseed cultivation continues to increase at the current trend, its contribution to the natural sources of methyl bromide could increase to 4.3% by 2050.

The rice varieties measured here emit methyl iodide at least three orders of magnitude lower than the range suggested by Lee-Taylor and Redeker (2005). A similar experiment where the rice plants are grown in saturated trays simulating a paddy field may provoke algal growth and associated methyl halide emissions, the change in growth media may invoke a flux similar to those observed by Lee-Taylor and Redeker (2005). However, the methyl bromide emission measured here is comparable with the figure reported by Lee-Taylor and Redeker (2005) used by the WMO in their latest ozone assessment report.

A temperature increase of +1°C by 2050 could increase the methyl bromide emission from rice by almost doubling its contribution to the natural methyl bromide budget. The

methyl iodide figures calculated in Table 5.6 show that for these climate change scenarios the methyl iodide emission from rice remains well below that reported from rice paddies by Lee-Taylor and Redeker (2005). There is scope to extend this sensitivity study to look at the changes in methyl halide emissions that would result from the temperature changes predicted for specific growing regions. This type of sensitivity study would also be applicable to the assessment of methyl halide emissions from tropical plant species such as those near the ground site of Bukit Atur during the OP3 project (Chapter 3).

Further experiments would greatly improve our understanding of how and why plants methylate the halides, particularly where the growth medium and substrate are analysed both before and after flux measurements, to quantify the halide content of the substrate and how much is readily available to the plant. The next step with the rice study is to identify the *hol* gene, or equivalent, in the rice plant to confirm that mutants in the rice family will also suppress the emission of methyl halides.

Chapter 6

Summary and Conclusions

A range of organohalogens and alkyl nitrates were successfully measured in Borneo during the OP3 project and the atmospheric composition of them described in Chapters 3 and 4 respectively.

The OP3 methyl chloride data showed higher values than the global atmospheric background levels, however, the values were not comparable with the mixing ratios reported by Yokouchi et al. (2002) (1,000 - 3,000 pptv in the ambient glasshouse air) or the emissions seen by Blei et al. (2010). The discrepancy between the leaf-level measurements of Blei et al. (2010) and the OP3 canopy-level measurements at Bukit Atur suggests that either methyl chloride has an unknown loss process in the rainforest environment, or that branch enclosure experiments force the plant's environment unrealistically and are not a sufficient representation of the ambient atmospheric composition. Greater understanding of why plants emit methyl halides could help explain why the methyl chloride signal is lost above the canopy: it could be that the plant emits methyl chloride to defend itself from pests and the interaction of the methyl chloride with the pest happens in a way that destroys the methyl chloride. This highlights the importance of an interdisciplinary approach to understanding plant emissions, such as that presented in Chapter 5 between the JIC and UEA that brings plant physiology and atmospheric chemistry together.

As current understanding of the atmospheric loss processes of methyl chloride do not support a hypothesis of a biological mechanism. The difference between sampling ambient air down an inlet, as described in Chapter 2, and branch enclosures, as in Blei

et al. (2010), is more likely to incur the discrepancy seen in the leaf-level and canopy-level data. To be certain of this, a series of validation experiments using the two methods could be undertaken involving plants with well characterised emissions, such as rapeseed or tobacco plants.

The organic bromine budgets calculated in Table 3.2 show that there is 6-7 pptv organic bromine available from short-lived brominated species (i.e. excluding methyl bromide), in the atmosphere over the landmass and seas of Sabah. This bromine could potentially contribute to the missing 3-5 pptv stratospheric bromine that is currently predicted (Montzka et al., 2010). The bromine budget calculated from the OP3 data confirms that the modelled 3-5 pptv contribution of short-lived brominated species is realistic.

The OP3 data presented in Chapter 3 suggests that the southeast coast is a source region for methyl bromide, methyl iodide and the short lived bromocarbons. The seaweed farms of the southeast coast are likely to be the source, supporting the work of Baker et al. (2001) and Yokouchi et al. (2005), amongst others, who reported high mixing ratios of these compounds from macroalgae. Furthering their work, the bromocarbon time series suggests that this coastal source could be diurnal. A further study to investigate the strength of this hypothesis would advance current understanding of the atmosphere-ocean exchange in the region. The daily variations in the time series from Bukit Atur may be a feature of the unusual nature of the site being within the daytime boundary layer but disconnected from the nocturnal boundary layer as hypothesised in Chapter 3.

The OP3 aircraft data and mean value maps confirmed the known sources of bromoform to be oceanic and so bromoform was used as an oceanic tracer. Periods of sustained elevated mixing ratios in the bromoform time series, termed 'events', were compared to variations with other compounds such as the alkyl nitrates: where the time series followed a similar variation, such as on the 28th April 2008, the change in mixing ratios was attributed to a change in air mass influencing the ground site.

Beyond the speciation of the atmospheric composition in the rainforest, data collected in the boundary layer over the oil palm plantations of Sabah showed high values of methyl chloride and chloroform. Flux measurements combined with canopy-level measurement

of these compounds in the oil palm plantations would clarify the role of the oil palms in the high mixing ratios of methyl chloride and chloroform observed.

Methyl nitrate was the dominant alkyl nitrate observed during the whole of the OP3 project. The mean concentration of methyl nitrate at the ground site of Bukit Atur increased from OP3-I to OP3-III, most likely this is linked to the change in prevailing wind direction between the two measurement periods. The methyl nitrate aircraft data in Chapter 4 shows that the highest mixing ratios were observed over the oil palm plantations of Sabah. Methyl and ethyl nitrate both show evidence of an alternative source besides their parent hydrocarbons (Chapter 4). The methyl and ethyl nitrate OP3 measurements support the literature by showing signs of marine influence, while introducing the hypothesis that oil palm plantations facilitate the formation of both nitrates. The oil palm plantations also appear to be a formation region for the propyl and butyl nitrates with 2-propyl nitrate average value almost 3 times higher than the average mixing ratio observed at the rainforest ground site for the same period. These findings provide a basic rationale for a study focusing on alkyl nitrates and their precursors in oil palm plantations. The contribution of the alkyl nitrates to the NO_y budget supports values in the literature for remote areas: the alkyl nitrates made up 3% of NO_y during OP3-I and 2% during OP3-III at the ground measurement site.

The periods of elevation seen in the propyl and butyl nitrate time series data for OP3-I and OP3-II are well correlated with anthropogenic precursors such as NO_x and the hydrocarbons, but also the bromocarbons confirming that changes in air mass are one of the greatest influences on the remote measurement site. The predominant factors influencing the variations observed at Bukit Atur appear to be meteorological, the origin of the air mass is important as well as the physical properties of the boundary layer.

The complexity of the OP3 data set leaves avenues of inquiry left open that could not be investigated here in this thesis. Further to the data collected as part of OP3, future ground based data in the oil palm plantations, at the coastlines and over the seas of Sabah would facilitate a fuller understanding of the emissions in these regions.

The laboratory and field experiments conducted between UEA and the JIC confirmed

that the *hol* gene is the gene responsible for methyl halide emission in *Arabidopsis thaliana* (Chapter 5), supporting the work of Rhew et al. (2003). The *Brassicaceae* plants studied emitted the methyl halides in the same preferential order, linking the trait between plants of this family and suggesting that the *hol* gene would be responsible for methyl halide emission across the *Brassicaceae* family.

This study suggests that the current value included in the WMO ozone assessment (2011) for rapeseed contribution to the natural sources of methyl bromide is too high at 5% compared to a contribution of 0.4% calculated in this work. However, its projected contribution to the natural sources of methyl bromide could increase to 4.3% by 2050 if production continued to follow the current trend. This work has shown that it is of paramount importance that freshweight is used in these calculations as opposed to dry weight which is the traditional unit employed in the literature to describe a plant emission rate. The FAO report their harvest figures in fresh weight and large errors are introduced if emission rates for dry weight are used.

The rice varieties measured and reported in Chapter 5 emit methyl iodide at least three orders of magnitude lower than the range suggested by Lee-Taylor and Redeker (2005). A similar experiment where the rice plants are grown in saturated trays simulating a paddy field may provoke algal growth and associated methyl halide emissions, the change in growth media may invoke a flux similar to those observed by Lee-Taylor and Redeker (2005). However, the methyl bromide emission measured here is comparable with the figure reported by Lee-Taylor and Redeker (2005) used by the WMO in their latest ozone assessment report (2011).

The findings of these novel experiments would justify further time and resources into this interdisciplinary field of crop genetics and atmospheric chemistry. As mentioned with regard to the methyl chloride data from OP3, these studies would benefit greatly from validation and comparison experiments. In this case it would be most informative to conduct a comparison of methyl halide mixing ratios from whole plant enclosures compared to grow room ambient air and the atmosphere above a field of the particular crop.

References

- Abarca, J. F., Casiccia, C. C. and Zamorano, F. D. (2002) Increase in sunburns and photosensitivity disorders at the edge of the antarctic ozone hole, southern chile, 1986-2000 *Journal of the American Academy of Dermatology* **46**(2) 193 – 199 doi:10.1067/mjd.2002.118556.
- AGAGE (2010) Advanced global atmospheric gases experiment *Technical report* URL <http://agage.eas.gatech.edu/data.htm>.
- Alam, M., Ali, M., Ruhul Amin, A. and Hasanuzzaman, M. (2009) Yield attributes, yield and harvest index of three irrigated rice varieties under different levels of phosphorus *Advances in Biological Research* **3**(3-4) 132–139.
- Armeanu-D'Souza, K. (2009) *Novel Halide Methyltransferases Catalyse the Synthesis of Methyl Halides in the Brassicales* Master's thesis John Innes Centre.
- Atkinson, R. and Arey, J. (2003) Gas-phase tropospheric chemistry of biogenic volatile organic compounds: a review *Atmospheric Environment* **37**, **Supplement 2**(0) 197–219 doi:10.1016/S1352-2310(03)00391-1.
- Atlas, E., Pollock, W., Greenberg, J. P., Heidt, L. and Thompson, T. M. (1993) Alkyl nitrates, nonmethane hydrocarbons, and halocarbon gases over the equatorial pacific ocean during Saga 3 *Journal of Geophysical Research* **98**(D9) 16,933–16,947.
- Attieh, J., Hanson, A. D. and Saini, H. S. (1995) Purification and characterization of a novel methyltransferase responsible for biosynthesis of halomethanes and methanethiol in brassica oleracea *Journal of Biological Chemistry* **270** 9250–9257.
- Attieh, J., Kleppinger-Sparace, K., Nunes, C., Sparace, S. and Saini, H. (2000) Evidence implicating a novel thiol methyltransferase in the detoxification of glucosinolate hydrolysis products in brassica oleracea l. *Plant Cell and Environment* **23** 165–174.

- Aucott, M., McCulloch, A., Graedel, T., Kleiman, G., Midgley, P. and Li., Y.-F. (1999) Anthropogenic emissions of trichloromethane (chloroform, CHCl₃) and chlorodifluoromethane (HCFC-22): Reactive chlorine emissions inventory *Journal of Geophysical Research* **104**(D7) 8405–8415 doi:10.1029/1999JD900053.
- BADC (2006) British Atmospheric Data Centre: European Centre for Medium-Range Weather Forecasts back trajectories <http://badc.nerc.ac.uk/data/ecmwf-op/> (last access: January 2011).
- Baker, J. M., Sturges, W. T., Sugier, J., Sunnenberg, G., Lovett, A. A., Reeves, C. E., Nightingale, P. D. and Penkett, S. A. (2001) Emissions of CH₃Br, organochlorines, and organoiodines from temperate macroalgae *Chemosphere - Global Change Science* **3**(1) 93–106 doi:10.1016/S1465-9972(00)00021-0.
- Bell, N., Hsu, L., Jacob, D. J., Schultz, M. G., Blake, D. R., Butler, J. H., King, D. B., Lobert, J. M. and Maier-Reimer, E. (2002) Methyl iodide: Atmospheric budget and use as a tracer of marine convection in global models *Journal of Geophysical Research* **107**(D17) 4340 doi:10.1029/2001jd001151.
- Bertman, S. B., Roberts, J. M., Parrish, D. D., Buhr, M. P., Goldan, P. D., Kuster, W. C., Fehsenfeld, F. C., Montzka, S. A. and Westberg, H. (1995) Evolution of alkyl nitrates with air mass age *Journal of Geophysical Research* **100**(D11) 22,805–22,813 doi:10.1029/95JD02030.
- Bill & Melinda Gates Foundation (2010) Progress Report: Stress-tolerant rice for farm households in africa and south asia URL <http://www.gatesfoundation.org/learning/Pages/2010-progress-report-irri-stress-tolerant-rice-development-for-farms-africa-asia.aspx> (last access: April 2011).
- Blake, N. J., Blake, D. R., Sive, B. C., Katzenstein, A. S., Meinardi, S., Wingenter, O. W., Atlas, E. L., Flocke, F., Ridley, B. A. and Rowland, F. S. (2003a) The seasonal evolution of NMHCs and light alkyl nitrates at middle to high northern latitudes during TOPSE *Journal of Geophysical Research* **108**(D4) 8359 doi:10.1029/2001JD001467.
- Blake, N. J., Blake, D. R., Swanson, A. L., Atlas, E., Flocke, F. and Rowland, F. S. (2003b) Latitudinal, vertical, and seasonal variations of C₁-C₄ alkyl nitrates in the troposphere over the Pacific Ocean during PEM-Tropics A and B: oceanic and continental sources *Journal of Geophysical Research* **108**(D2) 8242 doi:10.1029/2001JD001444.
- Blake, N. J., Blake, D. R., Wingenter, O. W., Sive, B. C., Kang, C. H., Thornton, D. C., Bandy, A. R., Atlas, E., Flocke, F., Harris, J. M. and Rowland, F. S. (1999) Aircraft measurements of the latitudinal, vertical, and seasonal variations of NMHCs, methyl nitrate, methyl halides, and DMS during the First Aerosol Characterization Experiment (ACE 1) *Journal of Geophysical Research* **104**(D17) 21,803–21,817 doi:10.1029/1999JD900238.

- Blei, E., Hardacre, C. J., Mills, G. P., Heal, K. V. and Heal, M. R. (2010) Identification and quantification of methyl halide sources in a lowland tropical rainforest *Atmospheric Environment* **44**(8) 1005–1010 doi:10.1016/j.atmosenv.2009.12.023.
- Butler, J. H., King, D. B., Lobert, J. M., Montzka, S. A., Yvon-Lewis, S. A., Hall, B. D., Warwick, N. J., Mondeel, D. J., Aydin, M. and Elkins, J. W. (2007) Oceanic distributions and emissions of short-lived halocarbons *Global Biogeochem. Cycles* **21**(1) GB1023 doi:10.1029/2006gb002732.
- Carpenter, L. and Liss, P. (2000) On temperate sources of bromoform and other reactive organic bromine gases *Journal of Geophysical Research* **105**(D16) 20,539– 20547 doi:10.1029/2000JD900242.
- Carpenter, L. J., Malin, G., Liss, P. S. and Küpper, F. C. (2000) Novel biogenic iodine-containing trihalomethanes and other short-lived halocarbons in the coastal east Atlantic *Global Biogeochemical Cycles* **14**(4) 1191– 1204 doi:10.1029/2000gb001257.
- Chuck, A., Turner, S. and Liss, P. S. (2002) Direct evidence for a marine source of C1 and C2 Alkyl Nitrates *Science* **297**(5584) 1151–1154 doi:10.1126/science.1073896.
- Cicerone, R. J., Stolarski, R. S. and Walters, S. (1974) Stratospheric ozone destruction by man-made chlorofluoromethanes **185**(4157) 1165–1167 doi:10.1126/science.185.4157.1165.
- Clemittshaw, K. C., Williams, J., Rattigan, O. V., Shallcross, D. E., Law, K. S. and Cox, R. A. (1997) Gas-phase ultraviolet absorption cross-sections and atmospheric lifetimes of several C2–C5 alkyl nitrates *J. Photoch. Photobio. A* **102** 117–126 doi:10.1016/S1010-6030(96)04458-9.
- Clerbaux, C., Cunnold, D., Anderson, J., Engel, A., Fraser, P., Mahieu, E., Manning, A., Miller, J., Montzka, S., Nassar, R., Prinn, R., Reimann, S., Rinsland, C., Simmonds, P., Verdonik, D., Weiss, R., Wuebbles, D. and Yokouchi, Y. (2007) *Scientific Assessment of Ozone Depletion: 2006* chapter 1: Long-lived compounds 50 World Meteorological Organization, Global Ozone Research and Monitoring Project, Geneva, Switzerland.
- Cox, M. L., Sturrock, G. A., Fraser, P. J., Siems, S. T. and Krummel, P. B. (2005) Identification of regional sources of methyl bromide and methyl iodide from AGAGE observations at cape grim, Tasmania *Journal of Atmospheric Chemistry* **50**(1) 59–77 doi:10.1007/s10874-005-2434-5.
- Crutzen, P. and Arnold, F. (1986) Nitric acid cloud formation in the cold antarctic stratosphere: a major cause for the springtime 'ozone hole' *Nature* **324**(6098) 651 – 655.
- Cullen, J. and Neale, P. (1994) Ultraviolet radiation, ozone depletion, and marine photosynthesis *Photosynthesis Research* **39** 303–320 ISSN 0166-8595 doi:10.1007/BF00014589.

- Dahl, E., Saltzman, E. and de Bruyn, W. (2003) The aqueous phase yield of alkyl nitrates from ROO+NO: implications for photochemical production in seawater *Geophysical Research Letters* **30**(6) 1271 doi: 10.1029/2002GL016811.
- Dahl, E. E. and Saltzman, E. S. (2008) Alkyl nitrate photochemical production rates in North Pacific seawater *Marine Chemistry* **112**(3-4) 137 – 141 doi:10.1016/j.marchem.2008.10.002.
- Day, D. A., Dillon, M. B., Wooldridge, P. J., Thornton, J. A., Rosen, R. S., Wood, E. C. and Cohen, R. C. (2003) On alkyl nitrates, O₃, and the 'missing NO_y' *Journal of Geophysical Research* **108**(D16) 4501 doi:10.1029/2003JD003685.
- Diepenbrock, W. (2000) Yield analysis of winter oilseed rape (*Brassica napus L.*): a review *Field Crops Research* **67** 35–49.
- Dimmer, C. H., Simmonds, P. G., Nickless, G. and Bassford, M. R. (2001) Biogenic fluxes of halomethanes from irish peatland ecosystems *Atmospheric Environment* **35**(2) 321 – 330 ISSN 1352-2310 doi:10.1016/S1352-2310(00)00151-5.
- Donner, L., Horowitz, L., Fiore, A., Seman, C., Blake, D. and Blake, N. (2007) Transport of radon-222 and methyl iodide by deep convection in the GFDL Global Atmospheric Model AM2 *Journal of Geophysical Research* **112**(D17303) doi:10.1029/2006JD007548.
- Fahey, D. and Hegglin, C., M.I. (2011) Twenty questions and answers about the ozone layer: 2010 update in *Scientific Assessment of Ozone Depletion: 2010* p. 72 World Meteorological Organization, Geneva, Switzerland [Reprinted from Scientific Assessment of Ozone Depletion: 2010, Global Ozone Research and Monitoring Project Report No. 52, 516 pp., World Meteorological Organization, Geneva, Switzerland, 2011.].
- FAOSTAT (2011) FAOSTAT-Agriculture *Technical report* Food and Agriculture Organization of the United Nations URL <http://faostat.fao.org/site/567/default.aspx#ancor>.
- Farman, J., Gardiner, B. and Shanklin, J. (1985) Large losses of total ozone in Antarctica reveal seasonal ClO_x/NO_x interaction *Letters to Nature* **315** 207 – 210 doi:10.1038/315207a0.
- Finlayson-Pitts, B. and Pitts, J. (2000) *Chemistry of the Upper and Lower Atmosphere: Theory, Experiments and Applications* Academic Press, San Diego.
- Fischer, H., de Reus, M., Traub, M., Williams, J., Lelieveld, J., de Gouw, J., Warneke, C., Schlager, H., Minikin, A., Scheele, R. and Siegmund, P. (2003) Deep convective injection of boundary layer air into the lowermost stratosphere at midlatitudes, *Atmospheric Chemistry and Physics* **3** 739–745 doi:10.5194/acp-3-739-2003.

- Flocke, F., Volz-Thomas, A., Buers, H.-J., Paitz, W., Garthe, H.-J. and Kley, D. (1998) Long-term measurements of alkyl nitrates in southern Germany 1. General behavior and seasonal and diurnal variation *Journal of Geophysical Research* **103**(D5) 5729–5746 doi:10.1029/97JD03461.
- Flocke, F., Volz-Thomas, A. and Kley, D. (1991) Measurements of alkyl nitrates in rural and polluted air masses *Atmospheric Environment. Part A. General Topics* **25**(9) 1951 – 1960 doi:DOI:10.1016/0960-1686(91)90276-D international Conference on the Generation of Oxidants Regional and Global Scales.
- Flury, M. and Papritz, A. (1993) Bromide in the natural environment: Occurrence and toxicity *Journal of Environmental Quality* **22** 747–758.
- Gan, J., Yates, S., Ohr, H. and Sims, J. (1998) Production of methyl bromide from terrestrial higher plants *Geophysical Research Letters* **25**(19) 3595–3598.
- Garratt, J. (1994) *The atmospheric boundary layer* Cambridge University Press, Cambridge.
- Gebhardt, S., Colomb, A., Hofmann, R., Williams, J. and Lelieveld, J. (2008) Halogenated organic species over the tropical rainforest *Atmospheric Chemistry and Physics Discussions* **8**(1) 1159–1190.
- Gettelman, A., Lauritzen, P. H., Park, M. and Kay, J. E. (2009) Processes regulating short-lived species in the tropical tropopause layer *Journal of Geophysical Research* **114**(D13303) doi:10.1029/2009JD011785.
- Goodwin, K. D., North, W. J. and Lidstrom, M. E. (1997) Production of bromoform and dibromomethane by giant kelp: Factors affecting release and comparison to anthropogenic bromine sources *Limnology and Oceanography* **42** 1725–1734.
- Gostlow, B., Robinson, A. D., Harris, N. R. P., O'Brien, L. M., Oram, D. E., Mills, G. P., Newton, H. M., Yong, S. E. and A Pyle, J. (2010) μ dirac: an autonomous instrument for halocarbon measurements *Atmospheric Measurement Techniques* **3** 507–521.
- Gribble, G. (1999) The diversity of naturally occurring organobromine compounds *Chemistry Society Reviews* **28** 335–346 doi:10.1039/a900201d.
- Gribble, G. (2000) The natural production of organobromine compounds *Environmental Science and Pollution Research* .
- Gross, J. (2011) *Mass Spectrometry* Springer Berlin / Heidelberg second edition edition.
- Guenther, A. (1995) A global model of natural volatile organic compound emissions *Journal of Geophysical Research* **100**(D5) 8873–8892.

- Guenther, A. (1997) Seasonal and spatial variations in natural volatile organic compound emissions *Ecological Applications* **7**(1) 34–45.
- Guenther, A. (2008) Are plant emissions green? *Nature* **452** 701–702.
- Gunasekera, C., Martin, L., Walton, G. and Siddique, K. (2001) Growth, dry matter production and seed yield of indian mustard (*brassica juncea* l.) in the mediterranean environment of south western australia, in *Proceedings of the 10th Australian Agronomy Conference: Science and Technology: Delivering Results for Agriculture?* The Australian Society of Agronomy, Hobart, Australia,.
- Hamilton, J., McRoberts, W., Keppler, F., Kalin, R. and Harper, D. (2003) Chloride methylation by plant pectin: An efficient environmentally significant process *Science* **301**(5630) 206–209.
- Hewitt, C. N., Lee, J. D., MacKenzie, A. R., Barkley, M. P., Carslaw, N., Carver, G. D., Chappell, N. A., Coe, H., Collier, C., Commane, R., Davies, F., Davison, B., DiCarlo, P., Marco, C. F. D., Dorsey, J. R., Edwards, P. M., Evans, M. J., Fowler, D., Furneaux, K. L., Gallagher, M., Guenther, A., Heard, D. E., Helfter, C., Hopkins, J., Ingham, T., Irwin, M., Jones, C., Karunaharan, A., Langford, B., Lewis, A. C., Lim, S. F., MacDonald, S. M., Mahajan, A. S., Malpass, S., McFiggans, G., Mills, G., Misztal, P., Moller, S., Monks, P. S., Nemitz, E., Nicolas-Perea, V., Oetjen, H., Oram, D. E., Palmer, P. I., Phillips, G. J., Pike, R., Plane, J. M. C., Pugh, T., Pyle, J. A., Reeves, C. E., Robinson, N. H., Stewart, D., Stone, D., Whalley, L. K. and Yin, X. (2010) Overview: oxidant and particle photochemical processes above a south-east asian tropical rainforest (the OP3 project): introduction, rationale, location characteristics and tools *Atmospheric Chemistry and Physics* **10**(1) 169–199 doi:10.5194/acp-10-169-2010.
- Hewitt, C. N., MacKenzie, A. R., Carlo, P. D., Marco, C. F. D., J. R. Dorsey, M. E., D. Fowler, M. W. G., Hopkins, J. R., Jones, C. E., Langford, B., Lee, J. D., Lewis, A. C., Lim, S. F., McQuaid, J., Misztal, P., Moller, S. J., Monks, P. S., Nemitz, E., Oram, D. E., Owen, S. M., Phillips, G. J., Pugh, T. A. M., Pyle, J. A., Reeves, C. E., Ryder, J., Siong, J., Skiba, U. and Stewart, D. J. (2009) Nitrogen management is essential to prevent tropical oil palm plantations from causing ground-level ozone pollution *Proceedings of the National Academy of Sciences of the United States of America, (PNAS)* **106**(44) 18447–18451.
- Holton, J. (2004) *Dynamic Meteorology* chapter 5: The planetary boundary layer, p. 969 Academic Press, San Diego.
- Hopkins, J. R., Boddy, R. K., Hamilton, J. F., Lee, J. D., Lewis, A. C., Purvis, R. M. and Watson, N. J. (2006) An observational case study of ozone and precursors inflow to south east england during an anticyclone *Journal of Environmental Monitoring* **8** 1195–1202 doi:10.1039/B608062F.

- Hopkins, J. R., Jones, C. E. and Lewis, A. C. (2011) A dual channel gas chromatograph for atmospheric analysis of volatile organic compounds including oxygenated and monoterpene compounds *Journal of Environmental Monitoring* **13** 2268–2276 doi:10.1039/C1EM10050E.
- Hubschmann, H.-J. (2009) *Handbook of GC/MS: Fundamentals and Applications* Wiley-VCH second edition.
- Jacob, D. (1999) *Introduction to Atmospheric Chemistry* Princeton University Press.
- James, R., Bonazzola, M., Legras, B., Surbled, K. and Fueglistaler, S. (2008) Water vapor transport and dehydration above convective outflow during asian monsoon *Geophysical Research Letters* **35**(L20810) doi:10.1029/2008GL035441.
- Keene, W. C., Khalil, M. A. K., Erickson, I., David J., McCulloch, A., Graedel, T. E., Lobert, J. M., Aucott, M. L., Gong, S. L., Harper, D. B., Kleiman, G., Midgley, P., Moore, R. M., Seuzaret, C., Sturges, W. T., Benkovitz, C. M., Koropalov, V., Barrie, L. A. and Li, Y. F. (1999) Composite global emissions of reactive chlorine from anthropogenic and natural sources: Reactive chlorine emissions inventory *Journal of Geophysical Research* **104**(D7) 8429–8440.
- Khalil, M. A. K., Moore, R. M., Harper, D. B., Lobert, J. M., Erickson, D. J., Koropalov, V., Sturges, W. T. and Keene, W. C. (1999) Natural emissions of chlorine-containing gases: Reactive chlorine emissions inventory *Journal of Geophysical Research* **104**(D7) 8333–8346.
- Khalil, M. A. K., Rasmussen, R. A. and Hoyt, S. D. (1983) Atmospheric chloroform (chcl₃): ocean-air exchange and global mass balance *Tellus B* **35B**(4) 266–274 doi:10.1111/j.1600-0889.1983.tb00029.x.
- Ko, M. K. W., Poulet, G., Blake, D. R., Boucher, B. J. C. M., O., Cox, R., George, C., Graf, H.-F., Holton, J., Jacob, D., Law, K. S., Lawrence, M. G., Midgley, P., Seakins, P., Shallcross, D. E., Strahan, S., Wuebbles, D. and Yokouchi, Y. (2003) in *Scientific Assessment of Ozone Depletion: 2002* chapter Chapter 2: Very short lived halogen and sulphur substances Global Ozone Research and Monitoring project, World Meteorological Organization, Geneva, Switzerland.
- Laternus, F., Haselmann, K., Borch, T. and Gron, C. (2002) Terrestrial natural sources of trichloromethane (chloroform, CHCl₃)-an overview *Biogeochemistry* **60**(2) 121–139.
- Laternus, F., Wiencke, C. and Adams, F. (1998) Influence of light conditions on the release of volatile halocarbons by antarctic macroalgae *Marine Environmental Research* **45**(3) 285 – 294 ISSN 0141-1136 doi:10.1016/S0141-1136(98)00025-7.
- Law, K., (Lead Authors), W. S., Blake, D., Blake, N., Burkholder, J., Butler, J., Cox, R., Haynes, P., Ko, M., Kreher, K., Mari, C., Pfeilsticker, K., Plane, J., Salawitch, R., Schiller, C., Sinnhuber, B.-M., von Glasow,

- R., Warwick, N., Wuebbles, D. and Yvon-Lewis., S. (2007) *Scientific Assessment of Ozone Depletion: 2006* chapter 2: Halogenated very short-lived substances, 50 World Meteorological Organization, Global Ozone Research and Monitoring Project, Geneva, Switzerland.
- Lee-Taylor, J. and Redeker, K. R. (2005) Reevaluation of global emissions from rice paddies of methyl iodide and other species *Geophys. Res. Lett.* **32**.
- Lelieveld, J., Butler, T. M., Crowley, J. N., Dillon, T. J., Fischer, H., Ganzeveld, L., Harder, H., Lawrence, M. G., Martinez, M., Taraborrelli, D. and Williams, J. (2008) Atmospheric oxidation capacity sustained by a tropical forest *Nature* **452**(7188) 737–740 ISSN 0028-0836.
- Lerdau, M. and Throop, H. (2000) Sources of variability in isoprene emission and photosynthesis in two species of tropical wet forest trees *Biotropica* **32**(4a) 670–676.
- Manley, S., Wang, N., Walser, M. and Cicerone, R. (2006) Coastal salt marshes as global methyl halide sources from determinations of intrinsic production by marsh plants *Global Biogeochemical Cycles* **20**.
- Manley, S. L. and Cuesta, J. L. d. I. (1997) Methyl iodide production from marine phytoplankton cultures *Limnology and Oceanography* **42**(1) 142–147 ISSN 00243590.
- Manley, S. L. and Dastoor, M. N. (1988) Methyl iodide (CH₃I) production by kelp and associated microbes *Marine Biology* **98** 477–482 doi:10.1007/BF00391538.
- Manley, S. L., Goodwin, K. and North, W. J. (1992) Laboratory production of bromoform, methylene bromide, and methyl iodide by macroalgae and distribution in nearshore southern California waters *Limnology and Oceanography* **37**(8) 1652–1659 ISSN 00243590.
- Manney, G. L., Santee, M. L., Rex, M., Livesey, N. J., Pitts, M. C., Veefkind, P., Nash, E. R., Wohltmann, I., Lehmann, R., Froidevaux, L., Poole, L. R., Schoeberl, M. R., Haffner, D. P., Davies, J., Dorokhov, V., Gernandt, H., Johnson, B., Kivi, R., Kyro, E., Larsen, N., Levelt, P. F., Makshtas, A., McElroy, C. T., Nakajima, H., Parrondo, M. C., Tarasick, D. W., von der Gathen, P., Walker, K. A. and Zinoviev, N. S. (2011) Unprecedented arctic ozone loss in 2011 *Nature* **478**(7370) 469–475 doi:10.1038/nature10556.
- McCulloch, A. (2003) Chloroform in the environment: occurrence, sources, sinks and effects *Chemosphere* **50**(10) 1291 – 1308.
- McKeen, S., Trainer, M., Hsie, E. Y., Tallamraju, R. K. and Liu, S. C. (1990) On the indirect determination of atmospheric OH radical concentrations from reactive hydrocarbon measurements *Journal of Geophysical Research* **95**(D6) 7493–7500.

- McKeen, S. A. and Liu, S. C. (1993) Hydrocarbon ratios and photochemical history of air masses *Geophysical Research Letters* **20**(21) 2363–2366.
- McMichael, A., Lucas, R., Ponsonby, A.-L. and Edwards, S. (2003) *Climate change and human health - risks and responses* chapter 8: Stratospheric ozone depletion, ultraviolet radiation and health World Health Organization, Geneva ISBN 9241590815.
- Mead, M. I., Khan, M. A. H., White, I. R., Nickless, G. and Shallcross, D. E. (2008a) Methyl halide emission estimates from domestic biomass burning in africa *Atmospheric Environment* **42**(21) 5241–5250 doi:10.1016/j.atmosenv.2008.02.066.
- Mead, M. I., White, I. R., Nickless, G., Wang, K. and Shallcross, D. E. (2008b) An estimation of the global emission of methyl bromide from rapeseed (*Brassica napus*) from 1961 to 2003 *Atmospheric Environment* **42**(2) 337–345 doi:10.1016/j.atmosenv.2007.09.020.
- Meehl, G., Stocker, T., Collins, W., Friedlingstein, P., Gaye, A., Gregory, J., Kitoh, A., Knutti, R., Murphy, J., Noda, A., Raper, S., Watterson, I., Weaver, A. and Zhao, Z.-C. (2007) *Global Climate Projections. In: Climate Change 2007: The Physical Science Basis. Contribution of Working Group I to the Fourth Assessment Report of the Intergovernmental Panel on Climate Change* chapter 10: Global Climate Projections Cambridge University Press, Cambridge, United Kingdom and New York, NY, USA.
- Midgley, P. M. and McCulloch, A. (1995) The production and global distribution of emissions to the atmosphere of 1,1,1-trichloroethane (methyl chloroform) *Atmospheric Environment* **29**(14) 1601–1608.
- Molina, M. and Rowland, F. (1974) Stratospheric sink for chlorofluoromethanes: chlorine atom-catalysed destruction of ozone *Nature* **249** 810 – 812 doi:10.1038/249810a0.
- Moller, S. (2010) *Nitrogen oxides in the remote boundary layer* Ph.D. thesis University of York, School of Chemistry.
- Montzka and Fraser (2003) Scientific assessment of ozone depletion: 2002 in *Global Ozone Research and Monitoring Project* volume Chapter 1, Section 1.2.5. World Meteorological Organization, Geneva.
- Montzka, S., Reimann, S., Engel, A., Kruger, K., O'Doherty, S., Sturges, W. T., Blake, D. R., Dorf, M., Fraser, P., Froidevaux, L., Jucks, K., Kreher, K., Kurylo, M., Mellouki, A., Miller, J., O.-J., N., Orkin, V., Prinn, R. G., Rhew, R., Santee, M., Stohl, A. and Verdonik, D. (2010) *Scientific Assessment of Ozone Depletion: 2010* chapter Chapter 1: Ozone-Depleting Substances (ODSs) and Related Chemicals Global Ozone Research and Monitoring project, World Meteorological Organization.
- Moore, R. (2008) A photochemical source of methyl chloride in saline waters *Environmental Science and Technology* **42**(6) 1933–1937.

- Moore, R. and Blough, N. (2002) A marine source of methyl nitrate *Geophysical Research Letters* **29**(15) 1–4.
- Moore, R., Gut, A. and Andreae, M. (2005) A pilot study of methyl chloride emissions from tropical woodrot fungi *Chemosphere* **58**(2) 221–225.
- Moore, R. M., Webb, M., Tokarczyk, R. and Wever, R. (1996) Bromoperoxidase and iodoperoxidase enzymes and production of halogenated methanes in marine diatom cultures *Journal of Geophysical Research* **101**.
- Muller, J. F., Stavrou, T., Wallens, S., Smedt, I. D., Roozendaal, M. V., Potosnak, M. J., Rinne, J., Munger, B., Goldstein, A. and Guenther, A. B. (2008) Global isoprene emissions estimated using MEGAN, ECMWF analyses and a detailed canopy environment model *Atmospheric Chemistry and Physics* **8**(5) 1329–1341.
- Muramatsu, Y. and Yoshida, S. (1995) Volatilization of methyl iodide from the soil-plant system *Atmospheric Environment* **29**(1) 21 – 25 doi:10.1016/1352-2310(94)00220-F.
- O'Brien, J. M., Shepson, P. B., Muthuramu, K., Hao, C., Niki, H., Hastie, D. R., Taylor, R. and Roussel, P. B. (1995) Measurements of alkyl and multifunctional organic nitrates at a rural site in Ontario *Journal of Geophysical Research* **100**(D11) 22,795–22,804.
- O'Doherty, L., S.J. and Carpenter (2007) *Volatile Organic Compounds in the Atmosphere* chapter 5: Halogenated Volatile Organic Compounds, pp. 173 – 220 Blackwell Publishing Ltd.
- O'Doherty, S., Simmonds, P. G., Cunnold, D. M., Wang, H. J., Sturrock, G. A., Fraser, P. J., Ryall, D., Derwent, R. G., Weiss, R. F., Salameh, P., Miller, B. R. and Prinn, R. G. (2001) In situ chloroform measurements at advanced global atmospheric gases experiment atmospheric research stations from 1994 to 1998 *Journal of Geophysical Research* **106**(D17) 20429–20444.
- Ohsawa, N., Ogata, Y., Okada, N. and Itoh, N. (2001) Physiological function of bromoperoxidase in the red marine alga, corallina pilulifera: production of bromoform as an allelochemical and the simultaneous elimination of hydrogen peroxide *Phytochemistry* **58** 683–692.
- Owen, S. M. and Hewitt, N. (2000) Extrapolating branch enclosure measurements to estimates of regional scale biogenic VOC fluxes in the northwestern mediterranean basin. *Journal of Geophysical Research* **105**(D9) 11,573 – 11,583.
- Pearson, G., Davies, F. and Collier, C. (2010) Remote sensing of the tropical rain forest boundary layer using pulsed doppler lidar *Atmospheric Chemistry and Physics* **10** 58915901.

- Peters, C., Pechtl, S., Stutz, J., Hebestreit, K., Hönninger, G., Heumann, K. G., Schwarz, A., Winterlik, J. and Platt, U. (2005) Reactive and organic halogen species in three different european coastal environments *Atmospheric Chemistry and Physics* **5**(12) 3357–3375.
- Piironen, A. K. (1994) *Analysis of volume imaging lidar signals* Ph.D. thesis University of Joensuu, Department of Physics.
- Prasad, P., Boote, K., Allen, L., Jr., Sheehy, J. and Thomas, J. (2006) Species, ecotype and cultivar differences in spikelet fertility and harvest index of rice in response to high temperature stress *Field Crops Research* **95**(2-3) 398 – 411 doi:10.1016/j.fcr.2005.04.008.
- Pyle, J. A., Ashfold, M. J., Harris, N. R. P., Robinson, A. D., Warwick, N. J., Carver, G. D., Gostlow, B., O'Brien, L. M., Manning, A. J., Phang, S. M., Yong, S. E., Leong, K. P., Ung, E. H. and Ong, S. (2011) Bromoform in the tropical boundary layer of the maritime continent during op3 *Atmospheric Chemistry and Physics* **11**(2) 529–542 doi:10.5194/acp-11-529-2011.
- Quack, B., Atlas, E., Petrick, G. and Wallace, D. W. R. (2007) Bromoform and dibromomethane above the mauritanian upwelling: Atmospheric distributions and oceanic emissions *Journal of Geophysical Research* **112**(D9) D09312 doi:10.1029/2006jd007614.
- Quack, B. and Wallace, D. (2003) Air-sea flux of bromoform: Controls, rates, and implications *Global Biogeochemical Cycles* **17**(1).
- Randel, W. J., Park, M., Emmons, L., Kinnison, D., Bernath, P., Walker, K. A., Boone, C. and Pumphrey, H. (2010) Asian monsoon transport of pollution to the stratosphere *Science* **328**(5978) 611–613 doi:10.1126/science.1182274.
- Read, K. A., Mahajan, A. S., Carpenter, L. J., Evans, M. J., Faria, B. V. E., Heard, D. E., Hopkins, J. R., Lee, J. D., Moller, S. J., Lewis, A. C., Mendes, L., McQuaid, J. B., Oetjen, H., Saiz-Lopez, A., Pilling, M. J. and Plane, J. M. C. (2008) Extensive halogen-mediated ozone destruction over the tropical atlantic ocean *Nature* **453**(7199) 1232–1235.
- Redeker, H., Wang, N.-Y., Low, J., McMillan, Tyler, S. and Cicerone, R. (2000) Emissions of methyl halides and methane from rice paddies *Science* **290**(5493) 966–969.
- Redeker, K. R., Andrews, J., Fisher, F., Sass, R. and Cicerone, R. J. (2002) Interfield and intrafield variability of methyl halide emissions from rice paddies *Global Biogeochem. Cycles* **16**(4).
- Redeker, K. R. and Cicerone, R. J. (2004) Environmental controls over methyl halide emissions from rice paddies *Global Biogeochem. Cycles* **18**.

- Reeves, C. E., Slemr, J., Oram, D. E., Worton, D., Penkett, S. A., Stewart, D. J., Purvis, R., Watson, N., Hopkins, J., Lewis, A., Methven, J., Blake, D. R. and Atlas, E. (2007) Alkyl nitrates in outflow from north america over the north atlantic during intercontinental transport of ozone and precursors 2004 *Journal of Geophysical Research* **112**.
- Rhew, L., R.C.and Ostergaard, Saltzman, E. S. and Yanofsky, M. (2003) Genetic control of methyl halide production in arabadopsis *Current Biology* **13** 1809–1813.
- Rhew, R. (2001) Shrubland fluxes of methyl bromide and methyl chloride *Journal of Geophysical Research* **106**(D18) 20,875–20,882.
- Rhew, R. C., Chen, C., Teh, Y. A. and Baldocchi, D. (2010) Gross fluxes of methyl chloride and methyl bromide in a california oak-savanna woodland *Atmospheric Environment* **44**(16) 2054 – 2061 ISSN 1352-2310 doi:10.1016/j.atmosenv.2009.12.014.
- Rhew, R. C., Miller, B. R. and Weiss, R. F. (2000) Natural methyl bromide and methyl chloride emissions from coastal salt marshes *Nature* **403** 292–295.
- Ricaud, P., Barret, B., Attié, J.-L., Motte, E., Le Flochmoën, E., Teyssèdre, H., Peuch, V.-H., Livesey, N., Lambert, A. and Pommereau, J.-P. (2007) Impact of land convection on troposphere-stratosphere exchange in the tropics *Atmospheric Chemistry and Physics* **7**(21) 5639–5657.
- Roberts, J. M. (1990) The atmospheric chemistry of organic nitrates *Atmospheric Environment* **24** 243287.
- Roberts, J. M., Bertman, S. B., Parrish, D. D., Fehsenfeld, F. C., Jobson, B. T. and Niki, H. (1998) Measurement of alkyl nitrates at chebogue point, nova scotia during the 1993 north atlantic regional experiment (nare) intensive *Journal of Geophysical Research* **103** 13,56913,580.
- Robinson, N., Newton, H., Allan, J. D., Irwin, M., Hamilton, J. F., Flynn, M., Bower, K. N., Williams, P. I., Mills, G., Reeves, C. E., McFiggans, G. and Coe, H. (2011) Source attribution of Bornean air masses by back trajectory analysis during the OP3 project *Atmospheric Chemistry and Physics* **11** 9605– 9630 doi:10.5194/acp-11-9605-2011.
- Russo, R. S., Zhou, Y., Haase, K. B., Wingenter, O. W., Frinak, E. K., Mao, H., Talbot, R. W. and Sive, B. C. (2010) Temporal variability, sources, and sinks of C1-C5 alkyl nitrates in coastal new england *Atmospheric Chemistry and Physics* **10** 1865– 1883.
- Saito, T., Yokouchi, Y., Kosugi, Y., Tani, M., Philip, E. and Okuda, T. (2008) Methyl chloride and isoprene emissions from tropical rain forest in southeast asia *Geophysical Research Letters* **35** doi: 10.1029/2008GL035241.

- Saxena, D., Aouad, S., Attieh, J. and Saini, H. S. (1998) Biochemical characterization of chloromethane emission from the wood-rotting fungus *phellinus pomaceus* *Applied Environmental Microbiology* **64** 2831–2835.
- Schall, C., Laturmus, F. and Heumann, K. (1994) Biogenic volatile organoiodine and organobromine compounds released from polar macroalgae *Chemosphere* **28**(7) 1315 – 1324 doi:10.1016/0045-6535(94)90076-0.
- Schauffler, S. M., Atlas, E. L., Blake, D. R., Flocke, F., Lueb, R. A., Lee-Taylor, J. M., Stroud, V. and Travnicek, W. (1999) Distributions of brominated organic compounds in the troposphere and lower stratosphere *Journal of Geophysical Research* **104**(D17) 21,513–21,535 doi:10.1029/1999JD900197.
- Shepson, P. (2007) *Volatile Organic Compounds in the Atmosphere* chapter 7: Organic nitrates, p. 500 Blackwell Publishing Ltd ISBN 978-1-4051-3115-5.
- Shepson, P. B., Anlauf, K. G., Bottenheim, J. W., Wiebe, H. A., Gao, N., Muthuramu, K. and Mackay, G. I. (1993) Alkyl nitrates and their contribution to reactive nitrogen at a rural site in ontario *Atmospheric Environment* **27** 749–757.
- Simpson, I., Meinardi, S., Blake, D. R., Blake, N. J. and Rowland, F. (2002) A biomass burning source of C1-C4 alkyl nitrates *Geophysical Research Letters* **29**(24) 2168.
- Simpson, I. J., Blake, N. J., Blake, D. R., Atlas, E., Flocke, F., Crawford, J. H., Fuelberg, H. E., Kiley, C. M., Meinardi, S. and Rowland, F. S. (2003) Photochemical production and evolution of selected C2-C5 alkyl nitrates in tropospheric air influenced by asian outflow *Journal of Geophysical Research* **108**.
- Simpson, I. J., Blake, N. J., Blake, D. R., Meinardi, S., Andersen, M. P. S. and Rowland, F. S. (2007) Strong evidence for negligible methyl chloroform (CH₃CCl₃) emissions from biomass burning *Geophysical Research Letters* **34**(10) L10805– doi:10.1029/2007GL029383.
- Simpson, I. J., Wang, T., Guo, H., Kwok, Y. H., Flocke, a. A. E., F., Meinardi, S., Rowland, F. S. and Blake, D. R. (2006) Long-term atmospheric measurements of C1-C5 alkyl nitrates in the pearl river delta region of southeast china *Atmospheric Environment* **40** 1619–1632.
- Sive, B. C., Varner, R. K., Mao, H., Blake, D. R., Wingenter, O. W. and Talbot, R. (2007) A large terrestrial source of methyl iodide *Geophysical Research Letters* **34**.
- Skoog, D., West, D., Holler, F. and Crouch, S. (2004) *Fundamentals of Analytical Chemistry* Brooks/Cole, Cengage Learning, 10 Davis Drive, Belmont, CA 94002-3098, USA eighth edition edition.

- Smith, R., Prezelin, B., Baker, K., Bidigare, R., Boucher, N., Coley, T., Karentz, D., MacIntyre, S., Matlick, H., Menzies, D. and et, a. (1992) Ozone depletion: ultraviolet radiation and phytoplankton biology in antarctic waters **255**(5047) 952–959 doi:10.1126/science.1546292.
- Smythe-Wright, D., Boswell, S. M., Breithaupt, P., Davidson, R. D., Dimmer, C. H. and Diaz, L. B. E. (2006) Methyl iodide production in the ocean: Implications for climate change *Global Biogeochemical Cycles* **20**(3) GB3003 doi:10.1029/2005gb002642.
- Solomon, S., Garcia, R. R. and Ravishankara, A. R. (1994) On the role of iodine in ozone depletion *Journal of Geophysical Research* **99**(D10) 20,491–20,499 doi:10.1029/94JD02028.
- Sommariva, R., Trainer, M., de Gouw, J. A., Roberts, J. M., Warneke, C., Atlas, E., Flocke, F., Goldan, P. D., Kuster, W. C., Swanson, A. L. and Fehsenfeld, F. C. (2008) A study of organic nitrates formation in an urban plume using a Master Chemical Mechanism *Atmospheric Environment* **42**(23) 5771 – 5786 doi: 10.1016/j.atmosenv.2007.12.031 selected Papers from the First International Conference on Atmospheric Chemical Mechanisms.
- Stroud, C. A. ., Roberts, J. M., Williams, J., Goldan, P. D., William C . Kuster, W., Ryerson, T. B., Sueper, D., Parrish, D. D., Trainer, M. and Fehsenfeld, F. C. (2001) Alkyl nitrate measurements during STERAO 1996 and NARE 1997: Intercomparison and survey of results *Journal of Geophysical Research* **106**(D19) 23043 – 23053.
- Sturges, D. E. C. L. J. P. S. A. E. A., William T. Oram (2000) Bromoform as a source of stratospheric bromine *Geophysical Research Letters* **27**.
- Sturges, G. C., W.T. and Buckley, P. (1992) Bromoform emission from arctic ice algae *Nature* **358** 660–662.
- Technologies, A. (1999) *5973 Network Mass Selective Detector: Hardware Manual* Agilent Technologies USA.
- von Glasow, R. and Cruzen, P. (2004) *The Atmosphere* chapter Tropospheric Halogen Chemistry, pp. 2–64 Elsevier ISBN 0-08-043751-6.
- Wayne, R. P. (1996) *Chemistry of Atmospheres* Oxford University Press.
- WMO (2003) Scientific assessment of ozone depletion: 2002 *Technical Report 47* World Meteorological Organization, Global Ozone Research and Monitoring Project Geneva.
- WMO (2007) Scientific assessment of ozone depletion: 2006 *Technical Report 50* World Meteorological Organization, Global Ozone Research and Monitoring Project Geneva.

- WMO (2010) Scientific assessment of ozone depletion: 2010 *Technical report* World Meteorological Organization, Global Ozone Research and Monitoring Project.
- Worton, D. (2005) *Alkyl nitrates (C1-C5), trihalomethanes and related compounds in contemporary air and air preserved in polar firn and ice*. Ph.D. thesis University of East Anglia, Environmental Sciences, Norwich, Doctor of Philosophy.
- Worton, D. R., Mills, G. P., Oram, D. E. and Sturges, W. T. (2008) Gas chromatography negative ion chemical ionization mass spectrometry: Application to the detection of alkyl nitrates and halocarbons in the atmosphere *Journal of Chromatography A* **1201**(1) 112–119 doi:10.1016/j.chroma.2008.06.019.
- Worton, D. R., Reeves, C. E., Penkett, S. A., Sturges, W. T., Slemr, J., Oram, D. E., Bandy, B. J., Bloss, W. J., Carslaw, N., Davey, J., Emmerson, K. M., Gravestock, T. J., Hamilton, J. F., Heard, D. E., Hopkins, J. R., Hulse, A., Ingram, T., Jacob, M. J., Lee, J. D., Leigh, R. J., Lewis, A. C., Monks, P. S. and Smith, S. C. (2010) Alkyl nitrate photochemistry during the tropospheric organic chemistry experiment *Atmospheric Environment* **44**(6) 773–785 doi:10.1016/j.atmosenv.2009.11.038.
- Worton, D. R., Sturges, W. T., Schwander, J., Mulvaney, R., Barnola, J. M. and Chappellaz, J. (2006) 20th century trends and budget implications of chloroform and related tri- and dihalomethanes inferred from firn air *Atmospheric Chemistry and Physics* **6**(10) 2847–2863 doi:10.5194/acp-6-2847-2006.
- Wuosmaa, A. and Hager, L. (1990) Methyl chloride transferase: a carbocation route for biosynthesis of halometabolites *Science* **249** 160–162.
- Yokouchi, Y., Hasebe, F., Fujiwara, M., Takashima, H., Shiotani, M., Nishi, N., Kanaya, Y., Hashimoto, S., Fraser, P., Toom-Sauntry, D., Mukai, H. and Nojiri, Y. (2005) Correlations and emission ratios among bromoform, dibromochloromethane, and dibromomethane in the atmosphere *Journal of Geophysical Research* **110**.
- Yokouchi, Y., Ikeda, M., Inuzuka, Y. and Yukawa, T. (2002) Strong emission of methyl chloride from tropical plants *Nature* **416** 163–165.
- Yokouchi, Y., Nojiri, Y., Barrie, L. A., Toom-Sauntry, D., Machida, T., Inuzuka, Y., Akimoto, H., Li, H. J., Fujinuma, Y. and Aoki, S. (2000) A strong source of methyl chloride to the atmosphere from tropical coastal land *Nature* **403**(6767) 295–298 ISSN 0028-0836 doi:10.1038/35002049.
- Yokouchi, Y., Saito, T., Ishigaki, C. and Aramoto, M. (2007) Identification of methyl chloride-emitting plants and atmospheric measurements on a subtropical island *Chemosphere* **69**(4) 549–553 doi:10.1016/j.chemosphere.2007.03.028.
- Yoshida, S. (1981) *Fundamentals of rice crop science* Manila International Rice Institute.

- Yuita, K. (1994) Overview and dynamics of iodine and bromine in the environment *Japan Agricultural Research Quarterly (JARQ)* **28** 90–111.
- Yvon-Lewis, S. A. and Saltzman, S. A., E. S. and (2009) Recent trends in atmospheric methyl bromide: analysis of post-montreal protocol variability *Atmospheric Chemistry and Physics* **9**(16) 5963–5974 doi: 10.5194/acp-9-5963-2009.
- Zhou, Y., Mao, H., Russo, R. S., Blake, D. R., Wingenter, O. W., Haase, K. B., Ambrose, J., Varner, R. K., Talbot, R. and Sive, B. C. (2008) Bromoform and dibromomethane measurements in the seacoast region of New Hampshire *Journal of Geophysical Research* **113** 2002–2004.
- Zhou, Y., Varner, R. K., Russo, R. S., Wingenter, O. W., Haase, K. B., Talbot, R. and Sive, B. C. (2005) Coastal water source of short-lived halocarbons in new england *Journal of Geophysical Research* **110**.
- Zimmerman, P. R., Greenberg, J. P. and Westberg, C. E. (1988) Measurements of atmospheric hydrocarbons and biogenic emission fluxes in the amazon boundary layer *Journal of Geophysical Research* **93**(D2) 1407–1416.

Source attribution of Bornean air masses by back trajectory analysis during the OP3 project

N. H. Robinson¹, H. M. Newton², J. D. Allan^{1,3}, M. Irwin¹, J. F. Hamilton^{4,5}, M. Flynn¹, K. N. Bower¹, P. I. Williams^{1,6}, G. Mills², C. E. Reeves², G. McFiggans¹, and H. Coe¹

¹Centre for Atmospheric Science, University of Manchester, Manchester, UK

²School of Environmental Sciences, University of East Anglia, Norwich, UK

³National Centre for Atmospheric Science, University of Manchester, Manchester, UK

⁴Department of Chemistry, The University of York, York, UK

⁵National Centre for Atmospheric Science, University of York, York, UK

⁶Facility for Groundbased Atmospheric Measurements, University of Manchester, UK

Received: 4 May 2011 – Published in Atmos. Chem. Phys. Discuss.: 18 May 2011

Revised: 5 September 2011 – Accepted: 13 September 2011 – Published: 16 September 2011

Abstract. Atmospheric composition affects the radiative balance of the Earth through the creation of greenhouse gases and the formation of aerosols. The latter interact with incoming solar radiation, both directly and indirectly through their effects on cloud formation and lifetime. The tropics have a major influence on incoming sunlight however the tropical atmosphere is poorly characterised, especially outside Amazonia. The origins of air masses influencing a measurement site in a protected rainforest in Borneo, South East Asia, were assessed and the likely sources of a range of trace gases and particles were determined. This was conducted by interpreting in situ measurements made at the site in the context of ECMWF backwards air mass trajectories. Two different but complementary methods were employed to interpret the data: comparison of periods classified by cluster analysis of trajectories, and inspection of the dependence of mean measured values on geographical history of trajectories. Sources of aerosol particles, carbon monoxide and halocarbons were assessed. The likely source influences include: terrestrial organic biogenic emissions; long range transport of anthropogenic emissions; biomass burning; sulphurous emissions from marine phytoplankton, with a possible contribution from volcanoes; marine production of inorganic mineral aerosol; and marine production of halocarbons. Aerosol sub- and super-saturated water affinity was found to be dependent on source (and therefore composition), with more hygroscopic aerosol and higher numbers of

cloud condensation nuclei measured in air masses of marine origin. The prevailing sector during the majority of measurements was south-easterly, which is from the direction of the coast closest to the site, with a significant influence inland from the south-west. This analysis shows that marine and terrestrial air masses have different dominant chemical sources. Comparison with the AMAZE-08 project in the Amazon basin shows Bornean composition to arise from a different, more complex mixture of sources. In particular sulphate loadings are much greater than in Amazonia which is likely to mainly be the result of the marine influence on the site. This suggests that the significant region of the tropics made up of island networks is not well represented by extrapolation from measurements made in the Amazon. In addition, it is likely that there were no periods where the site was influenced only by the rainforest, with even the most pristine inland periods showing some evidence of non-rainforest aerosol. This is in contrast to Amazonia which experienced periods dominated by rainforest emissions.

1 Introduction

In order to assess and predict the anthropogenic influence on climate, it is also important to understand the natural role of the biosphere. One way the biosphere can affect climate is through its role in aerosol production. This aerosol can then interact with solar radiation directly, acting to scatter short-wave radiation to space, and indirectly through its role as cloud condensation nuclei (CCN) acting to influence cloud brightness and persistence (Denman et al., 2007).



Correspondence to: H. Coe
(hugh.coe@manchester.ac.uk)

The tropics have a large influence on global climate due to the high surface flux of solar radiation, however to date the comprehensive data needed to fully characterise the gas and aerosol composition in these environments has been scarce. The tropics contain about half the World's forests (Food and Agriculture Organisation, 2010), playing a major role in the global biosphere. This natural background is being affected by anthropogenic activity such as deforestation and land use changes. It is important to assess the extent to which anthropogenic activities are affecting tropical aerosol, and their subsequent effects on climate.

Intensive field studies have been performed in Amazonia (ACP special issue OP3/ACES: Oxidant and particle photochemical processes above a south-east Asian tropical rain forest), Martin et al., 2010; JGR special issue 107, Avissar et al., 2002) and West Africa (ACPD special issue AMMA Tropospheric Chemistry and Aerosols; Lebel et al., 2010) but until now data from South East Asia has been limited. Specifically, the AMAZE-08 project in Amazonia found that sub-micron aerosol was dominated by biogenic secondary organic aerosol (BSOA) with elevated levels of oxidised organic aerosol (OOA) and sulphate during periods influenced by out-of-basin sources, which were attributed to biomass burning transport from Africa or a marine influence (Chen et al., 2009). The major source of submicron aerosol in West Africa is from biomass burning during the dry season and BSOA during the monsoon season (Capes et al., 2009, 2008). It also experiences high sulphate loadings which may be due to the influence of the Atlantic Ocean, although data coverage and quality did not allow this to be drawn as a conclusion.

Borneo is home to one of the largest expanses of rainforest in the world making it an important part of the biosphere and a potentially large source of volatile organic compounds (VOC) and associated BSOA. There is widespread deforestation on Borneo where land is being given over to logging and, particularly, palm oil production (McMorrow and Talip, 2001), meaning the role of the biosphere in the region is changing. Global palm oil production grew by 8% per year between 1976 and 2006, with the majority of production in Malaysia and Indonesia (Carter et al., 2007). It has been shown that oil palms are a large source of isoprene in Borneo (five times more than the rainforest; Hewitt et al., 2009). Isoprene has previously been found to produce secondary organic aerosol (SOA) in chambers and field studies (Claeys et al., 2004; Surratt et al., 2006, 2008; Paulot et al., 2009; Kleindienst et al., 2009; Surratt et al., 2010; Chan et al., 2010) and is thought to produce a substantial fraction of the SOA in Borneo (Robinson et al., 2011). As Borneo is an island, marine influences could be much larger than that in Amazonia and Africa. The oceans are a source of dimethyl sulphide (DMS) produced by phytoplankton (Kloster et al., 2006), minerals contained in sea water (Millero, 1974), halocarbons (Butler et al., 2007) and OA (O'Dowd et al., 2004; Novakov et al., 1997; Facchini et al., 2008). Borneo has a population of around 16 million people, mostly inhabiting

regions around the coast, so there is potential for influence of anthropogenic pollution in the form of combustion related emissions from transport, power stations or biomass burning. There is an abundance of volcanoes near Borneo which are a known source of sulphurous gases that are processed in the atmosphere to form aerosol (Pandis et al., 1995; Allen et al., 2002), which may contrast to other tropical studies that have not reported a volcanic influence (Chen et al., 2009; Capes et al., 2008).

Measurements were made as part of the Oxidant and Particulate Photochemical Processes Above a South East Asian Rainforest (OP3) project in protected rainforest in Sabah, Borneo (Hewitt et al., 2010). This region extends from around 4° N to the north coast of the island. Investigating the relationship between composition and synoptic flow can provide insight into significant regional sources. Two different but complementary methods employing back trajectories are used to attribute geographical sources, which can then be linked to likely emission sources. The focus of the paper is on species with a long enough atmospheric lifetime (hours or more) to be suitable for the analyses; mainly sub-micron aerosol composition and physical property measurements, but also long lived trace gases such as CO and halocarbons. Specifically the issues dealt with are the separation of atmospheric species originating on- and off-island and the attribution of likely sources.

2 Methods

2.1 Instrumentation

Measurements were performed at the Bukit Atur site (4°58'49.33" N, 117°50'39.05" E, 426 m a.s.l.) during two periods: 7 April–4 May (OP3-I) and 23 June–23 July (OP3-III). Measurements from the intervening period (OP3-II) were made from a different measurement site and are not detailed here. An overview of measurement techniques and a description of the measurement site can be found in the OP3 overview paper, Hewitt et al. (2010). There was poor data coverage during OP3-I and, though air mass characterisations of both periods are presented in Sect. 2 for reference, results presented here focus on OP3-III.

Aerosol composition was measured using a High Resolution Aerodyne Aerosol Mass Spectrometer (AMS; DeCarlo et al., 2006; Canagaratna et al., 2007) – a state of the art instrument capable of providing detailed bulk composition and aerodynamic sizing measurements of aerosols with a time resolution of minutes. It is limited to measurements of sub-micron non-refractory aerosol, where non-refractory (NR) is operationally defined as a species that volatilises quickly (on time-scales of less than a second) after impaction on the tungsten vaporiser (nominally run at 600 °C). Conversion of AMS aerosol mass loadings into total aerosol volume (assuming organic and inorganic densities as in Cross et al., 2007) allowed for comparison with a DMPS sampling from the same

inlet, and limited to the same size range. The instruments agreed and correlated well ($r = 0.92$) and a linear regression of AMS vs. DMPS volume series gave a gradient of 0.45. The collection efficiency (CE) factor accounts for the likelihood that a particle will be successfully vapourised and detected once in the AMS, and has typically been found to be around 0.5 in other projects (Matthew et al., 2008). The gradient of the linear regression is consistent with this and a CE of 0.5 has been applied to all the AMS data.

Despite extensive fragmentation, individual peaks in the mass spectrum provide more information about aerosol composition. Insight into the photochemical age of organic aerosols (OA) can be gained from the m/z 44 (mainly CO_2^+) to 43 (mainly $\text{C}_2\text{H}_3\text{O}^+$ and C_3H_7^+) peaks (Ng et al., 2010; Jimenez et al., 2009; Morgan et al., 2010). Organic spectra with a low f_{44} and high f_{43} (where f_x denotes the fraction of the organic mass at $m/z = x$) are less oxidised and can be thought of as semi-volatile aerosol (SV-OOA) which exist in an equilibrium between the gas and condensed phases. Aerosol with high f_{44} and low f_{43} are more oxidised and can be thought of as low volatility aerosol (LV-OOA) which exists mainly in the condensed phase.

In reality organic aerosol exist in a continuum between these two endpoints that can be expressed by points on a 2-D f_{44} vs. f_{43} space. The peak at m/z 60 can be used as a marker for fresh biomass burning (Alfarra et al., 2007; Capes et al., 2008), being a peak associated with levoglucosan and other anhydrous sugars which are compounds widely reported to be emitted during biomass burning (Simoneit et al., 1999; Jordan et al., 2006). It has been shown that as organic aerosol ages (with increasing f_{44} and decreasing f_{43}) its mass spectral signature becomes similar and dominated by m/z 44 regardless of source (McFiggans et al., 2005; Ng et al., 2010; Morgan et al., 2010).

The unit mass resolution organic aerosol data from the AMS were analysed using positive matrix factorisation (PMF). This is a multivariate technique that endeavours to explain the bulk organic AMS mass spectral time series in terms of time series of differing amounts of static “factor” spectra which can then be linked to distinct components of the ensemble organic aerosol mass (Paatero and Tapper, 1994; Paatero, 1997; Ulbrich et al., 2009). The details of the PMF analysis of the OP3 data were originally published in Robinson et al. (2011). The dependence of the solution on starting parameters (seeds) and rotational ambiguity (fpeak) was explored. In short, the most satisfactory solution was found to be the four factor solution. The results of the PMF analysis are discussed in more detail in Sect. 2.3. The high mass resolution of the AMS also enables the separation of ions at the same unit mass resolution by resolving the ion mass defects.

Subsaturated aerosol water affinity was measured as a function of size using a single column Hygroscopicity Tandem Differential Mobility Analyser (HTDMA; Cubison

et al., 2005; Gysel et al., 2009), which measures the size change of an aerosol experiencing a certain change in relative humidity (RH). This is expressed in terms of the growth factor (GF) defined as the ratio of the “dry” to “wet” size – in this case the sizes at <15% and 90% RH, respectively (GF_{90}). The supersaturation needed to activate a particle to a cloud droplet (critical supersaturation; SS_{crit}) was measured as a function of size using a Droplet Measurement Technologies dual column Cloud Condensation Nucleus counter (CCNc; DMT model 100; Roberts and Nenes, 2005; Lance et al., 2006; Irwin et al., 2011, 2010; Good et al., 2010a) downstream of a differential mobility particle sizer (DMPS; Williams et al., 2000, 2007). Both the HTDMA and CCNc perform measurements as a function of dry (<15% RH) aerosol size, selected using Vienna style differential mobility analysers (DMA; Winklmayr et al., 1991). The HTDMA measured at six sizes between 32 and 258 nm and the CCNc measured at 11 diameters between 57 and 224 nm. Aerosol optical absorption was measured with a Thermo Scientific model 5012 Multi Angle Absorption Photometer (MAAP; Petzold and Schonlinner, 2004) which reports in black carbon equivalent loading.

The halocarbon measurements were made using gas chromatography-mass spectrometry (GC-MS). The analysis was conducted on-site at Bukit Atur. Whole air samples were dried using a Nafion contra-flow drier and were pre-concentrated using a Markes International UNITY and Online Air Server with a Carbograph B and Carboxen 1000 trap. The UNITY was coupled to the Agilent 6890 GC and the MS5973 N mass spectrometer. The results presented here are from analysis on this GC-MS system in negative ion chemical ionization (NICI) mode (Worton et al., 2008). Litre samples were taken hourly (collected over a period of 40 min) from a position 30 m up the GAW tower (Hewitt et al., 2010) and separated on a Restek RTX-502.2 column. Calibrations were performed every 8 samples using the UEA 2006 Standard reference gas which is calibrated against the “NOAA 2003” scale for CHBr_3 , CH_2Br and CH_3Br and the “NOAA 2004” scale for CH_3I (Laboratory Earth Systems Research Global Monitoring Division, 2008). Gas phase CO measurements were made using an Aerolaser AL5002 fluorescence instrument (Gerbig et al., 1999).

2.2 Analysis of back trajectories

Backwards air mass trajectories (back trajectories) were generated using the British Atmospheric Data Centre Web Trajectory Service using European Centre for Medium-Range Weather Forecasts (ECMWF) wind fields (BADC, 2006a) at $1.125^\circ \times 1.125^\circ$ resolution. These trajectories show the modelled history of an air mass from a particular time and place in terms of geographical position and pressure altitude. One trajectory per hour was generated for the whole of the OP3 project – a total of 720 trajectories for OP3-I and 794 for OP3-III. Trajectories originate at the latitude and longitude

of the ground measurement site and a pressure altitude of 950 hPa, and were calculated backwards for the preceding seven days with a 30 min time resolution. No trajectories impacted the surface during the time-scales investigated.

Two distinct but complementary methods were used to interpret back trajectories: construction of a map showing the dependence of the mean value of the studied quantity measured at the site on air mass residence time in specific regions; and a comparison of periods classified by cluster analysis of trajectories. These methods provide a means of separating influences of different geographical locations on measurements made from the ground site. Elevated measurement values associated with regions can in turn be attributed to likely sources. Similar approaches have been used in the past to assess sources: for example, in Mace Head, Western Ireland, Cape et al. (2000) used trajectory cluster analysis to interpret trace gas measurements and Bassford et al. (1999) used a residence time analysis to separate two discrete sources of methyl iodide – a coastal source and a sub-tropical Atlantic ocean source. The trajectory residence time analysis was pioneered by Ashbaugh (1985) who used it to attribute measurements of sulphate aerosols made in the Grand Canyon National Park to source regions. These methods are particularly useful in analysing the OP3 data as the complex local topography at the measurement site means local wind vector data are likely not to be representative of the direction of air mass origin. While ECMWF trajectories do not explicitly represent complex terrain and boundary layer processes, they should still be a good indicator of regional synoptic transport over the time scales presented here. The analyses presented are suited to analysis of species with a long atmospheric lifetime compared to the trajectory durations used, i.e. for species such as aerosol particles, carbon monoxide and halocarbons which are the focus of this paper.

Typically, of the seven day trajectories, only the 36 h closest to the measurement site were used, although the seven day trajectories are discussed for context in Sect. 3.1. Many of the species studied here have atmospheric lifetimes longer than this and it is possible that more insight into far field sources could be gained from their use, however we focus on shorter trajectories to minimise the introduction of erroneous analysis. This is caused by: the “shadowing” effect demonstrated in Sect. 2.2.1 below; the dependence of the density of trajectory data points on proximity to the receptor site which is inherent in the polar geometry; and the increase in the error of modelled trajectories with increased time calculated backwards.

2.2.1 Residence time analysis of back trajectories

The statistical method first described by Ashbaugh (1985) was extended to give an indication of geographical origins of measurements made at the ground site. For a given measurement, a geographical grid is constructed – all grids presented here used a cell size of $0.1^\circ \times 0.1^\circ$. Maps of trajectory res-

idence time are shown in Fig. 1 for 36 h back trajectories during OP3-I and OP3-III. These are calculated by counting the number of trajectory data points in each cell for all trajectories and normalising to the probability density function inherent in the polar geometry. The polar probability density function can be calculated using

$$f_{ij}(r) = \frac{1}{2\pi Rr} \quad (1)$$

where R is the limit of the radial distance from the origin of the trajectories and r is the mean distance of each cell from origin of the trajectories (Ashbaugh, 1985). To assess the dependence of a measured quantity on air mass history, the value at the observing site at the time of arrival of a given trajectory is added to the grid cell that contains each trajectory point. Doing this for all trajectories and dividing by the total number of trajectory points in each cell gives the mean value measured at the ground site for an air mass that has passed over that cell. These plots are henceforth referred to as mean value maps.

Figure 2 shows an example mean value map of bromoform (CHBr_3) during OP3-III. Measurement techniques are detailed in Sect. 2.1. In interpreting mean value maps it is important to remember that air mass trajectories that regularly travel through a non-source region before travelling through a source region will show artificially elevated levels in the non-source region, henceforth called “shadowing”. For example, in Fig. 2 there appears to be bromoform south of the site in the region around 1.5°N , 117°E , however this may be artificial if the east coast is a source region. A similar argument can be made if trajectories regularly travel through a source region before travelling through a removal region (for example a region of elevated levels of precipitation acting to remove aerosol) resulting in the source region not being resolved. As a wider range of conditions are sampled, these artificial data would be expected to be of less importance with unaffected data dominating. It is also the case in general that increasing data coverage will tend to resolve sources more accurately as the influence of isolated events is outweighed by representative conditions. In order to assess the potential extent of these effects, the percentage of the entire set of calculated back trajectories that was used in the construction of each mean value map is displayed. It is also important to be able to quantify the degree of similarity between different mean value maps. This is done by calculating the Pearson's r of a scatter plot of the intensities of corresponding grid points.

2.2.2 Agglomerative hierarchical cluster analysis of back trajectories

Trajectories were processed using the custom made cluster analysis routine described in Morgan et al. (2009) based on the method described in Cape et al. (2000). At the start of the analysis, each trajectory is assigned its own cluster. An

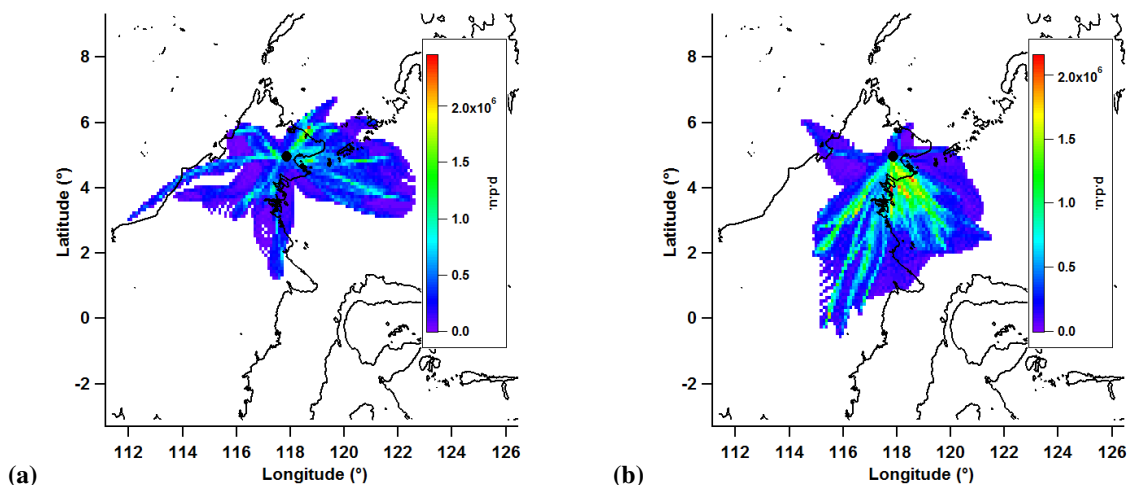


Fig. 1. Residence time of air masses in previous 36 h for all trajectories during (a) OP3-I and (b) OP3-III. Colour is number of trajectory data points (normalised to geometric probability density function), expressed in the resulting procedure defined units (p.d.u.). Trajectory receptor site (the measurement site) marked with a black dot.

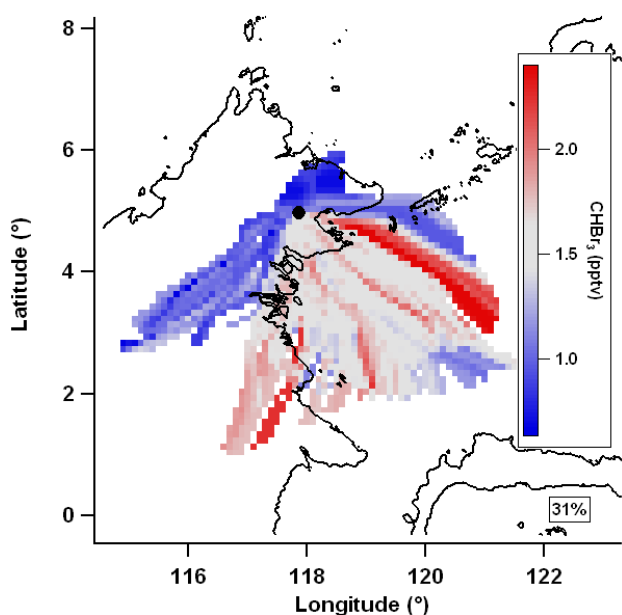


Fig. 2. Example mean value map of bromoform (CHBr_3) during OP3-III using 36 h trajectories. Grey is median value, red is greater than median, blue is less than median and white denotes no data coverage. Percentage of trajectories used denoted below key.

average linkage method was used based on calculating the squared distance between trajectories at each time step using

$$d(x_i, x_j) = \sum_k \left\{ (x_{ki} - x_{kj})^2 + (y_{ki} - y_{kj})^2 + (p_{ki} - p_{kj})^2 \right\} \quad (2)$$

where x_k , y_k and p_k are the coordinates of x_i or x_j . At each step in the analysis the two clusters with the lowest

squared distance are agglomerated. This continues until all trajectories are in one cluster. The optimum number of clusters may then be chosen, so as to maximize between cluster variance and minimize within cluster variance (Cape et al., 2000). The choice of the optimum number of clusters is subjective, however this has been shown to be the most appropriate technique for analysing meteorological trajectories (Kalkstein et al., 1987). The suitability of a solution of N clusters can be assessed using several scores. An increase in the root mean squared (RMS) distance between clusters indicates that two dissimilar clusters have been agglomerated (Cape et al., 2000). A sharp decrease of the coefficient of determination R^2 , defined as

$$R^2 = 1 - \frac{\sum_N (\text{within cluster variance})}{(\text{variance of all trajectories})} \quad (3)$$

is a subjective indicator of the number of clusters to retain (Kalkstein et al., 1987). Similarly to Morgan et al. (2009) and Cape et al. (2000), an indication of the number of major clusters is defined as the number of clusters containing more than 3% of the total number of trajectories.

The project was split into a series of successive twelve hour periods. These were classified according to the clusters that their constituent trajectories belonged to, similar to Cape et al. (2000): if trajectories belonging to more than one cluster were present, the period was deemed “unclassified”, otherwise it was deemed to be influenced by that cluster. This removes periods of transition between air mass cluster, leaving comparatively stable conditions and enabling comparison between measurements influenced by different clusters. Mean, median and percentiles of measured quantities were calculated for data influenced by each cluster. These cluster

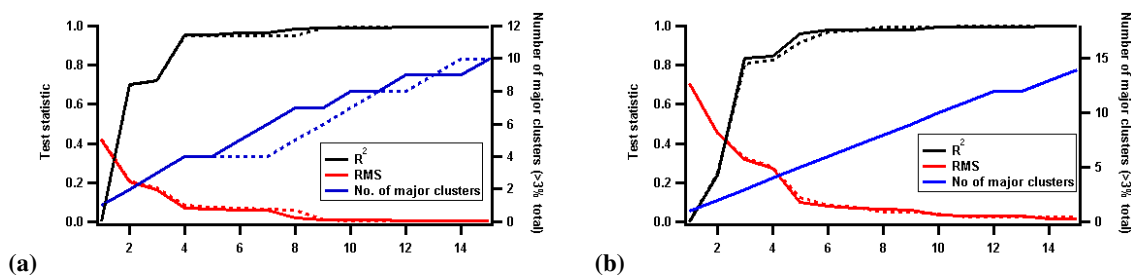


Fig. 3. R^2 , RMS and number of major clusters (containing $> 3\%$ of trajectories) as a function of number of clusters in solution for (a) OP3-I and (b) OP3-III. Solid lines are for one subset of trajectories and dashed lines are for the other.

averages are discussed in Sect. 3 and presented in full in Table 4.

In order to establish the robustness of the solution, the trajectories were split into two subsets: two day back trajectories of one hour time resolution released every two hours were used, with the alternate set similar but using trajectories from the intervening hours. The reduction in trajectory time resolution was necessary to improve computational efficiency. For both OP3-I and OP3-III, cluster scores (Fig. 3) and means (Figs. 4 and 5) show little difference between trajectory subset showing the cluster analysis solutions to be stable to perturbations, and are combined for classification and all subsequent analysis.

The scores for OP3-I (Fig. 3a) show the first major step change at the four cluster solution which is summarised in Fig. 4 and Table 1. *Italics* will be used for clarity when referring to cluster names, which are defined in Figs. 4 and 5. The main influence on the site is split evenly between the *North-easterly*, *Easterly* and *Terrestrial* clusters. Air masses associated with the *Westerly* cluster. Air masses associated with the *Westerly* cluster are of minor influence, making up only 3 % of the classified periods, and can generally be disregarded.

The scores from OP3-III (Fig. 3b) show the first major step change at the five cluster solution which is summarised in Fig. 5 and Table 2. The major influence on the site was from the south-westerly Marine cluster. The Coastal cluster from the south and the Terrestrial cluster from the south-west also had significant influence. There were two more clusters; the *North-easterly* and *Westerly* but both are of minor influence (consisting of 3 % and 5 % of classified periods, respectively) and can generally be disregarded. Figure 10, Sect. 3.1, shows the clusters influencing the measurement site during OP3-III (displayed as a coloured bar) for comparison to the aerosol composition data.

Table 1. Details of four cluster solution and resultant period classification for OP3-I.

Cluster name	No. of constituent trajectories (%)	No. of 12 h periods (%) attributed
North-easterly	221 (31 %)	15 (25 %)
Easterly	208 (29 %)	15 (25 %)
Terrestrial	236 (33 %)	18 (31 %)
Westerly	51 (7 %)	2 (3 %)
Unclassified		9 (15 %)

Table 2. Details of five cluster solution and resultant period classification for OP3-III.

Cluster name	No. of constituent trajectories (%)	No. of 12 h periods (%) attributed
North-easterly	41 (5 %)	2 (3 %)
Marine	460 (58 %)	33 (50 %)
Coastal	107 (14 %)	5 (8 %)
Terrestrial	141 (18 %)	10 (15 %)
Westerly	41 (5 %)	3 (5 %)
Unclassified		13 (20 %)

2.3 Positive matrix factorisation of organic aerosol mass spectra

Different PMF solutions were explored as a function of starting conditions (seed) and rotational ambiguity (fpeak) as detailed in Robinson et al. (2011), and the most satisfactory solution was a four factor solution with $f_{\text{peak}} = -1$. This solution was found to have negligible dependence on starting seed. Solutions with greater than four factors were found to be unsatisfactory due to “mixing” of factors (as described in Ulbrich et al., 2009), unrealistic factor spectra consisting of one or two peaks with little signal at other m/z s, or lack of convergence. The factor mass spectra are shown in Fig. 6 with the time series shown in Fig. 10.

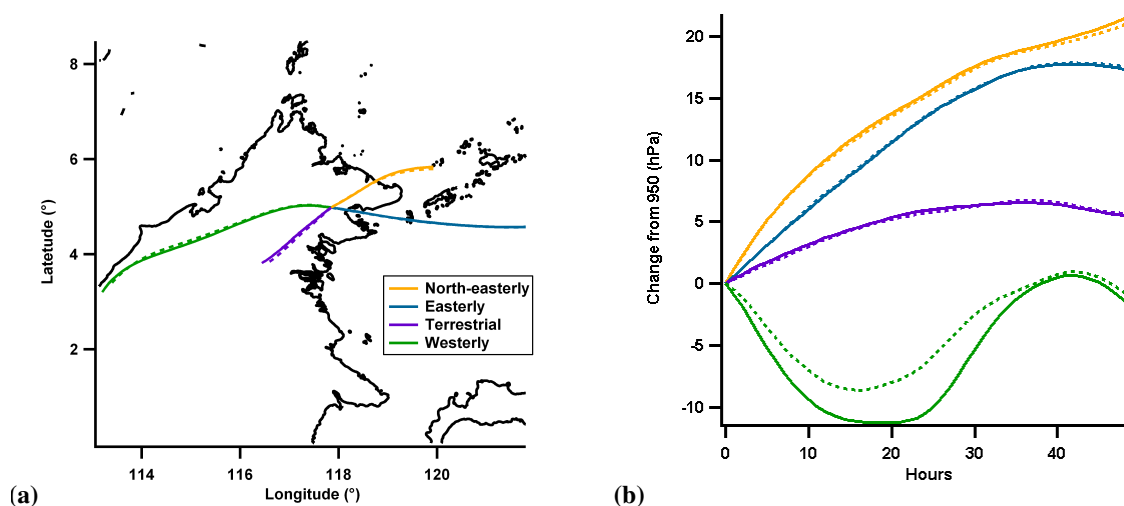


Fig. 4. OP3-I cluster mean (a) latitude and longitude and (b) pressure altitude in units of hPa different from starting altitude of 950 hPa. Colours are consistent between plots. Solid and dashed lines show solutions from each subset.

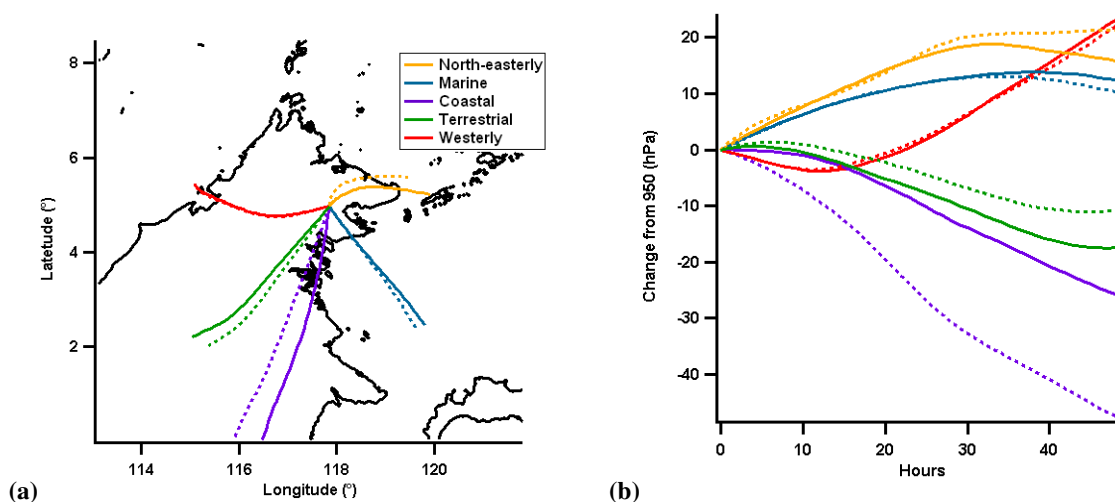


Fig. 5. OP3-III cluster mean (a) latitude and longitude and (b) pressure altitude in units of hPa different from starting altitude of 950 hPa. Colours are consistent between plots. Solid and dashed lines show solutions from each subset.

The four factors can be attributed sources from inspection of the mass spectral signature as follows. The first factor, named 91Fac, shows some similarities to previously published mass spectra of biomass burning emissions (Alfarra et al., 2007; Allan et al., 2010) for instance a prominent m/z 91 peak, which can be indicative of aromatic species. It does not show the m/z 60 and 73 peaks normally associated with levoglucosan, an established biomass burning marker in AMS measurements (Alfarra et al., 2007). However these levoglucosan peaks have been shown to reduce with ageing of biomass burning aerosol (Capes et al., 2008), implying the 91Fac may be from far field biomass burning emissions.

The second and third factors are named OOA1 and OOA2 respectively because of their similarity to previously pub-

lished spectra (Lanz et al., 2007; Zhang et al., 2007). Spectra such as OOA1 are considered highly oxidised and have been linked to low volatility oxygenated organic aerosol (LVOOA; McFiggans et al., 2005); similarly, spectra such as OOA2 are considered less oxidised and have been linked to semi-volatile organic aerosol (SVOOA; Jimenez et al., 2009). However such assertions are impossible without a direct volatility measurement. While these factors are resolved as separate factors, they represent what are in reality different ends of a continuum of OA oxidations (Ng et al., 2010; Morgan et al., 2010). OA is gradually oxidised from OOA2-like to OOA1-like aerosol over time, which would be represented by the PMF factors as a reduction in OOA2 and a concurrent increase in OOA1.

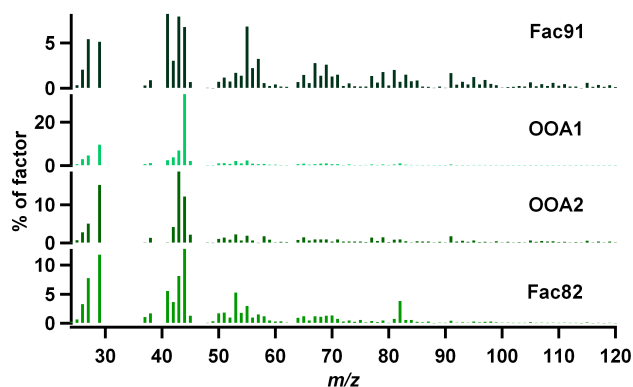


Fig. 6. Factor spectra for the four factor, $f_{\text{peak}} = -1$ solution of PMF analysis of organic mass spectra. From top to bottom, spectra are 91Fac, OOA1, OOA2 and 82Fac.

The last factor, named 82fac because of its prominent m/z 82 peak, is not similar to any mass spectra widely reported in the literature. Its measurement during the OP3 project was reported in Robinson et al. (2011) who provide evidence that it is associated that it is the product of isoprene oxidation. A similar factor has since been reported in rural North America where it was also associated with isoprene oxidation (Slowik et al., 2011). Further investigation into the likely sources linked to these factors will be made through the analysis presented in this paper.

3 Results

3.1 Overview of measurements and their regional setting

The major cities in Borneo are all located on the coast, with the biggest settlements on the south west of the island. The interior of Borneo is a mountainous unsettled and undeveloped region of rainforest. Average daily large scale precipitation from the ECMWF Integrated Forecasting System model reanalysis shows increased precipitation in the interior of Borneo (Fig. 7; BADC, 2006b). It is likely that this increased precipitation is due to the orography inland. Precipitation inhibits long range transport of aerosol. This means air masses from the southwest of the site will tend to have reduced concentrations of background aerosol. These air masses will have relatively greater amounts of locally produced aerosol.

Figure 8 shows a trajectory residence time plot, and the average minimum pressure (maximum altitude) of the trajectories passing through each cell, both using seven day back trajectories. These provide context for the more detailed analyses presented herein which use shorter (36 h) trajectories. This means the more detailed analyses only use trajectory data from relatively close to the receptor site where they are

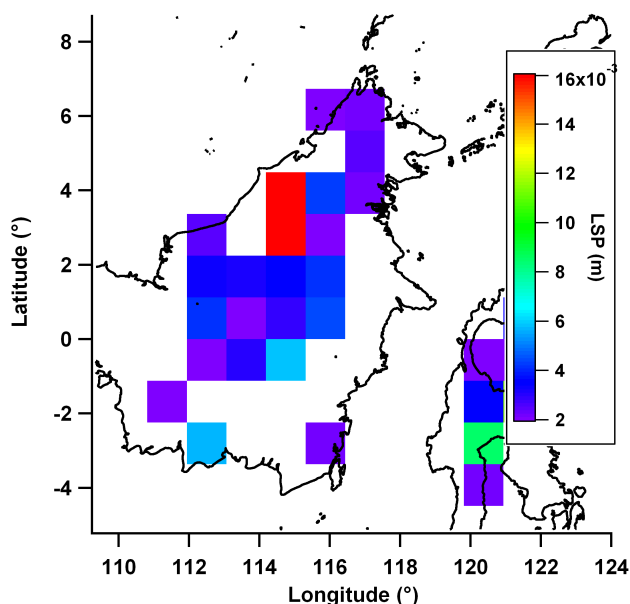


Fig. 7. Average daily large scale precipitation (m) from the European Centre for Medium-Range Weather Forecast Integrated Forecasting System model reanalysis (BADC, 2006b) at $1.125^\circ \times 1.125^\circ$ resolution during OP3-III. Values below 2×10^{-3} m are not shown for clarity.

most accurate and their density is highest. The residence time plot shows that the site is mostly influenced by air masses from the south east. There is no influence from the major urbanised regional areas in mainland Malaysia (around Kuala Lumpur, east of Borneo), Singapore (south west of Borneo) and Indonesia (around Jakarta, south west of Borneo). Many air masses travel over Sulawesi (around 2° S, 121° E). The majority of the 16 million people inhabiting Sulawesi live at the far south. The plot showing the average minimum pressure of trajectories passing over each cell shows trajectories travelling over the island to generally be from a greater maximum altitude than trajectories transported from the east coast of Borneo. The distribution of trajectory minimum pressures has a mean of 909 hPa, median of 938 hPa and a tenth percentile value of 821 hPa. This corresponds to a ninetieth percentile maximum altitude of approximately 1.8 km a.s.l. with the majority of trajectories having a maximum altitude close to that of the receptor site.

The Moderate Resolution Imaging Spectroradiometer (MODIS) fire count (Davies et al., 2009; Justice et al., 2002; Giglio, 2003) shows hotspots/open fires detected in the wider region during OP3-III in Fig. 9. The majority of fires are concentrated to the south west of the measurement site in Vietnam, mainland Malaysia, Sumatera, Indonesia and South Western Borneo. The seven day trajectories show none of these regions to be an influence on the measurement site. The trajectories that travel up from the south of the island (largely associated with the *Terrestrial* and *Coastal* clusters) are likely

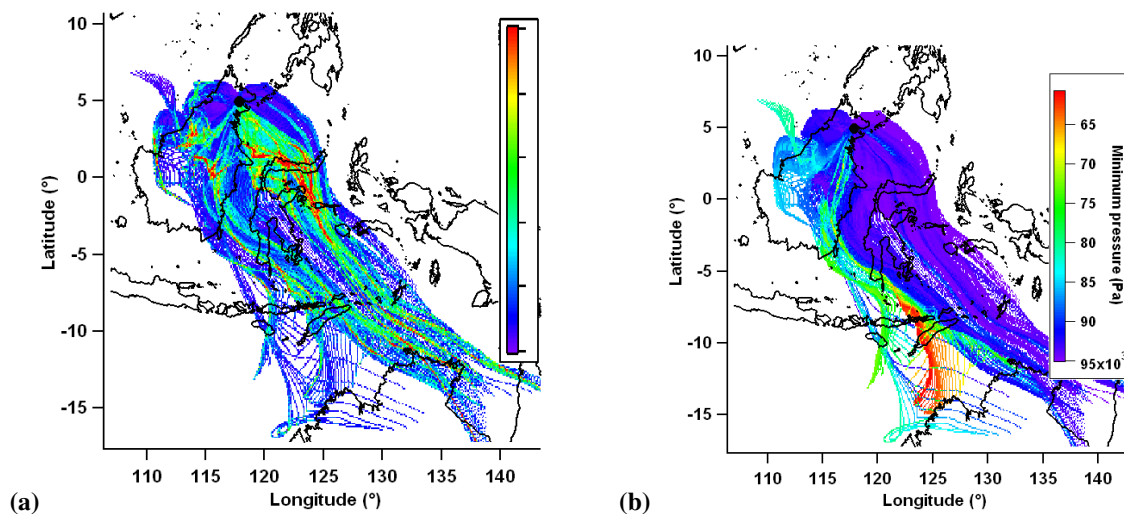


Fig. 8. (a) Residence time of air masses in previous 7 d for all trajectories during OP3-III. Colour is number of trajectory data points (normalised to geometric probability density function). (b) mean minimum pressure of trajectories passing through that cell in previous 7 d. Trajectory receptor site (the measurement site) marked with a black dot.

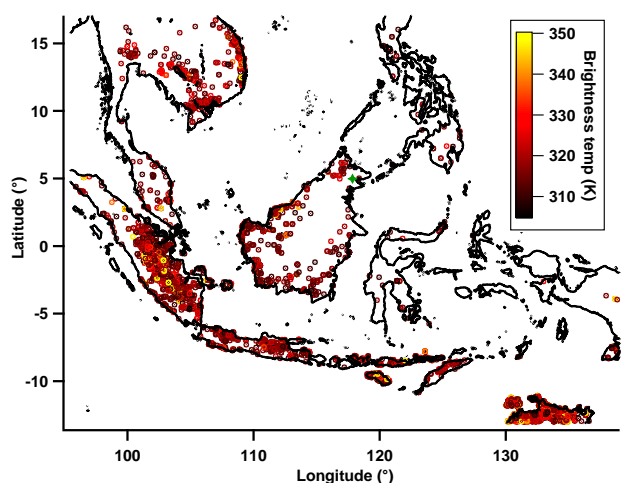


Fig. 9. MODIS hotspot/active fires coloured by temperature of event during OP3-III. Site marked with green star.

to have the most biomass burning influence due to on-island fires, and perhaps fires further afield on the Lesser Sunda Islands in South East Indonesia (around 7° S by 125° E).

Aerosol measurements made in Borneo show a contrasting situation to Amazonia with much higher sulphate and ammonium loadings, much more similar to those measured in West Africa (Table 3). The time series of aerosol composition is shown in Fig. 10 with a bar indicating the classification of the air mass (see Sect. 2.2.2) influencing the measurement site.

3.2 Halocarbons

The bromoform (shown previously in Fig. 2) and dibromomethane (CH_2Br_2 ; not shown) mean value maps show very similar profiles ($r = 0.90$) which is unsurprising as these compounds are well correlated in the atmosphere (Butler et al., 2007; Yokouchi et al., 2005; Zhou et al., 2008). The time series collected at Bukit Atur also confirms this as their time series are well correlated. Bromoform and dibromomethane show elevated levels over coastal and marine regions compared to terrestrial regions, this is consistent with other studies which have shown them to be produced by macro-algae (Carpenter and Liss, 2000; Goodwin et al., 1997; Quack et al., 2007). In particular the south-east coast of Sabah is a region of seaweed cultivation which is reflected in the high concentration seen in air masses from this region.

The methyl iodide mean value map (Fig. 11a) is similar to those of the polybrominated compounds, however, there are some differences in features (mean value map correlations of $r = 0.70$ with bromoform and with dibromomethane). Like the polybrominated compounds, the methyl iodide map shows high values to be predominantly attributable to off-island sources. This is consistent with whole air samples collected in the boundary layer during the OP3 flight campaign on the FAAM BAe-146 aircraft (Hewitt et al., 2009; Newton et al., 2011), and analysed on the same GC-MS system set-up as described in Sect. 2.1 of this paper. Data from this aircraft campaign showed a clear concentration gradient from sea-to-land, with highest concentrations of methyl iodide seen off the south-east coast of Sabah. The pattern of high values seen over the sea in the methyl iodide mean value map is similar to that seen in the polybrominated compound mean

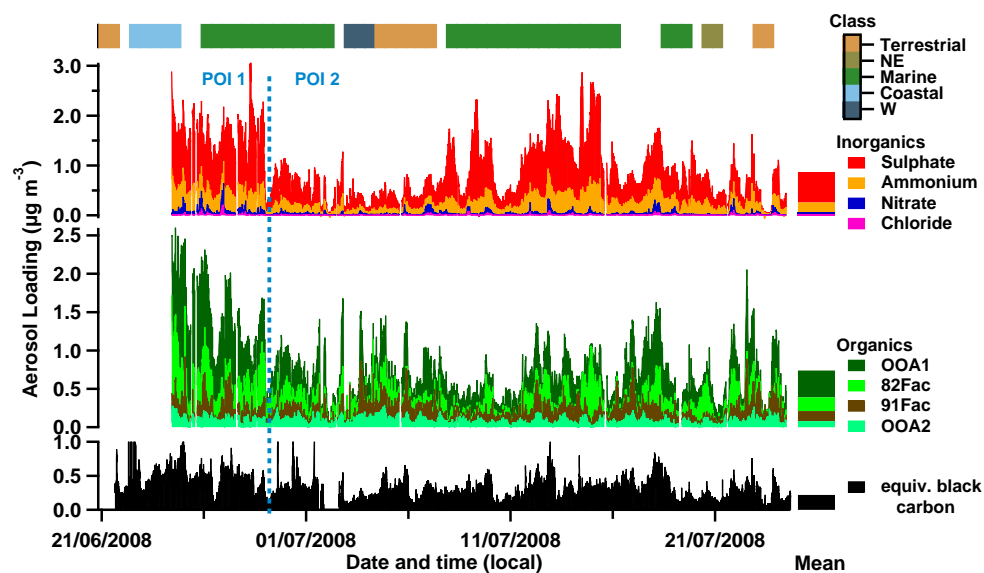


Fig. 10. Stacked time series of total sub-micron non-refractory aerosol split by composition (see Sect. 2.1) for OP3-III. The inorganics and organics are shown on separate axes, with the organics split into their constituent PMF factors. The split point between Period Of Interest (POI) One and Two is marked with a dashed blue line (see Sect. 3.6). The campaign mean aerosol loadings are shown as stacked bars to the right of the time series. Colour of bar at top indicates class of air mass influencing site (see Sect. 2). No bar indicates unclassified (changeable) air mass.

value maps. In particular the methyl iodide and polybrominated mean value maps all show a region of high values off the coast to the immediate east of Bukit Atur which extends east (to around 4° N, 120° E). This shared feature suggests a co-located source of methyl iodide and the polybrominated compounds; possibly it is even the same source, potentially macro algae, which have been shown to produce all three of these compounds (Carpenter and Liss, 2000; Manley et al., 1992). Other studies have observed correlations between methyl iodide and these polybrominated compounds, but noted the inconsistency of their correlation, suggesting different production mechanisms for the methyl iodide and polybrominated compounds (Butler et al., 2007). Methyl iodide shows less separation between terrestrial and marine air masses than the polybrominated compounds. This consistent with previous studies, which have shown methyl iodide to have a mixture of marine and terrestrial sources (Bell et al., 2002; Smythe-Wright et al., 2006; Sive et al., 2007) and be emitted during biomass burning (Cox et al., 2005; Mead et al., 2008).

In stark contrast to the other three halocarbons presented here the waters immediately east of Bukit Atur around 4° N, 120° E do not appear to be a productive region for methyl bromide (Fig. 11b). There is some marine contribution, predominantly from the coastal zone south of Sabah included in the extent of these maps, which is consistent with known marine sources of methyl bromide such as macro algae (Baker, 2001; Cox et al., 2005). Higher values (8–9 pptv) are seen over an area to the north of Bukit Atur (5.4 – 6° N) covering

Table 3. Comparison of sub-micron non-refractory aerosol loadings ($\mu\text{g m}^{-3}$) from different tropical campaigns. Bornean and Amazonian (Chen et al., 2009) measurements are campaign averages of ground site intensives. West African measurements are averages of low altitude data over several flights, screened to remove (local) biomass burning and anthropogenic influence (Capes et al., 2008, 2009).

	Borneo	Amazonia	West Africa
Organic	0.74	0.64	1.01
Sulphate	0.61	0.15	0.82
Ammonium	0.21	0.02	0.36
Total	1.6	0.82	2.26

both land and coastal areas. This area is known to comprise oil palm plantations and there are similarities between the methyl bromide mean value map and 82Fac (Fig. 14a) discussed in Sect. 3.4 although overall correlation is not high ($r = 0.32$). It is currently unknown whether oil palm trees are actually a source of methyl bromide. However, other activities associated with the oil palm plantations such as biomass burning, a known source of methyl bromide (Mead et al., 2008; Reeves, 2003), may also contribute to the localised high values. Moreover, a coastal source cannot be discounted as responsible for this feature, possibly a macro algae source. The mean value plot for methyl bromide shows an elevated feature to the south west of the measurement site,

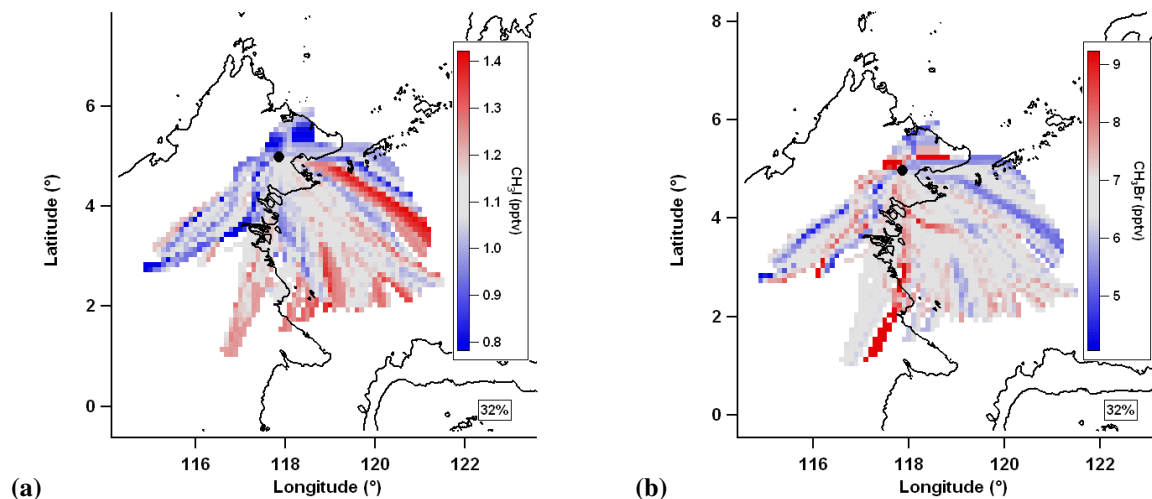


Fig. 11. Mean value maps for (a) methyl iodide, CH_3I and (b) methyl bromide CH_3Br . Grey is median value, red is greater than median, blue is less than median and white denotes no data coverage. 36 h trajectories used.

in a similar location to that seen in the methyl iodide map though the exact grid boxes differ. As discussed earlier small scale biomass burning may be a contributing factor to this feature, in addition tropical vegetation has been suggested as a weak source of methyl bromide (Blei et al., 2010).

3.3 Nitrate and chloride aerosol

The nitrate (Fig. 12) and chloride (not shown) mean value maps and time series are similar ($r = 0.76$) suggesting the two species may be components of the same aerosol. The greatest aerosol loadings are mostly associated with marine air from the south-east. Elevated loadings shown to the far south over the Sangkulirang Peninsula (around 1°N , 117.5°E) may be artificial, caused by the preceding or subsequent transit of the air mass over the sea. Cluster averages show nitrate and chloride to be associated with air of marine origin, with greater loadings in the *Marine* cluster than the *Terrestrial*. Campaign average loadings of nitrate ($0.03\ \mu\text{g m}^{-3}$) and chloride ($0.01\ \mu\text{g m}^{-3}$) are very low however they are high when compared to Amazonia ($0.01\ \mu\text{g m}^{-3}$ and $0.00\ \mu\text{g m}^{-3}$, respectively). The diurnal profile of nitrate and chloride loadings shows them to be strongly elevated around midnight with low levels throughout the day.

Nitrate (NO_3^-) is produced in the atmosphere by oxidation of NO_x on the time-scale of hours. Hewitt et al. (2009) found that NO_x levels in Borneo, while typically lower than those found in more developed countries such as USA and Europe, were highest over the oil palm plantations where the sources were vehicle emissions, combustion and crop fertilisation. The AMS nitrate loading is derived from two fragments (NO^+ and NO_2^+ at m/z 30 and 46) and during OP3 these varied, indicating that the nitrate that is detected is unlikely to be purely in the form ammonium nitrate (NH_4NO_3), as this is

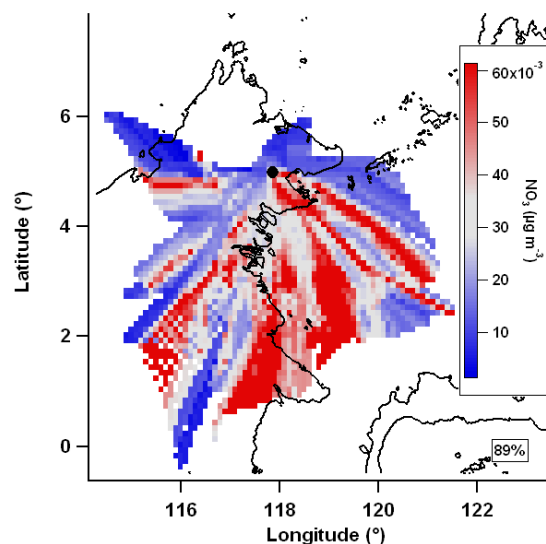


Fig. 12. Mean value map for nitrate. Grey is median value, red is greater than median, blue is less than median and white denotes no data coverage. 36 h trajectories are used.

known to fragment consistently. The ratio of the mean ambient NO^+ and NO_2^+ signals is significantly greater than during calibrations using ammonium nitrate (5.4 vs. 2.6). The AMS has been shown to be poor at measuring organic nitrates directly as $\text{C}_x\text{H}_y\text{N}^+$ or $\text{C}_x\text{H}_y\text{O}_z\text{N}^+$ (Farmer et al., 2010), with significant mass (30 %) detected at the NO_x^+ peaks (Rollins et al., 2010), which make up AMS “nitrate” measurements usually associated with inorganic nitrate. However the majority of organic nitrate mass is still thought to be measured at the $\text{C}_x\text{H}_y\text{N}^+$ and $\text{C}_x\text{H}_y\text{O}_z\text{N}^+$ peaks (Rollins et al., 2010) and there is little correlation of these signals with the NO^+

and NO_2^+ ($r = 0.29$), implying any role of organic nitrates to be low.

A likely source of chloride containing aerosol is sodium chloride particles from sea water, however the AMS cannot measure sea salt particles well as they are usually too large to be successfully sampled and they vapourise slowly (Allan et al., 2004). There is no excess ammonium (NH_4) detected after the neutralisation of sulphate in Borneo, meaning nitric acid will not readily be neutralised. The introduction of nitric acid (HNO_3) to aqueous sodium chloride particles would force the chloride to partition to the gas phase in the form of hydrogen chloride (HCl). This leads to aqueous sodium nitrate particles that are more easily volatilised by the AMS. The liberated hydrogen chloride can then react to form aerosol which is detected by the AMS. While there are no direct measurements of the composition of the chloride containing aerosol, it is likely that they are in the form ammonium chloride.

The nitrate and chloride diurnal profiles show a very strong increase at night, which may be driven by partitioning of vapours as the temperature reduces. A dense layer of fog formed across the forest every night which may have facilitated nitrate and chloride aerosol reformation occurring in the aqueous phase. Furthermore, the measurement site, located on a ridge top, protruded above the planetary boundary layer top every night (Pearson et al., 2010) which may have introduced more marine influenced aerosol that would be typical of the regional background.

3.4 Organic aerosol

The OOA1 mean value map shows both off-island and on-island sources (Fig. 13a). The *Marine* and *Terrestrial* period averages (0.33 and $0.29 \mu\text{g m}^{-3}$, respectively) show, while both sources are significant, the off island source is larger. The greatest concentrations of OOA1 are in marine/coastal air masses. These are likely to be the result of long range transport of highly oxidised regional emissions with a possible contribution from processed biomass burning at the start of the measurement period (see Sect. 3.6). It is likely that the on island source of OOA1 represents the aged component of BSOA from the rainforest and the components of regional long range transport aerosol that is not removed through wet deposition during transit across the island. The inland OOA1 is changeable, showing both high and low loadings, and it is conceivable that the amount of inland OOA1 is driven by the level of precipitation inland.

The OOA2 mean value map (Fig. 13b) shows a strongly terrestrial source of aerosol, with *Marine* and *Terrestrial* period loadings of 0.11 and $0.07 \mu\text{g m}^{-3}$, respectively. It shows elevated loadings across much of the island with the exception of the known oil palms to the immediate north and south of the measurement site. This suggests the rainforest is a source of freshly produced BSOA from the oxidation of rainforest VOC emissions which are represented by

the OOA2 factor. OOA2 is a relatively minor fraction of the total organic aerosol, making up only 11 % compared to OOA1 which makes up 47 %. This is expected in an environment such as Borneo where there are influences from far field sources such as off-island anthropogenic sources and OA from oceanic emissions, meaning more aged organic aerosol could dominate.

The ratio of mean value maps of OOA1 to OOA2 (extent of oxidation; Fig. 13) shows the oxidised aerosol to be originating externally to the island compared to the less oxidised aerosol which originates in the island interior. This implies the highly oxidised OA is from long range transport of aerosols that are emitted from sources external to the island, either biogenic or anthropogenic. Figure 13 shows low OA oxidation in air masses travelling across the centre of the island, a region of enhanced precipitation (Fig. 7). Wet removal of aerosol is likely to lead to depleted concentrations of regional aerosol (highly aged OA) and relatively increased concentrations of more locally produced aerosol. This local aerosol is likely to be BSOA generated from rainforest produced precursors as there were not any other major sources known to be nearby (e.g. biomass burning, large settlements), especially in the inland region.

The oil palm plantations in Borneo have been shown to be a substantial source of isoprene, with emissions per unit area five times higher than the rainforest (Hewitt et al., 2009). Robinson et al. (2011) showed that isoprene was a significant source of BSOA at the measurement site in Bukit Atur, linking isoprene derived BSOA to a distinctive m/z 82 peak in the AMS organic aerosol mass spectrum and the associated 82Fac PMF factor. The mean value map of 82Fac (Fig. 14a) shows higher than average loadings in air masses from the immediate north, north-east and south-east. These are all areas of oil palm agriculture, as shown in Fig. 1b of Hewitt et al. (2010). The air masses associated with these areas also have particularly low maximum altitudes meaning they are likely to be particularly influence by local surface emissions (Fig. 8). The cluster averages show higher 82Fac loadings from air masses associated with the *Marine* cluster than *Terrestrial* (0.18 vs. $0.12 \mu\text{g m}^{-3}$, respectively), which in this case corresponds to air masses from the Sempona Peninsula region to the immediate south-east of the site (approximately 4.5°N , 118°E). The north-easterly cluster, which corresponds to air mass from the oil palms to the north, shows high average loadings ($0.14 \mu\text{g m}^{-3}$), although there is a low amount of data from this period as stated earlier. Loadings are periodically high across the rest of the island signifying additional inland sources. The 82Fac OA makes up a significant proportion of the total OA (24 %). Robinson et al. (2011) speculated that the formation of isoprene SOA may be catalysed by the high sulphate loadings in Borneo: acidic sulphate has been shown to affect isoprene SOA formation in chambers (although through a mechanism unlikely to yield the m/z 82 marker detected in Borneo; Surratt et al., 2010) and acidic aerosol has been shown to catalyse the

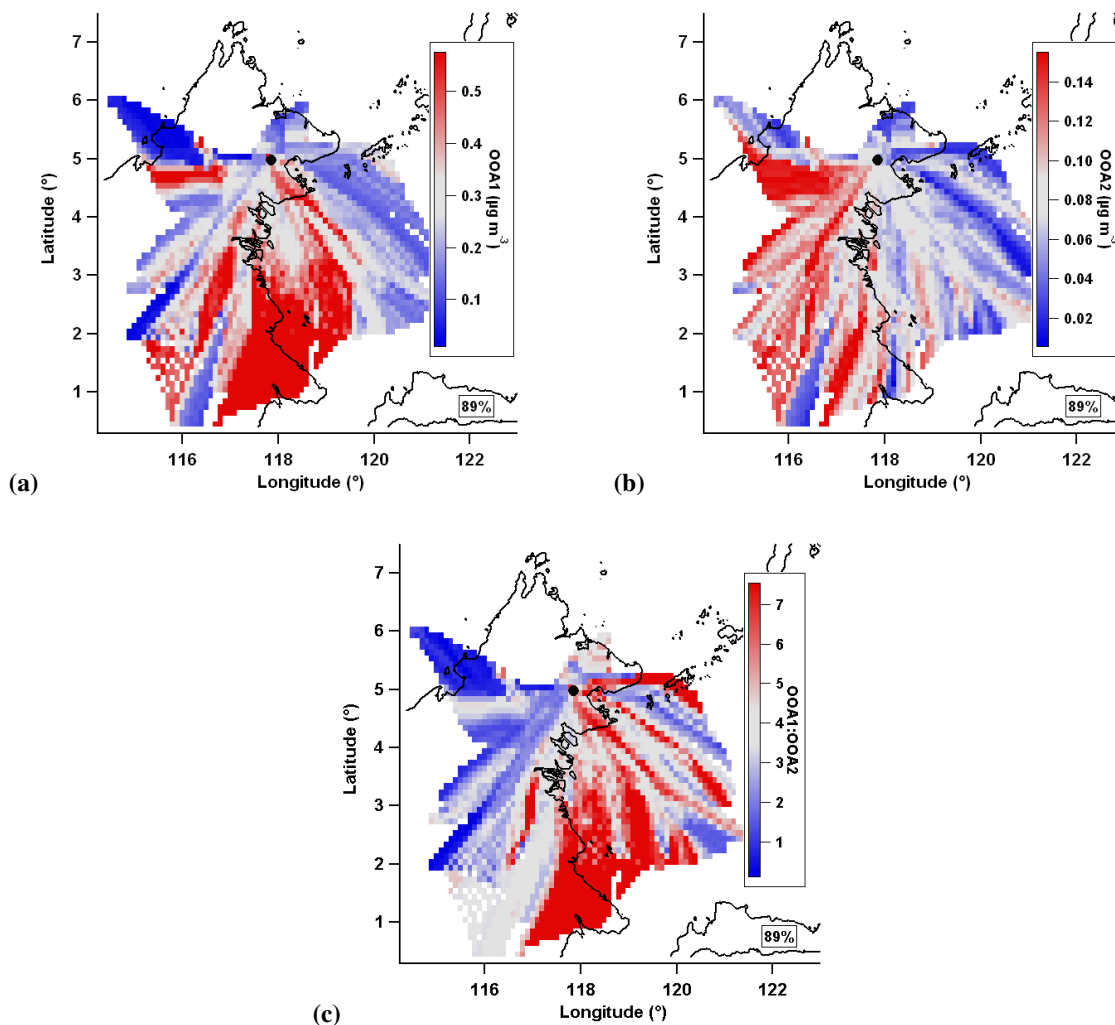


Fig. 13. (a) OOA1, (b) OOA2 and (c) the ratio of the OOA1 and OOA2 mean value maps, equivalent to OA oxidation. Grey is median value, red is greater than median, blue is less than median and white denotes no data coverage. 36 h trajectories are used.

heterogeneous reactive uptake of 1,4-hydroxycarbonyls (established isoprene oxidation products) to condensed phase species likely to yield the m/z 82 peak (Lim and Ziemann, 2009). The mean value map of excess sulphate (Fig. 14) shows the main source to the south-east of the site, in one of the regions associated with isoprene SOA. It should be noted that sulphate aerosol that is neutralised by the time of arrival at the measurement may be acidic closer to the coast where it has had less time to be neutralised by terrestrial ammonium sources.

3.5 Sulphate aerosol

The mean value map correlation ($r = 0.93$) suggests that sulphate (Fig. 15) and ammonium are components of the same aerosol, with the ion balance indicating this is likely in the form of ammonium sulphate. Cluster averages of ammonium

and sulphate show greater loadings in the *Marine* cluster than in the *Terrestrial* cluster (0.25 vs. $0.09 \mu\text{g m}^{-3}$ for ammonium and 0.75 vs. $0.25 \mu\text{g m}^{-3}$ for sulphate, respectively), which is consistent with the mean value maps.

Ammonia is produced from the natural breakdown of urea and uric acid excretion from animals and emissions from fertiliser. It is the primary basic gas in the atmosphere and would be expected to be present in Borneo. Sulphate aerosol is often produced from processing of anthropogenic emissions of SO_2 from fossil fuel combustion. South East Asia uses more sulphur rich vehicle fuel (International Fuel Quality Center, 2009) than western countries meaning anthropogenic fossil fuel combustion may be of particular influence in the region. Sulphate is also produced naturally by processing of phytoplankton DMS emission (Kloster et al., 2006) and gaseous sulphur emitted by volcanoes (Allen et al., 2002). Previous studies have used the methane sulphonic

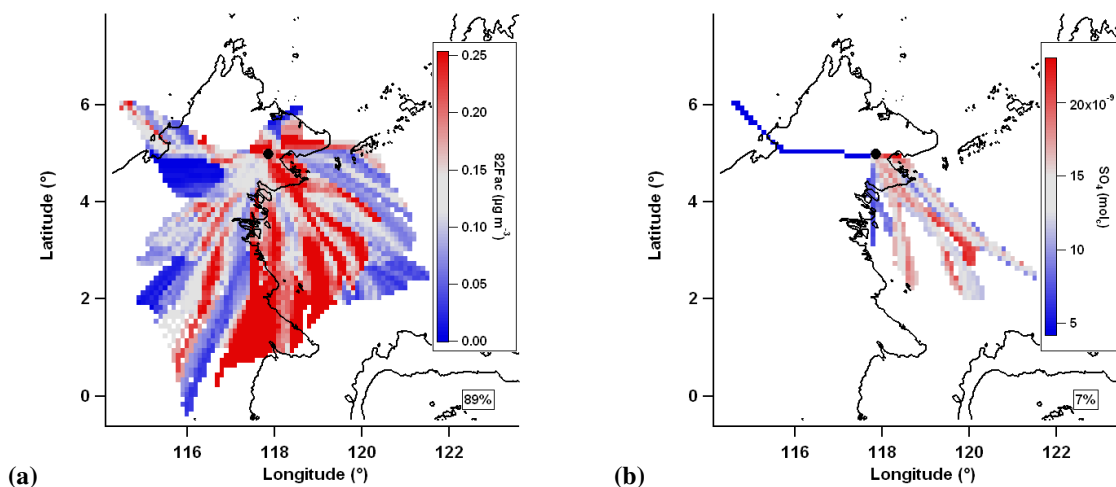


Fig. 14. Mean value maps of (a) 82Fac and (b) excess sulphate (defined as moles of charge of sulphate greater than moles of charge of ammonium plus 3×10^{-9} to account for spread of neutral values). Grey is median value, red is greater than median, blue is less than median and white denotes no data coverage. 36 h trajectories are used.

acid peak (MSA; $\text{CH}_3\text{SO}_3\text{H}$) of the high resolution AMS mass spectrum as a marker for DMS derived sulphate aerosol (Zorn et al., 2008). The yield of MSA relative to sulphate from atmospheric DMS oxidation has been shown to be much lower in tropical conditions (Bates et al., 1992; Allan et al., 2009) and no MSA signal was apparent in the Borneo dataset.

Volcanic activity was reported around the time of the OP3 project from Ruang (735 m), an island north of Sulawesi, Indonesia, East of Borneo and Mount Papandayan (2665 m) on Java, Indonesia, to the South of Borneo (Venzke et al., 2010), and could be responsible for some of the sulphate aerosol detected. However, if the back trajectories are assumed to be reliable when extended to the seven day limit (Fig. 8), these regions did not influence the site.

A scatter plot of sulphate loading vs. OA loading, coloured by cluster, is shown in Fig. 16, similar to the method used in Chen et al. (2009) when analysing aerosol composition in Amazonia. Figure S1 of the Supplement shows the same scatter plot coloured by m/z 44:43 (OA oxidation). Lines indicate the modal centres of the histogram of values of the sulphate to OA ratio. It should be noted that some level of correlation is to be expected between aerosol loadings due to shared removal processes, hence points at all three lines show a degree of correlation. Line A indicates points of high sulphate concentration with little dependence on OA loading, which are characteristically associated with the *Marine* cluster. They also show a varied level of OA oxidation. They are consistent with sources of sulphate external to Borneo that are not necessarily associated with production of OA – such as marine DMS production or volcanic emissions.

Line B indicates points of correlated high sulphate and OA concentration which are characteristically associated with

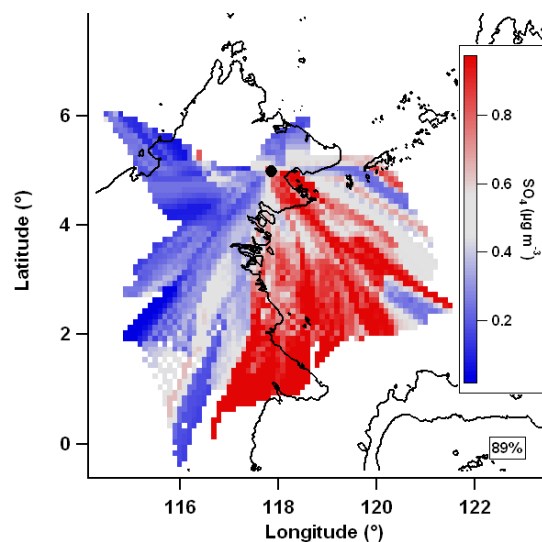


Fig. 15. Sulphate mean value map. Grey is median value, red is greater than median, blue is less than median and white denotes no data coverage. 36 h trajectories are used.

the *Marine*, *Coastal* and *North-easterly* clusters. These points show generally higher oxidation. This is consistent with an internally mixed regional background that is removed through wet deposition in inland Borneo. It is possible that the aerosol associated with line B could be sulphate from similar sources to that associated with line A, but with OA mass added during transit over conurbations on the east coast of Borneo, however this is not likely given the high level of OA oxidation which suggests long atmospheric lifetime, and the lack of association with individual cities. Most likely,

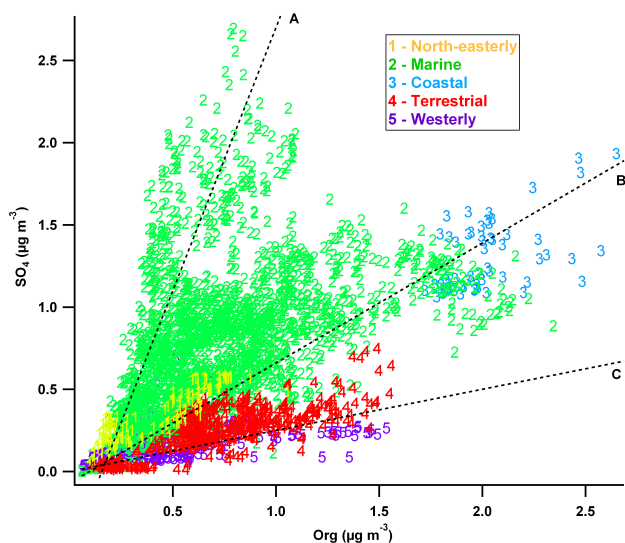


Fig. 16. SO_4 loading vs. OA loading coloured and numbered by cluster. Lines, labelled with letters, indicate different proposed dependencies. Lines represent modes of the SO_4 :org ratio histogram of values.

the aerosol whose sulphate and organic mass correlate along line B result from long range transport, which may well be a combination of anthropogenic and biogenic sources. Biogenic sources of organic matter are most likely to be of terrestrial origin and those of sulphate are likely to be marine in nature.

Line C indicates points of high OA loading with a weaker dependence on sulphate loading, which are characteristically associated with the *Terrestrial* and *Westerly* clusters. They show a range of levels of OA oxidation. This is consistent with biogenic production of SOA, providing a mixture of more and less aged OA.

For the region including the measurement site and the sea to the south-east, where the majority of sulphate containing air masses came from: DMS emissions from phytoplankton are predicted to contribute around 30–40 % of total column sulphate (Gondwe, 2003; Kloster et al., 2006); around 40–50 % of surface sulphate is predicted to be from anthropogenic emissions (Tsai et al., 2010) with < 10 % of surface sulphate concentrations predicted to be from shipping emissions (Capaldo et al., 1999); and around 30 % of surface sulphate predicted from volcanic emissions (Graf et al., 1997).

It is likely that the apparent elevated sulphate loadings over the oil palms to the south-east of the site are mainly due to the preceding transport of the air across marine source regions. There may also be elevated sulphate loadings due to the proximity of marine sources such as DMS production and shipping as well as an increased anthropogenic influence. The fact that sulphate and ammonium loadings are depleted inland is probably due to the wet removal of the aerosols as

they are transported through these regions of enhanced precipitation (Fig. 7).

3.6 Combustion emissions

High aerosol loadings at the beginning of the measurement period are associated with air masses from the south of the measurement site. This can be seen by splitting the data set into two periods of interest (POI): POI1 before 00:01 a.m. 29 June 2008 UTC and POI2 after. This point was chosen because of the drop in both organic and inorganic aerosol loadings and is indicated in Fig. 10. POI1 was influenced by air from the east coast of Borneo, and experienced greater amounts of OA (1.34 vs. $0.62 \mu\text{g m}^{-3}$), OOA1 (0.76 vs. $0.27 \mu\text{g m}^{-3}$), CO (177 vs. 98 ppb; Fig. 17), BC (0.36 vs. $0.18 \mu\text{g m}^{-3}$; Fig. 18) and 91Fac (0.15 vs. $0.12 \mu\text{g m}^{-3}$; Fig. 19) than POI2. These quantities are all indicative of pollution. The 91Fac factor may suggest biomass burning specifically due to its resemblance to previously reported biomass burning spectra (Alfarra et al., 2007; Allan et al., 2010), although it is a minor factor making up only 18 % of total OA mass over the whole project. Trajectories also tended to be influenced by air masses that have higher maximum altitudes during POI1 compared to POI2, with median minimum trajectory pressures of 880 hPa vs. 946 hPa and tenth percentile pressures of 653 hPa vs. 886 hPa, respectively.

During POI2, CO and 91Fac show strongly on-island sources implying that biomass burning still influences the site, albeit to a lesser extent. It is less evident that an on-island source of BC dominates during POI2, with elevated amounts to the south, both on and off-island. There is a disparity between inland BC and CO measurements during POI2, with the dominant CO source being inland and the dominant BC source being more coastal and marine. This would be explained if the BC and CO were emitted from biomass burning on the south coast of Borneo (or even further upwind) and then transported across the island. The BC would be depleted inland through wet removal but the CO concentrations would be largely unaffected. Any BC from shipping off the east coast that was insignificant compared to biomass burning emissions in POI1 would then be apparent in POI2. Modelled loadings of BC (0.2 – $0.5 \mu\text{g m}^{-3}$ for the region; Koch et al., 2009) are consistent with the BC equivalent loadings for POI1 and POI2.

The MODIS fire count shows more open fire activity on Borneo at the beginning of the campaign, with an average of 42 events per day in POI1 compared to 10 in POI2. The fires are mainly confined to the coast with particularly high activity on the south-west of the island. This is also true of the wider region as a whole, with an average of 193 events per day in POI1 compared to 176 in POI2 (for the region shown in Fig. 9). This is consistent with POI1 being particularly heavily influenced by aged biomass burning in the region, either transport of aged off-island biomass burning emissions,

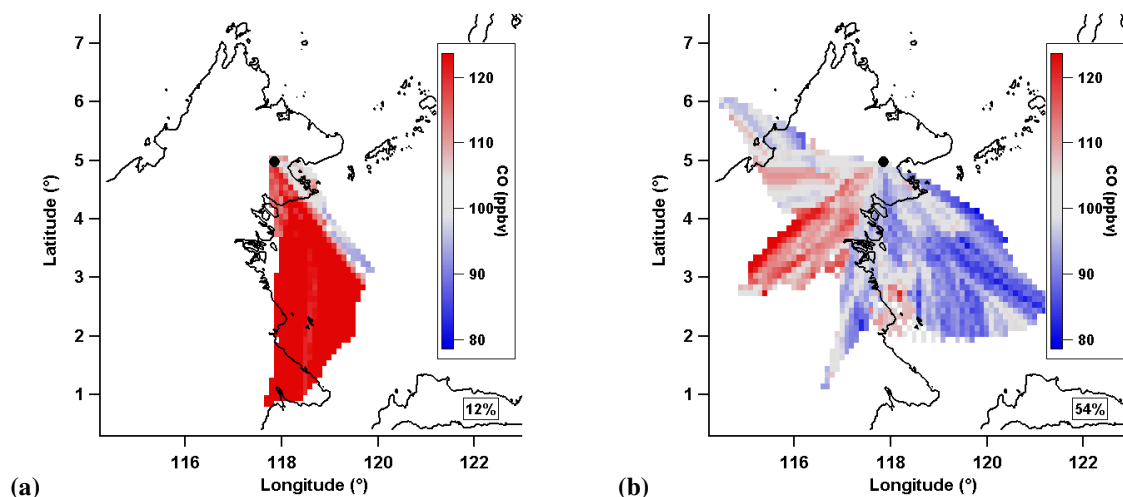


Fig. 17. Mean value maps of CO during (a) POI 1 and (b) POI 2. Colour scale is centred round the median value of the CO mean value map for the whole campaign.

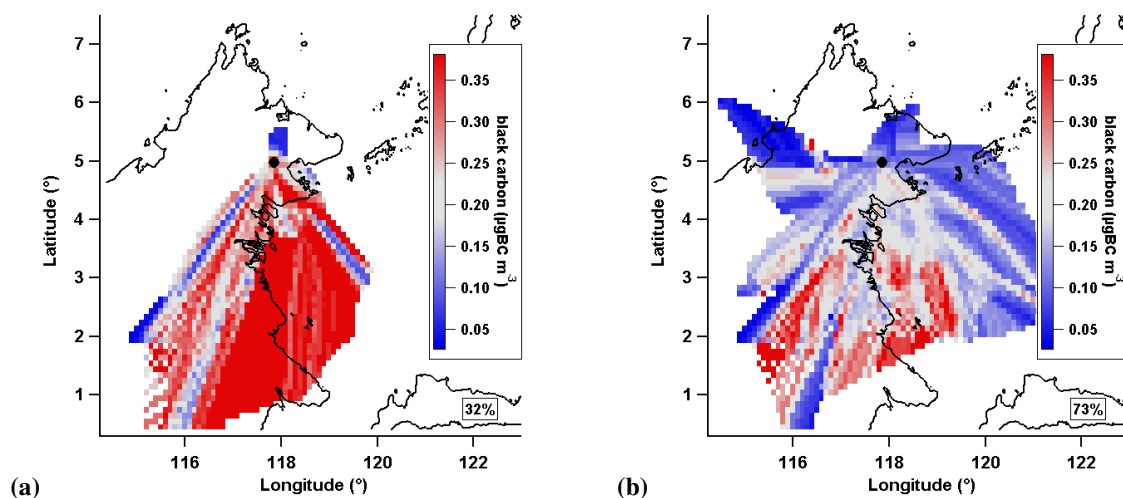


Fig. 18. Mean value maps of aerosol absorbance (expressed as black carbon equivalent loading) during (a) POI 1 and (b) POI 2. The colour scale is centred round the median value of the BC mean value map for the whole campaign.

or more local on-island biomass burning emissions. It is also the case that air masses during POI1 descended from higher altitudes than POI2, with mean minimum pressures of 838 hPa and 931 hPa and tenth percentile values of 652 hPa and 886 hPa, respectively. The introduction of free tropospheric air may increase the dominance of biomass burning species which are likely to be transported from their source to the upper troposphere by pyroconvection.

It is possible that there is an oxidised aerosol influence from the south eastern coast of the island, particularly during POI1. The enhanced OOA1 loadings during POI1 may be due to processed emissions from biomass burning. In POI2 the majority of oxidised aerosol is in air masses external to the island, implying long range transport of OA. Taking this

into consideration, it is likely that the OOA1 in POI1 is from a combination of long range transport of OA and on-island production and ageing of biomass burning OA. Further separation of these sources during POI1 is not possible given the short time scale and small range of trajectories sampled.

The inorganic aerosol components and 82Fac are also all greater in POI1 than POI2. There has been some evidence in the literature that sulphate gases produced from biomass burning can condense onto biomass burning aerosol downwind of fires, so this could be a potential sulphate source (Gao et al., 2003). However, coastal and marine air masses dominate POI1 compared to POI2, which has a more balanced mixture of coastal/marine and inland air masses. This would explain the greater inorganic loadings in POI1, as

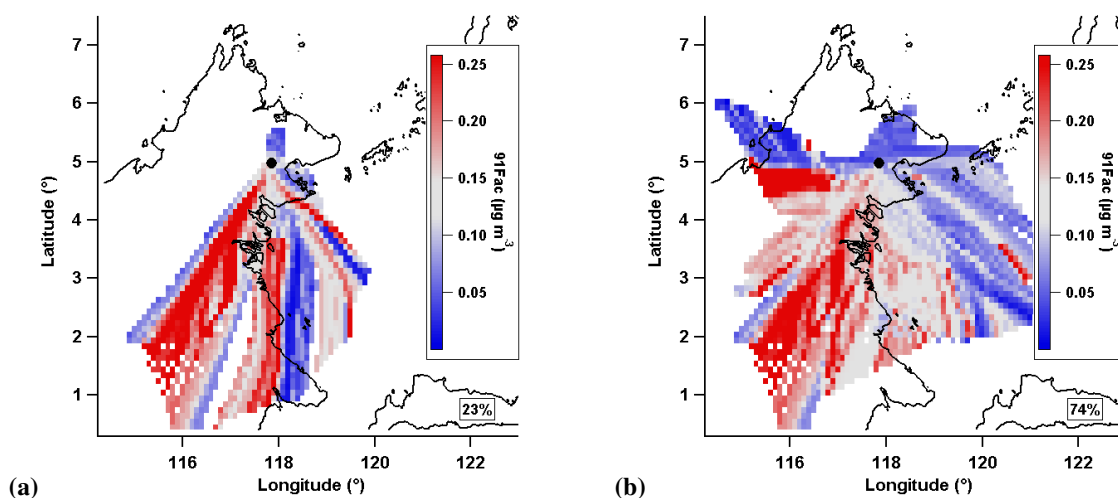


Fig. 19. Mean value maps of 91Fac during (a) POI 1 and (b) POI 2. Colour scale is the consistent between plots and is centred round the median value of the 91Fac mean value map for the whole campaign.

these aerosols are thought to be marine in origin (sulphate and chloride) or formed by reaction with marine aerosol (ammonium and nitrate). While 82Fac is not thought to be marine in origin, it is associated with marine air masses as these pass over the oil palm plantation to the south east of the site. It can also be speculated that some other controlling factor involved in the 82Fac OA was increased during POI1 (e.g. sulphate aerosol acidity or oxidation rates). Acidic sulphate has previously been shown to affect isoprene SOA formation and (Slowik et al., 2011) also showed their m/z 82 containing PMF factor may be associated with elevated sulphate concentrations. However, it appears that 82Fac shows little relation to the biomass burning markers throughout the project, suggesting that the increase during POI1 is unrelated to biomass burning. OOA2 showed a very slight decrease in loadings between POI1 and POI2 (0.09 vs. $0.08 \mu\text{g m}^{-3}$), however this change is so small as to be within the uncertainty of the instrument and analysis methods.

3.7 Dependence of hygroscopicity on regional source

Figure 20 shows mean value maps of hygroscopicity measurements for two given aerosol sizes. These are representative of other measured sizes, with an average $r = 0.9$ for six sizes between 32 and 258 nm for the GF_{90} mean value maps and an average $r = 0.7$ for ten sizes between 57 and 202 nm for the SS_{crit} mean value map. A complete discussion of aerosol hygroscopicity and its relation to composition and size is detailed in Irwin et al. (2010). The subsaturated growth factor (between 0 and 90 % relative humidity; GF_{90}) shows good separation between terrestrial and marine air masses for both sizes, with higher aerosol GF_{90} measured in air of marine origin. Critical supersaturation (SS_{crit}) shows highest values from the south-west and east

over Bongao island (5°N , 120°E), which are air masses associated with low sulphate levels (Fig. 13) and less oxidised aerosol (Fig. 13). As previously stated, the AMS does not efficiently measure sea salt, however if primary externally mixed sea salt aerosol was present it would be expected to be apparent in HTDMA data as a population of particles with a high (>2) growth factor in the upper dry size channels (Good et al., 2010a). Such a mode was not observed, justifying the comparison of AMS and hygroscopicity data. The hygroscopicity mean value maps are supported by the cluster averages. The hygroscopicity instruments have less data coverage than the AMS, not making measurements during the beginning of the measurement period when aerosol loadings were high in air mass from due south over the Sangkulirang Peninsula (1°N , 117.5°E). Taking this into account, higher GF_{90} and lower SS_{crit} values are measured in air masses associated with higher ammonium sulphate mass fraction, and conversely lower GF_{90} and higher SS_{crit} values are measured in air mass associated with lower ammonium sulphate mass fraction. This is consistent with the literature which shows ammonium sulphate to be more hygroscopic than atmospheric OA in both sub- and supersaturated regimes (Petters and Kreidenweis, 2007; Swietlicki et al., 2008). If a single hygroscopicity parameter can be used to explain water uptake then GF and SS_{crit} mean value plots would be expected to anti-correlate. While there is generally good anti-correlation, there are some exceptions. These should be the subject of further investigation to establish if this is due merely to instrumental or inversion artifacts, or if it is indicative of limitations of single variable parameterisations (as discussed by Good et al., 2010b; Irwin et al., 2010).

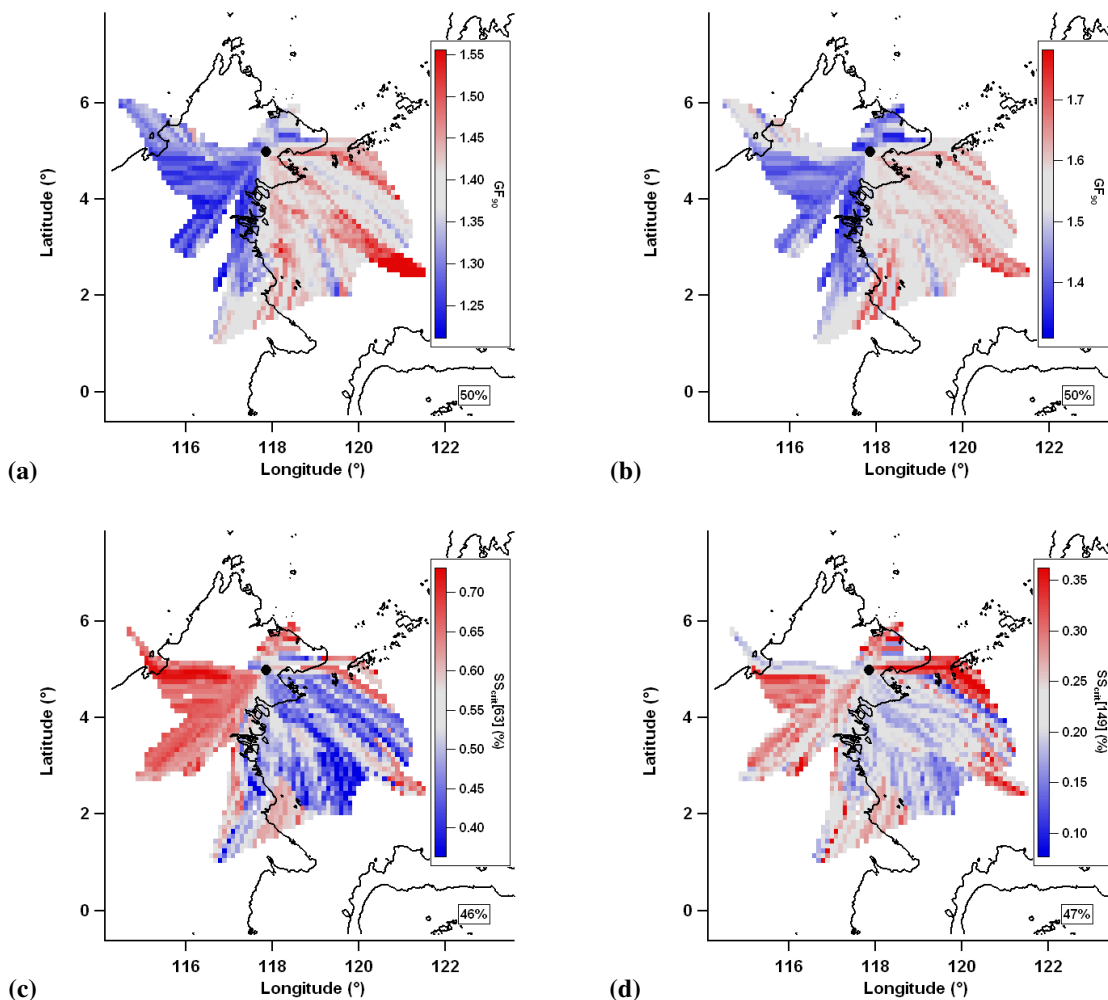


Fig. 20. Mean value maps of: sub-saturated growth factor for (a) 53 nm particles and (b) 155 nm particles; and critical supersaturation for (c) 63 nm particles and (d) 149 nm particles. Grey is median value, red is greater than median, blue is less than median and white denotes no data coverage. 36 h trajectories are used.

4 Summary

In general, many species demonstrated an association with either terrestrial or marine air masses. These are represented by data from the *Terrestrial* and *Marine* clusters which are displayed in Table 4. The analysis of halocarbons shows bromoform and dibromomethane to be strongly associated with coastal and marine air mass. These species are established marine tracers and this result provides validation for the back trajectory analysis presented here. Particularly high mixing ratios were observed in air masses associated with an area of seaweed cultivation directly east of the site. Methyl iodide was associated with similar air masses as the polybrominated compounds but it is unclear if it is produced from similar sources or by a different mechanism. It shows some departure from the polybrominated compounds, with inland levels not as uniformly low. Elevated inland values are also present in the methyl bromide mean value map. Methyl io-

dide has previously been reported from terrestrial vegetation and soil as well as biomass burning, all of which may contribute to the inland sources. Biomass burning has been reported as a source of methyl bromide and there is some evidence for emission from tropical vegetation. In contrast to the other halocarbons, the methyl bromide mean value map showed low mixing ratios in air masses directly east of the site. There does seem to be some marine contribution, specifically from the coast directly south of the site. It also showed some elevated mixing ratios in air masses from directly north and south of the site. This may be due to biomass burning associated with the oil palm plantations however other biomass burning markers were not observed to be significant of this region. It could also be due to the proximity of coastal sources such as macro algae. It is unclear if the oil palms themselves are a source of methyl bromide.

Table 4. Averages of data during 12 h periods classified as belonging to the *Marine* and *Terrestrial* clusters. Values quoted in the form mean (median_{75th %ile}, 25th %ile). *Marine* and *Terrestrial* data sets that are significantly different with a 95% confidence level (using the two tailed Mann-Whitney U test (Cheung et al., 1997), which is nonparametric) are marked with an asterisk.

	Borneo			Amazonia		
	Terrestrial	Marine	All	In basin	Out of basin	All
Aerosol composition						
Organics ($\mu\text{g m}^{-3}$)	0.68 (0.64 ^{0.89} _{0.47})	0.70 (0.62 ^{0.90} _{0.41})	0.74 (0.63 ^{0.95} _{0.43})	0.50	0.80	0.67
OOA1* ($\mu\text{g m}^{-3}$)	0.29 (0.25 ^{0.44} _{0.16})	0.33 (0.27 ^{0.43} _{0.16})	0.35 (0.27 ^{0.46} _{0.16})			
OOA2* ($\mu\text{g m}^{-3}$)	0.11 (0.10 ^{0.14} _{0.07})	0.07 (0.07 ^{0.10} _{0.04})	0.08 (0.07 ^{0.11} _{0.04})			
82Fac* ($\mu\text{g m}^{-3}$)	0.12 (0.09 ^{0.18} _{0.05})	0.18 (0.14 ^{0.25} _{0.06})	0.18 (0.13 ^{0.25} _{0.06})			
91Fac* ($\mu\text{g m}^{-3}$)	0.16 (0.15 ^{0.21} _{0.09})	0.12 (0.09 ^{0.15} _{0.05})	0.13 (0.10 ^{0.17} _{0.05})			
Sulphate* ($\mu\text{g m}^{-3}$)	0.27 (0.26 ^{0.35} _{0.19})	0.75 (0.71 ^{0.99} _{0.40})	0.61 (0.50 ^{0.89} _{0.28})	0.04	0.30	0.15
Ammonium* ($\mu\text{g m}^{-3}$)	0.09 (0.09 ^{0.12} _{0.05})	0.25 (0.24 ^{0.35} _{0.13})	0.21 (0.19 ^{0.31} _{0.09})			0.02
Nitrate* ($\mu\text{g m}^{-3}$)	0.03 (0.02 ^{0.04} _{0.01})	0.04 (0.03 ^{0.05} _{0.02})	0.04 (0.02 ^{0.05} _{0.01})			0.01
Chloride* ($\mu\text{g m}^{-3}$)	0.01 (0.00 ^{0.01} _{0.00})	0.01 (0.01 ^{0.01} _{0.00})	0.01 (0.01 ^{0.01} _{0.00})			0.00
Absorbance* ($\mu\text{g m}^{-3}$)	0.19 (0.16 ^{0.28} _{0.09})	0.21 (0.17 ^{0.29} _{0.09})	0.22 (0.18 ^{0.31} _{0.09})			
Hygroscopicity						
GF ₉₀ * [53 nm]	1.30 (1.29 ^{1.34} _{1.27})	1.42 (1.41 ^{1.45} _{1.36})	1.38 (1.38 ^{1.43} _{1.32})			
GF ₉₀ * [155 nm]	1.46 (1.49 ^{1.52} _{1.41})	1.58 (1.58 ^{1.62} _{1.53})	1.53 (1.54 ^{1.60} _{1.46})			
SS _{crit} * [63 nm]	0.63 (0.63 ^{0.67} _{0.61})	0.48 (0.47 ^{0.55} _{0.41})	0.53 (0.54 ^{0.63} _{0.45})			
SS _{crit} * [149 nm]	0.26 (0.25 ^{0.31} _{0.18})	0.20 (0.17 ^{0.23} _{0.15})	0.22 (0.20 ^{0.27} _{0.16})			
Gas composition						
CO* (ppbv)	111 (110 ¹¹⁶ ₁₀₅)	98.4 (94.3 ¹⁰⁸ _{86.8})	101 (100 ¹¹⁰ _{89.4})			
CHBr ₃ * (pptv)	1.10 (1.13 ^{1.28} _{0.96})	1.61 (1.56 ^{1.79} _{1.38})	1.48 (1.45 ^{1.75} _{1.17})			
CH ₂ Br ₂ * (pptv)	0.81 (0.83 ^{0.85} _{0.80})	0.95 (0.95 ^{0.99} _{0.91})	0.91 (0.93 ^{0.98} _{0.85})			
CH ₃ I* (pptv)	1.03 (1.08 ^{1.12} _{0.97})	1.09 (1.08 ^{1.18} _{0.99})	1.08 (1.08 ^{1.18} _{0.99})			
CH ₃ Br (pptv)	6.73 (6.68 ^{7.39} _{6.23})	6.92 (6.90 ^{7.23} _{6.35})	6.80 (6.69 ^{7.21} _{6.16})			

Particulate nitrate and chloride show very similar time series trends and their mean value maps show their association with marine air. They exhibit a consistent diurnal profile with sharply elevated levels around midnight. Inspection of the AMS mass spectral information shows that the nitrate is unlikely to be present as ammonium nitrate or organic nitrates. The sea is an established source of sodium chloride aerosol, however this is not generally detected due to its slow vapourisation time in the AMS. Nitric acid may be produced by processing of biogenic NO_x from soil (particularly from the fertilised oil palms plantations) and anthropogenic NO_x emissions from settlements on the coast. This nitric acid could displace chloride from marine sodium chloride particles to give aqueous sodium nitrate aerosol that is more efficiently vapourised by the AMS than sodium chloride. It is likely that the liberated chloride is detected in the form of ammonium chloride although it is unclear if this is the case. The

nocturnal profile may be caused by the reformation of nitrate and chloride aerosols in nocturnal fog droplets or their likely partitioning to the gas phase as the temperature increases during the day. It may also be associated with sampling of free tropospheric air when the boundary layer dropped below the measurement site, as was observed by LIDAR measurements (Pearson et al., 2010). While loadings of nitrate and chloride are small, they are higher than were measured in Amazonia which is consistent with greater influence of a marine source.

Levels of sulphate and ammonium are much higher than in the AMAZE-08 project in the rainforest of the Central Amazon basin where Chen et al. (2009) performed a similar analysis of sulphate and OA correlation to assess aerosol origin. This led to the classification of “in-basin” and “out-of-basin” influences. 40 % of the AMAZE-08 project was classified as being influenced by in-basin periods which were dominated by (relatively unoxidised) OA ($0.5 \mu\text{g m}^{-3}$), with

little sulphate influence ($0.04 \mu\text{g m}^{-3}$). These were deemed to be influenced mainly by BSOA freshly produced from rainforest VOC emissions. The out-of-basin periods, comprising 30% of the project, were less dominated by OA ($0.8 \mu\text{g m}^{-3}$), which was more oxidised, with more sulphate influence ($0.3 \mu\text{g m}^{-3}$). During these periods the measurement site was more influenced by long range transport of emissions from a variety of sources, probably processed DMS emissions from the Atlantic and biomass burning from West Africa. This is in contrast to Borneo which experienced much higher sulphate loadings ($0.61 \mu\text{g m}^{-3}$). A study in West Africa measured similarly high levels of sulphate as were observed during OP3, which may be due to the marine influences during the West African monsoon phase.

Organic aerosol is most oxidised in marine air masses. Sulphate was associated with marine air masses and showed varying levels of correlation with organic aerosol. Sulphate unassociated with organic aerosol showed an off-island source and is likely to be mainly from the processing of marine DMS emissions. Air masses travelling over the mountainous interior of Borneo show depressed levels of regional background aerosol which is probably due to greater wet removal by orographically induced convective precipitation. These air masses are also associated with less oxygenated OA, presumably because the removal of regional aerosol increases the relative dominance of BSOA produced close to the measurement site. It should be noted that the sulphate loading in *Terrestrial* air masses (which are most representative of rainforest conditions) is even greater than the out-of-basin classified data from Amazonia. This implies that, while regional aerosol is probably being depleted inland through wet deposition, a significant amount of aerosol is transported across the length of the island. Emissions from agriculture seemed to influence the site with isoprenoid BSOA showing elevated levels over the major oil palm plantations to the north and south of the site, which is consistent with measurements showing oil palm to emit five times as much isoprene as the natural rainforest (Hewitt et al., 2009).

OA associated with sulphate also showed an off-island source and an increased level of oxidation. This is likely to be long range transport of internally mixed aerosol. The sources are likely to be a combination of both anthropogenic and biogenic sources of both OA and sulphate but the OA has aged considerably during transport. It is unclear how much of this background signal is biogenic, anthropogenic or pyrogenic. It is also possible that the organic background may be wholly or in part due to marine biological sources (O'Dowd et al., 2004). A fraction of the OA showed only a weak association with sulphate. This predominantly arose during air periods influenced by on-island air masses and is likely to be biogenic aerosol from processing of VOCs emitted by the rainforest. Emissions from the rainforest in Borneo are likely to be measured at Bukit Atur as relatively fresh aerosol and so would be expected to be represented by OOA2 and 82Fac, plus some fraction of OOA1. Considering

only periods influenced by *Terrestrial* air masses, this gives an estimated loading of between 0.23 and $0.52 \mu\text{g m}^{-3}$, compared to $0.5 \mu\text{g m}^{-3}$ of OA seen in-basin in Amazonia. This lower contribution from the Bornean rainforest is likely to be mainly due to the difference in the size of the source regions.

The beginning of the campaign was dominated by high aerosol loadings, due in particular to sulphate and the organic OOA1 and 82Fac PMF factors. This period was also associated with increased CO, BC, 91Fac and all inorganic species. The MODIS satellite shows this to be a period of enhanced fire activity around the coast of Borneo, particularly on the southwest of the island. The beginning of the measurement period is influenced by coastal air running up the east coast of Borneo. It is likely that the increased biomass burning activity caused the increased CO, BC and 91Fac loadings. It is also likely that processed organic biomass burning emissions contributed to the increased OOA1 loadings. It is possible that some of the sulphate aerosol is from condensation of gases emitted from biomass burning. However, the correlation is not high ($r = 0.45$) between the OOA1 and sulphate time series during POI1 suggesting that, if this is occurring, it is a relatively small contribution. In addition to aerosol emissions from biomass burning, the enhanced inorganic and OOA1 aerosol loadings during POI1 could be due to the dominance of coastal air, a reduction in precipitation causing less wet removal, or an increase in oxidation rates. The latter two could themselves be consequences of biomass burning emissions.

Aerosol hygroscopicity showed marked differences between terrestrial and marine air masses, however the data coverage does not include the period of more intense biomass burning. The most hygroscopic aerosol associated with the same air masses as high ammonium sulphate concentrations. As sulphate aerosol is more hygroscopic than (even highly oxidised) organic aerosol, the sulphate to organic mass ratio would be expected to be the driving factor in the aerosol hygroscopicity.

5 Conclusions

The results are consistent with a regional background of sulphate and aged organic aerosol that is removed by wet deposition in the interior of Borneo. This may be expected on an island, where off-island sources are likely to be distant enough to contribute to an aged background. Seven day air mass trajectories show the site was influenced by the least populated areas with the least amount of detected fires, when compared to the wider region. Given this it is likely that biological sources dominated the regional background.

Both the Marine and Terrestrial clusters had much higher sulphate loadings (0.75 and $0.27 \mu\text{g m}^{-3}$, respectively) than were measured in Amazonia ($0.15 \mu\text{g m}^{-3}$), which is probably due to a greater marine influence. The rainforest ecosystem has also been reported as a minor source

of sulphur gases (and associated aerosol) in the Amazon (Andreae et al., 1990), but the analysis presented here shows if this is present it is a comparatively minor source, with *Terrestrial* air masses containing 65 % less sulphate than *Marine*.

The sulphate appears to be largely neutralised to ammonium sulphate by time of arrival at the site, probably by terrestrial ammonium. The rainforest and oil palms appear to be sources of BSOA, with an estimated mean concentration of $0.26 \mu\text{g m}^{-3}$, however there are no periods where local BSOA dominates as was the case in the AMAZE-08 project. The region is influenced by some level of biomass burning, although, apart from the beginning of the measurement period, this appears to be a relatively minor source. Far field biomass burning emissions may be so aged as to be part of the regional background, however inspection of seven day back trajectories were not associated with areas of particularly high fire activity in the region. There also appears to be a minor influence at night from marine chloride reacting with terrestrial nitrate.

In general Borneo shows a wider range of influences than Amazonia. Despite data coverage lower than other comparable analyses the methods proved useful in assessing the origin of species measured. This study shows that the Amazon, whilst clearly an important part of the biosphere, is not representative of the tropics as a whole. The “maritime continent” region needs to be considered separately from the Amazon, as being a heterogeneous and complex mixture of biogenic, marine and anthropogenic influence.

Supplementary material related to this article is available online at:

<http://www.atmos-chem-phys.net/11/9605/2011/acp-11-9605-2011-supplement.pdf>

Acknowledgements. Thanks to Gavin McMeeking (Colorado State University) and Mathew Evans (The University of Leeds) for useful conversations in the preparation of this manuscript. Thanks also to Minnie Wong (Fire Information and Resource Management System) for providing archived MODIS fire data. The OP3 project was funded by the UK Natural Environment Research Council [grant number NE/D002117/1]. We thank the Malaysian and Sabah Governments for their permission to conduct research in Malaysia; the Malaysian Meteorological Department (MMD) for access to the Bukit Atur Global Atmosphere Watch station and their long term ozone record; Leong Chow Peng (formerly of MMD) for her support in the early stages of the project; Waidi Sinun of Yayasan Sabah and his staff and Glen Reynolds of the Royal Society’s South East Asian Rain Forest Research Programme and his staff for logistical support at the Danum Valley Field Centre; the NERC Facility for Ground-based Atmospheric Measurements and Halo Photonics for support with the LIDAR deployment; Phua Mui How of the University Malaysia Sabah for his help with the land cover map; and the rest of the OP3 project team for their individual and collective efforts. This is paper number 525 of the Royal Society’s South East Asian Rainforest Research Programme.

Edited by: R. MacKenzie

References

- Alfarra, M. R., Prevot, A. S. H., Szidat, S., Sandradewi, J., Weimer, S., Lanz, V. A., Schreiber, D., Mohr, M., and Baltensperger, U.: Identification of the mass spectral signature of organic aerosols from wood burning emissions, *Environ. Sci. Technol.*, 41, 5770–5777, doi:10.1021/es062289b, 2007.
- Allan, J. D., Bower, K. N., Coe, H., Boudries, H., Jayne, J. T., Canagaratna, M. R., Millet, D. B., Goldstein, A., Quinn, P. K., Weber, R. J., and Worsnop, D. R.: Submicron aerosol composition at Trinidad Head, California, during ITCT 2K2: its relationship with gas phase volatile organic carbon and assessment of instrument performance, *J. Geophys. Res.*, 109, D23S24, doi:10.1029/2003JD004208, 2004.
- Allan, J. D., Topping, D. O., Good, N., Irwin, M., Flynn, M., Williams, P. I., Coe, H., Baker, A. R., Martino, M., Niedermeier, N., Wiedensohler, A., Lehmann, S., Müller, K., Herrmann, H., and McFiggans, G.: Composition and properties of atmospheric particles in the eastern Atlantic and impacts on gas phase uptake rates, *Atmos. Chem. Phys.*, 9, 9299–9314, doi:10.5194/acp-9-9299-2009, 2009.
- Allan, J. D., Williams, P. I., Morgan, W. T., Martin, C. L., Flynn, M. J., Lee, J., Nemitz, E., Phillips, G. J., Gallagher, M. W., and Coe, H.: Contributions from transport, solid fuel burning and cooking to primary organic aerosols in two UK cities, *Atmos. Chem. Phys.*, 10, 647–668, doi:10.5194/acp-10-647-2010, 2010.
- Allen, A. G., Oppenheimer, M. F., Baxter, P. J., Horrocks, L. A., Galle, B., McGonigle, A. J. S., and Duffell, H. J.: Primary sulfate aerosol and associated emissions from Masaya Volcano, Nicaragua, *J. Geophys. Res.*, 107, 4682, doi:10.1029/2002JD002120, 2002.
- Andreae, M. O., Berresheiem, H., Bingemer, H., Jacob, D. J., Lewis, B. L., Li, S.-M., and Talbot, R. W.: The atmospheric sulfur cycle over the Amazon Basin. II. Wet season, *J. Geophys. Res.*, 95, 16813–16824, doi:10.1029/JD095iD10p16813, 1990.
- Ashbaugh, L.: A residence time probability analysis of sulfur concentrations at grand Canyon National Park, *Atmos. Environ.*, 19, 1263–1270, doi:10.1016/0004-6981(85)90256-2, 1985.
- Avissar, R., Silva Dias, P., Silva Dias, M., and Nobre, C. A.: The Large-Scale Biosphere-Atmosphere Experiment in Amazonia (LBA): insights and future research needs, *J. Geophys. Res.*, 107, 8086, doi:10.1029/2002JD002704, 2002.
- British Atmospheric Data Centre: European Centre for Medium-Range Weather Forecasts back trajectories, <http://badc.nerc.ac.uk/data/ecmwf-op/> (last access: January 2010), 2006a.
- British Atmospheric Data Centre: European Centre for Medium-Range Weather Forecasts. ECMWF Operational Analysis data, http://badc.nerc.ac.uk/view/badc.nerc.ac.uk_ATOM.dataent_ECMWF-OP (last access: October 2010), 2006b.
- Baker, J.: Emissions of CH_3Br , organochlorines, and organoiodines from temperate macroalgae, *Glob. Change Sci.*, 3, 93–106, doi:10.1016/S1465-9972(00)00021-0, 2001.
- Bassford, M. R., Nickless, G., Simmonds, P. G., Lewis, A. C., Pilling, M. J., and Evans, M. J.: The concurrent observation of methyl iodide and dimethyl sulphide in marine air; implications for sources of atmospheric methyl iodide, *Atmos. Environ.*, 33, 2373–2383, doi:10.1016/S1352-2310(98)00403-8, 1999.
- Bates, T. S., Calhoun, J. A., and Quinn, P. K.: Variations in the methanesulfonate to sulfate molar ratio in submicrometer marine

- aerosol particles over the South Pacific Ocean, *J. Geophys. Res.*, **95**, 813–816, 1992.
- Bell, N., Hsu, L., Jacob, M., Schultz, M. G., Blake, D. R., Butler, J. H., King, D. B., Lobert, J. M., and Maier-Reimer, E.: Methyl iodide: atmospheric budget and use as a tracer of marine convection in global models, *J. Geophys. Res.*, **107**, 4340, doi:10.1029/2001JD001151, 2002.
- Blei, E., Hardacre, C. J., Mills, G. P., Heal, K. V., and Heal, M. R.: Identification and quantification of methyl halide sources in a lowland tropical rainforest, *Atmos. Environ.*, **44**, 1005–1010, doi:10.1016/j.atmosenv.2009.12.023, 2010.
- Butler, J. H., King, D. B., Lobert, J. M., Montzka, S. A., Yvon-Lewis, S. A., Hall, B. D., Warwick, N. J., Mondeel, D. J., Aydin, M., and Elkins, J. W.: Oceanic distributions and emissions of short-lived halocarbons, *Global Biogeochem. Cy.*, **21**, GB1023, doi:10.1029/2006GB002732, 2007.
- Canagaratna, M. R., Jayne, J. T., Jimenez, J. L., Allan, J. D., Alfarra, M. R., Zhang, Q., Onasch, T. B., Drewnick, F., Coe, H., Middlebrook, A., Delia, A., Williams, L. R., Trimborn, A. M., Northway, M. J., DeCarlo, P. F., Kolb, C. E., Davidovits, P., and Worsnop, D. R.: Chemical and microphysical characterization of ambient aerosols with the aerodyne aerosol mass spectrometer, *Mass Spectrom. Rev.*, **26**, 185–222, doi:10.1002/mas.20115, 2007.
- Capaldo, K., Corbett, J. J., Kasibhatla, P., Fischbeck, P., and Pandis, S. N.: Effects of ship emissions on sulphur cycling and radiative climate forcing over the ocean, *Nature*, **400**, 743–746, doi:10.1038/23438, 1999.
- Cape, J. N., Methven, J., and Hudson, L. E.: The use of trajectory cluster analysis to interpret trace gas measurements at Mace Head, Ireland, *Atmos. Environ.*, **34**, 3651–3663, doi:10.1016/S1352-2310(00)00098-4, 2000.
- Capes, G., Johnson, B., McFiggans, G., Williams, P. I., Haywood, J., and Coe, H.: Aging of biomass burning aerosols over West Africa: aircraft measurements of chemical composition, microphysical properties, and emission ratios, *J. Geophys. Res.*, **113**, D00C15, doi:10.1029/2008JD009845, 2008.
- Capes, G., Murphy, J. G., Reeves, C. E., McQuaid, J. B., Hamilton, J. F., Hopkins, J. R., Crosier, J., Williams, P. I., and Coe, H.: Secondary organic aerosol from biogenic VOCs over West Africa during AMMA, *Atmos. Chem. Phys.*, **9**, 3841–3850, doi:10.5194/acp-9-3841-2009, 2009.
- Carpenter, L. J. and Liss, P. S.: On temperate sources of bromoform and other reactive organic bromine gases, *J. Geophys. Res.*, **105**, 20539–20547, doi:10.1029/2000JD900242, 2000.
- Carter, C., Finley, W., Fry, J., Jackson, D., and Willis, L.: Palm oil markets and future supply, *Eur. J. Lipid Science Technol.*, **109**, 307–314, doi:10.1002/ejlt.200600256, 2007.
- Chan, M. N., Surratt, J. D., Claeys, M., Edgerton, E. S., Tanner, R. L., Shaw, S. L., Zheng, M., Knipping, E. M., Eddingsaas, N. C., Wennberg, P. O., and Seinfeld, J. H.: Characterization and quantification of isoprene-derived epoxydiols in ambient aerosol in the Southeastern United States, *Environ. Sci. Technol.*, **44**, 4590–4596, 2010.
- Chen, Q., Farmer, D. K., Schneider, J., Zorn, S. R., Heald, C. L., Karl, T. G., Guenther, A., Allan, J. D., Robinson, N., Coe, H., Kimmel, J. R., Pauliquevis, T., Borrmann, S., Pöschl, U., Andreae, M. O., Artaxo, P., Jimenez, J. L., and Martin, S. T.: Mass spectral characterization of submicron biogenic organic particles in the Amazon Basin, *Geophys. Res. Lett.*, **36**, L20806, doi:10.1029/2009GL039880, 2009.
- Cheung, Y. K., and Klot, J. H.: The Mann Whitney Wilcoxon Distribution Using Linked Lists, *Statistica Sinica*, **7**, 805–813, 1997.
- Claeys, M., Graham, B., Vas, G., Wang, W., Vermeylen, R., Pashynska, V., Cafmeyer, J., Guyon, P., Andreae, M. O., Artaxo, P., and Maenhaut, W.: Formation of secondary organic aerosols through photooxidation of isoprene, *Science*, **303**(5661), 1173–1176, doi:10.1126/science.1092805, 2004.
- Cox, M. L., Sturrock, G. A., Fraser, P. J., Siems, S. T., and Krummel, P. B.: Identification of regional sources of methyl bromide and methyl iodide from AGAGE observations at Cape Grim, Tasmania, *J. Atmos. Chem.*, **50**, 59–77, doi:10.1007/s10874-005-2434-5, 2005.
- Cross, E., Slowik, J., Davidovits, P., Allan, J., Worsnop, D., Jayne, J., Lewis, D., Canagaratna, M., and Onasch, T.: Laboratory and ambient particle density determinations using light scattering in conjunction with aerosol mass spectrometry, *Aerosol Sci. Technol.*, **41**, 343–359, doi:10.1080/02786820701199736, 2007.
- Cubison, M., Coe, H., and Gysel, M.: A modified hygroscopic tandem DMA and a data retrieval method based on optimal estimation, *J. Aerosol Sci.*, **36**, 846–865, doi:10.1016/j.jaerosci.2004.11.009, 2005.
- Davies, D. K., Ilavajhala, S., Wong, M. M., and Justice, C. O.: Fire information for resource management system: archiving and distributing MODIS active fire data, *IEEE Trans. Geosci. Remote S.*, **47**, 72–79, doi:10.1109/TGRS.2008.2002076, 2009.
- DeCarlo, P. F., Kimmel, J. R., Trimborn, A., Northway, M. J., Jayne, J. T., Aiken, A. C., Gonin, M., Fuhrer, K., Horvath, T., Docherty, K. S., Worsnop, D. R., and Jimenez, J. L.: Field-deployable, high-resolution, time-of-flight aerosol mass spectrometer, *Anal. Chem.*, **78**, 8281–8289, 2006.
- Denman, K., Brasseur, G., Chidthaisong, A., Ciais, P., Cox, P., Dickinson, R., Hauglustaine, D., Heinze, C., Holland, E., Jacob, D., Lohmann, U., Ramachandran, S., Dias, P. D. S., Wofsy, S., and Zhang, X.: Couplings Between Changes in the Climate System and Biogeochemistry, Chap. Couplings, Cambridge University Press, Cambridge, UK and New York, NY, USA, 2007.
- Facchini, M. C., Decesari, S., Rinaldi, M., Carbone, C., Finessi, E., Mircea, M., Fuzzi, S., Moretti, F., Tagliavini, E., Ceburnis, D., and O'Dowd, C. D.: Important source of marine secondary organic aerosol from biogenic amines, *Environ. Sci. Technol.*, **42**, 9116–9121, doi:10.1021/es8018385, 2008.
- Farmer, D. K., Matsunaga, A., Docherty, K. S., Surratt, J. D., Seinfeld, J. H., Ziemann, P. J., and Jimenez, J. L.: Response of an aerosol mass spectrometer to organonitrates and organosulfates and implications for atmospheric chemistry, *P. Natl. Acad. Sci. USA*, **107**, 6670–6675, doi:10.1073/pnas.0912340107, 2010.
- Food and Agriculture Organisation: Global Forest Resources Assessment 2010: Main Report, Bernan Assoc, Rome, <http://books.google.com/books?id=vEcJTweACA AJ&pgis=1> (last access: January 2011), 2010.
- Froyd, K. D., Murphy, S. M., Murphy, D. M., de Gouw, J. A., Eddingsaas, N. C., and Wennberg, P. O.: Contribution of isoprene-derived organosulfates to free tropospheric aerosol mass., *P. Natl. Acad. Sci. USA*, **107**, 21360–21365,

- doi:10.1073/pnas.1012561107, 2010.
- Gao, S., Hegg, D. A., Hobbs, P. V., Kirchstetter, T. W., Magi, B. I., and Sadilek, M.: Water-soluble organic components in aerosols associated with savanna fires in Southern Africa: identification, evolution, and distribution, *J. Geophys. Res.*, 108, 8491, doi:10.1029/2002JD002324, 2003.
- Gerbig, C., Schmitgen, S., Kley, D., Volz-Thomas, A., Dewey, K., and Haaks, D.: An improved fast-response vacuum-UV resonance fluorescence CO instrument, *J. Geophys. Res.*, 104, 1699–1704, doi:10.1029/1998JD100031, 1999.
- Giglio, L.: An enhanced contextual fire detection algorithm for MODIS, *Remote Sens. Environ.*, 87, 273–282, doi:10.1016/S0034-4257(03)00184-6, 2003.
- Gondwe, M.: The contribution of ocean-leaving DMS to the global atmospheric burdens of DMS, MSA, SO₂, and NSS SO₄⁻, *Global Biogeochem. Cy.*, 17, 1056, doi:10.1029/2002GB001937, 2003.
- Good, N., Topping, D. O., Allan, J. D., Flynn, M., Fuentes, E., Irwin, M., Williams, P. I., Coe, H., and McFiggans, G.: Consistency between parameterisations of aerosol hygroscopicity and CCN activity during the RHaMBLe discovery cruise, *Atmos. Chem. Phys.*, 10, 3189–3203, doi:10.5194/acp-10-3189-2010, 2010a.
- Good, N., Topping, D. O., Duplissy, J., Gysel, M., Meyer, N. K., Metzger, A., Turner, S. F., Baltensperger, U., Ristovski, Z., Weingartner, E., Coe, H., and McFiggans, G.: Widening the gap between measurement and modelling of secondary organic aerosol properties?, *Atmos. Chem. Phys.*, 10, 2577–2593, doi:10.5194/acp-10-2577-2010, 2010b.
- Goodwin, K. D., North, W. J., and Lidstrom, M. E.: Production of bromoform and dibromomethane by giant kelp: factors affecting release and comparison to anthropogenic bromine sources, *Limnol. Oceanogr.*, 42, 1725–1734, 1997.
- Graf, H.-F., Feichter, J., and Langmann, B.: Volcanic sulfur emissions: estimates of source strength and its contribution to the global sulfate distribution, *J. Geophys. Res.*, 102, 10727–10738, doi:10.1029/96JD03265, 1997.
- Gysel, M., McFiggans, G., and Coe, H.: Inversion of tandem differential mobility analyser (TDMA) measurements, *J. Aerosol Sci.*, 40, 134–151, doi:10.1016/j.jaerosci.2008.07.013, 2009.
- Hewitt, C. N., MacKenzie, A. R., Di Carlo, P., Di Marco, C. F., Dorsey, J. R., Evans, M., Fowler, D., Gallagher, M. W., Hopkins, J. R., Jones, C. E., Langford, B., Lee, J. D., Lewis, A. C., Lim, S. F., McQuaid, J., Misztal, P., Moller, S. J., Monks, P. S., Nemitz, E., Oram, D. E., Owen, S. M., Phillips, G. J., Pugh, T. A. M., Pyle, J. A., Reeves, C. E., Ryder, J., Siong, J., Skiba, U., and Stewart, D. J.: Nitrogen management is essential to prevent tropical oil palm plantations from causing ground-level ozone pollution, *P. Natl. Acad. Sci. USA*, 106, 18447–18451, doi:10.1073/pnas.0907541106, 2009.
- Hewitt, C. N., Lee, J. D., MacKenzie, A. R., Barkley, M. P., Carslaw, N., Carver, G. D., Chappell, N. A., Coe, H., Collier, C., Commane, R., Davies, F., Davison, B., DiCarlo, P., Di Marco, C. F., Dorsey, J. R., Edwards, P. M., Evans, M. J., Fowler, D., Furneaux, K. L., Gallagher, M., Guenther, A., Heard, D. E., Helfter, C., Hopkins, J., Ingham, T., Irwin, M., Jones, C., Karunaharan, A., Langford, B., Lewis, A. C., Lim, S. F., MacDonald, S. M., Mahajan, A. S., Malpass, S., McFiggans, G., Mills, G., Misztal, P., Moller, S., Monks, P. S., Nemitz, E., Nicolas-Perea, V., Oetjen, H., Oram, D. E., Palmer, P. I., Phillips, G. J., Pike, R., Plane, J. M. C., Pugh, T., Pyle, J. A., Reeves, C. E., Robinson, N. H., Stewart, D., Stone, D., Whalley, L. K., and Yin, X.: Overview: oxidant and particle photochemical processes above a south-east Asian tropical rainforest (the OP3 project): introduction, rationale, location characteristics and tools, *Atmos. Chem. Phys.*, 10, 169–199, doi:10.5194/acp-10-169-2010, 2010.
- International Fuel Quality Center: International Desil Rankings – Top 100 Sulphur, [http://www.ifqc.org/UserFiles/file/Misc/DieselRankings0909\(1\).pdf](http://www.ifqc.org/UserFiles/file/Misc/DieselRankings0909(1).pdf), (last access: April 2010), 2009.
- Irwin, M., Good, N., Crosier, J., Choulaton, T. W., and McFiggans, G.: Reconciliation of measurements of hygroscopic growth and critical supersaturation of aerosol particles in central Germany, *Atmos. Chem. Phys.*, 10, 11737–11752, doi:10.5194/acp-10-11737-2010, 2010.
- Irwin, M., Robinson, N., Allan, J. D., Coe, H., and McFiggans, G.: Size-resolved aerosol water uptake and cloud condensation nuclei measurements as measured above a Southeast Asian rainforest during OP3, *Atmos. Chem. Phys. Discuss.*, 11, 3117–3159, doi:10.5194/acpd-11-3117-2011, 2011.
- Jimenez, J. L., Canagaratna, M. R., Donahue, N. M., Prevot, A. S. H., Zhang, Q., Kroll, J. H., DeCarlo, P. F., Allan, J. D., Coe, H., Ng, N. L., Aiken, A. C., Docherty, K. S., Ulbrich, I. M., Grieshop, A. P., Robinson, A. L., Duplissy, J., Smith, J. D., Wilson, K. R., Lanz, V. A., Hueglin, C., Sun, Y. L., Tian, J., Laaksonen, A., Raatikainen, T., Rautiainen, J., Vaattovaara, P., Ehn, M., Kulmala, M., Tomlinson, J. M., Collins, D. R., Cubison, M. J., Dunlea, E. J., Huffman, J. A., Onasch, T. B., Alfarra, M. R., Williams, P. I., Bower, K. N., Kondo, Y., Schneider, J., Drewnick, F., Borrmann, S., Weimer, S., Demerjian, K., Salcedo, D., Cottrell, L., Griffin, R., Takami, A., Miyoshi, T., Hatakeyama, S., Shimono, A., Sun, J. Y., Zhang, Y. M., Dzepina, K., Kimmel, J. R., Sueper, D., Jayne, J. T., Herton, S. C., Trimborn, A. M., Williams, L. R., Wood, E. C., Middlebrook, A. M., Kolb, C. E., Baltensperger, U., and Worsnop, D. R.: Evolution of organic aerosols in the atmosphere, *Science*, 326, 1525–1529, doi:10.1126/science.1180353, 2009.
- Jordan, T., Seen, A., and Jacobsen, G.: Levoglucosan as an atmospheric tracer for woodsmoke, *Atmos. Environ.*, 40, 5316–5321, doi:10.1016/j.atmosenv.2006.03.023, 2006.
- Justice, C., Giglio, L., Korontzi, S., Owens, J., Morisette, J., Roy, D., Descloitres, J., Alleaume, S., Petitcolin, F., and Kaufman, Y.: The MODIS fire products, *Remote Sens. Environ.*, 83, 244–262, 2002.
- Kalkstein, L. S., Tan, G., and Skindlov, J. A.: An evaluation of three clustering procedures for use in synoptic climatological classification, *J. Appl. Meteorol.*, 26, 717–730, 1987.
- Kleindienst, T. E., Lewandowski, M., Offenber, J. H., Jaoui, M., and Edney, E. O.: The formation of secondary organic aerosol from the isoprene + OH reaction in the absence of NO_x, *Atmos. Chem. Phys.*, 9, 6541–6558, doi:10.5194/acp-9-6541-2009, 2009.
- Kloster, S., Feichter, J., Maier-Reimer, E., Six, K. D., Stier, P., and Wetzell, P.: DMS cycle in the marine ocean-atmosphere system – a global model study, *Biogeosciences*, 3, 29–51, doi:10.5194/bg-3-29-2006, 2006.
- Koch, D., Schulz, M., Kinne, S., McNaughton, C., Spackman, J. R., Balkanski, Y., Bauer, S., Berntsen, T., Bond, T. C., Boucher, O., Chin, M., Clarke, A., De Luca, N., Dentener, F., Diehl, T.,

- Dubovik, O., Easter, R., Fahey, D. W., Feichter, J., Fillmore, D., Freitag, S., Ghan, S., Ginoux, P., Gong, S., Horowitz, L., Iversen, T., Kirkevåg, A., Klimont, Z., Kondo, Y., Krol, M., Liu, X., Miller, R., Montanaro, V., Moteki, N., Myhre, G., Penner, J. E., Perlwitz, J., Pitari, G., Reddy, S., Sahu, L., Sakamoto, H., Schuster, G., Schwarz, J. P., Seland, Ø., Stier, P., Takegawa, N., Takemura, T., Textor, C., van Aardenne, J. A., and Zhao, Y.: Evaluation of black carbon estimations in global aerosol models, *Atmos. Chem. Phys.*, 9, 9001–9026, doi:10.5194/acp-9-9001-2009, 2009.
- Laboratory Earth Systems Research Global Monitoring Division: NOAA Calibration Scales for Various Trace Gases, <http://www.esrl.noaa.gov/gmd/ccl/scales.html> (last access: August 2008), 2008.
- Lance, S., Medina, J., Smith, J. N., and Nenes, A.: Mapping the operation of the DMT continuous flow CCN counter, *Aerosol Sci. Technol.*, 40, 242–254, 2006.
- Lanz, V. A., Alfarra, M. R., Baltensperger, U., Buchmann, B., Hueglin, C., and Prévôt, A. S. H.: Source apportionment of sub-micron organic aerosols at an urban site by factor analytical modelling of aerosol mass spectra, *Atmos. Chem. Phys.*, 7, 1503–1522, doi:10.5194/acp-7-1503-2007, 2007.
- Lebel, T., Parker, D. J., Flamant, C., Bourlès, B., Marticorena, B., Mougou, E., Peugeot, C., Diedhiou, A., Haywood, J. M., Ngamini, J. B., Polcher, J., Redelsperger, J.-L., and Thorncroft, C. D.: The AMMA field campaigns: multiscale and multidisciplinary observations in the West African region, *Q. J. Roy. Meteor. Soc.*, 136, 8–33, doi:10.1002/qj.486, 2010.
- Lim, Y. B. and Ziemann, P. J.: Kinetics of the heterogeneous conversion of 1,4-hydroxycarbonyls to cyclic hemiacetals and dihydrofurans on organic aerosol particles., *Phys. Chem. Chem. Phys.*, 11, 8029–8039, doi:10.1039/b904333k, 2009.
- Manley, S. L., Goodwin, K., and North, W. J.: Laboratory production of bromoform, methylene bromide, and methyl iodide by macroalgae and distribution in nearshore Southern California waters, *Limnol. Oceanogr.*, 37, 1652–1659, 1992.
- Martin, S. T., Andreae, M. O., Althausen, D., Artaxo, P., Baars, H., Borrmann, S., Chen, Q., Farmer, D. K., Guenther, A., Gunthe, S. S., Jimenez, J. L., Karl, T., Longo, K., Manzi, A., Müller, T., Pauliquevis, T., Petters, M. D., Prenni, A. J., Pöschl, U., Rizzo, L. V., Schneider, J., Smith, J. N., Swietlicki, E., Tota, J., Wang, J., Wiedensohler, A., and Zorn, S. R.: An overview of the Amazonian Aerosol Characterization Experiment 2008 (AMAZE-08), *Atmos. Chem. Phys.*, 10, 11415–11438, doi:10.5194/acp-10-11415-2010, 2010.
- Matthew, B., Middlebrook, A., and Onasch, T.: Collection efficiencies in an aerodyne aerosol mass spectrometer as a function of particle phase for laboratory generated aerosols, *Aerosol Sci. Technol.*, 42, 884–898, doi:10.1080/02786820802356797, 2008.
- McFiggans, G., Alfarra, M. R., Allan, J., Bower, K., Coe, H., Cubison, M., Topping, D., Williams, P., Decesari, S., Facchini, C., and Fuzzi, S.: Simplification of the representation of the organic component of atmospheric particulates, *Faraday Discuss.*, 130, 341, 341–362, doi:10.1039/b419435g, 2005.
- McMorrow, J. and Talip, M. A.: Decline of forest area in Sabah, Malaysia: relationship to state policies, land code and land capability, *Global Environ. Change*, 11, 217–230, doi:10.1016/S0959-3780(00)00059-5, 2001.
- Mead, M., Khan, M., White, I., Nickless, G., and Shallcross, D.: Methyl halide emission estimates from domestic biomass burning in Africa, *Atmos. Environ.*, 42, 5241–5250, doi:10.1016/j.atmosenv.2008.02.066, 2008.
- Millero, F. J.: The physical chemistry of seawater, *Annu. Rev. Earth Planet. Sci.*, 2, 101–150, doi:10.1146/annurev.ea.02.050174.000533, 1974.
- Morgan, W. T., Allan, J. D., Bower, K. N., Capes, G., Crosier, J., Williams, P. I., and Coe, H.: Vertical distribution of sub-micron aerosol chemical composition from North-Western Europe and the North-East Atlantic, *Atmos. Chem. Phys.*, 9, 5389–5401, doi:10.5194/acp-9-5389-2009, 2009.
- Morgan, W. T., Allan, J. D., Bower, K. N., Highwood, E. J., Liu, D., McMeeking, G. R., Northway, M. J., Williams, P. I., Krejci, R., and Coe, H.: Airborne measurements of the spatial distribution of aerosol chemical composition across Europe and evolution of the organic fraction, *Atmos. Chem. Phys.*, 10, 4065–4083, doi:10.5194/acp-10-4065-2010, 2010.
- Ng, N. L., Canagaratna, M. R., Zhang, Q., Jimenez, J. L., Tian, J., Ulbrich, I. M., Kroll, J. H., Docherty, K. S., Chhabra, P. S., Bahreini, R., Murphy, S. M., Seinfeld, J. H., Hildebrandt, L., Donahue, N. M., DeCarlo, P. F., Lanz, V. A., Prévôt, A. S. H., Dinar, E., Rudich, Y., and Worsnop, D. R.: Organic aerosol components observed in Northern Hemispheric datasets from Aerosol Mass Spectrometry, *Atmos. Chem. Phys.*, 10, 4625–4641, doi:10.5194/acp-10-4625-2010, 2010.
- Newton, H. M., Reeves, C. E., Mills, G. P., and Oram, D. E.: Organohalogenes in and above the rainforest of Borneo, to be submitted to *Atmos. Chem. Phys.*, 2011.
- Novakov, T., Corrigan, C., Penner, J., Chuang, C., Rosaria, O., and Bracero, O. M.: Organic aerosols in the Caribbean trade winds: a natural source?, *J. Geophys. Res.-Atmos.*, 102, 21307–21313, 1997.
- O'Dowd, C. D., Facchini, M. C., Cavalli, F., Ceburnis, D., Mircea, M., Decesari, S., Fuzzi, S., Yoon, Y. J., and Putaud, J.-P.: Biogenically driven organic contribution to marine aerosol, *Nature*, 431, 676–680, 2004.
- Paatero, P.: Least squares formulation of robust non-negative factor analysis, *Chemometr. Intell. Lab.*, 37, 23–35, doi:10.1016/S0169-7439(96)00044-5, 1997.
- Paatero, P. and Tapper, U.: Positive matrix factorization: a non-negative factor model with optimal utilization of error estimates of data values, *Environmetrics*, 5, 111–126, doi:10.1002/env.3170050203, 1994.
- Pandis, S. N., Wexler, A. S., and Seinfeld, J. H.: Dynamics of tropospheric aerosols, *J. Phys. Chem.*, 99, 9646–9659, doi:10.1021/j100024a003, 1995.
- Paulot, F., Crounse, J. D., Kjaergaard, H. G., Kürten, A., St. Clair, J. M., Seinfeld, J. H., and Wennberg, P. O.: Unexpected epoxide formation in the gas-phase photooxidation of isoprene., *Science*, 325, 730–733, doi:10.1126/science.1172910, 2009.
- Pearson, G., Davies, F., and Collier, C.: Remote sensing of the tropical rain forest boundary layer using pulsed Doppler lidar, *Atmos. Chem. Phys.*, 10, 5891–5901, doi:10.5194/acp-10-5891-2010, 2010.
- Petters, M. D. and Kreidenweis, S. M.: A single parameter representation of hygroscopic growth and cloud condensation nucleus activity, *Atmos. Chem. Phys.*, 7, 1961–1971, doi:10.5194/acp-7-1961-2007, 2007.
- Petzold, A. and Schonlinner, M.: Multi-angle absorption photome-

- ter – a new method for the measurement of aerosol light absorption and atmospheric black carbon, *J. Aerosol Sci.*, 35, 421–441, doi:10.1016/j.jaerosci.2003.09.005, 2004.
- Quack, B., Peeken, I., Petrick, G., and Nachtigall, K.: Oceanic distribution and sources of bromoform and dibromomethane in the Mauritanian upwelling, *J. Geophys. Res.*, 112, C10006, doi:10.1029/2006JC003803, 2007.
- Reeves, C. E.: Atmospheric budget implications of the temporal and spatial trends in methyl bromide concentration, *J. Geophys. Res.*, 108, 4343, doi:10.1029/2002JD002943, 2003.
- Roberts, G. and Nenes, A.: A continuous-flow streamwise thermal-gradient CCN chamber for atmospheric measurements, *Aerosol Sci. Technol.*, 39, 206–221, doi:10.1080/027868290913988, 2005.
- Robinson, N. H., Hamilton, J. F., Allan, J. D., Langford, B., Oram, D. E., Chen, Q., Docherty, K., Farmer, D. K., Jimenez, J. L., Ward, M. W., Hewitt, C. N., Barley, M. H., Jenkin, M. E., Rickard, A. R., Martin, S. T., McFiggans, G., and Coe, H.: Evidence for a significant proportion of Secondary Organic Aerosol from isoprene above a maritime tropical forest, *Atmos. Chem. Phys.*, 11, 1039–1050, doi:10.5194/acp-11-1039-2011, 2011.
- Rollins, A. W., Fry, J. L., Hunter, J. F., Kroll, J. H., Worsnop, D. R., Singaram, S. W., and Cohen, R. C.: Elemental analysis of aerosol organic nitrates with electron ionization high-resolution mass spectrometry, *Atmos. Meas. Tech.*, 3, 301–310, doi:10.5194/amt-3-301-2010, 2010.
- Simoneit, B., Schauer, J. J., Nolte, C. G., Oros, D. R., Elias, V. O., Fraser, M. P., Rogge, W. F., and Cass, G. R.: Levoglucosan, a tracer for cellulose in biomass burning and atmospheric particles, *Atmos. Environ.*, 33, 173–182, doi:10.1016/S1352-2310(98)00145-9, 1999.
- Sive, B. C., Varner, R. K., Mao, H., Blake, D. R., Wingenter, O. W., and Talbot, R.: A large terrestrial source of methyl iodide, *Geophys. Res. Lett.*, 34, L17808, doi:10.1029/2007GL030528, 2007.
- Slowik, J. G., Brook, J., Chang, R. Y.-W., Evans, G. J., Hayden, K., Jeong, C.-H., Li, S.-M., Liggio, J., Liu, P. S. K., McGuire, M., Mihele, C., Sjostedt, S., Vlasenko, A., and Abbatt, J. P. D.: Photochemical processing of organic aerosol at nearby continental sites: contrast between urban plumes and regional aerosol, *Atmos. Chem. Phys.*, 11, 2991–3006, doi:10.5194/acp-11-2991-2011, 2011.
- Smythe-Wright, D., Boswell, S. M., Breithaupt, P., Davidson, R. D., Dimmer, C. H., and Eiras Diaz, L. B.: Methyl iodide production in the ocean: implications for climate change, *Global Biogeochem. Cy.*, 20, GB3003, doi:10.1029/2005GB002642, 2006.
- Surratt, J. D., Murphy, S. M., Kroll, J. H., Ng, N. L., Hildebrandt, L., Sorooshian, A., Szmigielski, R., Vermeylen, R., Maenhaut, W., Claeys, M., Flagan, R. C., and Seinfeld, J. H.: Chemical composition of secondary organic aerosol formed from the photooxidation of isoprene, *J. Phys. Chem. A*, 110, 9665–9690, 2006.
- Surratt, J. D., Gomez-Gonzalez, Y., Chan, A. W. H., Vermeylen, R., Shahgholi, M., Kleindienst, T. E., Edney, E. O., Offenberg, J. H., Lewandowski, M., Jaoui, M., Maenhaut, W., Claeys, M., Flagan, R. C., and Seinfeld, J. H.: Organosulfate formation in biogenic secondary organic aerosol, *J. Phys. Chem. A*, 112, 8345–8378, doi:10.1021/jp802310p, 2008.
- Surratt, J. D., Chan, A. W. H., Eddingsaas, N. C., Chan, M., Loza, C. L., Kwan, A. J., Hersey, S. P., Flagan, R. C., Wennberg, P. O., and Seinfeld, J. H.: Atmospheric chemistry special feature: reactive intermediates revealed in secondary organic aerosol formation from isoprene., *P. Natl. Acad. Sci. USA*, 15, 6640–6645, doi:10.1073/pnas.0911114107, 2010.
- Swietlicki, E., Hansson, H.-C., Hameri, K., Svenningsson, B., Massling, A., McFiggans, G., McMurry, P. H., Petaja, T., Tunved, P., Gysel, M., Topping, D., Weingartner, E., Baltensperger, U., Rissler, J., Wiedensohler, A., and Kulmala, M.: Hygroscopic properties of submicrometer atmospheric aerosol particles measured with H-TDMA instruments in various environments – a review, *Tellus B*, 60, 432–469, doi:10.1111/j.1600-0889.2008.00350.x, 2008.
- Tsai, I.-C., Chen, J.-P., Lin, P.-Y., Wang, W.-C., and Isakson, I. S. A.: Sulfur cycle and sulfate radiative forcing simulated from a coupled global climate-chemistry model, *Atmos. Chem. Phys.*, 10, 3693–3709, doi:10.5194/acp-10-3693-2010, 2010.
- Ulbrich, I. M., Canagaratna, M. R., Zhang, Q., Worsnop, D. R., and Jimenez, J. L.: Interpretation of organic components from Positive Matrix Factorization of aerosol mass spectrometric data, *Atmos. Chem. Phys.*, 9, 2891–2918, doi:10.5194/acp-9-2891-2009, 2009.
- Venzke, E., Wunderman, R. W., McClelland, L., Simkin, T., Luhr, J. F., Siebert, L., and Mayberry, G. (Eds.): *Global Volcanism, 1968 to the Present*, Smithsonian Institution, Global Volcanism Program Digital Information Series, GVP-4, <http://www.volcano.si.edu/reports/> (last access: February 2009), 2010.
- Williams, I., Gallagher, M. W., Choulaton, T. W., Coe, H., Bower, K. N., and McFiggans, G.: Aerosol development and interaction in an urban plume, *Aerosol Sci. Technol.*, 32, 120–126, doi:10.1080/027868200303821, 2000.
- Williams, P. I., McFiggans, G., and Gallagher, M. W.: Latitudinal aerosol size distribution variation in the Eastern Atlantic Ocean measured aboard the FS-Polarstern, *Atmos. Chem. Phys.*, 7, 2563–2573, doi:10.5194/acp-7-2563-2007, 2007.
- Winklmayr, W., Reischl, G. P., Lindner, A. O., and Berner, A.: A new electromobility spectrometer for the measurement of aerosol size distributions in the size range from 1 to 1000 nm, *J. Aerosol Sci.*, 22, 289–296, 1991.
- Worton, D. R., Mills, G. P., Oram, D. E., and Sturges, W. T.: Gas chromatography negative ion chemical ionization mass spectrometry: application to the detection of alkyl nitrates and halocarbons in the atmosphere, *J. Chromatogr. A*, 1201, 112–119, 2008.
- Yokouchi, Y., Hasebe, F., Fujiwara, M., Takashima, H., Shiotani, M., Nishi, N., Kanaya, Y., Hashimoto, S., Fraser, P., Toom-Saunty, D., Mukai, H., and Nojiri, Y.: Correlations and emission ratios among bromoform, dibromochloromethane, and dibromomethane in the atmosphere, *J. Geophys. Res.*, 110, D23309, doi:10.1029/2005JD006303, 2005.
- Zhang, Q., Jimenez, J. L., Canagaratna, M. R., Allan, J. D., Coe, H., Ulbrich, I., Alfarra, M. R., Takami, A., Middlebrook, A. M., Sun, Y. L., Dzepina, K., Dunlea, E., Docherty, K., DeCarlo, P. F., Salcedo, D., Onasch, T. B., Jayne, J. T., Miyoshi, T., Shimo, A., Hatakeyama, S., Takegawa, N., Kondo, Y., Schneider, J., Drewnick, F., Borrmann, S., Weimer, S., Demerjian, K., Williams, P., Bower, K. N., Bahreini, R., Cottrell, L., Griffin, R. J., Rautiainen, J., Sun, J. Y., Zhang, Y. M., and Worsnop, D. R.: Ubiquity and dominance of oxygenated species in organic aerosols in anthropogenically-influenced Northern

- Hemisphere midlatitudes, *Geophys. Res. Lett.*, 34, 101029, doi:10.1029/2007GL029979, 2007.
- Zhou, Y., Mao, H., Russo, R. S., Blake, D. R., Wingenter, O. W., Haase, K. B., Ambrose, J., Varner, R. K., Talbot, R., and Sive, B. C.: Bromoform and dibromomethane measurements in the seacoast region of New Hampshire, 2002–2004, *J. Geophys. Res.*, 113, D08305, doi:10.1029/2007JD009103, 2008.
- Zorn, S. R., Drewnick, F., Schott, M., Hoffmann, T., and Borrmann, S.: Characterization of the South Atlantic marine boundary layer aerosol using an aerodyne aerosol mass spectrometer, *Atmos. Chem. Phys.*, 8, 4711–4728, doi:10.5194/acp-8-4711-2008, 2008.